UNITED STATES DEPARTMENT OF COMMERCE
JESSE H. JONES, Secretary
NATIONAL BUREAU OF STANDARDS
Lyman J. Briggs, Director

✦

Journal of Research

of the

National Bureau of Standards

✦

Volume 28, Number 4
April 1942

[Published with approval of the Director of the Budget]

UNITED STATES
GOVERNMENT PRINTING OFFICE
WASHINGTON : 1942

For sale by the Superintendent of Documents, Washington, D. C. - - - - Price 30 cents
$3.50 per year on subscription

The prices of the separate Research Papers appearing in this JOURNAL are given on the front cover page. If 100 or more copies of any separate are ordered, a discount of 25 percent is allowed. Those who desire copies of separate Research Papers should send their orders and remittances without delay to the Superintendent of Documents, U. S. Government Printing Office, Washington, D. C. This will aid him to determine the number of copies to be printed for sale. Research Papers are not printed from electrotypes, and usually no more reprints can be had when the first and only printing is exhausted.

MATHEMATICAL TABLES

A list of the mathematical tables now obtainable from the National Bureau of Standards is printed on page 3 of the Journal cover. New tables will be announced from time to time as they become available.

U. S. Department of Commerce National Bureau of Standards

RESEARCH PAPER RP1461

Part of Journal of Research of the National Bureau of Standards, Volume 28, April 1942

SOME PROPERTIES OF THE DRY AIR-SETTING TYPE OF REFRACTORY BONDING MORTAR

By Raymond A. Heindl and William L. Pendergast

ABSTRACT

Seventeen brands of air-setting refractory mortars of the type marketed in the dry condition were investigated in the unheated state with regard to tempering water, fineness of grain, soluble alkali content, pyrometric-cone equivalent, suitability for troweling and dipping, drying and setting properties, and strength. After heat treatments at various final temperatures the strengths of the mortars were determined. In rupturing assemblages of two half-brick and mortar, the types of failure were noted. The tendency of the mortars to shrink, crack, and flow when exposed to high temperatures, both in fusion blocks and in units of three brick each, was also investigated.

The ingredients of the mortars were all fine-grained, only a small amount being retained on a No. 40 sieve. The strengths of the neat mortars covered a wide range; the strengths of those received and stored in metal drums indicated the desirability of storage in airtight containers. In a series of heat treatments the neat mortars in general were found to have the least strength when preheated at 750° C. However, the least strengths of the majority were noted in assemblages of brick and mortar preheated at 1,000° C. The mechanical troweling machine gave a better indication of the workability of the mortars than did the time-of-set test. Observations made on the mortars heated in fusion blocks in general corroborated the shrinkage, cracking, and fusion of the same mortars heated in brick piers.

CONTENTS

	Page
I. Introduction	402
II. Materials and containers	402
III. Preparation of specimens and methods of testing	402
1. Mortar	402
(a) Mixing and mixing water	402
(b) Sieve analysis	403
(c) Soluble alkali content	403
(d) Pyrometric-cone equivalent	403
(e) Fusion-block test	403
(f) Flow-table test	403
(g) Troweling and drying properties	403
(1) Appearance before drying	403
(2) Appearance after drying	404
(h) Dipping	404
(i) Transverse strength and linear shrinkage	404
2. Assemblage of two half-brick and mortar	404
(a) Preparation	404
(b) Setting time of mortar	405
3. Pier of three brick and mortar	405
IV. Results and discussion	405
1. Mortar	405
(a) Mixing water	405
(b) Sieve analysis	408
(c) Soluble alkali content	408

IV. Results and discussion—Continued. Page
Mortar—Continued.
(d) Pyrometric-cone equivalent ... 408
(e) Fusion-block test ... 408
(f) Flow-table test ... 408
(g) Troweling ... 408
(1) Appearance before drying ... 408
(2) Appearance after drying ... 409
(h) Dipping ... 409
(i) Transverse strength and linear shrinkage ... 409
2. Assemblage of two half-brick and mortar ... 412
(a) Setting time of mortar, or water-retention test ... 412
(b) Transverse strength ... 412
(c) Types of failure ... 413
(d) Relation of water content to setting time and to flow ... 413
(e) Effect of atmosphere during heating on strength ... 413
3. Pier of three brick and mortar ... 414
V. Summary and conclusions ... 415

I. INTRODUCTION

Air-setting refractory mortars may be purchased either in the wet condition, ready for use, or dry, requiring only the addition of water. A report [1] giving the results of a study of the wet type has been published. The results of a somewhat similar investigation of the dry type are herein reported.

Preliminary to the latter study, it was deemed advisable to determine suitable soaking and mixing periods for the average mortar after adding the water required for bringing it to the necessary consistency for use. The results of this preliminary investigation have also been reported.[2]

The information made available in the present report will be used as a basis for Federal specifications governing this commodity.

II. MATERIALS AND CONTAINERS

Seventeen air-setting mortars of the type marketed in the dry condition, 4 of which had a chromite base, were furnished by 12 manufacturers. As indicated in table 1, 6 of these mortars were received in sealed sheetiron drums and 11 in paper-lined burlap or jute sacks. The length of time of storage after receipt is reported, since storage in nonairtight containers causes deterioration in the strength of such mortars.

III. PREPARATION OF SPECIMENS AND METHODS OF TESTING

1. MORTAR

(a) MIXING AND MIXING WATER

Each mortar was mechanically mixed with water for 1 hour, soaked overnight (19 hours), and then mixed for an additional 4 hours before it was tested. The consistencies for troweling and for dipping were judged by "feel."

The loss in weight, assumed to indicate the water content or mixing water, was obtained by drying samples of approximately 200 g

[1] Raymond A. Heindl and William L. Pendergast, *Properties of air-setting refractory bonding mortars of the wet type*, J. Research NBS **23**, 7 (1940) RP1219.

[2] Raymond A. Heindl and W. L. Pendergast, *Effect of water content and mixing time on properties of air-setting refractory mortars containing sodium silicate*, Bul. Am. Ceram. Soc. **19**, 430 (1940).

to a constant weight at about 105° C. In most cases the drying time required was 96 hours.

(b) SIEVE ANALYSIS

The sieve analysis was made by the wet method [3] on a sample of about 100 g. Two tests were made—the first after slaking the mortar for 1 hour, and the second after machine-mixing 1 hour, soaking 19 hours, and machine-mixing 4 additional hours. The dried residue was sieved, using United States Standard Sieves Nos. 20, 40, 60, 100, and 200, mechanically vibrated.

(c) SOLUBLE ALKALI CONTENT

The soluble alkali content of each mortar was determined on an unfired sample, weighing approximately 20 g, taken from the bar specimens. The dried sample was digested with 200 ml of water on a steam bath overnight, filtered, and the residue leached a second time overnight with the same quantity of water. The alkali content of the combined filtrates was determined by titration with 0.2 *N* hydrochloric acid, using methyl red as the indicator.

(d) PYROMETRIC-CONE EQUIVALENT

The pyrometric-cone equivalents (softening points) were determined according to the ASTM standard method, serial designation C 24–35.[4] Cones were made from the mortars both before and after calcining at approximately 1,200° C. In both cases, after placing the cones in plaques, they were heated to about 1,200° C and cooled before testing.

(e) FUSION-BLOCK TEST

The pyrometric-cone equivalent of the fusion block was 32. Two blocks were used for each mortar, the compartments for holding the test materials being approximately ½ in. and ⅛ in. deep, respectively. Samples of the mortars sufficiently large to fill the compartments were taken from the machine-mixed batches prepared for other tests. The blocks containing the mortar samples were heated at 110°, 750°, 1,000°, 1,350°, and 1,500° C. After cooling the mortars they were examined for shrinkage, bubbles, glassiness, and flow.

(f) FLOW-TABLE TEST

The flow-table test is described in Federal Specification SS–C–158 [5] and also in the ASTM Standard for Masonry Cement, serial designation C 91–40.[6]

(g) TROWELING AND DRYING PROPERTIES

The troweling tests were made with the machine described by Heindl and Pendergast.[7] A ¼-in. layer of mortar was spread evenly by hand-troweling on the upper 9- by 4½-in. face of a brick by means of a template. Using such specimens, four tests of troweling properties were made by reducing this ¼-in. layer to ⅛ in. in 1 stroke, to 1/16 in. in 1 stroke, to ⅛ in. in 25 strokes (0.005 in. per stroke), and to 1/16 in. in 37 strokes.

(1) *Appearance before drying.*—The mortar caps were examined for uniformity of thickness and adherence to the brick, which are indications of satisfactory troweling properties.

[3] In general the test was similar to that described in Method C 92-36, p. 195, Am. Soc. Testing Materials, Standards, pt. 2, Non-Metals (1939).
[4] Am. Soc. Testing Materials, Standards, pt. 2, Non-Metals, p. 214 (1939).
[5] Cements, hydraulic; General Specification.
[6] Am. Soc. Testing Materials, Standards, Supplement, pt. 2, p. 1–7 (1940).
[7] J. Research NBS **23**, 7 (1940) RP1219.

(2) *Appearance after drying.*—The mortared specimens were dried at room temperature and ordinary atmospheric conditions, and the mortar caps inspected for cracks, curling, and separation from the brick.

(h) DIPPING

A joint of mortar approximately 1/16 in. thick, obtained by dipping the brick in a slurry, is frequently recommended by the manufacturers when mortars of this type are used for laying brick. Hence, testing the adaptability of the various mortars for conversion to the dipping condition was important. This was accomplished by placing a quantity of the mortar, which was in a troweling condition, in a pan and mixing it by hand with measured amounts of water until the desired consistency was obtained.

(i) TRANSVERSE STRENGTH AND LINEAR SHRINKAGE

The transverse strength (modulus of rupture) was determined on mortar bars 6 by 1 by 1/4 in. over a 5-in. span. The bars were formed by placing the mortar in brass molds under which were slips of newspaper resting on glass plates. The mold and bar were then removed from the glass and, with the attached paper down, placed on a firebrick. An initial set occurred within a few minutes, and the mold was then removed from the mortar bar with the aid of a safety razor blade. To prevent warping, the following drying schedule was used. The mortar bars were stored (1) in a constant-humidity room maintained for 48 hours at 60- to 65-percent humidity and 20° to 22° C, (2) 18 hours (overnight) at ordinary laboratory temperature and humidity, and (3) 27 hours in a drying oven at 105° to 110° C. The paper was removed from the mortar bars in the constant-humidity room when they had become sufficiently hard to permit handling without breakage. Hereafter the "positions" of the mortar bars will be designated as "original" (the side next to the paper being down) and "inverted" (the side next to the paper being up). In making the transverse-strength tests, half of the 10 mortar bars were tested in the "original" position in the cross-breaking machine and the other half in the "inverted" position.

2. ASSEMBLAGE OF TWO HALF-BRICK AND MORTAR

(a) PREPARATION

The standard 9-in. dry-pressed brick used in the test specimens for determining the strength of brick-to-mortar bond had a moderately coarse texture, an absorption of 8.6 percent, and a transverse strength of 590 lb/in^2. By means of an abrasive wheel the brick were cut, parallel to the 2½- by 4½-in. faces, into two equal parts. A laboratory screwpress [8] was employed in the operation of bonding the two half-brick with mortar. The press had an attached jig, or alining guide, to prevent lateral motion of the two halves of the brick when forced together with mortar between them. Uniform thickness of mortar joints, 1/16 and 1/4 in., for testing bonding strength and "time of set", respectively, was obtained by using properly sized spacers. The operation of bonding was as follows. After rigidly clamping the halves of brick against the jig, the end-molded faces and spacer were brought in contact by lowering the upper half-brick. This position, indicated by a scale attached to the frame of the machine, being

[8] J. Research NBS 23, 7 (1940) RP1219.

noted, the upper half of the brick was raised, the spacer removed, and approximately double the amount of mortar required for the joint was placed between the two half-brick. The upper portion was again lowered until it occupied the same position as when the spacers were used. The excess mortar was removed and the specimen taken from the press and subjected to the drying treatment described in the preparation of the mortar bars. These brick-and-mortar assemblages were heated simultaneously with the mortar bars made from the corresponding mortar. The modulus of rupture of the mortar joint was determined over an 8-in. span.

(b) SETTING TIME OF MORTAR

The time elapsing between placing the mortar on the brick and the attainment of sufficient mortar stiffness to prevent flow under a constant load of 50 lb. was designated "time of set." When removed from the press, the assemblage (¼-in. mortar joint) in its original vertical position stood for 3 minutes from the time the mortar was first placed on the brick before being gently loaded with a 50-lb. weight. It was noted whether such loading caused mortar to be squeezed from the joint. If no flow occurred, additional tests with newly prepared assemblages were made and the original time of 3 minutes was reduced to 2 minutes. If, however, flow was observed, then the original time was increased by 3-minute increments until the mortar was set and no flow occurred. The final time was then reduced by one or two 1-minute decrements until the mortar was again squeezed from the joint.

3. PIER OF THREE BRICK AND MORTAR

A second type of brick-and-mortar assemblage was made which consisted of a pier of two standard-size brick and two half-brick laid flat to give one vertical and two horizontal joints. Three of these piers were laid up with a 1/16-in. dipped joint and three with a ⅛-in. troweled joint, spacers being used to obtain the desired joint thickness.

The piers were examined for defects of the mortar and mortar joint after curing and drying and after heating them at 750° C for 24 hours, at 1,350° C for 1 hour, and at 1,500° C for 1 hour.

IV. RESULTS AND DISCUSSION

1. MORTAR

(a) MIXING WATER

The amounts of water, in percentages of the dry weight of the mortar, used for bringing the mixtures to the proper consistencies for making test bars, troweling, and dipping, respectively, are given in table 1, columns 11, 15, and 20.

The percentages of water ranged from 12.8 to 36.9 in the bars, 16.6 to 43.0 in the mortars of troweling consistency, and 20.7 to 60.1 in those of dipping consistency.

In opposition to the general trend, there were two cases in which the water content used for troweling was less than that in the bars and five cases in which approximately the same content of water was used for both purposes.

Without exception the water content of the mortar adjusted to a dipping consistency was greater than that of troweling consistency.

TABLE 1.—*Some properties of air-setting refractory*

Mortar	Container [1]	Stored before testing	Sieve analysis [2]				Alkali as Na_2O	Pyrometric-cone equivalent		Water content of neat mortar used in bar specimens
			Retained on No. 40	Passed No. 40; retained on No. 60	Passed No. 60; retained on No. 100	Passed No. 100, retained on No. 200		Raw	Calcined	
(1)	(2)	(3)	(4)	(5)	(6)	(7)	(8)	(9)	(10)	(11)
		Months	*Percent*	*Percent*	*Percent*	*Percent*	*Percent*	*Cone*	*Cone*	*Percent*
A-3	Bag	1	0.6 3.2	5.4 6.5	15.6 17.1	23.3 25.5	0.57	34	34	25.9
A-4	do	2	0.6 .6	1.9 2.4	10.0 9.8	17.4 16.5	.10	33	32 to 33	32.5
B-1	Metal drum	48	0 .1	5.4 8.1	15.3 15.5	14.8 17.2	1.90	30 to 31	30 to 31	18.6
D-1	do	48	0 1.7	7.5 12.5	15.5 14.5	16.6 16.4	0.71	37	37	24.0
E-2	Bag	48	0.8 2.1	6.7 8.4	27.3 27.2	16.6 16.3	.87	26	27	30.5
F-1	Metal drum	48	0.2 3.6	17.6 21.8	18.0 16.2	13.9 11.5	1.53	26 28	26 28	21.0
F-2	do	¼	0 0	2.5 2.3	26.5 23.9	24.1 26.8	1.03	27	27	36.9
G-1	Bag	6	0 .2	3.4 3.5	13.5 12.7	16.4 16.1	0.27	27	27	26.0
H-1	do	7	0 .1	2.2 3.6	12.9 15.3	19.1 19.7	1.86	29	29	32.9
I-1	do	49	0.7 3.4	9.6 9.0	12.6 11.0	16.0 15.2	0.03	Above 38	Above 38	14.4
L-1	do	13	2.4 22.7	25.7 24.1	15.1 10.7	12.1 10.3	1.02	[3] 19 to 23	20	22.8
M-1	Metal drum	49	0.6 .4	8.8 11.0	11.5 15.0	10.8 17.2	1.03	Above 35	Above 35	12.8
O-2	Bag	¼	.1	2.6	6.1	10.4	1.08	Above 36	Above 36	21.7
R-2	do	3	3.3 1.9	21.3 20.6	15.4 15.6	11.9 12.3	1.27 1.27	31	31	25.8
W-1	do	48	0.4 1.1	11.7 13.5	19.8 19.5	15.5 16.0	0.88	31	31	26.3
X-1	Metal drum	34	0.6 1.1	2.3 2.7	8.4 8.0	14.7 16.0	0	27 to 28	27	27.1
Z-1	Bag	½	0 .2	11.7 13.0	14.5 15.3	13.0 14.6	2.13	31	31	18.8

[1] In most cases the bags were of burlap lined with moisture-proof paper.
[2] First values obtained after mixing 1 hour, soaking 19 hours, and mixing 4 hours; second values after 1-hour slaking only.
[3] Unable to obtain satisfactory end point.

mortars marketed in the dry condition

Time of set of mortars used for troweling	Troweling; spreading and reducing layer		Water content of mortars used in troweling tests	Flow-table reading	Troweling and drying properties		Dipping consistency		
	From ¼″ to 1/8″ and ¼″ to 1/16″ in 1 stroke and ¼″ to ⅛″ in 25 strokes	From—¼″ to 1/16″ in 37 strokes			Curled	Cracked	Obtained easily	Water-content of mortars	Workability
(12)	(13)	(14)	(15)	(16)	(17)	(18)	(19)	(20)	(21)
Minutes			*Percent*					*Percent*	
1	Good	Fair	24.4	100	No	Slightly	Yes	30.4	Good.
5	do	Good	32.5	26	do	do	do	59.1	Good. Very sticky.
10	do	do	25.6	86	do	do	do	31.3	Good.
8.5	do	do	20.9	78	Moderately	Badly	do	32.4	Do.
10	do	do	33.3	62	Slightly	Moderately	No	49.2	Poor. Did not stay in suspension.
5	do	do	21.9	95	No	No	Yes	27.7	Good.
3	do	Fair	40.4	84	do	do	do	60.1	Do.
10	do	Good	36.3	70	Moderately	Badly	No	42.4	Poor. Did not stay in suspension.
3	do	do	39.9	66	do	do	do	53.8	Fair. Dried too rapidly.
5	do	Fair	21.9	80	No	Slightly	Yes	42.3	Good.
1	do	do	26.0	110	do	No	do	35.3	Fair. Dried too rapidly.
3	do	Good	16.6	64	No	do	No	20.7	Good.
30	do	do	25.0	77	Moderately	Moderately	Yes	43.4	Do.
3	do	do	25.8	24	No	Badly	do	36.6	Fair. Did not stay in suspension.
3	do	do	43.0	66	Slightly	do	No	50.0	Poor.
20	do	Fair	28.0	77	No	No	Yes	42.8	Fair. Dried too slowly.
16	do	Good	20.1	64	do	do	do	32.4	Good.

(b) SIEVE ANALYSIS

The results of the sieve analysis are given in table 1, columns 4, 5, 6, and 7. The differences between the first and second series of values for each mortar are accounted for by the fact that the longer time of soaking and mixing caused a gradual breaking down of the particles. This disintegration was more pronounced in some mortars than in others, as illustrated by mortar *D*–1 versus *X*–1. The disintegration also proceeded further in the mortars containing the greater fractions of coarse particles, as illustrated by mortar *L*–1 versus *G*–1. In a number of instances (examples *A*–4, *F*–1, *L*–1, etc.) the percentages of the fractions retained on the No. 100 and No. 200 sieves were increased at the expense of the coarser fractions when the mortar was mixed for the longer period. Although no values for material retained on the No. 20 sieve are shown in the table, in no case was this residue as much as 0.5 percent; in fact, for most of the mortars no residue was noted. No significant relation was apparent between percentage of material not passing the No. 200 sieve and other properties, although in most cases the time of set of the mortars was shortest in those containing the greatest quantity of coarse particles. That no definite relation existed was not surprising, since the mortars contain different amounts of sodium silicate and other ingredients which tended to upset any such relation.

(c) SOLUBLE ALKALI CONTENT

The soluble alkali content of the mortars, in terms of sodium oxide, ranged from 0 to 1.90 percent. This free alkali in all probability represented in most cases only a portion of that originally added. As shown by Geller and Caldwell,[9] considerable amounts of alkali can be absorbed by clays and its presence not detected by an indicator.

(d) PYROMETRIC-CONE EQUIVALENT

The pyrometric-cone equivalent (pce, or softening point) of the mortars listed in table 1, columns 9 and 10, ranged from 19 to above 38 for the uncalcined material and from 20 to above 38 for the calcined mortars. The end points obtained indicate little difference in pce between the uncalcined and calcined materials. In some cases, however, the end points of the uncalcined material were more difficult to obtain because of the tendency of the cones to twist and curl.

(e) FUSION-BLOCK TEST

The conclusions drawn from the appearance of the mortar in the fusion-block tests, relative to adherence, flow, shrinkage, and cracking (see table 3) correlate in general so well with those drawn from the pier specimens that no separate discussion is considered necessary.

(f) FLOW-TABLE TEST

The results of the flow-table test of the mortars in a troweling consistency are given in table 1, column 16. The values range from 24 to 110. This range is rather broad; consequently it would be impracticable to specify a troweling consistency for different mortars based on a definite flow-table reading, as was the original intention when the tests were started.

(g) TROWELING

(1) *Appearance before drying.*—The results of the troweling tests are given in table 1, columns 13 and 14. The troweling tests gave

[9] *Absorption of sodium hydroxide by kaolins*, J. Am. Ceram. Soc. **4**, 468 (1921).

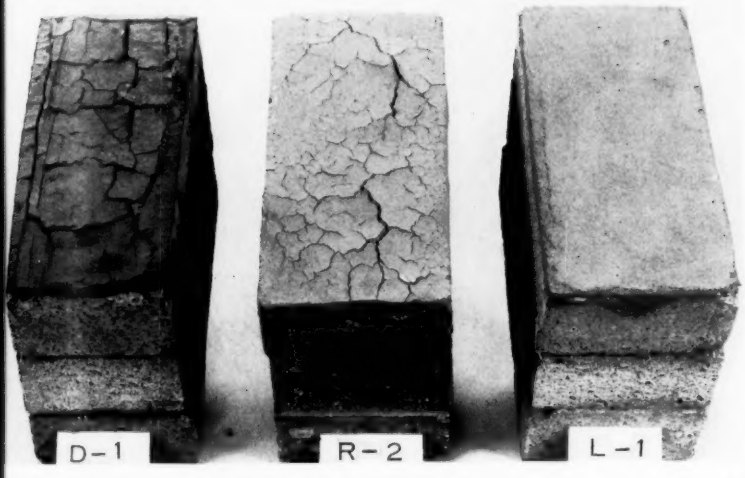

IGURE 1.—*Desirable drying properties are illustrated by mortar L–1 and undesirable ones by mortars D–1 and R–2.*

UNIV. OF MICH.

both an indication of the comparative ease with which a mortar could be satisfactorily spread, and of its water retentiveness. With the mortars in a troweling consistency, as judged by the investigator, there was no difficulty in spreading and reducing layers from ¼ to ⅛ in. in 1 stroke, from ¼ to 1/16 in. in 1 stroke, or from ¼ to⅛ in. in 25 strokes, when a mechanical trowel was used. When, however, the layer was reduced from ¼ to 1/16 in. in 37 strokes, five of the mortars (*A*–3, *F*–2, *I*–1, *L*–1, *X*–1) showed distinct signs of deterioration as far as their working properties were concerned.

(2) *Appearance after drying.*—Observations on the tendency of the mortars to curl and crack are given in table 1, columns 17 and 18, respectively. These observations were made on the mortar caps of the thicknesses produced by the mechanical troweling tests (see table 1, columns 13 and 14). The following ratings, based on the appearance of the mortars after drying on the brick, were given to differentiate the several degrees to which the mortars were curled or cracked: "no", "slightly", "moderately", and "badly." The mortars as a whole showed remarkably little curling, 13 of the 17 mortars being either free or practically free of this undesirable feature. Serious cracking, on the other hand, occurred in 7 of the 17 mortars during drying. The extremes in appearance after drying are illustrated by the three mortars in figure 1.

(h) DIPPING

The observations given in table 1, column 19, indicate that 5 of the 17 mortars were converted from a troweling to a dipping consistency with difficulty, requiring at least half an hour of mixing with water to produce the conversion. The workability (column 21) of the mortars when in a dipping consistency varied widely, with seven of them considered as unsatisfactory. In 3 of these 7 mortars the solids had a decided tendency to separate from the liquid, requiring almost constant agitation of the suspension during the process of dipping the brick. In two cases (*H*–1, *L*–1) the water retention was poor, as indicated by too rapid drying of the mortars. Mortar *X*–1, however, was of the opposite type, drying so slowly that it oozed almost completely from the joints of brick piers. This particular mortar could not be classed as smooth-working, since, starting with a troweling consistency, the process of mixing for one-half hour and screening to break up the lumps failed to produce a satisfactory slip consistency.

(i) TRANSVERSE STRENGTH AND LINEAR SHRINKAGE

In table 2 are given the transverse strengths of the neat-mortar bars, previously heated at various temperatures and cooled. In each case three values are given: (1) the average for not less than five bars broken with the surface that was originally at the bottom in compression (the "inverted" position); (2) a similar average for bars with the surface that was originally at the bottom in tension (the "original" position); and (3) the average for both positions. With comparatively few exceptions, the strength was significantly greater when the bars were broken in the "original" position. This difference in strength may be related to the differences in concentration of the alkali salts near the two surfaces.[10]

[10] *Properties of air-setting refractory bonding mortars of the wet type*, J. Research NBS **23**, 7 (1939) RP1219.

The strength of the mortar bars (average for the two positions) after drying at 105° C. ranged from 250 to 4,990 lb/in². The mortars that were received in burlap sacks and stored in the laboratory for an appreciable period of time (table 1, column 2) showed much lower dry strengths, as a group, than those stored in sealed metal drums.[11]

TABLE 2.—*Transverse strength of neat mortar bars and two-half-brick-and-mortar assemblages, and length changes of mortars*

Mortar	Transverse strength,[1] neat-mortar bars after heating at ° C				Transverse strength, two-half-brick-and-mortar assemblage, after heating at ° C, and manner of failure[2]					Length changes[3] after heating at—		
	105	750	1,000	1,350	105	750	1,000	1,350	1,500	105° C	750° C	1,350° C
	*lb/in.*²	*lb/in.*²	*lb/in.*²	*lb/in.*²	*lb/in.*²	*lb/in.*²	*lb/in.*²	*lb/in.*²	*lb/in.*²	%	%	%
A-3	280	540	1, 320	1, 715	45	45	30	260	390	3.0	+0.2	+5.5
	785	745	2, 080	1, 700	M	M	M	B & M	M			
	560	645	1, 700	1, 705								
A-4	2, 170	1, 120	3, 035	3, 575	55	0	0	80	415	4.9	+.2	+1.4
	2, 040	1, 000	2, 610	2, 805	J	J	J	J	J & M			
	2, 105	1, 060	2, 825	3, 190								
B-1	1, 500	1, 445	2, 350	3, 110	425	380	320	365	----------	3.4	+.1	2.2
	1, 950	1, 785	2, 350	3, 510	B	B & J	B	B & M	----------			
	1, 725	1, 615	2, 350	3, 310								
D-1	1, 035	1, 570	2, 450	[4] 1, 450	350	300	185	465	----------	8.0	.5	-----
	1, 475	1, 740	2, 875	1, 655	B & M	B, M,& J	B & M	B	----------			
	1, 275	1, 655	2, 740	1, 555								
E-2	625	270	270	720	160	35	0	105	----------	7.3	+1.2	2.0
	1, 050	295	260	750	M & J	M & J	J	M & J	----------			
	835	280	265	735								
F-1	930	520	820	860	355	145	230	335	----------	2.9	+0.6	1.9
	1, 415	940	1, 250	785	B	M	M	B & M	----------			
	1, 195	730	1, 035	820								
F-2	530	530	380	1, 030	205	25	0	0	175	2.0	+.6	+3.5
	1, 060	745	875	1, 900	M	M & J	M & J	M & J	M			
	795	635	625	[5] 1, 405								
G-1	315	230	680	1, 700	80	20	20	70	760	5.7	+.5	2.1
	585	355	800	2, 135	M & J	M & J	M & J	M & J	B			
	450	295	740	1, 920								
H-1	400	760	1, 725	2, 050	45	20	0	30	----------	5.5	.3	3.1
	620	750	1, 420	1, 565	M & J	J	J	J	----------			
	510	755	1, 575	1, 805								
I-1	405	1, 115	920	2, 690	110	40	0	75	355	2.6	.3	0.5
	390	915	785	2, 560	J	J	J	J	M			
	400	1, 015	850	2, 625								
L-1	600	325	430	1, 360	180	55	0	125	----------	2.6	+.3	1.8
	870	365	575	1, 155	J & M	M & J	M	M & J	----------			
	750	345	500	1, 260								
M-1	2, 610	2, 610	2, 910	5, 730	480	355	230	410	500	4.5	+.8	2.3
	3, 830	2, 700	3, 380	7, 540	B, M, &J	B, M, & J	B & J	B, J, & M	B, M, & J			
	3, 220	2, 650	3, 145	[6] 6,635								
O-2	5, 255	1, 855	2, 195	5, 940	240	100	110	350	----------	7.0	1.2	5.5
	4, 775	3, 510	4, 435	4, 740	J	J	J	B, J, & M	----------			
	4, 990	2, 685	3, 315	5, 275								
R-2	675	700	990	1, 100	120	35	150	255	----------	6.2	0.2	1.3
	900	780	1, 075	1, 020	M	M & J	M & J	M & J	----------			
	[5] 785	740	1, 030	1, 060								
W-1	210	530	1, 040	2, 040	[5] 35	15	0	60	----------	3.8	.3	3.3
	290	575	1, 185	1, 720	J & M	J	----------	J & M	----------			
	250	555	1, 115	1, 880								

See footnotes at end of table.

[11] *Effect of water content and mixing time on properties of air-setting refractory mortars containing sodium silicate*, Bul. Am. Ceram. Soc. **19**, 430 (1940).

TABLE 2. (Continued)—*Transverse strength of neat mortar bars and two-half-brick-and-mortar assemblages, and length changes of mortars*

Mortar	Transverse strength, neat-mortar bars after heating at ° C				Transverse strength, two-half-brick-and-mortar assemblage, after heating at ° C, and manner of failure					Length changes after heating at—		
	105	750	1,000	1,350	105	750	1,000	1,350	1,500	105° C	750° C	1,350° C
	lb/in.[2]	*lb/in.*[2]	*lb/in.*[2]	*lb/in.*[2]	*lb/in.*[2]	*lb/in.*[2]	*lb/in.*[2]	*lb/in.*[2]	*lb/in.*[2]	%	%	%
X-1	710	500	1,460	3,485	290	30	95	420	.....	4.4	.2	6.1
	1,180	555	1,425	2,970	M	J & M	M & J	B & M	.....			
	950	525	1,440	3,330								
Z-1	1,965	1,900	2,310	2,805	380	205	320	305	.....	5.0	.4	2.6
	2,700	1,850	2,275	2,320	B, J, & M	B, J, & M	B, M, & J	B, M, & J	.....			
	[4] 2,335	1,880	2,295	2,560								

[1] The 3 values for each mortar at the various temperatures represent, in the order given, the average of: (1) 5 specimens broken with the surface that was originally at the bottom during drying, in compression; (2) 5 specimens with the surface that was originally on the bottom, in tension; (3) all specimens.

[2] B, J, and M indicate failure occurred in brick, joint, or mortar, respectively.

[3] Except the values for 105° C, which represent the drying shrinkage, the length changes given represent changes between the dry length and the length after heating. "+" indicates expansion. Measurements made of bar specimens of neat mortars. For water content, see column 11 of table 1.

[4] Overfired.

[5] Average of 7 specimens broken over a 3-in. span.

[6] Average of 5 specimens.

The majority of the mortars were weaker after heating at 750° C than when dried at 150° C. The air-setting strength was generally equalled or exceeded, however, by heating at 1,000° and 1,350° C. In this respect the trend of strength-temperature relations (see footnote 10) is similar to that found in previous tests on air-setting refractory mortars of the wet type. The following is a grouping of the 17 mortars, of the dry type, according to strength changes resulting from heat treatment at three temperatures, compared with the dry strength: (1) Eleven had lower strength at 750° and higher strength at 1,000° and 1,350° C; (2) Four had increased strength with increased temperature; and (3) two had lower strength with increased temperature.

The ranges of the coefficient of variation in transverse strength of the neat-mortar bars preheated at the several temperatures are as follows: (1) 0.7 to 21.1 percent (⅝ of them below 10 percent) at 105° C, (2) 3.2 to 19.8 percent (⅝ of them below 10 percent) at 750° C, (3) 1.7 to 37.3 percent (⅜ of them below 10 percent) at 1,000° C, (4) 1.0 to 34 percent (¾ of them below 10 percent) at 1,350° C.

Values for the changes in length of the mortar bars preheated at 105°, 750°, and 1,350° C are given in table 2, each value being the average length change of three bars. The shrinkages of the mortar bars dried overnight at approximately 105° C ranged from 2.0 to 8.0 percent. Preheating at 750° C resulted in little additional shrinkage, eight mortars in fact showing a slight expansion. After heating at 1,350° C, all but four mortars (*A*–3, *A*–4, *F*–2, and *D*–1, which were badly warped) showed shrinkages ranging from 0.5 to 6.1 percent. It is rather significant that all of the mortars, except *A*–4, having a drying shrinkage greater than 5 percent cracked moderately or badly, whereas those, except *W*–1, having 5 percent or less showed either no cracks or barely perceptible ones (see column 18, table 1) when the mechanical troweling and drying were completed.

2. ASSEMBLAGE OF TWO HALF-BRICK AND MORTAR

(a) SETTING TIME OF MORTAR, OR WATER-RETENTION TEST

The time required for the mortars, placed between firebrick, to air-set, or stop flowing under load, ranged from 1 to 30 minutes (table 1, column 12); seven, however, set in 3 minutes or less.

Because this test, that is, time of set, or water-retention test, may be made without special equipment, it would be preferable to a mechanical-troweling test, provided it gave the desired information regarding workability. However, some of the mortars which would be rated as satisfactory on the basis of the setting time (*F*–2, *I*–1, and *X*–1) were unsatisfactory as far as workability was concerned, as indicated by the mechanical trowel. It appears, therefore, that the time of set is not a satisfactory criterion of workability. Furthermore, the mechanical-troweling test is the more inclusive workability test, since it not only gives information on the water retentiveness of a mortar but also gives information as to its troweling properties, such as ease of spreading and smoothness. Thus there is a lapse of 3½ minutes between the time a ¼-in. layer of mortar is placed on the face of a brick and the reduction of this layer to $\frac{1}{16}$ in. in 37 strokes of the trowel. If the mortar sets too quickly, it will not give good results in the troweling test, as was indicated by mortars *A*–3 and *L*–1. Therefore, since the time-of-set, or water-retention, test failed to differentiate between mortars of good and poor workability in 3 of the 17 mortars tested, the value of such a test in a specification is questionable.

(b) TRANSVERSE STRENGTH

The results of the transverse-strength tests made on assemblages of the two half-brick and mortar, preheated simultaneously with the mortar bars, are given in table 2. The strengths of the assemblages after drying at 105° C ranged from 35 to 480 lb/in.^{2}, eight of the values being not less than 200 lb/in.^{2}. The assemblages containing 11 of the 17 mortars had the least strength after the 1,000° C heat treatment. This is in contrast to the strengths of the neat-mortar bars, whose lowest values were found, in general, after the 750° C heat treatment. Furthermore, after the 1,000° C heat treatment, seven mortars had no apparent bonding strength—that is, the specimens failed during handling. This is in sharp contrast to the strengths of the air-setting mortars of the wet type,[12] where none was without some bonding strength and only two had strengths less than 100 lb/in.^{2} after a similar heat treatment.

The strengths of assemblages bonded with six different mortars were obtained after heating at 1,500° C for 1 hour. The values showed great increases in strength in comparison with those obtained after heating at 1,350° C, as given in table 2.

The ranges of the coefficient of variation in strength of the assemblages previously heated at the several temperatures are as follows: (1) 105° C, 8.3 to 73 percent; (2) 750° C, 18 to 79 percent; (3) 1,000° C, 35 to 65 percent, and (4) 1,350° C, 8.3 to 64 percent. In general the high coefficients of variation are associated with low mean values.

A direct relation was indicated between the dry strengths (105° C) of the neat-mortar bars and those of the assemblages, except in two cases (*A*–4 and *O*–2), where failures occurred in the joint or at the mortar-

[12] *Properties of air-setting refractory-bonding mortars of the wet type*, J. Research NBS **23**, 7 (1939) RP1219.

brick interface. Because of these exceptions, it would appear desirable to state a strength requirement for the assemblage in a specification.

(c) TYPES OF FAILURE

In testing the cross-breaking strength of the assemblages, the four following types of failure were observed. The fracture occurred (1) in the brick, (2) at the mortar-brick interface, (3) in the mortar, (4) some combination of (1), (2), and (3). In table 2 these types of failure are respectively indicated B, J, M and the proper combination of B, J, and M.

(d) RELATION OF WATER CONTENT TO SETTING TIME AND TO FLOW

Small changes in the water content of an air-setting refractory mortar may greatly alter some of its properties, such as time of set

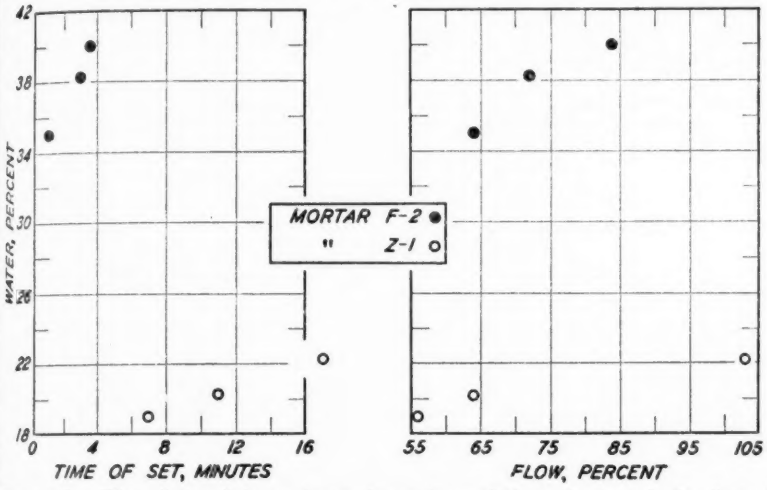

FIGURE 2.—*The relation between tempering-water and time of set, and also flow of mortars F–2 and Z–1.*

and flow (consistency). Mortars are differently affected by a uniform change in their water content.

Two mortars, *F*–2 and *Z*–1, containing 40.1 and 20.1 percent of water, respectively (see table 1, column 15), were used in investigating these relations. Figure 2, showing the effect of small changes in tempering-water on the time of set and on the flow of these mortars, indicates that *Z*–1 is more sensitive than *F*–2 to such changes. A 3.2-percent increase in the water content of *Z*–1 increased the time of set 10 minutes (7 to 17 minutes) and the flow 50 percent (56 to 106 percent), whereas a 5-percent increase in the water content of *F*–2 increased the setting time slightly more than 2 minutes (1 to +3 minutes) and the flow only 20 percent (64 to 84 percent).

The information thus obtained indicates that attempts to place any limitations on the technical requirements, such as the time of set and its influence on other properties, should not be made without giving some consideration to the factor of the sensitivity of mortars to changes in water content.

(e) EFFECT OF ATMOSPHERE DURING HEATING ON STRENGTH

The results of the transverse-strength tests, reported in table 2, were obtained from mortar specimens heated in an oxidizing atmos-

phere. Additional tests were required to determine the effect of a reducing atmosphere.

Three mortars (*I*–1, *M*–1, *O*–2) having a chromite base and three (*B*–1, *F*–1, *X*–1) having a fire-clay base were used for this purpose. The test specimens, consisting of mortar bars and assemblages (two half-brick and mortar), were heated at 1,350° C in a strongly reducing atmosphere, which was mechanically controlled.[13]

The results of the transverse-strength tests are given in table 3. For comparison, data (table 2, columns 5 and 9) obtained on similar test specimens heated at 1,350 °C in an oxidizing atmosphere are included.

These results indicate that the heating at 1,350° C in a reducing atmosphere had no significant effect on the strength of the mortars containing large percentages of chromite; but the fire-clay mortars, with one exception (*F*–1, bonded brick), showed decreases in strength up to 50 percent.

TABLE 3.—*Strengths of neat-mortar bars and of assemblages (two half-brick and mortar) after heating at 1,350° C in oxidizing or reducing atmosphere*

Mortar and type	Atmosphere			
	Oxidizing		Reducing	
	Neat-mortar bars	Assemblages	Neat-mortar bars [1]	Assemblages [1]
	*lb/in.*²	*lb/in.*²	*lb/in.*²	*lb/in.*²
B–1, fire clay	3,310	365	1,620	245
F–1, fire clay	820	335	485	340
I–1, chrome	2,625	75	2,950	73
M–1, chrome	[2] 5,670	410	5,800	295
O–2, chrome	5,275	350		385
X–1, fire clay	3,330	420	2,320	325

[1] Average of 8 specimens.
[2] Average of 5 specimens.
[3] Represents average of a different lot of specimens from that given in table 2.

3. PIER OF THREE BRICK AND MORTAR

The results of the visual examination of the mortars used in the piers are given in table 4.

The quality of the mortars, as indicated by cracking, already was evident after air-drying. Four of the mortars (*D*–1, *G*–1, *H*–1, *O*–2) in the group having the greatest drying shrinkage cracked badly in the ⅛-in. joints, but, with the exception of *D*–1, showed no serious cracking in the 1/16-in. joints. On the other hand, mortar *R*–2, in the same shrinkage group, had cracked badly in the 1/16-in. joint only.

Observations on the adherence of mortar to brick showed that the nonadherent areas of the mortar caps amounted to 25 to 50 percent for six mortars and an estimated 5 to 10 percent for four others after drying at 105° C. No improvement in the percentage of adherence resulted after heating at the higher temperatures. In fact, the tendency for more of the cap to become loosened was increased. Apparently the lack of adherence of the mortar caps was no indication that low strengths (table 2, *B*–1, *D*–1) of the piers would necessarily follow except (*A*–4 and *O*–2) where low strength was caused by failure at the mortar-brick interface.

[13] By means of a CO_2 meter.

TABLE 4.—*Appearance of mortar in fusion block, cap, and in joints of three-brick-and-mortar assemblag*

Mortar	Appearance [1] of mortar after drying			Appearance [1] of mortar after heating 24 hours at 750° C			Appearance [1] of mortar after heating 1 hour at 1,350° C			Appearance [1] of mortar after at 1,500° C	
	In joint		As cap, ⅛"	In joint		As cap, ⅛"	In joint		As cap, ⅛"	In joint, ⅛"	A
	1/16"	⅛"		1/16"	⅛"		1/16"	⅛"			
A-3	Good	Good	Very good	‖ cracks	‖ and ⊥ cracks	Good	⊥ cracks	‖ cracks	Good	‖ cracks	Good
A-4	⊥ and ‖ cracks	‖ cracks	25% not bonded	⊥ cracks	do	25% not bonded	⊥ and ‖ cracks	⊥ and ‖ cracks	50% not bonded	Bad ⊥ and ‖ cracks	Slight not
B-1	do	⊥ and ‖ cracks	Moderately cracked. 10% not bonded.	Good	do	Moderately cracked. 25% not bonded.	do	do	Moderately cracked. 25% not bonded.	⊥ crack	Badly
D-1	Bad ⊥ and ‖ cracks	Bad ⊥ cracks	Badly cracked. 50% not bonded.	Bad ⊥ cracks	Bad ⊥ and ‖ cracks	Badly cracked. 75% not bonded.	Bad ⊥ and ‖ cracks	Bad ⊥ and ‖ cracks	Badly cracked. 50% not bonded. Glassy.	Bad ⊥ cracks	Badly shri
E-2	⊥ and ‖ cracks	Moderate ⊥ and ‖ cracks.	Slightly cracked. 10% not bonded.	⊥ and ‖ cracks	‖ cracks	Slightly cracked. 50% not bonded.	⊥ and ‖ cracks	⊥ and ‖ cracks	Moderately cracked. 75% not bonded.	Fused and flowed from joint.	Fused age
F-1	Good	Good	Very good	Good	Good	Very good	‖ cracks. Glassy	‖ cracks. Glassy	Slightly cracked. 5% not bonded.	do	Fused
F-2	do	do	Good		‖ cracks	do	⊥ and ‖ cracks	⊥ and ‖ cracks	No cracks. 100% not bonded.	⊥ and ‖ cracks. Glassy.	100%
G-1	⊥ and ‖ cracks	Bad ⊥ and slight ‖ cracks.	Good. 5% not bonded.	⊥ and ‖ cracks	⊥ and ‖ cracks	Slightly cracked	Bad ⊥ and ‖ cracks	Bad ⊥ and ‖ cracks	Slightly cracked	Bad ⊥ and slight ‖ cracks.	Mode
H-1	do	Bad ⊥ and ‖ cracks	Badly cracked. 10% not bonded.	do	do	Badly cracked	Glassy. Bulged	Glassy. Bulged	Badly cracked. 15% not bonded.	Glassy. Bulged	Badly not
I-1	Good	Good	Very good	Good	Good	Good	⊥ and ‖ cracks	Bad ⊥ and ‖ cracks	Slightly cracked	Slightly glassy	Mod
L-1	do	do	do	do	do	Very good	Good	Good	Very good	Good	Very
M-1	do	do	do	do	do	do	Moderate ⊥ and ‖ cracks.	⊥ and ‖ cracks	Slightly cracked	Moderate ⊥ cracks. Slightly glassy.	Sligh
O-2	Moderate ⊥ and ‖ cracks.	Bad ⊥ and ‖ cracks	Moderately cracked. 25% not bonded.	Bad ⊥ and ‖ cracks.	Bad ⊥ and ‖ cracks	Badly cracked. 50% not bonded.	Bad ⊥ and ‖ cracks	Bad ⊥ and ‖ cracks	Badly cracked. 50% not bonded.	⊥ and ‖ cracks	Badl
R-2	Bad ⊥ and ‖ cracks	Moderate ⊥ and ‖ cracks.	Cracked and warped. 35% not bonded.	do	Moderate ⊥ and ‖ cracks.	Cracked and warped. 65% not bonded.	⊥ and ‖ cracks	Moderate ⊥ and ‖ cracks.	50% curled and not bonded.	Moderate ⊥ and ‖ cracks.	Badl no
W-1	⊥ cracks	do	Badly cracked. 50% not bonded.	do	Bad ⊥ and ‖ cracks	Moderately cracked. 30% not bonded.	Bad ⊥ and ‖ cracks	do	Badly cracked. 30% not bonded.	Bad ⊥ cracks	Badl no
X-1	do	Moderate ⊥ cracks	Good	⊥ and ‖ cracks	Moderate ⊥ and ‖ cracks.	Good	⊥ and ‖ cracks	⊥ and ‖ cracks	Moderately cracked	Bad ⊥ and ‖ cracks	Badl
Y-1	do	⊥ cracks	Moderately cracked. 50% not bonded.	‖ cracks	Bad ⊥ cracks	Badly cracked and and warped. 50% not bonded.	‖ cracks	Bad ⊥ cracks	⊥ and ‖ thermal cracks.	Good	Goo

[1] Cracks occurring in horizontal joint are labeled "‖", those in the vertical joint "⊥".
[2] Fusion blocks heated simultaneously with brick-and-mortar assemblages. No reference to "adherence" indicates that bonding had taken place between mortar and fusion block.

joints of three-brick-and-mortar assemblages or piers

ur at 1,350° C	Appearance [1] of mortar after heating 1 hour at 1,500° C		Condition [2] of mortar in fusion block after heating at—			
As cap, ⅛"	In joint, ⅛"	As cap, ⅛"	105° C	750° C	1,350° C	1,500° C
ood	‖ cracks	Good	Good	Good	Good. Slight expansion	Good. Slight expansion.
% not bonded	Bad ⊥ and ‖ cracks	Slightly cracked. 50% not bonded.	Good. No adherence	Good. No adherence	Good. No adherence	Good. No adherence.
oderately cracked. 25% not bonded.	⊥ crack	Badly cracked	Badly cracked	Badly cracked	Badly cracked	Badly cracked.
adly cracked. 50% not bonded. Glassy.	Bad ⊥ cracks	Badly cracked. High shrinkage.	do	Badly cracked	Badly cracked. High shrinkage.	Badly cracked. High shrinkage.
oderately cracked. 75% not bonded.	Fused and flowed from joint.	Fused. High shrinkage.	No adherence. Moderate shrinkage.	No adherence. Moderate shrinkage.	No adherence. High shrinkage.	Fused and flowed slightly.
ightly cracked. 5% not bonded.	do	Fused	Good. Slightly cracked.	Moderately cracked	Moderate shrinkage. Glassy	Fused and flowed slightly. Moderate shrinkage.
o cracks. 100% not bonded.	⊥ and ‖ cracks. Glassy.	100% not bonded	Good	Good	Good. No adherence	Good. Glassy.
ightly cracked	Bad ⊥ and slight ‖ cracks.	Moderately cracked	High shrinkage. No adherence.	Moderate shrinkage. No adherence.	High shrinkage. No adherence.	High shrinkage. No adherence.
adly cracked. 15% not bonded.	Glassy. Bulged	Badly cracked. 15% not bonded.	High shrinkage. No adherence.	High shrinkage. No adherence.	do	Do.
ightly cracked	Slightly glassy	Moderately cracked	Good. No adherence	Moderate shrinkage. No adherence.	Moderate shrinkage. No adherence.	High shrinkage. No adherence.
ery good	Good	Very good	do	Good	Good	Good.
ightly cracked	Moderate ⊥ cracks. Slightly glassy.	Slightly cracked	do	do	Moderate shrinkage	Moderate shrinkage.
adly cracked. 50% not bonded.	⊥ and ‖ cracks	Badly cracked	Badly cracked	Badly cracked. No adherence.	Badly cracked. Bloated on surface. High shrinkage.	Badly cracked and fused.
% curled and not bonded.	Moderate ⊥ and ‖ cracks.	Badly cracked. 25% not bonded.	Moderate shrinkage. No adherence.	Moderate shrinkage. No adherence.	High shrinkage. No adherence.	High shrinkage. No adherence.
adly cracked. 30% not bonded.	Bad ⊥ cracks	Badly cracked. 25% not bonded.	No adherence. High shrinkage.	Cracked. No adherence.	High shrinkage. No adherence.	High shrinkage. No adherence.
oderately cracked	Bad ⊥ and ‖ cracks	Badly cracked	Good	Slightly cracked	High shrinkage	High shrinkage. Glassy.
and ‖ thermal cracks.	Good	Good	do	Good	Moderate shrinkage	Moderate shrinkage.

UNIV OF MICH

After heating the piers at 1,500° C, the mortars having low pyrometric-cone equivalents (*E*–2, *F*–1, *F*–2, *G*–1, and *X*–1) indicated their lack of refractoriness by becoming glassy. In addition, several mortars (*I*–1, *M*–1, *O*–2) of highest refractoriness also showed signs of fusion, apparently because of the migration of salts to the surface.

As stated in section IV–e, the conclusions drawn from the appearance of the mortar after heating in the fusion blocks (table 4) correlate well with those drawn from an examination of the piers; that is, much pertinent information relative to the quality of the mortar may be obtained from the former test.

V. SUMMARY AND CONCLUSIONS

Seventeen air-setting refractory mortars (four of which had a chromite base) marketed in the dry condition and furnished by 12 manufacturers were subjected to a series of tests. Different amounts of water were added to the mortars to obtain consistencies suitable for preparing specimens of the neat mortar and for use in bonding brick by troweling and dipping methods.

Six of the mortars were furnished in metal drums and the remainder in paper-lined jute sacks. They remained in storage from 1 week to 49 months before being tested.

The water required for bringing the mortars to a troweling consistency ranged from 16.6 to 43 percent, and that required for a dipping consistency ranged from 20.7 to 60.1 percent. The ease of troweling on brick, determined mechanically, was considered satisfactory for all but five of the mortars. The workability of seven of the mortars was considered unsatisfactory when of a dipping consistency. The percentage flow (consistency), as determined with a flow table, ranged from 24 to 110, with 12 of the mortars ranging between 62 and 86. After slaking in water 1 hour, 16 of the 17 mortars showed less than 4 percent retained on a No. 40 United States Standard Sieve, and in no case was the residue on a No. 20 sieve greater than 0.5 percent. The free-alkali content, expressed as sodium oxide, ranged from 0 to 1.90 percent. The pyrometric-cone equivalents of the mortars ranged from 20 to above 38, with very little difference between the end points of calcined and uncalcined materials. Eight of the mortars, mechanically troweled on brick and dried, cracked seriously. The time required for the mortars to air-set (indication of water retention), indicated by their resistance to flow under load, ranged from 1 to 30 minutes when used to bond firebrick of 8.6-percent absorption.

The average transverse dry strengths of the air-set neat mortars ranged from 250 to 4,990 lb/in^2. With three exceptions, the strength of the test specimens was considerably greater when the surface uppermost during drying was in tension in the breaking test. Eleven of the mortars showed lower strengths after heating at 750° C than after heating at 1,000° or 1,350° C. four being weakest after air-drying and two strongest.

The bonding strength of the dried mortars in assemblages of two half-brick and mortar ranged from 45 to 480 lb/in^2.

Brick specimens bonded with 11 of the 17 mortars were weaker after heating at 1,000° C than after drying or heating at 750° C. Furthermore, seven of the mortars preheated at 1,000° C had prac-

446682—42——2

tically no bonding strength. In these tests, failure of the assembly occurred either in the brick, in the mortar, in the joint, or in some combination of these.

Piers of two standard-size brick and two half-brick (making two horizontal and one vertical joint) were made up with ⅛-in. and 1/16-in. joints. The mortar joints of piers for five of these mortars, all of which had high drying shrinkages, were badly cracked after drying. Also, as a result of the heating at 1,500° C, eight of the mortars had either become fluid enough to bulge from the joints or had cracked.

Some of the mortars shipped and stored in sacks, rather than in airtight containers, would undoubtedly have had better strength and bonding properties if they had been tested soon after manufacture.

The mechanical-troweling test is a much better measure of the workability of a mortar than is the water-retention or time-of-set test.

The failure of a cap of mortar to adhere to brick was no indication of its bonding properties.

Much pertinent information relative to the quality of a mortar may be obtained from the fusion-block test.

The technical requirements in a Federal specification for this commodity will be based on the results of tests made in this investigation. The requirements for such a specification will probably cover fineness, bonding strength, refractoriness, and workability. If the limits for these properties are so chosen as to insure a product of the proper quality, then from the results of this investigation it may be concluded that because so few will fall within those limits, airsetting mortars of the dry type as a class may possibly be greatly improved.

WASHINGTON, January 16, 1942.

U. S. DEPARTMENT OF COMMERCE NATIONAL BUREAU OF STANDARDS

RESEARCH PAPER RP1462

Part of Journal of Research of the National Bureau of Standards, Volume 28, April 1942

CREEP RATES OF COLD-DRAWN NICKEL-COPPER ALLOY (MONEL METAL)

By John A. Bennett and Dunlap J. McAdam, Jr.

ABSTRACT

A description is given of new equipment recently assembled at this Bureau for testing the creep of metals.

The apparatus was used to study the creep rate of cold-drawn nickel-copper alloy over a wide range of stress and temperature. Each specimen was used for a series of tests, which allowed a more rapid determination of the characteristic creep rates than using a single specimen for each test. The data indicate that the characteristic creep rate depends only on the stress and temperature, and is not affected by prior stresses or temperatures. The influence of stress on the rate of creep increases with increasing stress, while the influence of temperature on the rate of creep decreases with increasing temperature. The results of the tests are shown in graphs, as no mathematical expression was found which would represent them.

CONTENTS

	Page
I. Introduction	417
II. Apparatus	418
1. Specimen and methods of loading	418
2. Furnaces and temperature control	419
3. Measurement of extension	421
III. Time-extension data for the nickel-copper alloy	423
1. Procedures and material	423
2. Results from specimens supporting different loads at the same temperature	424
3. Results from specimens supporting the same load at different temperatures	431
4. Supplemental tests	432
IV. The stress-temperature creep-rate relationship of nickel-copper alloy	434
V. Summary and conclusions	437
VI. References	437

I. INTRODUCTION

It is well known that if the temperature is sufficiently high, all metals will deform continuously under a constant stress. This time rate of change of deformation is called creep. About 20 years ago it began to be realized that the tensile strength as determined by a short-time test does not give reliable information on the ability of metals to withstand stress at elevated temperature and that such information can be obtained only by measuring the deformation of the material over long periods of time.

A considerable amount of the pioneer work on the creep of metals

was done by H. J. French and associates [1] [1] at this Bureau. Since then there has been great improvement in creep-testing equipment. For the present investigation at this Bureau, therefore, it was necessary to design new apparatus in accordance with present standards. This apparatus is described in the first part of this report.

In the temperature range where creep occurs, the instantaneous elastic extension is followed by plastic extension at a decreasing rate. If this plastic extension is plotted against time, the slope is found to approach a constant value whose magnitude depends on the stress and temperature. The period of decreasing creep rate is followed by a period of increasing rate, which leads to fracture. For comparatively low stresses and temperatures (such as those which would be encountered in service), the period of decreasing creep is so long that it is not practicable to run tests until the fracture period starts. This fact makes it difficult to define a creep rate which is characteristic of a certain stress-temperature combination. However, since the creep rate during much of the decreasing period is very nearly constant, it has been found possible to estimate a characteristic rate from the time-extension diagram after the initial rapid change in rate.

This paper gives results showing the influence of stress and temperature on this characteristic creep rate for a single material. A nickel-copper alloy was chosen in order that the results would not be complicated by allotropic transformations and by the presence of more than one phase.

II. APPARATUS

1. SPECIMEN AND METHODS OF LOADING

The new apparatus consists of 12 static tensile testing units each fitted with a furnace for maintaining the specimen at a uniform and

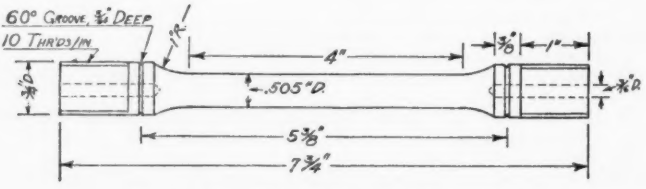

FIGURE 2.—*Standard creep-test specimen.*

constant temperature over long periods. Tensile creep tests were decided upon in preference to other types—such as bending, torsion, etc.—because of the uniformity of the stress distribution.

To conserve space, the loading framework was made as compact as possible by putting 12 units in 2 opposed, staggered rows, with the weights of 1 row hanging near the furnaces of the other. The whole framework, one side of which is shown in figure 1, rests on compression springs to reduce vibration. The standard specimen for use in the apparatus has a 4-in. gage length of 0.505-in. diameter (fig. 2). Universal joints are used above and below the specimen adapters to reduce nonaxial loading.

[1] Figures in brackets indicate the literature references at the end of this paper.

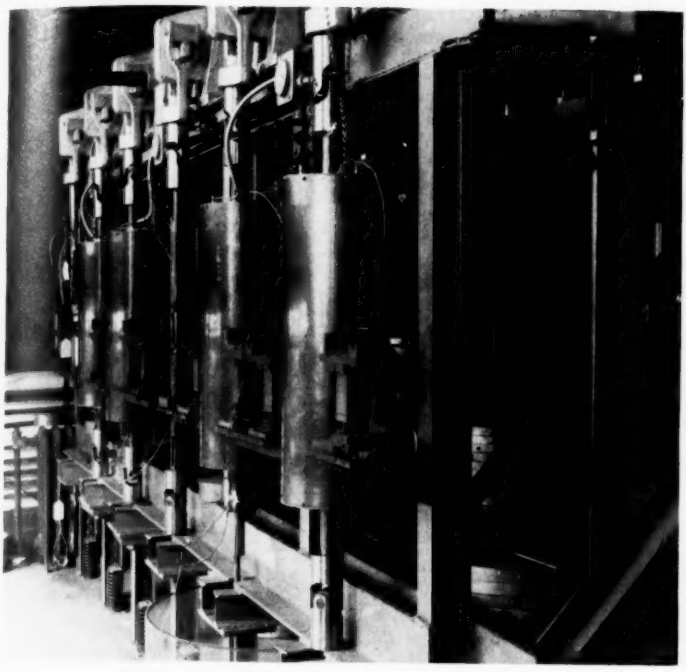

FIGURE 1.—*Creep-test apparatus.*

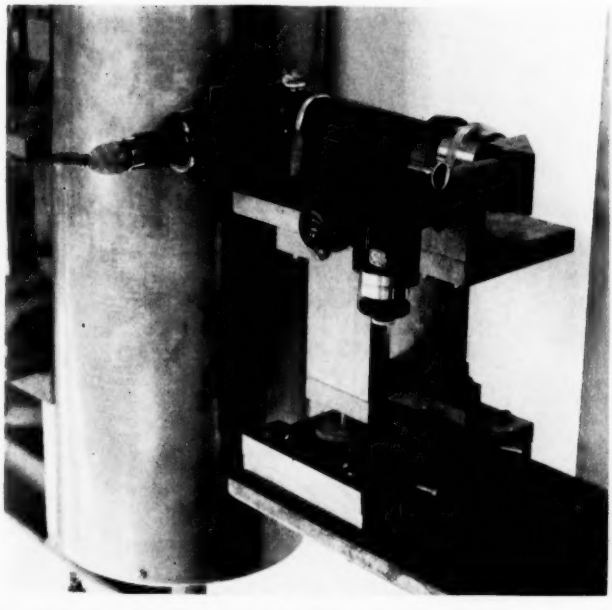

FIGURE 5.—*The extensometer microscope in place at a creep furnace.*

In order to maintain suitable accuracy in the application of low stresses without the necessity of using an excessive number of weights for applying large loads, three loading systems have been provided. For low stresses the weights are hung directly on the specimen, at *A* in figure 3. For intermediate stresses a single lever having a ratio of 9:1 is used with the weights loaded at *B*. In the highest range of stress, two levers having an over-all factor of 54:1 are used with weights hung at *C*. In this way stresses as low as 80 lb./in.^{2} and as high as 90,000 lb./in.^{2} can be applied easily and accurately.

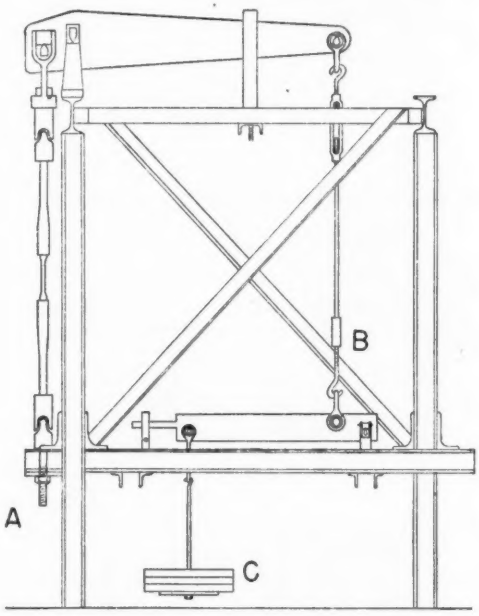

FIGURE 3.—*Methods of loading the specimen.*

1. Low stresses; weights are loaded at *A*. 2. Intermediate stresses; weights are loaded at *B*. 3. High stresses; weights are loaded at *C*.

2. FURNACES AND TEMPERATURE CONTROL

The furnaces are the conventional tube type, the over-all dimensions being 24 in. long by 7 in. in diameter. The Alundum inner tube has a 1½-in. bore, and the space between this tube and the outer brass shell is filled with Sil-O-Cel insulation. At the center of each furnace are two windows 180° apart for sighting on the gage bars. These windows consist of Alundum tubes, closed on the inside by a quartz disk set into the furnace tube, and on the outside by a Pyrex disk (fig. 4). The furnace winding is spaced to give, as nearly as possible, uniform temperature along the gage length, and four taps are provided for final temperature adjustment.

In each furnace there are three thermocouples, for controlling, recording, and checking the furnace temperature. All of the couples may be read with a stationary precision potentiometer by selecting the desired couple on multiple-point switches.

The location of the control couple is important. If it is outside

the winding, the furnace temperature varies with the room temperature. This variation can be eliminated by placing the bead of the couple inside the winding. This is done by drilling two holes in the

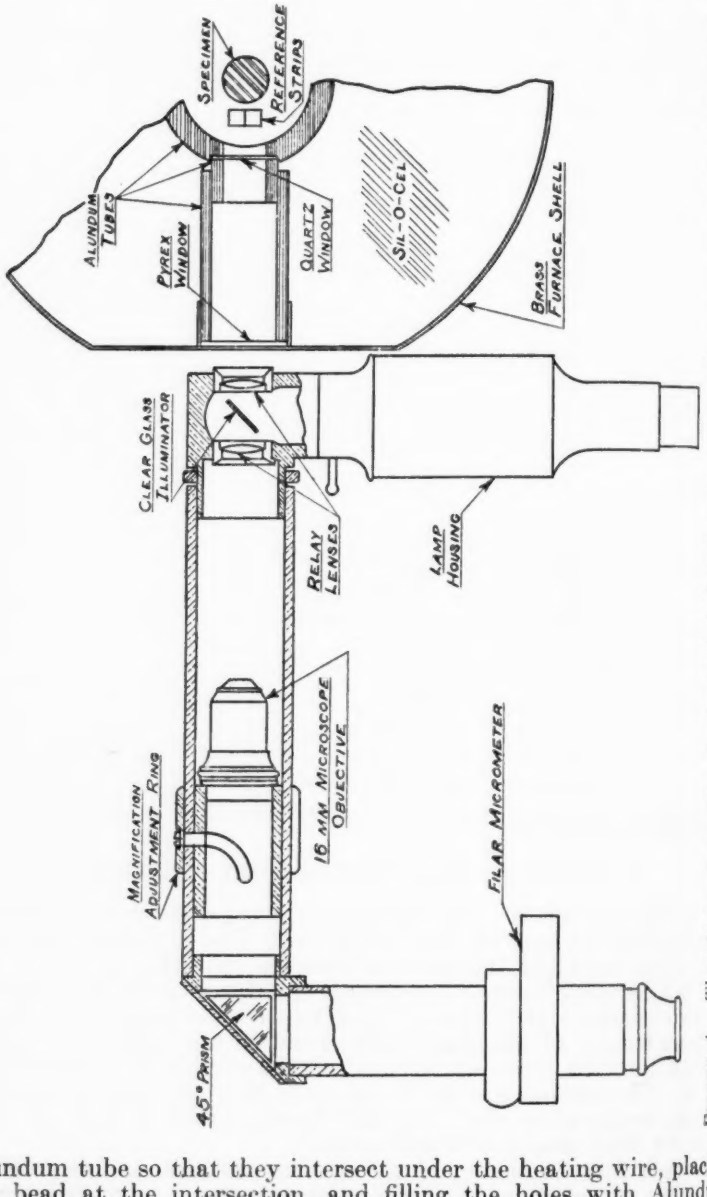

FIGURE 4.—*The extensometer system, showing method of constructing windows in furnace and details of microscope.*

Alundum tube so that they intersect under the heating wire, placing the bead at the intersection, and filling the holes with Alundum cement. The control couple for each furnace is connected to a photoelectric-type controller which changes the power input to the furnace by 25 or 30 percent between off and on. The cold junctions

of the control thermocouples are kept in constant-temperature boxes mounted on the framework. These boxes are controlled by a bimetal strip at a temperature somewhat higher than the maximum probable room temperature.

The recording and checking couples are placed in holes at each end of the specimens (fig. 2), and the lead wires are brought out through longitudinal holes in the adapters. The recording couple in the top shoulder of the specimen is connected to a six-point recording millivoltmeter, but this gives only a rough measure of the actual temperature and is supplemented every few days by reading the electromotive force of the third couple, which is in the bottom shoulder, with the cold junction in ice. Either of these couples may be removed for comparison against a standard without disturbing the test. With these precautions, the temperature at any one point on a specimen is held constant during a test within less than $\pm 2°$ F.

Before a test is started, the furnace is calibrated to give a uniform temperature along the gage length by placing suitable resistances in parallel with certain sections of the winding. The temperature distribution is determined on a dummy specimen of the same dimensions as the test specimen, but having five thermocouples placed 1 in. apart along the reduced section. Norton [2] stated that this method of calibration was unsatisfactory owing to the variation in heat conductivity across the threads to the adapter with different specimens and different loads. He recommends having thermocouples fastened along the gage length throughout the test. In the present investigation, one actual test specimen was set up in this way in order to see if it was necessary with the 24-in. furnaces. No significant difference in the temperature distribution along the specimen could be found, either between the dummy and the test specimen or for stresses from 10,000 to 65,000 lb/in ^{2}.

The variation of temperature along the gage length was not more than $\pm 5°$ F, and in most cases was considerably less. There was a section opposite the windows which was slightly cool in all of the furnaces, but the rest of the specimen was in all cases within $\pm 3.5°$ F.

Abrupt changes in the room temperature are eliminated by thermostatically controlled heating or ventilating, but no effort is made to maintain the same temperature winter and summer.

3. MEASUREMENT OF EXTENSION

The extensometer is of the optical type, with no parts extending out of the furnace (figs. 4 and 5). Extension is determined by measuring the distance between reference marks on two adjacent gage bars with a microscope. One end of each bar is fastened to a shoulder of the specimen, the other ends of the bars being held by a guide in such a way that they are free to slide along one another when the specimen is deformed. The gage bars are Nichrome, but the reference marks are made on platinum strips welded to these bars so that the marks remain well defined after long exposure to elevated temperatures. Each specimen is provided with two pairs of gage bars placed 180° apart.

The measuring microscope consists of a relay lens which forms a full-size image of the reference marks, followed by a 16-mm objective and 7.5× eyepiece which give a magnification of about 75 diameters. The magnification can be adjusted by means of a collar which moves the objective relative to the relay lens and eyepiece. In order to observe the two pairs of gage bars from the front of the frame, a right-angle prism was placed between the objective and eyepiece. Actual measuring is done with the filar micrometer. The extensometer microscope can be easily moved from one unit to another. All the focusing is done by moving the whole mounting, so once this is done properly, the extensometer is always in focus when set in the V-blocks which support it.

The relay lens has a diameter of 0.6 in. and a working distance of 3 in., giving a numerical aperture of 0.10 and a theoretical resolving

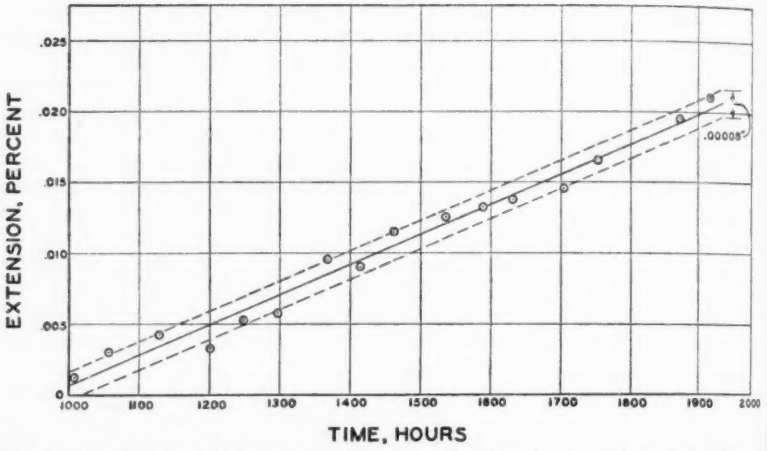

FIGURE 6.—*Portion of a typical creep curve, showing the precision of the observed extension values.*

power of about 4 microns for yellow light. This resolving power is sufficient so that by averaging two readings for each observation of the extension, the probable error of an observation is less than 1 micron (0.00004 in.), or 0.001 percent of the gage length. There are several other factors which may cause an error in the measurement of extension, such as variation in temperature of the specimen, change in the positioning of the microscope relative to the gage bars, inequalities in the pitch of the micrometer screw, etc. Figure 6 shows the deviations from a straight line of a series of observations on a typical creep test, and indicates that the combined influence of all the above-mentioned factors results in a precision of ±1 micron. The dashed lines in this figure are drawn a distance of 1 micron above and below the best average line through the points.

Several checks on the accuracy of the extensometer are provided. The magnification of the microscope is set at a value which gives a convenient conversion factor, and this setting is checked at intervals

by measurements on a stage micrometer. The total extension of the specimen as measured with the extensometer is checked by measuring, before and after testing, the distance between the grooves on the shoulders of the specimen. The extension as measured by the extensometer must be corrected for the deformation in the shoulder of the specimen. This correction is made from the uncorrected stress-rate relationship, assuming a uniform stress distribution throughout the cross section in the fillet (neglecting the part of the shoulder whose diameter is larger than the root of the groove). Measurements on the reduced section indicated that these assumptions and approximations give a sufficiently good approach to the true correction. Before a test is started, small platinum beads are welded at each end of the gage length, and the distance between reference marks made on these beads is measured before and after test. The average difference between the total plastic extension measured in this way and that obtained from the corrected extensometer readings is 1.5 percent for the specimens included in this report.

When the creep rate is high (above about 0.5 percent per 1,000 hours) and maximum precision is less important than the ease and rapidity with which readings can be made, the extensometer field is photographed with a 35-mm camera, and the extension measurements are made later by projecting the negatives in an enlarger. For very high rates of creep (5 percent per 1,000 hours or more), the movement of the end of the loading lever is measured with a dial gage, and the extension of the specimen is determined from these measurements by calibrating them with camera or micrometer observations.

III. TIME-EXTENSION DATA FOR THE NICKEL-COPPER ALLOY

1. PROCEDURES AND MATERIAL

When a metal is subjected to stress and elevated temperature, the various factors influencing its resistance to deformation gradually approach a condition of equilibrium as evidenced by the approach of the creep rate to a constant value. Since the metal actually undergoes alteration during this period, it is difficult to correlate the equilibrium rates for different stress-temperature combinations. In order to minimize the time required for this alteration of the metal, however, a single specimen was used for several different stress-temperature combinations. After each change of stress, the rate was determined shortly after the period of rapid change.

To obtain information concerning the effect of the alteration in structure of the metal, several different procedures were used in determining characteristic rates. In some cases the temperature was held constant and the rate determined for a series of progressively higher stresses (up-step procedure) or for progressively lower stresses (down-step procedure). Most of the results given in this report were obtained with one or the other of these procedures or a combination of the two. It was thus possible in many instances to obtain characteristic rates for certain stresses at different stages in the total plastic extension of a specimen. Another procedure was to

maintain the load constant and determine the characteristic rate at various temperatures.

The material from which specimens were made was ⅞-in. rod of nickel-copper alloy provided by the International Nickel Co. Since it was desired to run tests on both the annealed and cold-worked material, the stock was cold-drawn to a reduction of area of 40 percent, which was sufficient to give uniform hardness and microstructure throughout the cross section. All of the specimens came from the same heat. The composition of the monel metal used in the tests was as follows:

Element	Percentage
Ni	69. 02
Cu	28. 46
Si	0. 10
S	. 007
Fe	1. 24
Mn	0. 94
C	. 18

2. RESULTS FROM SPECIMENS SUPPORTING DIFFERENT LOADS AT THE SAME TEMPERATURE

Tests in which the temperature was held constant throughout a series were made at the following temperatures; 700, 800 (two series), 905, 1,000, 1,100, 1,225° F. The creep curves for six of these series are shown in figures 7 to 12, inclusive. As the test at 700° F is still in operation, this series is not shown in the figures. The points plotted are the experimental points, and have not been corrected for the extension of the fillet. Each figure shows the results obtained on a single specimen at a single temperature. The time scale was started from zero each time the load was changed, but the ordinates give the total extension of the specimen. The chronological order of the tests is given by the letter adjacent to each curve, while the stress is shown by the numbers above or below each curve. The asterisks near certain curves indicate that these curves were not used in determining the characteristic creep rate. Reasons for this distinction are discussed later.

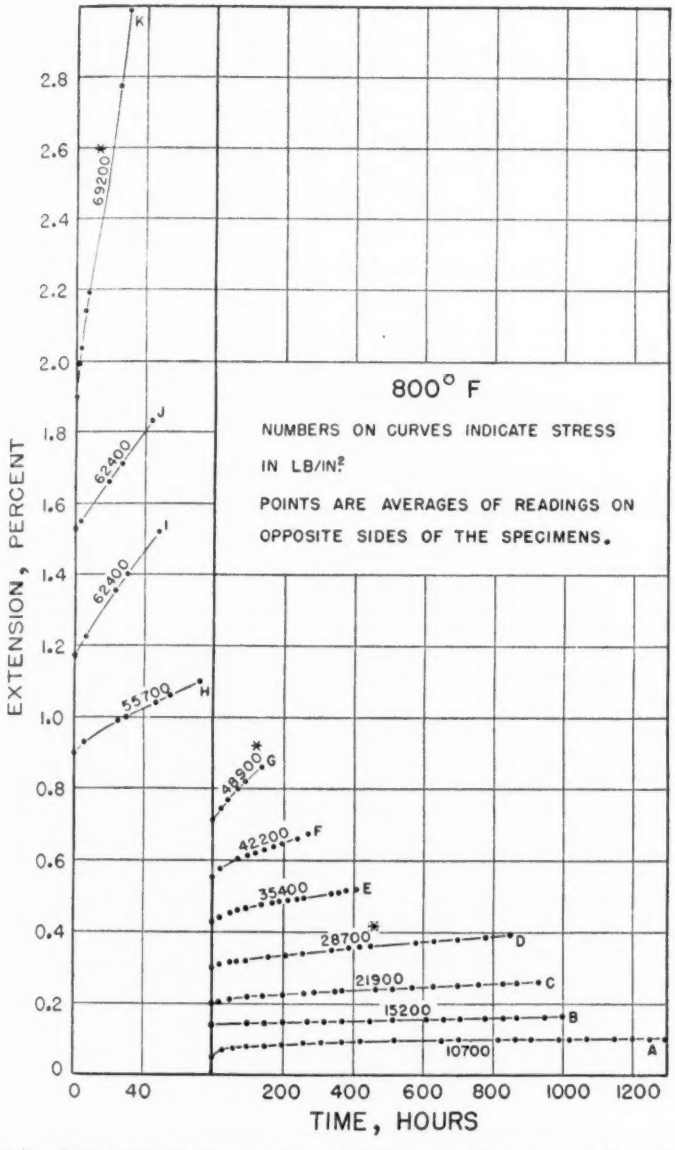

FIGURE 7.—*Time-extension curves for a specimen supporting various loads at 800 °F.*
The chronological order of the tests is indicated by the letters on the curves.

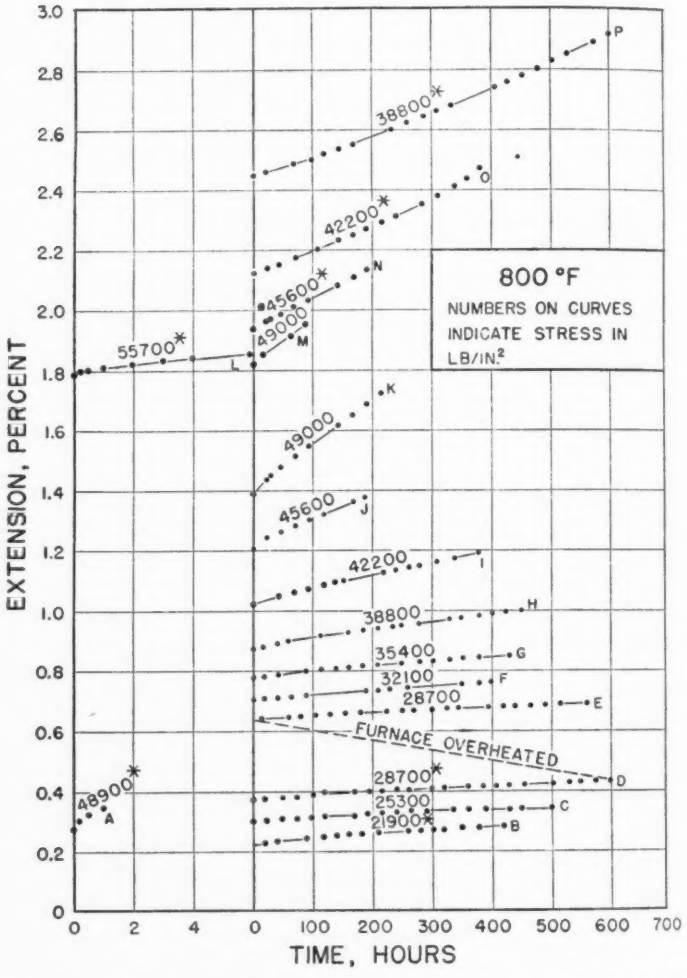

FIGURE 8.—*Time-extension curves for a specimen supporting various loads at 800° F.*

The chronological order of the tests is indicated by the letters on the curves. These tests were made on a different specimen from those shown in figure 7.

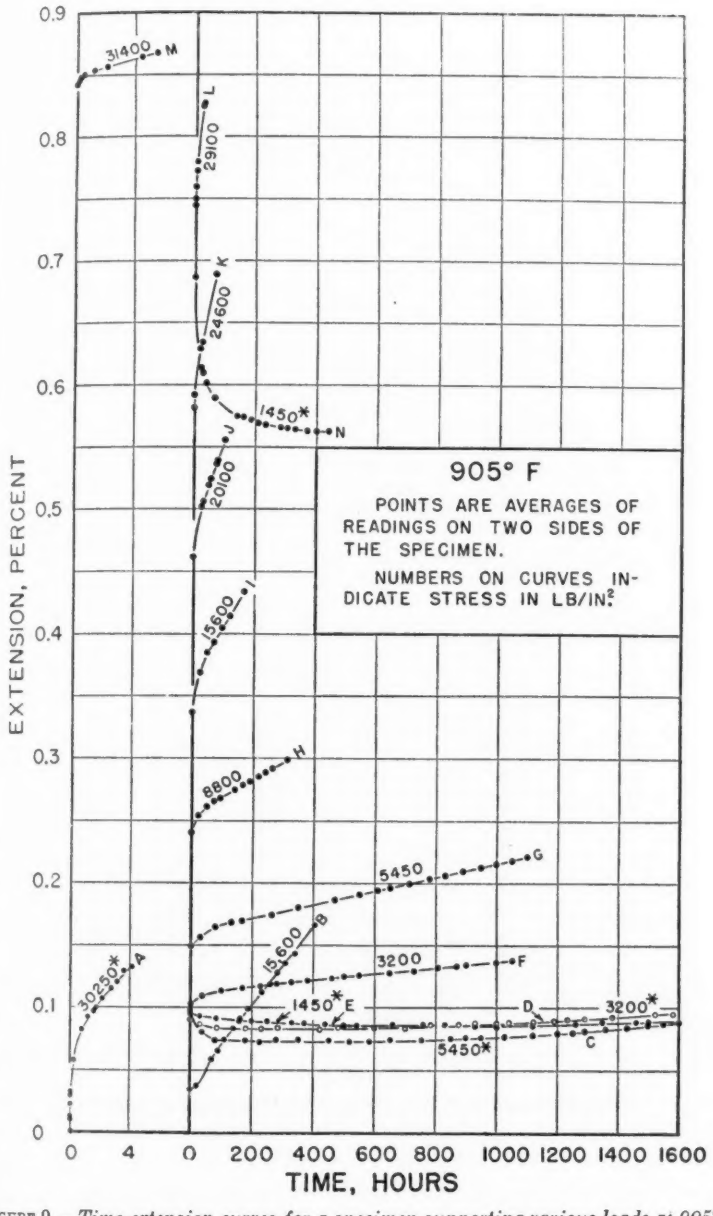

FIGURE 9.—*Time-extension curves for a specimen supporting various loads at 905° F.*

The chronological order of the tests is indicated by the letters on the curves. The elastic extension occurring upon application of the first load is not shown.

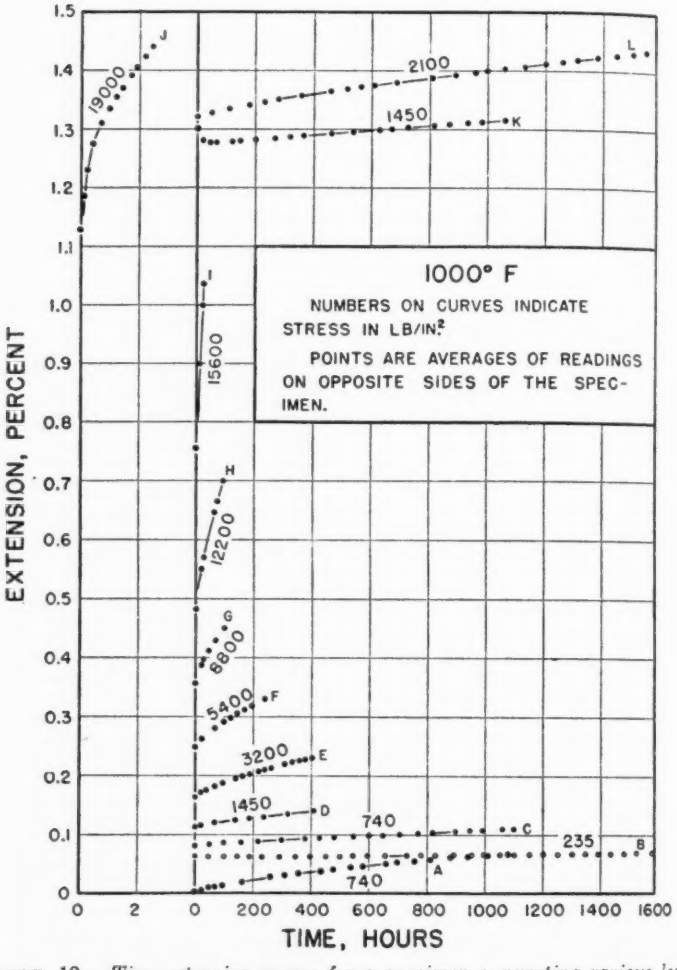

FIGURE 10.—*Time-extension curves for a specimen supporting various loads at 1,000° F.*

The chronological order of the tests is indicated by the letters on the curves.

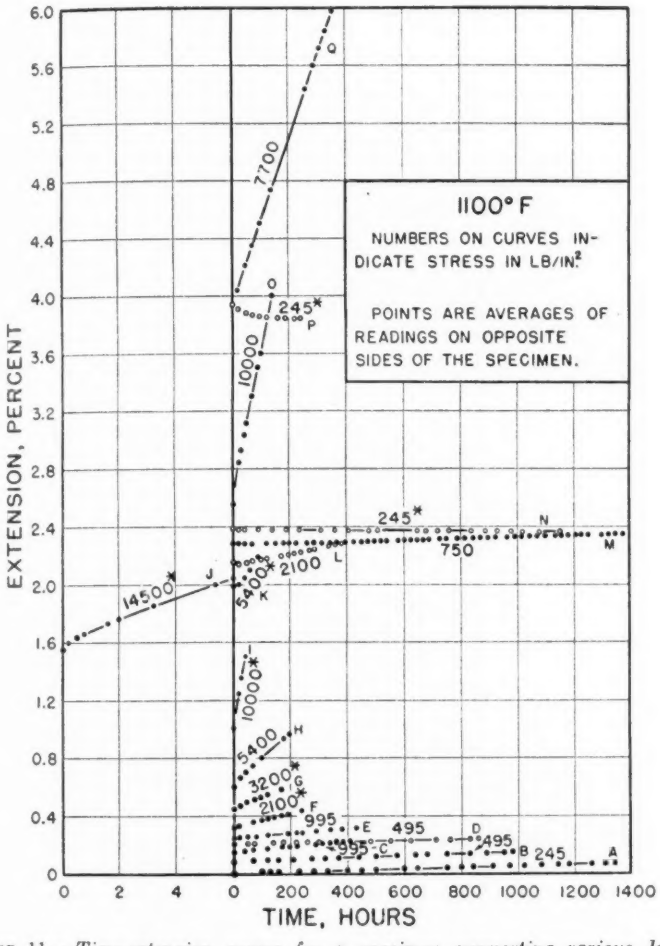

FIGURE 11.—*Time-extension curves for a specimen supporting various loads at 1,100° F.*

The chronological order of the tests is indicated by the letters on the curves.

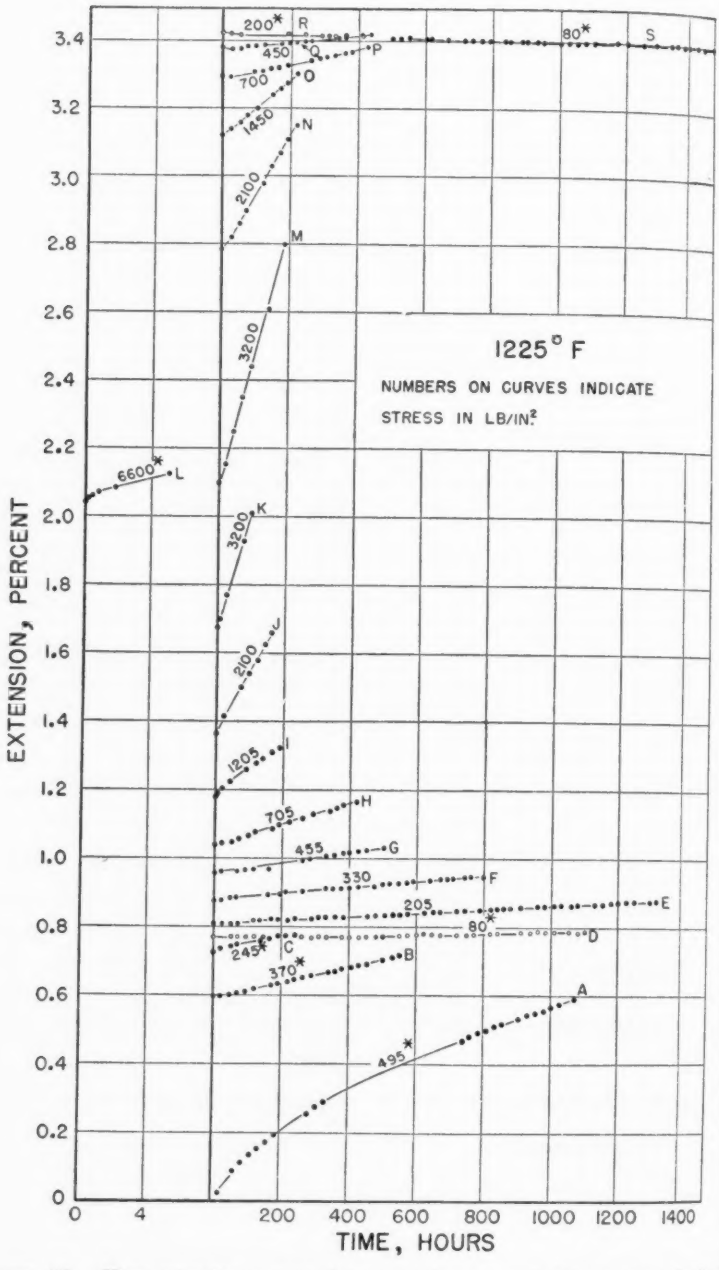

FIGURE 12.—*Time-extension curves for a specimen supporting various loads at 1,225° F.*

The chronological order of the tests is indicated by the letters on the curves.

3. RESULTS FROM SPECIMENS SUPPORTING THE SAME LOAD AT DIFFERENT TEMPERATURES

A similar series of curves is shown in figure 13 for the tests made by holding the load constant and varying the temperature between tests. Because the relative thermal expansion of the specimen and the exten-

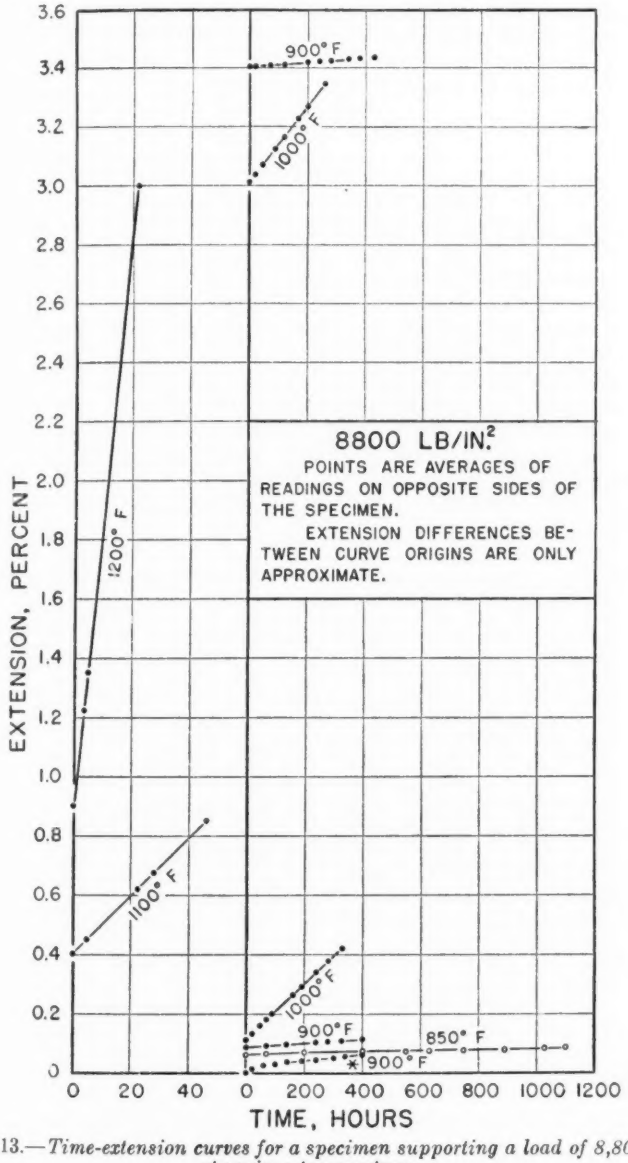

FIGURE 13.—*Time-extension curves for a specimen supporting a load of 8,800 lb/in.² at various temperatures.*

The chronological order of the tests is indicated by the position of the curves above the *x* axis.

446682—42——3

someter bars was not known with much accuracy, the extension which took place during the periods when the temperature was being changed could not be determined. Therefore the position of the curves above the base line in the graph must be considered as only approximate.

An inspection of the curves in figure 13 shows that for all tests except the first, a constant creep rate was attained almost immediately after each change of temperature. This indicates that once the initial rapid change in creep rate has occurred at a certain stress and temperature, a steady flow is again attained in much less time on changing the temperature than on changing the stress.

4. SUPPLEMENTAL TESTS

After a specimen was removed from the creep test, it was first measured in the various ways mentioned above (section II–3) to check the accuracy of the extensometer and to obtain the extension of the gage length. Then a tensile test specimen having a gage section 2 in. long and 0.333 in. in diameter was machined from the reduced section of the creep specimen, and the tensile properties were determined at room temperature. The results of these tests, given in table 1, will be discussed later, in connection with the selection of characteristic creep rates from time-extension curves.

A microscopic examination was also made of each creep specimen, both in the reduced section and near the end, where there was little stress. The specimens that had been tested at 1,000° F and higher were found to be recrystallized. A comparison of the curves in figures 14 to 16, however, shows that this had little or no effect on the creep resistance.

TABLE 1.—*Room-temperature mechanical properties of specimens after creep test*

Specimen	Creep test temperature	Total creep extension	Yield stress	Ultimate stress	True breaking stress	Elongation in 2 in.	Reduction of area	Hardness number
	°F	Percent	Lb/in.²	Lb/in.²	Lb/in.²	Percent	Percent	Rockwell "B"
Original material			122,000	128,000	219,000	12	64	102
ZA2[1]	800	2.3	90,000	105,700	119,000	7	11	95
ZA7	800	2.6	101,400	114,800	138,000	11	21	99
ZA3	905	0.8	64,000	97,600	163,000	21	53	92
ZA10	900	2.8	78,800	96,000	109,000	7	12	98
ZA5	1,000	1.2	31,000	77,900	156,000	40	62	69
ZA8	1,100	5.6	32,300	77,300	146,000	35	57	66
ZB1[1]	1,225	2.5	29,000	77,500	158,000	39	63	65
ZB3[1]	850 to 1,200	3.1	37,800	85,500	176,000	39	65	87

[1] These specimens were annealed 4 hours at 1,200° F before the creep test.

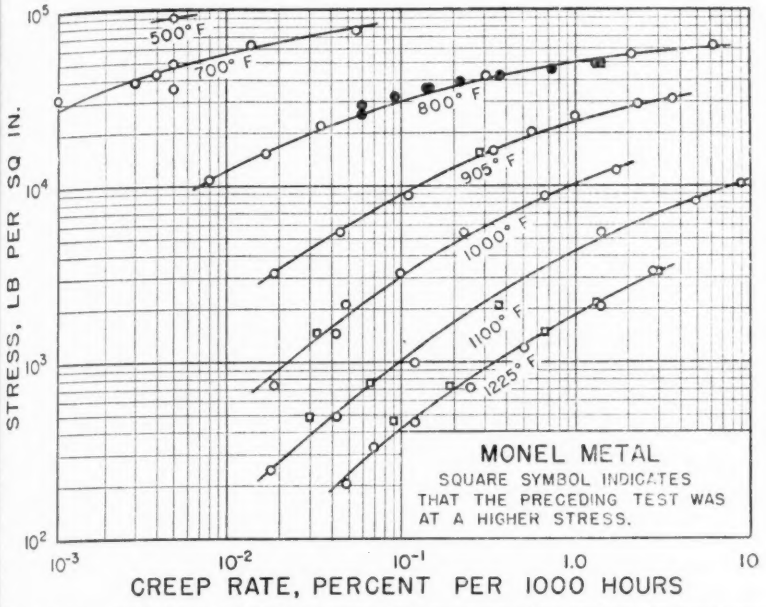

FIGURE 14.—*Relationship between stress and creep rate for various temperatures, obtained from the time-extension curves of figures 7 to 12.*

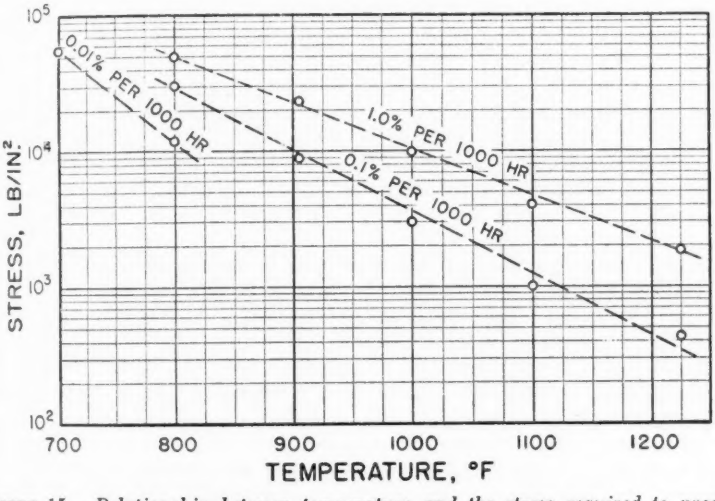

FIGURE 15.—*Relationship between temperature and the stress required to produce certain creep rates, as derived from figure 14.*

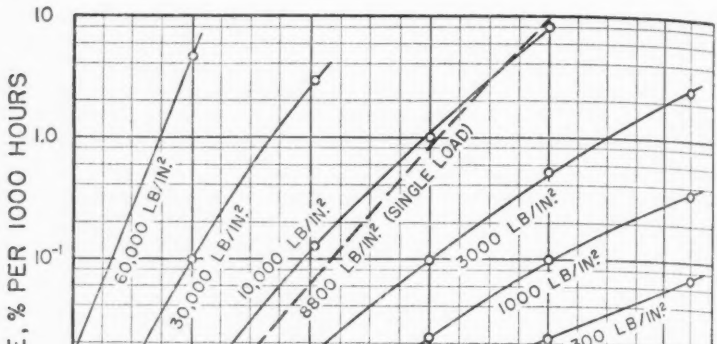

FIGURE 16.—*The relationship between temperature and creep rate for various stresses, as derived from figure 14.*

The dashed line is the curve of figure 17.

IV. THE STRESS-TEMPERATURE CREEP-RATE RELATIONSHIP OF NICKEL-COPPER ALLOY

An increase of stress causes an immediate increase in the rate of creep, but the rate then decreases and approaches a nearly constant rate (figs. 7 to 12). It is this nearly constant rate which is chosen as being characteristic of the stress-temperature combination. A decrease of stress tends to cause negative creep.[2] If the stress is decreased to zero or to a sufficiently low value, actual negative creep begins and proceeds at a decreasing rate. It may, however, merely cause the creep curve to be convex downward, thus indicating that negative creep has been superposed on a continuing positive creep. In some instances the initial downward convexity is followed by upward convexity.

In determining characteristic creep rates, therefore, more care generally is necessary after a decrease of stress than after an increase of stress. After considerable negative creep, a characteristic rate generally was not estimated unless the negative creep was followed by enough positive creep to cause considerable net extension. Moreover, characteristic rates were not estimated until the initial extension of the specimen had been enough to put the metal in a relatively stable condition as regards resistance to creep. No characteristic creep rates, for example, were estimated from curves *C*, *D*, and *E* of figure 9, or from curves *A* to *D* of figure 12. After total extension beyond a certain amount, moreover, creep may tend to proceed at a continuously increasing rate, probably because permanent damage to the material has resulted. Evidence of such permanent damage was seen in the microstructure and in the mechanical properties at room temperature (table 1), the reduction in ductility of the damaged

[2] Negative creep is here used to mean any plastic contraction, regardless of the direction of the stress change preceding it.

specimens (*ZA2, ZA7, ZA10*) being very marked. Such a condition evidently is the cause of the continued downward convexity and the relatively rapid creep rate represented by the upper three curves of figure 8. For these reasons, a few curves at the top of some of the series were not used in estimating characteristic rates. The curves that were not used in estimating characteristic creep rates are indicated by asterisks.

In the actual determination of creep rates, the time-extension data were plotted on larger and more appropriate scales than those of figures 7 to 13, and the correction for extension in the shoulders of the specimen was made. The estimated characteristic rates are plotted against stress in figure 14. No consistent differences are found between the experimental points obtained after a decrease of stress and the points obtained after an increase of stress. These results, therefore, do not confirm the conclusions reached by some investigators as a result of experiments with steels. White and Clark [3] presented results of up-step, down-step, and single-step tests on steel, which indicated that the down-step method of loading gave the lowest creep rate for a certain stress, the single-step method next, and the up-step method the highest creep rate. The evidence in figure 14, however, suggests that the direction of previous change of stress has (of itself) practically no effect on the *characteristic* creep rate.

A comparison between the characteristic creep rate as determined in these tests and the minimum rate, which is reached just before the final stage of creep begins, was provided by a test run at a single load until the rate was definitely accelerating. The temperature was 900° F, the stress was 30,200 lb/in.^{2}, and the minimum rate, which was reached after 900 hours, was 0.92 percent per 1,000 hours. From figure 14 the characteristic rate at this stress at 905° F is 2.8 percent per 1,000 hours.

As indicated by the varying slopes of the curves in figure 14, the influence of a stress variation on the rate of creep increases with increase of the stress, and with decrease of the temperature for a constant rate. Two other aspects of the three-dimensional relationship represented in figure 14 are shown in the derived diagrams, figures 15 and 16. In each of these diagrams, temperatures are represented by linear coordinates. As illustrated by figure 16, the influence of temperature on the creep rate increases with decrease in the temperature (contrary to the prevalent view), and with increase in the stress.

It has been pointed out that the time-extension curves, figure 13, representing data obtained with a specimen supporting the same load at different temperatures, indicate a characteristic rate after a very short adjustment period. These rates are plotted against temperature in figure 17. It will be noted that the relationship can be represented by a curve which is more nearly straight than that representing the stress-rate relationships. This means that the results can be interpolated and extrapolated more reliably than can the stress-rate curves. Kanter and Sticha [4] have suggested the plotting of the logarithm of the creep rate against the reciprocal of the absolute temperature. With the data obtained in this test, however, the resulting curve was not so straight as that in figure 17.

The curve on figure 17 is included as a dashed line in figure 16 for comparison with the data from the constant-temperature tests. As the agreement evidently is good, it can be concluded that the characteristic creep rate obtained from time-extension data is independent

of previous temperatures and stresses, and is dependent only on the particular stress-temperature combination.

This conclusion assumes considerable importance when it is remembered that the time-extension curves for tests at constant load and different temperatures show little or no adjustment period. If the conclusion is supported by additional creep-test data, much time evidently may be saved by determining creep rates with this type of test rather than with the conventional single-load constant-temperature tests now commonly used.

Another interesting point is brought out by the agreement between the two types of curves of figure 16. The dashed curve was obtained

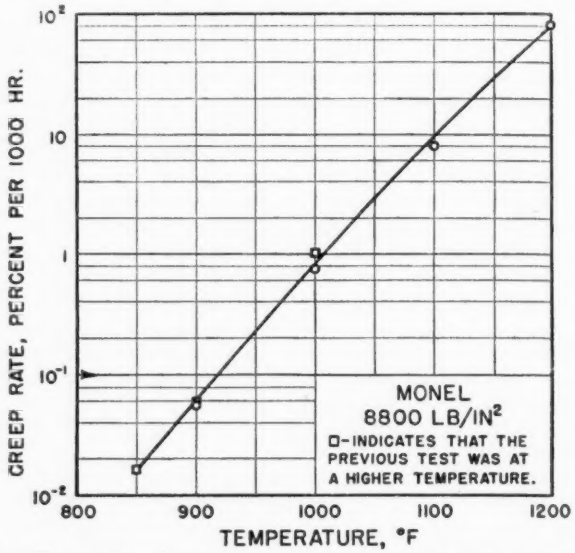

FIGURE 17.—*The relationship between temperature and creep rate for a load of 8,800 lb/in.², as derived from the time-extension curves of figure 13.*

on an annealed specimen, while all of the constant-temperature tests (except the one at 1,225° F) were made on cold-drawn specimens. This difference in the material, therefore, evidently has little effect on the characteristic creep rate for this alloy. This does not mean, however, that the rate would be the same if some structural change, such as recrystallization, were taking place during the test.

None of the mathematical relationships suggested in the literature [5] were found to agree with the creep data determined in this investigation, and it is thought that the data can be represented satisfactorily only in graphs. Since the stress-temperature and creep-rate-temperature curves are nearly straight, the relationship between these two pairs of variables may be represented approximately by exponential equations, but the agreement with experiment is not sufficiently close to be of particular value.

The closest approximation to the time-elongation curves is obtained with an equation of the form

$$d=d_0+vt-Ce^{-\alpha t},$$

where d_0, C, and α are constants, d is total extension, t is time, and v

is the minimum creep rate. This cannot be made to fit well near the beginning of the test, and is certainly not the true relationship, but it is the only type of equation which gives a reasonably good approach to the curves for both the up-step and down-step tests.

V. SUMMARY AND CONCLUSIONS

Details of the creep-testing apparatus recently installed at the National Bureau of Standards are described. It consists of 12 independent units for testing specimens having a 4-in. reduced section. On a 0.505-in. diameter specimen, loads from 80 to 90,000 lb./in.^{2} can be conveniently applied. The temperature is controlled within $\pm 5°$ F up to 1,200° F, and the extensometer readings have a probable error of less than 0.00004 in. The extension is measured between the shoulders of the specimen, so that a correction is required, but the accuracy of the corrected extension averages within 1½ percent.

Time-extension data were obtained with specimens of severely cold-worked nickel-copper alloy. The stress range investigated covered the full range of the apparatus, while the temperatures used varied from 700° to 1,225° F. In general, one specimen was tested at a single temperature and a series of different stresses.

The results show that a nearly constant creep rate, characteristic of a stress-temperature combination, was attained after a period of adjustment. The use of a single specimen for a series of stresses allowed more rapid determination of this characteristic rate than a single load test. With a single specimen, therefore, a series of characteristic creep rates could be determined, for different applied stresses. One series of tests, made under a single load at a series of different temperatures, resulted in little or no period of adjustment, yet these rates were consistent with those determined from the constant-temperature tests. The results as a whole indicate that there was only one characteristic rate for each stress-temperature combination irrespective of the previous stresses or temperatures.

Diagrams are given showing the relationship between the variables stress, temperature, and creep rate. No mathematical function could be found to describe the creep test data.

Daniel H. Gagon, formerly of this Division, assisted with the construction of the furnaces and with the measurement of extension during tests.

VI. REFERENCES

[1] W. A. Tucker and S. E. Sinclair, *Creep and structural stability of nickel-chromium-iron alloys at 1,600° F*, BS J. Research **10**, 851 (1933) RP572.

[2] F. H. Norton, *Pyrometry in connection with creep tests.* Symposium on Temperature: Its Measurement and Control in Science and Industry, p. 963 (Reinhold Publishing Co., New York, N. Y., 1939).

[3] A. E. White and C. L. Clark, *Creep characteristics of metals at elevated temperatures*, Trans. Am. Soc. Steel Treating **21**, 1 (1933).

[4] J. J. Kanter and E. A. Sticha, *Creep rates from tests of short duration*, Trans. Am. Soc. Metals **28**, 257 (1940).

[5] A. Eichinger, *Mathematical treatment of creep curves*, Arch. Eisenhüttenw. **13**, 397 (1940).

Washington, January 8, 1942.

U. S. Department of Commerce · National Bureau of Standards

RESEARCH PAPER RP1463

Part of Journal of Research of the National Bureau of Standards, Volume 28, April 1942

FRICTIONAL PROPERTIES OF RUBBER

By Frank L. Roth, Raymond L. Driscoll, and William L. Holt

ABSTRACT

Laboratory measurements of coefficients of friction of soft rubber compounds were made by towing specimens on horizontal tracks and by allowing them to slide down inclined tracks. The specimens were prepared by attaching the rubber to a metal backing and molding it against glass surfaces having different degrees of roughness. The coefficients increase markedly with speed, ranging from about 1 at 10^{-4} cm/sec to more than 4 at 5 cm/sec. The occurrence of vibrations prevented observations at higher speeds. Static friction is greater than dynamic friction for speeds appreciably less than 10^{-3} cm/sec and less than dynamic friction for greater speeds. The coefficients decrease slightly with increasing pressures and are independent of the size of the specimen. Except at very low speeds the smoother surfaces yield the higher coefficients. Materials such as talc or bloom on the sliding surfaces cause large decreases in the coefficients.

Attention is called to the dependence of the coefficients of friction on the speed, which is shown in several previous investigations on rubber and other materials.

CONTENTS

	Page
I. Introduction	440
II. Experimental procedure	440
1. Earlier experiments	441
(a) Apparatus and procedure	441
(b) Rubber compounds investigated	441
(c) Rubber sliding on tracks of different degrees of roughness	442
(d) Steel sliding on a rubber track	443
(e) Effects of certain lubricants	444
(f) Abrasion of specimens on a smooth track	445
2. Later experiments	445
(a) Compounds investigated	445
(b) Apparatus and procedure	446
(1) General description	446
(2) Specimens	446
(3) Tracks for frictional measurements	448
(4) Mounting and loading of specimen	448
(5) Measurement of the frictional forces	448
(6) Sliding speeds	449
III. Results	449
1. Changes in frictional forces at the start of slide	449
2. Coefficient of static friction	450
3. Coefficient of dynamic friction	451
4. Relation between static and dynamic coefficients	451
5. Effects of various factors on the coefficients of dynamic friction	452
(a) Sliding speed	452
(b) Roughness of the sliding surfaces	454
(c) Surface area and normal pressure	455
(d) Vibration of the apparatus	455

III. Results—Continued. Page
5. Effects of various factors on the coefficients of dynamic friction—Continued.
(e) Composition of the rubber compound ... 455
(f) Cleaning the specimens ... 456
(g) Moisture ... 457
6. Summary of results ... 457
IV. Discussion ... 457
1. Sliding speed ... 458
(a) Change of friction with speed ... 458
(b) Vibrations ... 459
2. Changes in friction at the start of slide ... 460
3. Roughness of the sliding surfaces ... 461
4. Composition of the rubber compound ... 461
V. References ... 461

I. INTRODUCTION

The coefficients of friction of soft vulcanized rubber compounds have been studied by numerous investigators. The data reported for many of the investigations previous to March 1934 have been collected and tabulated by Dawson and Porritt [1].[1] Most of the studies of the frictional properties of rubber deal with particular kinds of rubber goods, such as tires, power-transmission belts, soles and flooring, and water-lubricated bearings. In such studies the experimental conditions are those under which the products are commonly used. For example, the motion between the friction surfaces for tires or belts is a combination of rolling and sliding. Foreign materials, many of which act as lubricants, are nearly always present between the surfaces. Often, sliding is accompanied by vibration of the rubber, as in the case of the skidding of tires, where the vibration is distinctly audible.

In the present investigation, which is a part of a more general investigation on the abrasive wear of rubber, the specimens and tracks were prepared in the laboratory. This procedure makes it possible to employ a relatively wide range of experimental conditions and to exercise control over the composition and the surface of the specimens. No attempt was made to determine the skidding resistance of tires; instead the study was limited to the frictional characteristics of clean, soft rubber compounds, particularly those of the type used in tire treads, when sliding on clean smooth tracks. The effects of the presence of certain types of lubricants were briefly studied in order that the results might be compared with those for relatively clean surfaces. Conditions of slide under which the specimens vibrate or chatter were not studied except to note that the average force required to pull the specimen decreased considerably when chattering began. Because of chattering of the specimens, the maximum speeds for which friction was studied were limited to 10 cm/sec. Also, because of difficulties experienced in preventing the specimens from buckling or otherwise deforming greatly, the maximum normal pressures between the specimens and the tracks were limited to 40 lb/in.^{2} for most of the work.

II. EXPERIMENTAL PROCEDURE

Since this investigation was begun several years ago and then was discontinued for nearly 2 years before it was again resumed, the experi-

[1] Figures in brackets indicate the literature references at the end of this paper.

mental procedure and data are presented in two parts. The first part was more in the nature of an exploratory investigation consisting in brief studies for a relatively large variety of experimental conditions. The second part was a more detailed study of a rather limited field. Different samples, different apparatus, and different experimental techniques were employed in these two parts of the investigation but the results are similar in many respects and lead to the same general conclusions.

1. EARLIER EXPERIMENTS

(a) APPARATUS AND PROCEDURE

The rubber specimens for most of this work were in the form of three circular disks, which were cemented to one surface of a rectangular metal plate in such a way that they shared equally the weight of the plate and the additional load. The disks were 1/16 in. thick and the diameters for different sets ranged from 5/16 to 1/2 in. For some of the work the rubber disks were replaced with steel and the track was cut from the rubber to be studied. In some of the tests the metal plate and disks were towed along the friction track by means of a cord which was wound on a drum. A motor and reduction gear served to rotate the drum, and a spring scale in the tow line served to measure the frictional force. In other tests a circular friction track about 2 ft. in diameter was rotated at the desired speed by means of the motor, and the specimens were held at rest by the tow line and spring scale.

(b) RUBBER COMPOUNDS INVESTIGATED

The compositions of the rubber compounds used in the specimens are given in table 1. One is a typical pure-gum compound; the other is the standard abrasion compound described in the Federal Specification for Rubber Goods No. ZZ–R–601a. These compounds were selected for study because of their great difference in resistance to abrasion and in order to determine whether the coefficients were characteristic of the filler or of the rubber. Since specimens made from the soft pure-gum compound distorted greatly under conditions of slide, the larger part of the study was made on the standard abrasion compound and on specimens cut from a rubber conveyor belt the exact composition of which was not known.

TABLE 1.—*Composition of rubber compounds*

[The standard abrasion and pure-gum compounds were press-vulcanized 60 and 30 minutes, respectively, at 142° C.]

Ingredients	Rubber compounds	
	Standard abrasion	Pure-gum
	Parts by weight	*Parts by weight*
Rubber (smoked sheets)	100	100
Sulfur	3.5	3
Zinc oxide	20	5
Stearic acid	2	1
Diorthotolylguanidine	1.25	.....
Mercaptobenzothiazole (Captax)	.....	1
Phenylbetanaphthylamine	1	.....
Channel-black (Micronex)	30	.....
Total	157.75	110

(c) RUBBER SLIDING ON TRACKS OF DIFFERENT DEGREES OF ROUGHNESS

Coefficients of friction for the standard abrasion compound sliding on steel, and on different grades of abrasive materials are plotted against the logarithm of the sliding speed in figure 1. The logarithmic scale is used for the speed in this and subsequent figures for convenience in showing the coefficients over a large range of speeds. The smoothest track was steel polished with No. 0 polishing paper. Various grades of abrasive papers, fixed on a rigid base, served as rough tracks. Figure 1 shows that for every track the coefficient of friction increased with the speed. At the higher speeds the smoother tracks yielded the greater coefficients; but for speeds approaching zero, the rough tracks yielded the greater coefficients. Each point represents the average of several observations. Except for the steel

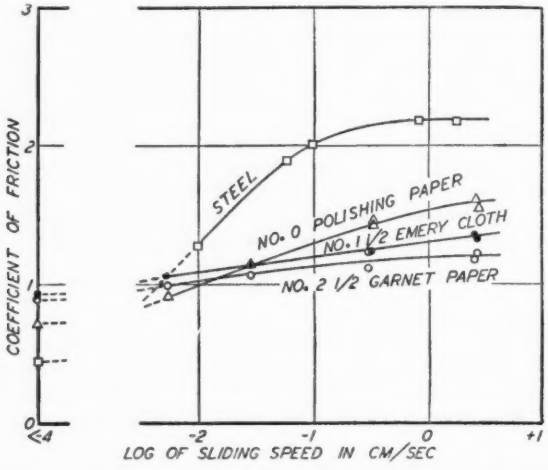

FIGURE 1.—*Coefficient of friction of rubber sliding at different speeds on surfaces of varying degrees of roughness.*

The composition of the rubber is that given for the standard abrasion compound in table 1.

track the data for the different points in each curve, particularly where two points occur for one speed, were obtained at various times over a period of more than a year. The values shown for the lowest speed were obtained by observing the spring scale after stopping the motor. The specimens continued to move on the track under the action of the spring for some time after the motor was stopped. Readings were taken when the specimen had apparently stopped. The normal pressures between the specimens and the track were 25 to 30 lb/in.^{2}

Figure 2 shows coefficients of friction obtained with the pure-gum compound on the steel track. The values for the standard abrasion compound shown in figure 1 are also reproduced here for purposes of comparison. For these two compounds the increases of the coefficients with speed are similar. At speeds approaching 10 cm/sec the values of the coefficients became equal; but since the specimens vibrated at these speeds, the values were not plotted.

(d) STEEL SLIDING ON A RUBBER TRACK

For the study of steel sliding on rubber, the rubber disks were replaced by steel disks of about the same size. The track, which was circular in form, was cut from a rubber-covered conveyor belt. Por-

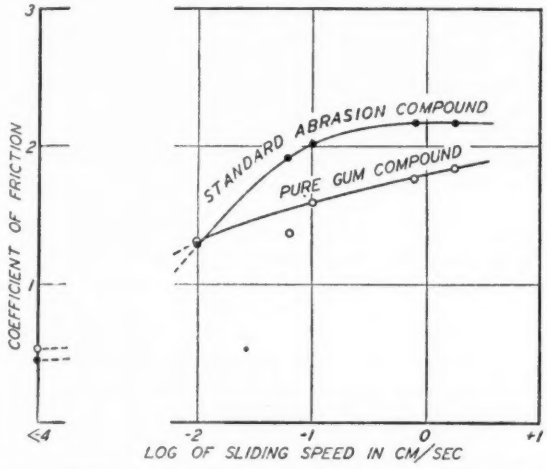

FIGURE 2.—*Comparison of the coefficients of friction of the two rubber compounds described in table 1 when sliding at different speeds on a steel track.*

The data for the standard abrasion compound are those shown for the steel track in figure 1.

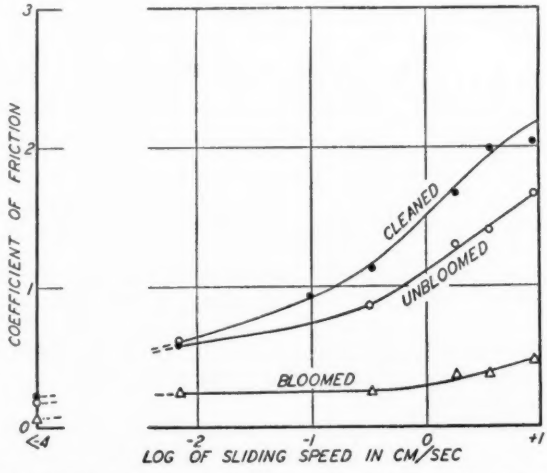

FIGURE 3.—*Coefficients of friction of steel on rubber, showing the effect of the presence of bloom on the rubber surface.*

tions of this belt showed a decided tendency to bloom. The curves in figure 3 show, respectively, the coefficient of friction plotted against the logarithm of the speed for the steel disks sliding on a bloomed portion of the rubber, on a portion which showed no apparent bloom, and on a portion which had been cleaned with acetone the day before

the observations were made. As in the previous experiments, the coefficients increased with speed in every case, although the presence of bloom sharply reduced the observed values.

(c) EFFECTS OF CERTAIN LUBRICANTS

Since bloom or other materials which may be present on rubber compounds cause appreciable decreases in the observed coefficients of friction, a brief study was made of the effects of several materials which may have lubricating properties when present on the sliding surfaces. The materials selected were talc, spherulized kaolin,[2] a thick soap solution, graphite, castor oil, and water. Talc is often used to facilitate the sliding of one rubber article on another, as in the case of an inner tube in a tire. Spherulized kaolin might be expected to possess

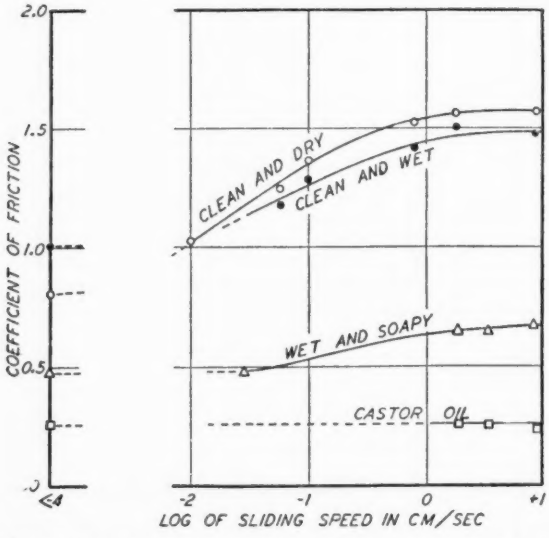

FIGURE 4.—*Coefficients of friction of rubber on rubber showing the effects of the presence of water, soap solution, and castor oil on the track.*

lubricating properties because of its rounded particles. Soap, graphite, and castor oil are well known lubricants. Petroleum oils were not tried, since they cause swelling of the rubber. The effects of talc, spherulized kaolin, and graphite were studied for steel sliding on rubber and for rubber on rubber. The other substances were tried only for rubber on rubber.

In our experiments, talc and soap reduced the observed coefficients, but the increases in the coefficients with speed were still evident. Spherulized kaolin reduced the coefficients to a greater extent than talc did, but slight increases of the coefficients with speed still persisted. The presence of graphite or castor oil on the sliding surfaces further reduced the coefficients, and the increases of the coefficients with speed disappeared completely.

[2] The spherulized kaolin was prepared by blowing kaolin powder through an oxy-hydrogen flame and collecting the rounded particles thus produced. The particles were of the order of 1 micron in diameter.

For rubber sliding on rubber, wetting the surfaces with water caused a small decrease in the coefficients for the higher speeds and a small increase as the speed approached zero. No general conclusions can be drawn from a single experiment of this kind. Observations reported later in this paper show that when rubber slides on glass, the presence of water causes a sharp decrease in the observed coefficients. Reports on the frictional characteristics of rubber sliding on glass and on roadway materials [2], of tires on roads [3], and of water-lubricated bearings [4] show that the effect of water between the sliding surfaces depends markedly on the thickness of the water film and on other factors—such as the speed, the normal pressure, the nature and smoothness of the surfaces, and the presence of foreign materials in the water film.

(f) ABRASION OF SPECIMENS ON A SMOOTH TRACK

In an attempt to determine whether any rubber was abraded from the specimens in sliding on a relatively smooth metal track, the specimens and plate to which they were cemented were weighed to 0.1 mg before and after towing them several hours at about 3 cm/sec on the track. The procedure was repeated for increasing normal pressures between the specimens and track up to the point at which the specimens were torn apart by the frictional forces. No definite loss by abrasion could be detected for pressures up to 260 lb/in.^{2}

2. LATER EXPERIMENTS

(a) COMPOUNDS INVESTIGATED

A large proportion of the measurements of coefficients of friction were carried out on specimens made from a channel-black compound containing 49 parts of carbon black to 100 parts of crude rubber. The composition is shown in table 2. This compound is one of those used in an investigation of stress-strain properties at different rates of stretch [5]. Except for the omission of softeners or plasticizers which would facilitate manufacturing processes, it is a typical tire-tread compound.

TABLE 2.—*Composition of rubber compounds*

[The specimens were press-vulcanized for 15 minutes at about 142° C.]

Ingredients	Rubber compounds	
	Channel-black	Clay
	Parts by weight	*Parts by weight*
Rubber (smoked sheets)	100	100
Sulfur	3	3
Zinc oxide	5	5
Stearic acid	2	2
Benzothiazyl disulfide (Altax)	1	1
Tetramethylthiuram disulfide (Tuads)	0.1	0.1
Phenyl-beta-naphthylamine	1.5	1.5
Channel-black (Micronex)	49	
Clay (Dixie)		140
Total	161.6	252.6

Several specimens were also made of a compound in which the channel-black was omitted. Because of distortions of the soft rubber under frictional forces, it was impossible to obtain satisfactory results with these specimens. Specimens were then made with a body of the channel-black compound and a thin layer of the soft compound on the sliding surface. These specimens chattered at the higher speeds, and at low speeds the frictional forces repeatedly increased to a maximum and dropped to a lower value.

Specimens were also made from a compound in which 70 parts of clay filler was substituted for the channel-black. This amount of clay is equal in volume to the amount of channel-black which it replaced. These specimens jumped and chattered for speeds of 0.01 cm/sec or greater.

A number of satisfactory measurements of the coefficient of friction were obtained, however, on specimens made from a compound containing 140 parts of clay instead of the channel-black. This compound, referred to in table 2 and elsewhere as the clay compound, possesses a hardness measured by resistance to indentation which is about equal to that of the channel-black compound.

(b) APPARATUS AND PROCEDURE

(1) *General description.*—A schematic diagram of the two arrangements used in determining the coefficients of friction is shown in figure 5. The horizontal track was suspended by four wires from points about 6 feet above it, and the specimen was pulled along the track at a constant speed by means of a motor and reduction gears. The frictional force was determined by measuring the force required to hold the track at rest while the specimen was being moved. The coefficient of friction in this arrangement is the ratio of the measured force to the total weight on the specimen.

In the inclined-track arrangement the specimen was allowed to slide down the track under the action of the combined weights of the specimen carriage and the additional load which was hung from it. In this case the frictional force remained constant, and the speed of slide was measured. The coefficient of friction is equal to the tangent of the angle made by the plane of the track and the horizontal.

(2) *Specimens.*—Attempts were made to use specimens which were cut from a sheet of rubber and fitted snugly into a recess in the under side of the carriage. As these specimens slid along the track, they became shorter and thicker, leaving an open space at the leading end of the recess, and finally they buckled. This excessive distortion was eliminated by vulcanizing the rubber stock to rectangular pieces of steel ⅛ in. thick which fit into the recess. The rubber in these specimens was usually about 1/16 in. thick, but increasing the thickness to ⅛ in. produced no noticeable difference in the coefficients of friction. Most of the specimens had dimensions of either 5/16 by 1⅛ in. or ¾ by 1½ in. The direction of slide was parallel to the larger dimension, and the leading end was beveled to prevent the edge from rolling under.

The sliding surfaces of the specimens were of three types. The first, a smooth surface, was obtained by molding the rubber against plate glass. When these specimens were pressed against a glass surface, only part of their areas made actual contact with the glass.

Interference fringes were observed around the boundaries of the contact areas, and considerable force was required to lift the specimens off the glass. The coefficients of friction observed differed greatly between individual specimens and between different observations on the same specimen. Examination of the specimens after they were allowed to slide on the track showed that only parts of their surfaces

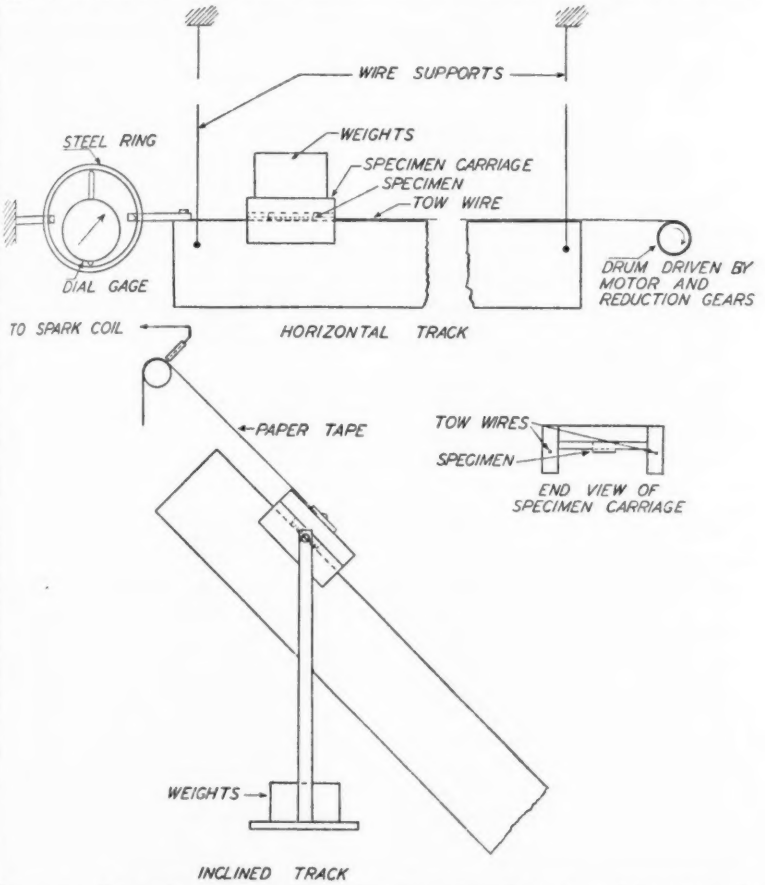

FIGURE 5.—*Schematic diagram of the two arrangements used in determining the coefficients of friction.*

made contact and that the proportion of each specimen which made contact varied considerably between individual specimens.

In order to obtain more uniform conditions of contact and to get the pressure between the specimen and the track distributed more uniformly over the entire surface, specimens were made by molding the rubber against plate glass which had been roughened with an abrasive. Two degrees of roughness were obtained, one by roughening the glass with carborundum flour and the other by the use of 150-mesh carborundum. Much of the work reported here was done using these two types of specimens, which are referred to as specimens

446682—42——4

type *F*, and type 150, respectively. Photomicrographs of two specimens of type *F* and one of type 150 are shown in figure 6. The specimen represented by the photomicrograph labeled *D* was obtained by cutting a piece of rubber from the tread of a used tire and cementing it to a rigid fiber back. The rubber was about 3/32-in. thick, and care was taken to get the thickness nearly uniform. The tread surface shown here was used as the friction surface. Examination of figure 6 shows that, except for a few relatively deep marks in the direction of the rotation of the tire, the roughness of this specimen is intermediate between specimens type 150 and type *F*. Only one such specimen was investigated.

(3) *Tracks for frictional measurements.*—Two kinds of friction tracks were used; one was a ground-steel surface and the other was plate glass. The steel track was made from a piece of cold-rolled steel 1½ in. wide, 3 in. thick, and about 40 in. long. The friction surface was ground smooth with a high-speed, fine-abrasive wheel. This surface was not polished and consequently was not as smooth as the glass track. Rusting of the steel, when not in use, was prevented by a coating of Alox rust preventive dissolved in Stoddard solvent. This coating was removed with gasoline followed by acetone prior to each use of the track.

The glass surface was obtained by clamping a strip of plate glass on top of the steel track. The glass was usually cleaned with soap and warm water followed by clean water, and usually dried with acetone. The use of acetone, though not necessary, was a quick and convenient means of drying the track. Occasionally the glass track was cleaned by immersing it for several hours in chromic acid. It was found that this occasional cleaning was sufficient to give reproducible results.

(4) *Mounting and loading of specimen.*—In order to keep the pressure between the specimen and the track uniform over the entire specimen surface, the carriage was so constructed that its center of gravity lay in the center of the surface of the specimen. When the carriage was used on the horizontal track, it was towed by means of two wires fastened equidistant from the specimen on either side and in the plane of the track. Any additional weights were placed centrally over the specimen on the top of the carriage. When the carriage was used on the inclined track, the additional weights were hung from pins placed in its sides equidistant from the specimen and in the plane of the track.

The loads applied to the specimens were such that the normal pressure on the sliding surfaces ranged from 2.5 to 15 lb/in.^{2} for the large specimens and from 7.5 to 40 lb/in.^{2} for the small ones. A large proportion of the work was done using 10 lb/in.^{2} on the large specimens and 20 lb/in.^{2} on the small ones.

(5) *Measurement of the frictional forces.*—The force to be measured in the horizontal-track arrangement was that required to keep the track from moving when the specimen was pulled. Since it was desired to measure this force with a minimum of displacement of the track, it was determined by measuring the distortion it produced when applied to a steel ring. The ring had an outside diameter of about 3.6 in., and an inside diameter of about 3.3 in., and was about 0.6 in. wide. It was fastened between the track and a fixed support, as shown in figure 5, so that the force to be measured acted along the

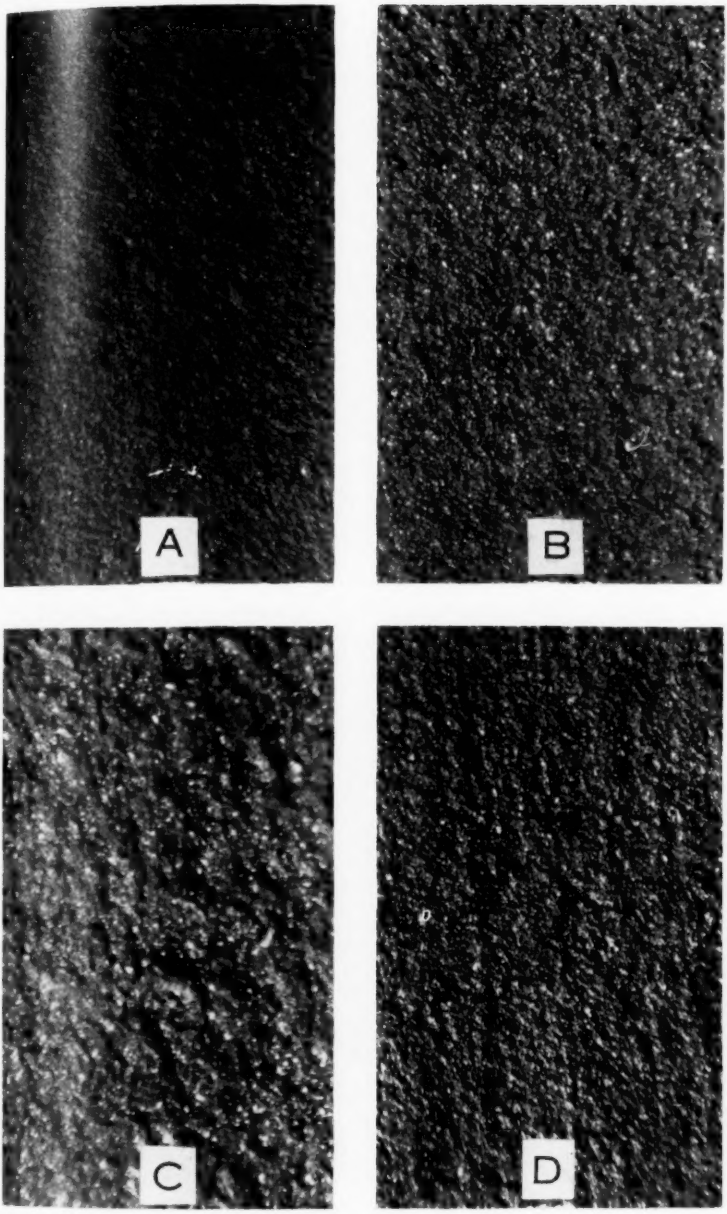

FIGURE 6.—*Photomicrographs of the sliding surfaces of the rubber specimens.*

A and *B* are type *F*, *C* is type 150, and *D* is the specimen from a used-tire tread. Magnification 48×.

horizontal diameter. The distortion in the direction of the vertical diameter was measured by means of a sensitive dial gage graduated to ten-thousandths of an inch. The distortion shown by the gage rarely exceeded 0.008 in. (80 divisions), and calibration over this range showed that it was proportional to the force applied, the calibration factor being 305 g per division.

(6) *Sliding speeds.*—The speeds on the horizontal track ranged from 0.0001 to 7 cm/sec. Since observations became increasingly tedious as the speed was decreased, and since the coefficients at very low speeds were markedly affected by vibrations in the building, no attempt was made to extend the investigation on the horizontal track to speeds below this range. The maximum speeds, from 1 to 7 cm/sec, were limited by jumping and chattering of the specimens on the track.

In the case of the inclined track, the speed was the quantity to be measured, while the forces acting on the specimen remained constant. As a convenient means of determining the speed, a paper tape was fastened to the specimen carriage and towed through a spark gap. Sparks produced at desired intervals punctured the tape, making a permanent record of the position of the specimen as a function of time. The force required to pull the tape was negligible.

Usually the angle of incline was adjusted before the specimen was placed on the track; but when the equilibrium speed was over 0.01 cm/sec, it was often necessary to allow the specimen to begin sliding with the track at a relatively low angle of incline, and to increase the angle as the speed decreased. Determinations of the speed were not made until the desired angle of incline was reached.

III. RESULTS

1. CHANGES IN FRICTIONAL FORCES AT THE START OF SLIDE

It was noted throughout the later experiments (section II–2) that when a specimen was towed at constant speed on a horizontal track, the force of friction did not become constant until the specimen had moved several centimeters. Likewise, a specimen sliding down an inclined track moved several centimeters before it attained a constant equilibrium speed. Figure 7 shows the results of a study of these changes for typical specimens of type 150 and type *F* when sliding on a glass track. For the horizontal track the points on the graphs refer to readings of the force of friction which were taken at predetermined intervals of time. Care was taken at the start of slide to allow all the slack and stretch in the apparatus to be taken up before observations were begun. For the low speeds, readings were not taken until the specimen was allowed to move about half of a millimeter. In the case of the inclined track the position of the specimen was recorded at various intervals of time and the average speed for each interval was plotted.

These changes in the frictional characteristics of the specimens at the start of slide were first thought to be due to nonuniformities in the friction track, but this explanation was ruled out by the fact that the phenomenon occurred on any portion of the track and on all the glass tracks which were used in the tests. Also, when the specimen was stopped during its slide and was started again, it repeated the changes which were observed at the beginning of the test and approached the same equilibrium conditions of slide. Furthermore, similar results were observed for specimens sliding on the steel track.

It appears that these changes of frictional properties at the start of slide are transitions from static conditions of contact between the friction surfaces to dynamic conditions and are regarded as such in the more detailed discussions which follow, but it is not clear why the effect should extend over such a large distance of slide.

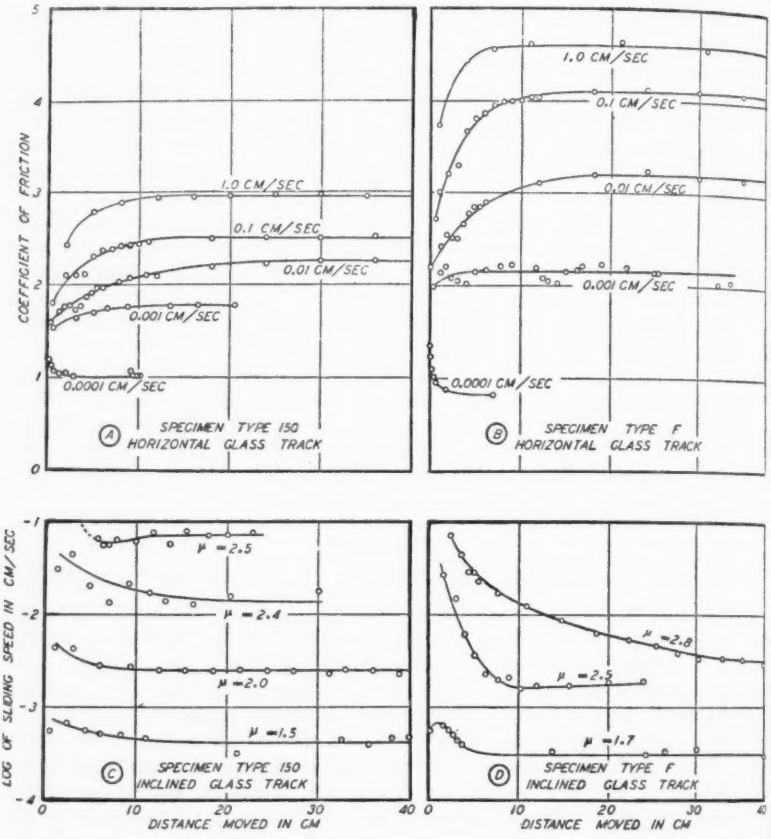

FIGURE 7.—*Changes in frictional properties of rubber at the start of slide.*

Results are shown for two types of surfaces on horizontal and inclined glass tracks. μ is the tangent of the angle of incline and is equal to the coefficient of friction.

2. COEFFICIENT OF STATIC FRICTION

If the curves in figure 7 (*A* and *B*) are extended back, one would expect them to intersect the zero ordinate at a point which corresponds to the coefficient of static friction. This point appears to lie somewhere between the values 1.2 and 1.5 for the specimen type 150 and between 1.5 and 2.0 for type *F*. Accordingly, if the specimens are placed on the inclined glass track, the maximum angle of repose should be between $\tan^{-1}$ 1.2 and $\tan^{-1}$ 1.5 for the specimen type 150 and between $\tan^{-1}$ 1.5 and $\tan^{-1}$ 2.0 for type *F*. It was found that the specimen type 150 always started sliding when the angle of incline was $\tan^{-1}$ 1.3 or greater, seldom started when the angle was $\tan^{-1}$ 1.2,

and never started for angles appreciably less than $\tan^{-1}$ 1.2. The maximum angle of repose for the specimen type *F* was similarly about $\tan^{-1}$ 1.6.

3. COEFFICIENT OF DYNAMIC FRICTION

If one regards the changes of the frictional forces during the first several centimeters of slide on the horizontal track as transitions from static to dynamic conditions, the relatively constant coefficient finally reached is the coefficient of dynamic friction for that particular speed. Likewise the nearly constant speed which is attained after the first several centimeters of motion down the inclined track represents the equilibrium speed for that particular angle of incline.

The data from the equilibrium conditions shown in figure 7 have been plotted in figure 8 to show the relation between the coefficient of dynamic friction and the speed, and to show the correlation between tests made on the horizontal track and those made on the inclined

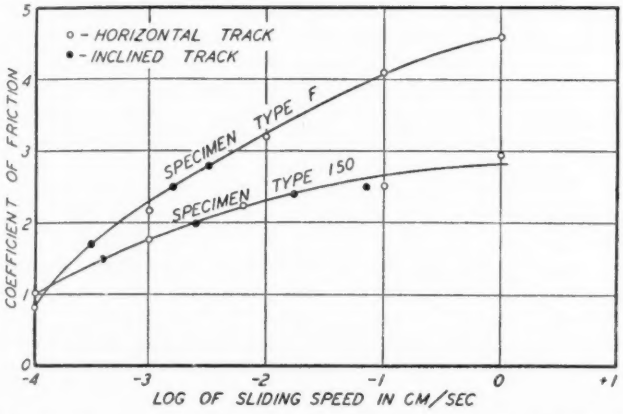

FIGURE 8.—*Coefficients of friction of channel-black rubber sliding at different speeds on a glass track.*

The data were taken from the equilibrium conditions of slide in figure 7 and show the correlation between tests made on the horizontal and inclined tracks.

track. This graph indicates that the coefficients obtained by use of the horizontal and inclined tracks are in agreement, that the coefficients of friction for both specimens increase as the speeds increase, and that except for the lowest speed the coefficients for the surface with the finer texture, type *F*, are greater than those for type 150. These observations have been substantiated by results from several similar specimens (see fig. 9).

4. RELATION BETWEEN STATIC AND DYNAMIC COEFFICIENTS

It is evident from figure 7 that the coefficients of dynamic friction for speeds of 10^{-3} cm/sec or more are greater than the coefficient of static friction, but it appears that at a speed of 10^{-4} cm/sec the dynamic coefficients are the smaller. This phenomenon leads one to believe that if a specimen were once sliding under nearly equilibrium conditions, it should continue to slide down a track which is inclined at an angle less than the angle of repose. Accordingly, a specimen of type

150, for which several determinations showed that the angle of repose was not less than $\tan^{-1}$ 1.2, was placed on the inclined glass track and allowed to slide about 2 hours with the angle of incline at $\tan^{-1}$ 1.3. The angle was then decreased by small amounts at intervals of from 1 to several hours until it reached a value of $\tan^{-1}$ 1.1, where it was left for nearly 3 days. During this time the specimen slid about 12 cm, with an average and nearly constant speed of slide of 4.8×10^{-5} cm/sec. The angle was again decreased by small steps until a value of $\tan^{-1}$ 1.0 was reached. With the track at this angle the specimen slid continuously for about 9 days, moving 16.5 cm at an average speed of 2.1×10^{-5} cm/sec. Thus experiments with both horizontal and inclined tracks show that at very low speeds the coefficient of dynamic friction is less than the static coefficient.

5. EFFECTS OF VARIOUS FACTORS ON THE COEFFICIENTS OF DYNAMIC FRICTION

The effects produced on the coefficients of dynamic friction by changes of several experimental conditions are shown in figures 9, 10, and 11. Each experimental point in these figures represents the nearly constant coefficient attained after several centimeters of slide. The four graphs of data plotted in figure 9 show principally comparisons between the coefficients of friction of channel-black specimens of type 150 and type *F*, when sliding at different speeds on glass and on steel. The individual graphs show the effects of changing other conditions, but these will be discussed under separate headings. Much of the work presented in this figure has been substantiated by experiments on inclined tracks; but in order to avoid further complications of the graphs, these data have been omitted. Figure 10 shows the coefficients of friction for one channel-black specimen of each of the two sizes, when sliding under different normal pressures at a speed of 0.1 cm/sec on glass. Figures 7 and 10 were obtained from specimens which were cleaned with acetone prior to each test, but figure 11 shows the effect of omitting this precaution.

(a) SLIDING SPEED

The data for coefficients of friction of rubber presented in figures 8, 9, and 11 have been plotted as a function of the speed. In every case the coefficient increases with the speed. This increase becomes relatively more pronounced for smoother and for cleaner sliding surfaces. In most cases the rate of increase of the coefficient in respect to the speed becomes less for speeds over 0.1 cm/sec.

Similar increases in the coefficients are also shown throughout the earlier experiments (section II–1), where the conditions were quite different from those in the later experiments. The only cases in which the coefficients are independent of the speed are those for which the sliding surfaces were lubricated with graphite or castor oil.

Large decreases in the coefficients of all the specimens were observed when the speed reached a value at which the specimen began to vibrate or chatter. Chattering usually occurred between 5 and 10 cm/sec for the channel-black specimens of types *F* and 150. Specimens of softer compounds and those with smoother surfaces began to chatter at lower speeds.

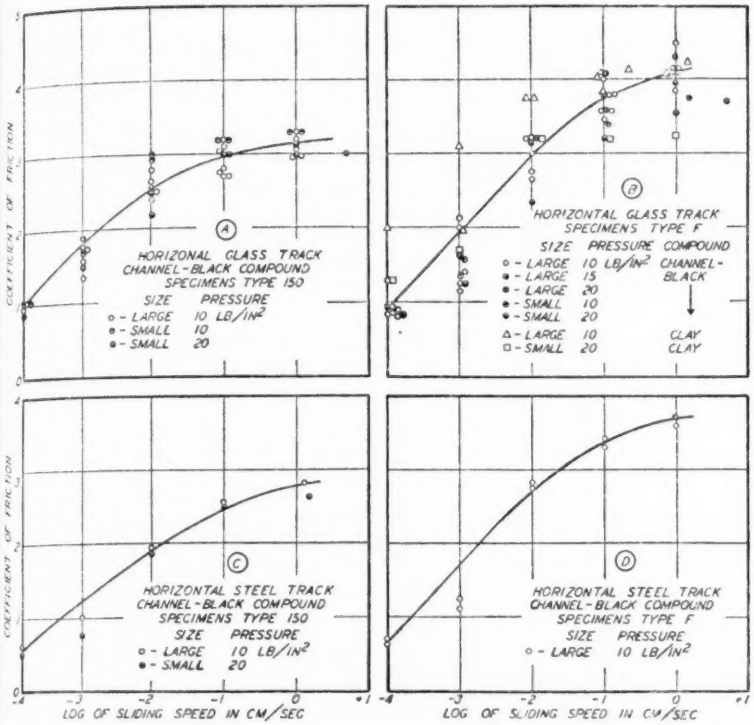

FIGURE 9.—*Comparison between the coefficients of friction of channel-black specimens type 150 and type F when sliding on glass and on steel tracks.*

The individual graphs show variations in the coefficients for nominally identical specimens, for specimens of different sizes, and for various pressures. The dimensions of the large and small specimens are, respectively, ¾ by 1½ in. and 5/16 by 1⅛ in. Graph *B* also compares coefficients obtained for the channel-black and clay compounds.

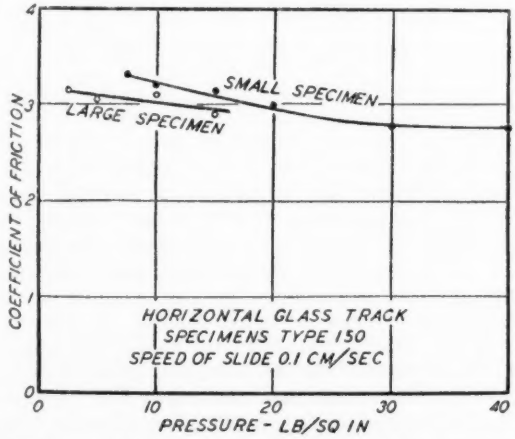

FIGURE 10.—*Coefficients of friction of rubber when sliding under different normal pressures on a glass track.*

(b) ROUGHNESS OF THE SLIDING SURFACES

The data obtained in this investigation indicate that, except for very low speeds, less than 10^{-3} cm/sec, the rougher the specimen surface or the rougher the friction track, the lower are the observed coefficients of friction.

The effect of the roughness of the specimen surface on the observed coefficients is suggested in part by the data shown in figure 9, where at any given speed except the lowest, the coefficients for specimens type *F* sliding on either glass or on steel are greater than the corresponding coefficients for specimens type 150. Additional confirmation of this effect is shown by a study of several specimens which had been molded against unroughened plate glass. The results obtained from these

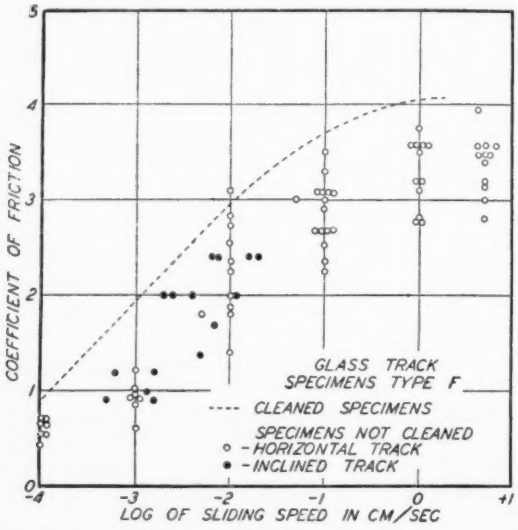

FIGURE 11.—*Coefficients of friction of rubber on glass, showing the effect of omitting the precaution of cleaning the surface of the specimens with acetone prior to the test.*

The broken-line curve is the curve shown in figure 9 (*B*).

specimens are not shown here because it was evident from the appearance of the sliding surfaces that only parts of them had actually come into contact with the track, and that the proportion of each specimen surface which made contact with the track varied considerably between individual specimens. However, it could be seen in spite of the great scattering of the data, that the coefficients for the smooth specimens were appreciably higher, especially for intermediate speeds, than those for specimens type *F*. Furthermore, it was found that there were appreciable differences in the coefficients obtained for individual specimens of type *F*, figure 9 (*B*). A closer examination of some of these specimens revealed that there were slight differences in the apparent roughness of these specimens, those showing the higher coefficients having a finer surface texture. For instance, in figure 6, *A* and *B* are both photomicrographs of specimens type *F*, but the surface of *A* appears to be of a finer texture than that for *B*. Correspondingly, the coefficients obtained from *A* are appreciably higher.

The effect of the roughness of the track is illustrated by the data presented in figure 1. In this work the rubber specimens were drawn over various abrasive tracks, and, except for the lowest speed, the smaller the abrasive particles the higher were the coefficients obtained. Further evidence, though not conclusive in itself, is shown by figure 9, where the coefficients for rubber on steel were found to be slightly less than the coefficients for corresponding specimens at the same speeds on glass. This difference might be due to differences in the nature of the materials, but it seems more likely to be due to the relative smoothness of the surfaces of the tracks, the glass track being somewhat smoother than the steel.

(c) SURFACE AREA AND NORMAL PRESSURE

There seems to be no relationship between the coefficients and the specimen sizes. The data in figure 9 show that differences between nominally identical specimens are of the same order as the differences between specimens of the two sizes employed. Figure 10 shows that the coefficients decrease only slightly with increasing pressure. In this figure the coefficients are plotted as a function of the normal pressure for one channel-black specimen of each of the two sizes when sliding on glass at a speed of 0.1 cm/sec. The range of pressures investigated, 2.5 to 40 lb/in.^{2}, was determined by limitations of the apparatus.

(d) VIBRATION OF THE APPARATUS

The values shown in figure 9 (*C* and *D*) for the coefficients of friction at the speed of 10^{-3} cm/sec seem to be somewhat lower than would be expected from the values at the other speeds. A comparison of these coefficients with the results obtained from the inclined track also showed some discrepancy. It was found that the motor was causing vibration in the apparatus at this speed. When this vibration was eliminated, the observed coefficients became somewhat higher and in better agreement with those obtained from the inclined track. The values shown in figures 7 and 8, and part of those shown in figure 9 (*A* and *B*) were obtained after the vibration had been eliminated. Further indications of the effect of vibration on the observed coefficients of friction is shown by the data for the lowest speeds plotted in figure 7 (*A* and *C*). In the case of the horizontal track, figure 7 (*A*), the seventh point represents an observation taken early in the morning, before general activity in the building began. The value of this coefficient is higher than those observed later in the day and during the previous day. Likewise, the seventh point for the inclined track, figure 7 (*C*) represents the average speed during the night. This point is well below the other points, all of which represent speeds during the 2 days. Observations such as these have been made repeatedly.

(e) COMPOSITION OF THE RUBBER COMPOUND

The frictional properties of a rubber compound seem to be dependent more on the rubber matrix than on the compounding ingredients or fillers. Since cleaned specimens of very soft rubber compounds show a strong tendency to chatter or vibrate on the tracks even at relatively low speeds, only a limited amount of work was done with such compounds. Observations were made of the clay compound

described in table 2, and data for three specimens of this compound were plotted in figure 9 (*B*) for the purpose of comparing them with the data for channel-black specimens which had similar sliding surfaces. The surfaces of the specimens of both compounds were produced by molding them against plate glass which had been roughened with carborundum flour. The size of the clay specimens was the same as for the larger channel-black specimens, and the normal pressure was 10 lb/in.^{2} The values of the coefficients for the clay specimens are rather widely scattered, but for any one specimen the general changes in the coefficients in respect to speed are quite similar to those obtained for the channel-black specimens.

A specimen taken from the tread of a used tire also showed frictional properties which were similar to those obtained from the prepared channel-black specimens. The surface of this specimen, shown in figure 6 (*D*), had some rather high and low regions, but the general surface texture seemed to be not far different from some of the prepared specimens. Because the cement bond between the rubber and the rigid back for this specimen was not so strong as the bond between the rubber and the steel on the other specimens, the pressure was limited to about 6 lb/in^2. The values of the coefficients of dynamic friction obtained on the horizontal glass track for this specimen, after cleaning it with acetone, were 1.3, 1.7, 2.1, 2.4, 3.0, and 3.4, respectively, for speeds of 0.0001, 0.001, 0.01, 0.1, 1.0, and 5 cm/sec. These values are in approximate agreement with those given in figure 9 (*A*) for specimens of type 150. The coefficients observed before cleaning ranged from 0.7 at 0.01 cm/sec to 1.1 at 1.0 cm/sec. The frictional forces for the clean specimen showed the usual increase in value during the first several centimeters of slide at speeds over 0.001 cm/sec, and a decrease in value during the first several millimeters of slide at 0.0001 cm/sec. Chattering of the specimen occurred during part of the sliding at speeds of 1 and 5 cm/sec.

Another comparison between coefficients of friction of two widely differing compounds is shown in figure 2. Because of the differences in the experimental procedures, the actual values of the coefficients in this figure cannot be compared to those obtained in the later experiments (section II–2), but it can be seen that the coefficients for these two compounds do not differ greatly over the range of speeds investigated.

(f) CLEANING THE SPECIMENS

The specimens which were used for obtaining the data shown in figures 7 to 10 were cleaned with acetone prior to each test. This procedure made possible more uniform results than could be obtained otherwise, and the actual values observed for the coefficients were not greatly different from those obtained when the specimens were tested immediately after removing them from the molds. Cleaning the specimens also permitted using them repeatedly with no observable change in frictional properties, whereas uncleaned specimens showed progressively lower coefficients as blooming progressed. Consequently, by cleaning the specimens it was possible to determine the equilibrium coefficients of dynamic friction of the same specimen for various conditions of slide (different speeds, normal pressure, horizontal and inclined tracks, etc.) instead of using a new specimen for each test and introducing unavoidable differences in surface roughness.

As an illustration of the effects of omitting the precaution of cleaning the specimens, a number of coefficients of dynamic friction for uncleaned specimens are plotted as a function of the logarithm of the speed in figure 11. The specimens for this work were left in the mold about 2 days after vulcanizing and were placed on the friction apparatus as soon after removing them from the mold as possible. This procedure kept the specimens relatively clean and free from bloom, though probably not entirely so. As a means of comparing these values with those obtained from specimens which were cleaned with acetone, the curve from figure 9 (*B*) is shown as a broken line. The data for both graphs were obtained from specimens with the same type of surface, namely type *F*. Figure 11 shows that the values of the coefficients for the uncleaned specimens scatter rather widely, but approach the values of the cleaned specimens as an upper limit. Similar observations have been made for specimens type 150.

(g) MOISTURE

Although the relative humidities in the laboratory ranged from 10 to 80 percent during the investigation of the coefficients of friction of rubber on steel and rubber on glass, there was no observable correlation between the coefficients observed and the relative humidity. In the case of rubber sliding on glass, the presence of visible water on the track or the specimen resulted in a sharp decrease in the coefficients observed. When the track was submerged in water, the values of the coefficients decreased to about 4 or 5 percent of the values obtained for dry surfaces. Coefficients obtained after wetting the track and the specimen with water and allowing it to evaporate until all the visible water disappeared were not observably different from coefficients obtained after drying the surfaces with acetone. No attempts were made to remove adsorbed water from the glass surface.

The effects of water on the coefficient of friction of rubber on steel were not studied, because of the possibility of changes in the nature of the steel surface due to corrosion.

6. SUMMARY OF RESULTS

The experimental results obtained from this investigation may be briefly summarized as follows:

1. Dynamic friction increases with speed up to a certain critical speed at which the specimens chatter. The dynamic friction is less than static friction only at speeds less than about 10^{-3} cm/sec.

2. Clean rubber specimens slide several centimeters before the friction becomes constant.

3. Except for very low speeds, the rougher the surfaces the lower are the observed coefficients.

4. The coefficient of friction of a rubber compound seems to be dependent more on the rubber matrix than on the compounding ingredients and fillers.

IV. DISCUSSION

The four generalizations listed in the foregoing summary of results are discussed in order here under separate headings.

1. SLIDING SPEED

The increase of friction with speed for speeds ranging from 10^{-4} to 10 cm/sec was evident throughout the investigation. At the lowest speeds the values of the coefficients were seldom much over unity and were usually somewhat less. For speeds greater than the order of about 10^{-3} cm/sec. the dynamic friction became greater than the static friction. For the highest speeds at which the specimens slid smoothly, the coefficients reached values ranging from somewhat over 2 to more than 4, depending on the cleanliness and smoothness of the sliding surfaces. The limiting speed of smooth sliding seemed to be determined by the properties of the specimen, being nearly 10 cm/sec for the channel-black compound and less for softer compounds. The effect of the geometry of the specimen on this limiting speed was not studied, although there was no observable difference between the two sizes of specimens employed in the investigation.

(a) CHANGE OF FRICTION WITH SPEED

Observations of coefficients of static friction which were less than dynamic coefficients and observations of dynamic friction which increased with speed have been reported at various times for rubber and for other materials. However, the reports do not include observations of such high values for the coefficients as have been found in the present investigation on rubber. That the static friction for rubber was less than dynamic friction was reported by W. S. James in 1924 [6], and by J. B. Derieux in 1934 [7], for sections of tires sliding on various surfaces. Derieux also reported that the friction increases with speed. R. Ariano [8] found that when a rubber belt was allowed to slip over a pulley, the coefficient of friction increased with the speed of slip. In an investigation of the frictional properties of small rubber blocks sliding on wet and on dry roadway materials, Papenhuyzen [2] also showed coefficients of friction which increased with the speed.

A large proportion of the investigations on the frictional properties of rubber has dealt with the skidding of tires on roads. In many of the earlier investigations the tire was dragged on the road and the forces for starting the motion and for maintaining it at some constant speed were used in determining, respectively, the coefficients of static and dynamic friction. Sliding speeds of less than 3 mph (about 135 cm/sec) were seldom studied. It can be seen that if the coefficient increases sharply with speed and reaches a maximum value at a speed much lower than the one investigated, this maximum coefficient would be reached before the observer was aware that the specimen was moving and consequently would appear to the observer to be the coefficient of static friction. Thus one may readily account for the many observations of static coefficients which were greater than the dynamic coefficients. In more recent investigations [3, 9, 10] the coefficients were determined for various amounts of slip as the tire rolls along the road. In general, when braking forces or accelerating forces are applied, the tires begin to slip, so that the speed of rotation is not equal to the speed of a free-rolling wheel.

When a braking force is applied to the wheel, the amount of this slippage increases with the force until the wheel locks and slides. Moyer [3] showed that for a speed of 20 mph on wet concrete, the coefficients of friction increased sharply with increasing percentage of

slip, reaching a maximum value when the slip reached about 18 percent of the vehicle velocity. The coefficient of friction reached 90 percent of its maximum value at about 5-percent slip. A slip of 5 percent at 20 mph corresponds to a sliding speed of 45 cm/sec. The coefficients decreased as the slip increased above 18 percent. Schmid [9] showed similar results for various types of roads by means of autographic recording of the braking force and the angular speed of the wheel. At 4 kilometers per hour (about 2.5 mph) the coefficient of friction rose sharply with increasing slip up to 10 percent of the speed of the vehicle and then rose less rapidly as the slip increased to about 20 percent. Beyond 20-percent slippage the wheel often locked and the coefficient decreased. Because of the tendency for the wheel to lock, difficulty was encountered in determining coefficients for slippages above the point at which the coefficient reached a maximum value. Similar increases of friction with increasing slip have been obtained for various types of roads at the National Physical Laboratory [10].

(b) VIBRATIONS

It is well known that when rubber slides on a solid surface, as in the case of a tire on the road, a distinctly audible vibration often occurs. In most of the investigations on frictional properties of tires, or of other rubber products, such vibrations seem not to have been given much attention. The coefficient of friction is usually regarded as the ratio of the average towing force to the load irrespective of the condition of slide. Papenhuyzen [2], however, does study such vibrations for rubber sliding on glass and for rubber sliding on roadway materials. Employing an apparatus in which one end of a cylindrical rubber specimen was held coaxially against the face of a rotating disk of glass or of roadway material, he found that vibrations occurred at a critical speed which was greater for the roadway material than for glass. Below this critical speed, sliding was smooth, that is, no vibration occurred. Examination of the vibratory motion at speeds immediately above the critical speed by means of motion pictures showed that the cycle of vibration consisted of two parts, one in which the specimen was distorted and the other in which the specimen "broke free" [3] and quickly receded to a position of much less distortion. The time required for the specimen to reach its maximum distortion depended on the speed of the disk and the amount the specimen slipped during the time of the distortion. This slippage was small, but observable. The time of relaxation depended largely on the physical characteristics of the specimen.

Vibrations of this type are known as mechanical relaxation oscillations [11]. Analogous oscillations occur in certain electric circuits. Mechanical relaxation oscillations are observed in oscillating systems of small inertia, where the restoring force increases with the displacement. An extensive study of such oscillations has been made of the bowed violin string [12]. Oscillations of this type have been explained [11, 13, 14] as being due to a decrease in friction with increasing speed. The decrease in friction with increasing speed was not actually observed in the present investigation, but figures 1, 2, 4, and 9 indicate that the friction approached a maximum at the speed at which chat-

[3] In our investigation with tracks which were inclined at relatively large angles, specimens often "broke free" from a condition of uniform speed and slid down the rest of the track with greatly accelerated motion.

tering occured. Thus, it is reasonable to suppose that the chatter was accompanied by a decrease in friction beyond this maximum and that the chattering was a manifestation of relaxation oscillations.

Mechanical relaxation oscillations have been observed for materials other than rubber, metals in particular, but only with measuring apparatus which possesses certain dynamical properties. Kaidanovsky and Haykin [11] studied such oscillations for a lubricated cylindrical journal bearing and stated that in order to obtain such oscillations it was necessary that the dynamic friction decrease with speed. Haykin, Lissovsky, and Solomonsky [15] describe these experiments in English and account for the "stick-slip" phenomenon of Bowden and Leben [16], in which no lubricant was employed, as a manifestation of such oscillations. Extensive studies of mechanical relaxation oscillations for both lubricated and unlubricated metals have been recently reported by Morgan, Muskat, and Reed [17].

In a theoretical discussion of relaxation oscillations, H. Blok [13] points out that these oscillations are not necessarily audible, but that they may be either subsonic or ultrasonic, depending on the characteristics of the sliding system. He also shows that for certain materials and under certain conditions the amplitude of the vibrations may be very small, and he calls such oscillations "micro-vibrations."

2. CHANGES IN FRICTION AT THE START OF SLIDE

It was shown in figure 7 that when a rubber specimen was towed on the friction track, the coefficient of friction changed during the first several centimeters of slide. These changes were apparently from a value which may be regarded as the static coefficient to a constant equilibrium value, which may be regarded as the coefficient of dynamic friction for that particular speed. For speeds greater than 10^{-3} cm/sec the coefficient increased from the initial value, and at speeds appreciably less than 10^{-3} cm/sec the coefficient decreased. This change in friction may be connected with the peculiar properties of thin films of water which may be present on the sliding surfaces. Derjaguin [18] has shown that thin films of water possess definite and measurable shear moduli and yield points. A further confirmation of the rigid properties of thin films of water has recently been reported by Eversole and Lahr [19]. An explanation of this property of the film supposes the existence of long chains of oriented water molecules extending from the solid surfaces into the interior of the liquid. Papenhuyzen [2] supposes that the presence of such films on the sliding surfaces would account for values of friction which are higher than would otherwise be observed. In addition he supposes that the orientation of the molecules and the formation of the chains would be enhanced by sliding of the surfaces, and that a certain time would be required for the formation of these chains. This idea is similar to that presented by Hardy and Doubleday [20] in explanation of the time required to reach equilibrium conditions of slide when certain oils are employed as boundary lubricants.

If one were to apply this idea to the data in figure 7, one would arrive at a chain formation time of about 10 seconds for the speed of 1.0 cm/sec, 100 seconds of 0.1 cm/sec, and so on. At the speed of 10^{-4} cm/sec, however, the chains do not seem to be formed, since the friction decreases to its equilibrium value.

3. ROUGHNESS OF THE SLIDING SURFACES

That the higher coefficients are obtained with the smoother surfaces is in contradiction to frictional characteristics for many commonly observed sliding conditions. This conclusion, however, applies only to the range of speeds from about 10^{-3} cm/sec to speeds at which the specimens vibrate. Below 10^{-3} cm/sec it appears that the rougher surfaces show the higher coefficients. It will be noted that the speed of about 10^{-3} cm/sec is also the critical speed above which the coefficients at the start of slide increase, and below which they decrease.

Since measurements of the area of contact could not be made without considerable difficulty, no attempt was made to correlate the various coefficients with the actual contact area of the specimens. The finer surfaces present more points of contact than do the coarser surfaces, but this fact does not indicate the relative contact areas.

4. COMPOSITION OF THE RUBBER COMPOUND

Since rubber is the external phase in a rubber-filler system, one might expect that the filler should not greatly affect the frictional properties of the compound. Changes in other physical properties, modulus of rigidity for example, would necessarily affect the critical speed at which vibrations in the specimen occur. The inclusion of waxes, oils, or other materials in the compound which come to the surface would be likely to affect the coefficients greatly, and were avoided as far as possible in this work. Cleaning the specimens prevented lubrication due to blooming of the ingredients which were employed.

V. REFERENCES

[1] T. R. Dawson and B. D. Porritt, Rubber, Physical and Chemical Properties, p. 381 (Research Assoc. of British Rubber Manufacturers, Croydon, England, 1935.)

[2] P. J. Papenhuyzen, *Friction experiments in connection with the slipping of automobile tires*, De Ingenieur, **53–2,** p. V.75 (1938).

[3] R. A. Moyer, *Skidding characteristics of road surfaces*, Proc. 13th Ann. Meeting Highway Res. Board, pt. 1, p. 123 (1933); see also, Iowa State College Eng. Exp. Sta. Bul. 120 (1934).

[4] W. F. Busse and W. H. Denton, *Water lubricated bearings*, India Rubber J. **84,** 347 (1932).

[5] F. L. Roth and W. L. Holt, *Tensile properties of rubber compounds at high rates of stretch*, J. Research NBS **23,** 603 (1939) RP1256.

[6] W. S. James, *Brake-performance studies*, J. Soc. Automotive Engrs. **14,** 236 (1924).

[7] J. B. Derieux, *The coefficient of friction of rubber*, J. Elisha Mitchell Sci. Soc. **50,** 53 (1934); Rubber Chem. Tech. **8,** 441 (1935).

[8] R. Ariano, *The coefficient of friction between rubber and various materials—Part II*, Politecnico, No. 10 and 11 (1929); India Rubber J. **79,** 56 (1930); Rubber Chem. Tech. **3,** 287 (1930).

[9] C. Schmid, *Frictional forces between tire and road*, Automobiltech. Z. p. 392 (Aug. 10, 1938); Abstract, Inst. Automobile Eng. J. (London) **7,** 57 (1930).

[10] J. Bradley and R. F. Allen, *Factors affecting the behavior of rubber-tired wheels on road surfaces*, Proc. Inst. Automobile Eng. (London) **25,** 63 (1930).

[11] N. Kaidanovsky and S. Haykin, *Mechanical relaxation oscillations*, J. Tech. Phys. (U. S. S. R.) **3,** 91 (1933).

[12] C. V. Raman, *On the mechanical theory of vibrations of bowed strings and of musical instruments of the violin family, with experimental verification of the results; Part I*, Indian Assoc. Cultivation Sci. Bul. No. 15 (1918).

[13] H. Blok, *Fundamental mechanical aspects of boundary lubrication*, J. Soc. Automotive Eng. **46,** 54 (1940).

[14] J. P. Den Hartog, Mechanical Vibrations (McGraw-Hill Book Company, New York, N. Y. 1934).

[15] S. Haykin, L. Lissovsky, and A. Solomonsky, *On the "jerky character" of frictional force*, J. Phys. (U. S. S. R.) **2,** 253 (1940).
[16] F. P. Bowden and L. Leben, *The nature of sliding friction and analysis of friction*, Proc. Roy. Soc. (London) [A] **169,** 371 (1938).
[17] F. Morgan, M. Muskat, and D. W. Reed, *Friction phenomena and the stick-slip process*, J. Applied Phys. **12,** 743 (1941).
[18] B. Derjaguin, *Shear elasticity of water films*, Z. Physik **84,** 657 (1933).
[19] W. G. Eversole and Paul H. Lahr, *The thickness of the rigid water film at a quartz-water interface from a measurement of Newton's rings*, J. Chem. Phys. **9,** 686, (1941).
[20] W. B. Hardy and Ida Doubleday, *Boundary lubrication:—The latent period and mixtures of two lubricants.* Proc. Roy. Soc. (London) [A] **104,** 25 (1923).

WASHINGTON, February 13, 1942.

U. S. DEPARTMENT OF COMMERCE NATIONAL BUREAU OF STANDARDS

RESEARCH PAPER RP1464

Part of Journal of Research of the National Bureau of Standards, Volume 28, April 1942

THE FIRST SPECTRUM OF ANTIMONY

By William F. Meggers and Curtis J. Humphreys

ABSTRACT

The spectrum emitted by neutral antimony atoms has been photographed, measured, and analyzed. Measured wavelengths and estimated relative intensities are given for 466 lines, ranging from 1388.91 to 12466.75 A in wavelength and from 1 to 2500 in intensity. Nearly 80 percent of these lines are classified as combinations of 60 even energy levels arising from $5s^2\,5p^2\,ns$, $5s^2\,5p^2\,nd$, and $5s5p^4$ electron configurations and 31 odd levels from $5s^2\,5p^3$, $5s^2\,5p^2\,np$, and possibly $5s^2\,5p^2\,nf$. The average difference between observed and computed wave numbers is 0.15 cm^{-1}. A paucity of lines in the visible spectrum and intense radiation of antimony atoms in the ultraviolet and infrared are seen to be consequences of the relative values of various groups of levels. Although it is not possible to give a complete quantum interpretation of all the levels, several spectral series of the type $5s^2\,5p^3-5s^2\,5p^2\,ns$ are proposed, and an absolute value of 69700 cm^{-1} is deduced for the ground state, $5s^2\,5p^3.{}^4S_{3/2}$, of neutral antimony atoms. From spectroscopic data, the principal ionization potential of antimony is calculated to be 8.64 volts.

CONTENTS

	Page
I. Introduction	463
II. Experiments	465
III. Results	467
1. Wavelengths of Sb I lines	467
2. Term structure of the Sb I spectrum	472
3. Spectral series and ionization potential	474
IV. References	478

I. INTRODUCTION

During the past 90 years the emission spectra of antimony have been described and discussed in scientific literature more than 100 times, but unfortunately it remained true that information on this subject was far from complete or satisfactory. Undoubtedly, this state of affairs for the first spectrum of antimony is attributable, at least in part, to the extraordinary character of this spectrum. When antimony atoms are excited to radiate in flames or in electric arcs they emit next to nothing in the visible range but radiate powerfully in the ultraviolet and infrared. Under similar circumstances most metals emit atomic spectra with maximum intensity in or near the visible and with relatively little strength in the shorter ultraviolet or longer infrared.

Several years ago when improved infrared-sensitive photographic plates became available we succeeded in recording all antimony waves previously observed only radiometrically, and in addition found many

446682—42——5

new lines of long wavelength. Efforts to classify the new lines as combinations of known energy levels disclosed the fact that relatively little was known about the structure of this spectrum. Discrepancies among the data and interpretations of different workers appeared to be explained mainly by incomplete and unreliable descriptions. We, therefore, decided to observe the entire spectrum more carefully. The arc spectrum of antimony was accordingly photographed and measured from its limit below 1400 A in the ultraviolet to wavelengths exceeding 12000 A in the infrared. The results of this investigation are reported in this paper.

References to 54 publications dealing with the spectra of antimony previous to 1912 have been compiled and discussed by Kayser [1].[1] About 50 more papers concerned with antimony spectra have since appeared, but only those which are considered relevant to the description and analysis of the Sb I spectrum will be mentioned here. It may be noted that the first useful measurements of antimony arc spectra were made by Kayser and Runge [2] in 1893. They measured the wavelengths of 70 Sb arc lines (5730.52 to 2068.54 A) on Rowland's scale and at the same time discovered the first regularities in this spectrum. Schippers [3], a student of Kayser's, measured both the arc and the spark spectrum of antimony relative to international standards for the first time in 1912. In the arc spectrum he measured 94 lines (2068.38 to 6648.134 A), but 2 of these (5700, 5782) represent copper, and 15 others (5774 to 6648 A) have not been confirmed as characteristic of antimony. Walters [4] in 1921 photographed 75 antimony arc lines with wavelengths between 5531.89 and 9132.30 A, using plates sensitized by bathing in solutions of pinacyanol and dicyanin. The only other long-wave antimony data published heretofore are wavelengths and galvanometer deflections for 16 lines (9519.9 to 12118.9 A) detected radiometrically by Randall [5] in a 20-ampere carbon arc in which antimony metal was vaporized. An attempt by Lehmann [6] to observe the infrared arc spectrum of antimony by means of phosphorophotography did not yield any important results.

The first investigation of the arc spectrum of antimony for emission shorter than 2000 A was made in 1917 by Takamine and Nitta [7], who photographed, with a small quartz spectrograph, 13 lines with wavelengths ranging from 1989.3 to 1890.3 A. McLennan, Young, and Ireton [8], working with a small fluorite spectrograph in 1920, reported 36 lines (1931.0 to 1437.0 A) as characteristic of the antimony arc in a vacuum. During the past 20 years the only other attempt to describe the first spectrum of antimony in the extreme ultraviolet is that of L. and E. Bloch [9], who varied conditions in an electrodeless discharge and separated the observed lines into five successive stages of ionization. Unfortunately, the electrodeless discharge gave a very feeble Sb I spectrum, so that only six lines shorter than 2000 A (1970.88 to 1698.91 A) were assigned to the first spectrum. Comparison of the above lists with each other shows little or no agreement and brands each and all of them entirely inadequate as a useful description of the extreme ultraviolet Sb I spectrum.

The most direct manner of determining the normal state of any atom is to observe which of its characteristic atomic spectral lines are absorbed by unexcited atoms. Attempts to do this for antimony

[1] Figures in brackets indicate the literature references at the end of this paper.

have been made by Dobbie and Fox [10], Grotrian [11], Ruark, et al. [12], Narayan and Rao [13], McLennan and McLay [14], Frayne and Smith [15], Zumstein [16], and Charola [17]. Most of these observers found only banded and continuous absorption, indicating that unexcited antimony vapor is usually polyatomic. McLennan and McLay [14] reported finding four lines absorbed in the extreme ultraviolet (1525.2, 1514.1, 1483.5, and 1481.0 A), but it is doubtful if any of these represent antimony. By slowly admitting antimony vapor into a hot carbon tube at about 1,400° C, Zumstein [16] obtained a dissociation of the molecules into atoms, and observed five absorption lines with wavelengths 2311.50, 2175.88, 2127.46, 2068.38, and 2023.86 A. These lines are shown by analysis of spectral structure to result from combinations of the ground state with the first five excited states; they are the only ones longer than 2000 A that can be absorbed by neutral antimony atoms.

It has been observed repeatedly that many ultraviolet antimony lines are more or less self-reversed in the ordinary arc and in the underwater spark. An investigation of the latter phenomenon was made in 1924 by Hulburt [18], who found that for antimony the underwater spark reversals included all the observed arc reversals and seven lines in addition (2224.98, 2220.80, 2207.7, 2145.03, 2141.8, 2139.76, 2127.55 A). Buffam and Ireton [19] also studied the underwater spark of antimony but observed only eight lines (2790.50, 2769.97, 2670.81, 2652.73, 2598.24, 2528.68, 2311.71, 2288.99 A), the first of which belongs to Sb II.

The Zeeman effect of antimony lines has been measured by van der Harst [20] and by Löwenthal [21]. The former observed 29 lines (2311 to 4352 A), but all patterns are given as triplets except 4 quartets and 1 quintet. Löwenthal published only 18 lines (2311 to 4033 A) but employed higher resolution, which permitted the calculation of precise values for the splitting factors and absolute determination of the inner quantum numbers of the atomic energy levels.

Further publications dealing with antimony spectra will be noted below in connection with the discussion of our results.

II. EXPERIMENTS

This new description of the Sb I spectrum was obtained by employing conventional arcs (and sparks) at atmospheric pressure and photographing the spectra from 2000 to 13000 A with large concave gratings. Arcs were operated on a direct-current circuit with 220 volts applied potential, and with a series resistance to regulate the current between 6 and 12 amperes, except for the ultraviolet, as described below. Antimony has a relatively low melting point (630°C), and for this reason it is not possible to use solid electrodes in the arc. Lumps of pure antimony were burned in an arc having a pure copper rod (6 mm in diameter) as upper electrode and a pool of molten antimony in a cupped lower electrode of copper (12 mm in diameter). Comparison spark spectra of antimony were made throughout the visible and ultraviolet to 2000 A, so that any lines belonging to ionized atoms which might appear on the arc spectrograms could be recognized and removed from the final list of Sb I lines.

The extreme ultraviolet data for wavelengths shorter than 2000 A were obtained from arc spectrograms made by A. G. Shenstone at

Princeton University. Shenstone used arcs of 1 to 2½ amperes between water-cooled electrodes of pure antimony, or antimony versus copper or carbon, in an atmosphere of pure nitrogen. The interval 1200 to 2200 A was recorded on Ilford Q plates with a normal-incidence vacuum spectrograph [22] having a 2–m glass grating ruled 30,000 lines to the inch. The dispersion is 4.2 A/mm and the definition and resolving power are excellent, although the photographic contrast of the plates used is rather low. Full exposures were obtained in 30 minutes.

On spectrograms made by Shenstone, it was easy to distinguish between lines characteristic of neutral atoms and those arising from ionized atoms because the latter appeared only (or greatly enhanced) at the electrodes. Among some 300 antimony lines appearing in arc spectrograms from 1239 to 2200 A, at least 70 were recognized as belonging to ionized atoms.

Spectrograms covering the range 2000 to 13000 A were made at this Bureau with stigmatic concave-grating spectrographs [23]. An aluminized Pyrex grating (22 ft in radius) ruled 30,000 lines per inch was used in the first order from 2000 to 8200 A and in the second order from 2500 to 4300 A. In the second order the dispersion averages 1 A/mm. The entire infrared photographically accessible was recorded with a speculum grating ruled with 7,500 lines per inch, giving a scale of 10 A/mm. With these spectrographs and with the photographic plates listed below, exposure times required to photograph the arc spectrum of antimony ranged from 1 or 2 minutes in the near ultraviolet to 4 hours for the infrared limit. The following types of spectroscopic plates supplied by the Research Laboratory of the Eastman Kodak Co. [24] were used. Plates coated with No. 33 emulsion were employed in the range 2000 to 4800 A, *F*-sensitized plates from 4500 to 6800 A, *N*-sensitized from 6500 to 8500 A, *Q*-sensitized from 8000 to 11000 A, and *Z*-sensitized from 10000 to 13000 A.

The wavelengths of antimony lines were measured by interpolating between standard lines of iron, the iron arc spectrum being photographed adjacent to antimony on all spectrograms except those in the extreme ultraviolet, which had sufficient lines of copper, carbon, nitrogen, or oxygen to fix the scale and corrections for each exposure. These antimony wavelengths are thus based on international secondary standards of iron [25] or on interferometer values of iron and copper lines by Burns and Walters [26], supplemented in the extreme ultraviolet by values of carbon, nitrogen, and oxygen "impurity" lines recommended as tentative standards by Boyce and Robinson [27]. In the infrared and ultraviolet, outside the present limits of international secondary standards (6700 to 2500 A) interferometer values of iron lines measured at this Bureau [28] were used as standards. Beyond 8600 A the first-order grating spectrum of antimony was usually measured relative to iron lines in the second or third order, doubling or trebling the interpolated values of the apparent wavelengths of antimony lines to obtain their true values. It will be understood that the first-order was photographed with an infrared filter interposed between source and slit, whereas the second and third orders were recorded by removing the filter.

All spectrograms were measured both direct and reversed on a comparator reading to 0.001 mm, and all lines were observed on four

or more spectrograms except the faintest, which were discarded unless confirmed by a second exposure. It is difficult to determine the wavelengths of antimony lines from conventional sources within 0.01 A because most of the line images are either hazy, wide, and unsymmetrical, or wide and more or less self-reversed. Nevertheless, the agreement between results from different spectrograms, and the establishment of additional energy levels reported below, indicate that the description of the first spectrum of antimony has been improved as well as greatly extended.

III. RESULTS

1. WAVELENGTHS OF Sb I LINES

Data for 466 lines characteristic of neutral antimony atoms are presented in table 1, where wavelengths, relative intensities, vacuum wave numbers, term combinations of classified lines, and differences of observed and calculated wave numbers appear in successive columns. Since the wavelengths shorter than 2000 A are vacuum values, the corresponding wave numbers are direct reciprocals of the observed wavelengths. The remaining wavelengths are valid for standard air and must be multiplied by the refractive index of air to convert them to vacuum values. Vacuum wave numbers for lines between 2000 and 10000 A were taken directly from Kayser's "Tabelle der Schwingungszahlen" [29], but for lines of longer wavelengths the values were obtained by computing the reciprocals of the wavelengths which have been corrected to vacuum with the aid of the dispersion formula of Meggers and Peters [30].

TABLE 1.—*First spectrum of antimony* (Sb I)

λ_{air} A	Intensity, character	$\nu_{vac.}$ cm^{-1}	Combination	$\nu_{obs.}-\nu_{calc.}$ 0.1 cm^{-1}	λ_{air} A	Intensity, character	$\nu_{vac.}$ cm^{-1}	Combination	$\nu_{obs.}-\nu_{calc.}$ 0.1 cm^{-1}
12466.75	2	8019.14	5–13°	−1	10794.11	80	9261.79	10°–36	0
12276.6	2	8143.35	4–8°	0				5–16°	0
12116.06	5	8251.25	2–7°	−2	10773.84	10	9279.21	10–21°	+1
11957.7	1	8360.5	12–21°	+3	10741.94	800	9306.76	2–10°	−2
11863.37	30	8427.01	10–19°	−2	10717.89	4h	9327.64	12–27°	+1
					10711.94	6h	9332.82	13°–48	−2
11518.7	2h	8649.1	11°–36	−3					
11455.2	10d+Sn	8727.3	14–25°	+4	10677.41	1000	9363.01	1–6°	+1
11403.72	3	8766.67			10648.9	15h	9388.1		
11381.25	6	8783.98	11–21°	0	10645.19	5h	9391.35	8–21°	−2
11318.8	1	8832.4	12–24°	+1	10620.32	2h	9413.33		
					10616.57	2	9416.67		
11315.08	3h	8835.34							
11274.93	3	8866.81			10585.60	200	9444.22	5–17°	0
11272.27	9h	8868.90			10576.1	4h	9452.7	7°–31	0
11266.23	150	8873.66	4–11°	0	10488.3	50*H*	9531.8		
11227.61	10h	8904.18			10460.56	6h	9557.10	13°–50	+1
					10405.1	5h	9608.0		
11189.61	30	8934.42			10382.2	3h	9629.2	7°–32	−3
11183.66	2h	8939.17			10364.33	50	9645.83	10–22°	+1
11112.82	4h	8996.16	7°–29	−2	10265.2	6h	9739.0	11–26°	−2
11108.52	50h	8999.64	11–*64728.0*	−1	10261.01	300	9742.96	4–14°	0
11104.84	50h	9002.62	4–12°	−1				10–24°	+2
					10252.14	2h	9751.39	11–27°	+1
11084.98	30h	9018.75	6°–25	0	10245.15	5	9758.04	8–22°	−2
11079.95	40h	9022.84			10163.77	6h	9836.18	8–23°	−1
11012.79	300	9077.87	4–13°	+1	10135.70	2h	9863.41	8–24°	−3
10925.29	15	9150.57	11–22°	0	10108.8	2	9889.7	6°–27	0
10879.55	400	9189.04	2–8°	0	10078.49	200	9919.40	2–11°	0
10868.58	200	9198.32	5–15°	−1	10060.5	1*H*	9937.1	17–31°	+1
10848.0	4h	9215.8			10045.24	1	9952.24		
10839.73	600	9222.79	2–9°	−1	9987.3	2*H*	10010.0	8°–39	−4
10832.8	8h	9228.7	11–23°	0	9973.1	2*H*	10024.2		
10801.0	3h	9255.9	11–24°	−2	9949.14	400	10048.37	2–12°	0

TABLE 1.—*First spectrum of antimony* (Sb I)—Continued

λ_{air} A	Intensity, character	$\nu_{vac.}$ cm^{-1}	Combination	Obs.–Calc. 0.1 cm^{-1}	λ_{air} A	Intensity, character	$\nu_{vac.}$ cm^{-1}	Combination	Obs.–Calc. 0.1 cm^{-1}
9866.78	30	10132.24	7−19°	+1	7834.2	5*H*	12761.0		
9854.67	2	10144.69	11°−44	0	7817.0	7*Hw*	12789.1		
9847.80	4	10151.77	10°−42	0	7765.4	20*Hw*	12874.1		
9775.13	20	10227.24	10−25°	+1	7755.83	15	12889.98	2−17°	
9766.88	5	10235.88	7°−35	−1	7648.28	30*h*	13071.24		+1
			9°−42	0					
					7593.06	8*h*	13166.30		
9756.72	25	10246.54	10−27°	+1	7556.32	3*h*	13230.32	7°−52?	
9746.69	2	10257.08	4−15°	+1	7405.05	8*H*	13500.58	6°−45	−1
9705.38	2*H*	10300.75	11−29°	0	7361.84	4*h*	13579.82	7−*67108.0*	+1
9675.69	4	10332.35	9−26°	0	7136.40	5*h*	14008.81	3−18°	−1
9672.8	1	10335.4	10−28°	0					
					7033.04	4*h*	14216.7		
9669.16	4	10339.33	8−25°	−3	7006.17	4*h*	14269.2	5−19°	−1
9662.5	20	10346.5	8−26°	−3	6811.38	2	14677.3		
9661.6	7	10347.4	6°−28	−4	6640.63	2*h*	15054.7	2−18°	+1
9602.94	20	10410.62			6611.49	20	15121.0	5−21°	−1
9568.94	4*h*	10447.61	8−28°	−3					
					6517.07	6	15340.1	1−15°	
9546.12	10*h*	10472.59	16−31°	0	6490.23	4	15403.5	1−16°	0
9518.68	400	10502.78	4−17°	0	6454.97	8	15487.7	5−22°	−1
9455.80	4*h*	10572.62	7°−37	0	6221.44	15*h*	16069.0	5−25°	−1
9448.75	1	10580.51	6°−29	−3	6213.94	6*h*	16088.4	5−27°	−1
9392.77	4	10643.57							
					6179.81	5*h*	16177.3	5−28°	−1
9390.2	1	10646.5	7°−38	+2	6178.82	7*h*	16179.8	4−21°	0
9386.8	2*h*	10650.3			6097.71	4	16395.1		
9315.4	8*H*	10732.0			6097.53	5	16395.5	4−*64728.0*	0
9265.9	1	10789.3			6013.53	2*h*	16624.6	4−23°	+1
9262.8	2	10792.9							
					5948.27	3*h*	16807.0	3−*63798.1*	0
9260.3	2*h*	10795.8	10−29°	0	5912.32	9*h*	16909.2	3−20°	0
9251.9	2*h*	10805.6			5830.34	60*h*	17446.2	5−30°	+1
9212.93	1	10851.33			5707.48	8*h*	17516.0		
9164.8	2*h*	10908.3	8−29°	0	5691.15	4*h*	17566.3		
9132.21	30	10947.25	1−7°	−2					
					5660.72	4*h*	17660.7		
9019.24	10	11084.37	3−14°	0	5632.02	100*hl*	17750.7	1−18°	+1
8999.52	1	11108.66	11−30°	−1	5602.19	30*hl*	17845.2		
8860.0	7*h*	11283.6	10°−47	0	5599.83	15*hl*	17852.7	2−*63798.1*	0
8816.6	6*H*	11336.6	14−31°	+1	5567.97	8*h*	17954.9	2−20°	0
8789.34	5*h*	11374.30							
					5556.10	40*h*	17993.2	3−24°	0
8742.1	2*H*	11435.8	6−22°	+2	5531.67	4*h*	18072.7		
8734.8	20*Hl*	11445.3			5490.32	30*h*	18208.8	4−*66541.8*	0
8719.87	7	11464.91	2−13°	0	5473.85	2*h*	18263.6		
8700.1	10*H*	11491.0	10°−48	−1	5414.38	8	18464.2		
8682.7	30*h*	11514.0	6−23°	+3					
					5402.57	15*hl*	18504.6	4−30°	0
8667.2	8*H*	11534.6			5384.44	15	18566.9	2−21°	0
8619.55	100	11598.35	3−15°	0	5280.17	8	18933.5	2−22°	0
8617.6	10*Hl*	11601.0	6°−33	−3	5250.90	4*h*	19039.1	2−24°	+1
8611.8	4*h*	11608.8	5−18°	−1	5117.82	3	19534.1	2−27°	−1
			8°−48	−1					
8594.6	4*h*	11632.0			4854.00	2	20595.8	2−*665 415*	−1
					4841.06	6	20650.9	1−20°	0
8572.64	150	11661.82	4−16°	0	4754.99	6*h*	21024.7		
8533.4	3*h*	11715.4	10°−50?	+5	4742.81	4*h*	21078.7	3−31°	−1
8532.7	1*h*	11716.4	8−30°	0	4599.60	4	21735.0	1−24°	0
8526.9	7*h*	11724.4	12−*67876.6*	−1					
8463.2	6*h*	11812.6	7°−44	0	4033.55	200	24785.1	5°−1	+2
					3722.79	200*r*	26854.0	4°−1	+2
8457.9	2*h*	11820.0			3637.83	250	27481.1	5°−2	+2
8411.69	60	11884.95	1−8°	0	3504.48	50	28526.8	5°−3	+2
8388.5	4*H*	11917.8	12−31°	0	3383.15	100	29549.8	4°−2	0
8378.40	8*h*	11932.18	7−25°	+2					
8349.94	4*h*	11972.85	9−*67108.0*	0	3347.10	5	29868.0	5°−4	+1
					3267.51	700*r*	30595.6	4°−3	+1
8314.25	20*h*	12024.24	6−26°	0	3232.52	600*r*	30926.7	5°−5	+1
8302.99	2*h*	12040.55	7−28°	+3	3029.83	500*r*	32995.6	4°−5	+1
8289.3	20*Hw*	12.060.4			2877.92	1000*R*	34737.2	2°−1	−1
8270.11	20*h*	12088.48							
8257.8	15*H*	12106.4							
					2858.03	20	34978.9	5°−6	+1
8244.8	2*h*	12125.5	6−28°	+2	2851.11	100	35063.8	5°−7	0
8241.71	7	12130.07	2−14°	0	2769.95	400*R*	36091.1	3°−2	−1
8238.9	3*h*	12134.2			2727.23	80	36656.4	5°−8	+1
8062.2	20*Hw*	12400.2			2726.20	4	36670.2	5°−9	+1
7969.55	40*H*	12544.30							
					2718.90	150*r*	36768.7	5°−10	0
7924.65	200	12615.38	1−11°	0	2692.25	120	37132.6	4°−7	0
7906.67	10	12644.08	2−15°	0	2682.76	200*r*	37264.0	5°−11	+1
7867.17	20	12707.56	2−16°	+1	2670.64	300*r*	37433.1	2°−2	+1
7844.44	80	12744.39	1−12°	0	2652.60	200*r*	37687.7	5°−12	
7837.29	10*h*	12756.01	8−*67876.6*	+1					

TABLE 1.—*First spectrum of antimony* (Sb I)—Continued

λ_{air} A	Intensity, character	$\nu_{vac.}$ cm^{-1}	Combination	Obs.–Calc. 0.1 cm^{-1}	λ_{air} A	Intensity, character	$\nu_{vac.}$ cm^{-1}	Combination	Obs.–Calc. 0.1 cm^{-1}
2614.66	30	38234.5	5°−13	0	2098.01	10*h*	47649.0	5°−45	+5
2612.31	300*r*	38268.9	5°−14	0	2090.25	30	47825.9	4°−34	+1
2598.09	500*R*	38478.3	3°−4	−1	2087.47	25	47889.6	5°−46	+1
2598.05	1500*R*	38478.9	2°−3	−1	2081.05	10	48037.3	4°−35	0
2575.03	5	38822.9	5°−15	+2	2079.56	100	48071.7	5°−47	+2
2574.06	150	38837.5	4°−10	−1	2074.60	4	48186.6	2°−13	−3
2554.64	80	39132.7	5°−16	−1	2073.11	40	48221.3	2°−14	0
2526.52	2000*R*	39536.9	3°−5	−1	2068.33	1000*R*	48332.7	1°− 4	+2
2520.14	50	39668.4	5°−17	0	2066.57	7	48373.8	4°−37	−1
2514.56	40	39756.4	4°−12	−1	2063.43	50	48447.4	4°−38	−2
2510.54	100	39820.1	2°−4	−3	2057.36	10*h*	48590.3	5°−51?	
2481.74	40	40282.1	5°−18	0	2051.62	3	48726.3		
2480.44	150	40303.2	4°−13	−1	2049.57	150*R*	48775.0	2°−15	−1
2478.32	400	40337.7	4°−14	−1	3046.57	20	48846.5	4°−40	−9
2474.57	80	40398.8	5°−19	0	2045.93	2	48861.8	4°−41	−4
2445.51	400*r*	40878.9	2°−5	−1	2044.63	25	48892.8	3°−18	+3
2426.35	250	41201.7	4°−16	0	2040.96	4	48980.7		
2422.13	150	41273.4	5°−20	0	2039.77	70*r*	49009.3	3°−19 4°−42	0 +7
2395.22	100	41737.1	4°−17	−2					
2383.64	300*h*	41939.8	5°−21	+2	2036.62	9	49085.1	2°−16	−1
					2036.39	7	49090.7		
2373.67	400*h*	42116.0	5°−22	+3					
2360.50	80	42350.9	4°−18	−1	2031.53	3	49208.1		
2352.21	50	42500.2	5°−23	0	2029.49	60*r*	49257.5	4°−43	−1
2329.10	50	42921.8	5°−24	0					
2315.89	150	43166.6	5°−25	−1	2027.45	2	49307.1		
					2024.00	50	49391.1	1°− 5	0
2311.47	2500*R*	43249.2	1°−1	−2	2014.91	3	49613.9	4°−44	0
2306.46	300*r*	43343.1	4°−20 5°−26	+8 −12	2014.63	20	49620.8	2°−17	0
2293.44	150*r*	43589.2	3°−6	0	2012.33	20*h*	49677.5	5°−56	+5
2288.98	120	43674.1	3°−7	−1	2001.01	3	49958.5	4°−46	+1
2270.07	80	44037.8	5°−27	+1	$\lambda_{vac.}$ A				
2262.51	300*r*	44185.0	4°−22	−2	1996.25	15*h*	50093.9		
2235.00	4	44728.8	5°−29	0	1990.67	40	50234.3	2°−18	−2
2224.93	120*r*	44931.2	2°−6	0	1987.16	2	50323.1		
2221.98	100	44990.9	4°−24	+2	1986.05	60	50351.2	2°−19	−1
2220.73	150*r*	45016.2	2°−7	0	1982.82	15*h*	50433.2	4°−49	+2
2218.96	5	45052.1	5°−30	0	1979.15	20*h*	50526.7	5°−58	+2
2212.42	20	45185.2	5°−31	+1	1978.23	30	50550.2	3°−21	+2
2208.45	300*r*	45266.5	3°−8	−1	1974.07	5	50656.8	4°−51	−2
2207.73	20	45281.2	3°−9	+1	1971.34	20	50726.9	3°−22	+2
2203.81	10	45361.8	5°−32	−1	1966.03	10*h*	50863.9		
2202.97	10	45379.0	3°−10	−1	1964.3	80*H*	50909.		
2201.32	200*r*	45413.1	4°−26	−1	1959.55	2	51032.1	4°−52	0
2190.81	5	45630.9			1957.00	7*h*	51098.6		
2185.15	20	45749.1	5°−33	−2	1956.54	20	51110.6	3°−23	0
2184.7	5	45758.	5°−34		1952.15	10	51225.6	2°−20	−2
2183.54	20	45782.8			1950.39	200*r*	51271.8		
2179.19	250*r*	45874.2	3°−11	0	1944.42	3	51429.2	5°−59	+4
2175.81	1500*R*	45945.4	1°− 2	0	1943.82	10*h*	51445.1	4°−54	+4
2174.72	10	45968.5	5°−35	+1	1931.36	40	51777.0	3°−25	−1
2170.88	15	46049.8	5°−36	+1	1927.08	100	51892.0	2°−21	0
2159.24	40	46298.0	3°−12	0	1925.82	10	51925.9		
2158.91	50	46305.1	5°−37	+1	1924.74	8	51955.1	3°−25	+4
2155.48	20	46378.7	5°−38	0	1920.53	10	52069.0	2°−22	+3
2149.14	10	46515.5			1913.48	30*H*	52260.8		
2146.88	15	46564.5	4°−28	+1	1907.82	5*h*	52415.8	5°−60	0
2144.86	100*R*	46608.4	2°− 8	−2	1906.47	7	52453.0	2°−23	+4
2144.17	10	46623.2	2°− 9	+1	1904.2	10*H*	52516.		
2141.83	50*r*	46674.3			1900.72	2	52611.6		
2141.55	20	46680.4	5°−39	+1	1899.39	70	52648.5	3°−27	+4
2139.69	100*R*	46721.0	2°−10	−1	1893.16	2	52821.7		
2137.05	50*r*	46778.7	5°−40	+2	1891.28	70	52874.2	2°−24	0
2136.4	3	46793.	5°−41		1890.41	2	52898.6		
2136.15	5	46798.4	4°−29	+7	1887.5	40*Hw*	52980.		
2132.46	2	46879.3	3°−14	0	1882.56	150*r*	53119.2	2°−25	+1
2127.39	100*R*	46991.0	1°− 3	−1	1876.29	20	53296.7	2°−26	0
2118.48	80*r*	47188.7	5°−43	0	1874.80	40	53339.0	3°−29	−2
2117.25	40	47216.1	2°−11	−1	1871.15	300*R*	53443.1	1°−6	−2
2107.66	20	47430.9	4°−32	+1	1869.23	5	53498.0	4°−59	+3
2100.53	4	47591.8			1868.17	50*r*	53528.3	1°−7	0
2098.41	50*r*	47639.9	2°−12	−1	1863.50	30	53662.5	3°−30	0

TABLE 1.—*First spectrum of antimony* (Sb I)—Continued

$\lambda_{vac.}$ A	Intensity, character	$\nu_{vac.}$ cm^{-1}	Combination	$\nu_{obs.}-\nu_{calc.}$ 0.1 cm^{-1}	$\lambda_{vac.}$ A	Intensity, character	$\nu_{vac.}$ cm^{-1}	Combination	$\nu_{obs.}-\nu_{calc.}$ 0.1 cm^{-1}
1858.89	60	53795.5	3°−31	0	1644.37	20h	60813.6		
1852.18	20	53990.4	2°−27	+3	1640.32	15	60963.7	1°−23	
1842.72	20	54267.6			1638.65	8	61025.8	3°−60	−10
1839.59	4	54359.9	3°−33	+2	1629.17	10	61380.9	2°−59	−4
1839.33	7	54367.6	3°−34	+3	1629.03	10	61386.2	1°−24	−3
									−1
1836.61	20	54448.1	2°−28	+2	1623.3	100*Hw*	61600.		
1832.21	40	54578.9	3°−35	+1	1622.55	8	61631.4	1°−25	
1829.50	100	54659.7	3°−36	−4	1617.90	10	61808.5	1°−26	+2
1828.78	10	54681.3	2°−29	+1	1612.8	200*Hw*	62004.		−3
1818.02	3	55004.9	2°−30	+4	1600.91	3h	62464.5		
1814.20	80r	55120.7	1°−8	0	1599.96	80*R*	62501.6	1°−27	
1813.65	20	55137.4	2°−31	−1	1588.32	8	62959.6	1°−28	−6
1810.50	50r	55233.4	1°−10	+2	1582.46	40*R*	63192.8	1°−29	−4
1808.62	25	55290.8	3°−39	+1	1574.41	30*R*	63515.9	1°−30	−5
1807.84	8	55314.6	2°−32	+3	1571.10	15	63649.7	1°−31	−1
									+1
1805.40	30	55389.4	3°−40	+5	1566.76	15r	63826.0	1°−32	−4
1800.18	150	55550.0	3°−42	−4	1557.29	30r	64214.1	1°−33	+3
1795.28	10	55701.6	2°−33	−1	1557.13	10	64220.7	1°−34	−1
1795.03	3	55709.4	2°−34	+1	1552.01	3	64432.6	1°−35	−3
1788.24	100r	55920.9	2°−35	+1	1543.96	20r	64768.5	1°−37	+2
									−10
1785.64	15	56002.3	2°−36	+2	1535.06	80*R*	65144.0	1°−39	−1
1782.79	9	56091.9			1532.74	120*R*	65242.6	1°−40	−4
1780.87	100r	56152.3	1°−12	+2	1532.38	15r	65258.0	1°−41	+2
1777.50	20	56258.8	{3°−45	−1	1523.15	4	65653.4	1°−43	+2
			{2°−37?		1516.35	8r	65947.8		
1775.21	20	56331.4	2°−38	+3					
					1514.64	6r	66022.3		
1765.76	100h	56632.8	2°−39	+1	1512.57	50*R*	66112.6	1°−45	−4
1764.23	15	56681.9	3°−47	0	1503.50	2	66511.5		
1763.69	40r	56699.3	1°−13	+3	1491.36	40h	67052.9	1°−51	+3
			{1°−14		1486.57	20r	67268.9		
1762.68	40r	56731.8	{2°−40						
1762.24	20	56746.0	2°−41	+3	1483.07	5	67427.7	1°−52	0
					1481.47	5r?	67500.5		
1757.79	50	56889.6	3°−48	0	1475.04	*R*10	67794.8	1°−53	+2
1755.18	10h	56974.2	3°−49	−3	1474.05	*R*3	67840.3	1°−54	0
1750.91	15	57113.2	3°−50	0	1469.60	*R*5	68045.7	1°−55	−1
1750.06	15	57140.9	2°−43	−2					
1748.30	6h	57198.4	3°−51	−1	1468.76	*R*60	68084.6		
					1467.54	*R*10	68141.2	1°−56	−3
1745.59	9	57287.2	1°−15	0	1467.05	*R*5	68164.0		
1739.21	20	57497.4	2°−44	0	1464.19	10h?	68297.1		
1738.95	25	57506.0			1463.96	*R*15	68307.9		
1736.19	100r	57597.4	1°−16	0					
1728.86	15	57841.6	2°−46	−3	1463.45	*R*10	68331.7		
					1463.08	*R*10	68349.0	1°−57	0
1724.56	2	57985.8	3°−54	−4	1462.20	*R*20	68390.1		
1723.43	150r	58023.8	2°−47	−1	1459.79	*R*8	68503.0	1°−68503	
1720.19	4	58133.1	1°−17	+2	1458.88	*R*20	68545.7		
1717.45	150r	58225.9							
1716.93	80r	58243.5			1456.62	*R*30	68652.1	1°−68652	
					1449.46	*R*5	68991.2	1°−58	+2
1715.64	2	58287.3	3°−56	−1	1442.40	*R*10	69328.9		
1714.78	2	58316.5	2°−49	0	1441.39	*R*40	69377.5		
1709.21	15h	58506.6			1430.76	10	69892.9	1°−59	−4
1703.45	30	58704.4							
1702.22	20	58746.8	1°−18	+2	1420.60	*R*10	70392.8		
					1416.95	*R*10	70574.1		
1698.85	50	58863.4	1°−19	0	1415.79	*R*100	70631.9		
1697.34	2	58915.7	2°−52	+1	1413.98	*R*100	70722.4		
1695.15	7h	58991.8			1410.82	*R*5	70880.8	1°−60	+3
1691.02	30h	59135.9	3°−58	−10					
1688.06	30h	59239.6			1406.68	*R*20	71089.4	1°−71089	
					1401.60	*R*10	71347.0		
1686.84	20h	59282.4	2°−53	−1	1393.96	*R*15	71738.1		
1679.72	*R*5	59533.7	2°−55	0	1392.12	*R*10	71832.9		
1676.48	6h	59648.8			1391.46	*R*25	71867.0		
1673.98	10	59737.9	1°−20	0					
1671.21	5	59836.9	2°−57	0	1390.32	*R*50	71925.9		
					1389.63	*R*10	71961.6		
1665.35	3	60047.4			1388.91	*R*40	71998.9		
1662.6	100*Hw*	60145.							
1655.52	10r	60403.9	1°−21	−2					
1651.20	50h	60562.0							
1650.70	3	60580.4	1°−22	−4					

Our relative intensities of antimony lines, being based on visual estimates of the densities and widths of photographic images, are subject to progressive errors near the infrared limit of photographic sensitivity, but should be comparable elsewhere because sensitivity variations were usually compensated by choosing exposures which gave a nearly uniform background throughout the spectrum. Besides intensities, column 2 of table 1 contains some notes on the character of certain lines, the symbols for this purpose being those adopted by the International Astronomical Union [31]. The physical appearance of line images is an important aid in the analysis of spectral structure, remembering that self-reversals are always associated with low energy states and haziness with highly excited states. The widest reversals (*R*) involve the ground state of the atom, and narrower ones (*r*) usually indicate that the transition is to some metastable low state. Many of the emission lines of antimony between 3723 and 1500 A exhibit more or less self-reversal. Scarcely any Sb I lines appear in emission shorter than 1500 A, but several groups of absorption lines can be seen against the continuous background to 1388 A, which appears to be the short wave limit of the Sb I spectrum. Only a portion of these absorbed lines has been classified, but it is significant that all thus far interpreted as resulting from transitions between established levels possess the ground level as their final state.

Seventy-four percent of the observed Sb I lines have now been interpreted as transitions between established atomic energy states. Applying the combination principal as a test of the precision with which relative values of wavelengths have been measured, it is found that the average difference, $\nu_{obs}-\nu_{calc.}$, is 0.15 cm^{-1}, which corresponds to 0.15 A in the infrared at 10000 A, 0.05 A in the yellow at 5800 A, 0.01 A in the ultraviolet at 2600, and 0.003 A at 1500 A.

The most intense line of the Sb I spectrum has the wavelength 2311.47 A and the term combination $(5s^2\ 5p^3)\ {}^4S^\circ_{1½}-(5s^2\ 5p^2\ 6s)\ {}^4P_{0½}$. It is the *raie ultime* for spectrographic detection of traces of antimony, and as such it obeys the rule [32] that these lines arise from the electronic transition $s\leftrightarrow p$. It is also the resonance line of neutral antimony atoms and therefore susceptible of the widest self-reversal in the arc or the strongest absorption in atomic vapor. Other things being equal, the relative intensities of spectral lines are proportional to the statistical weights $(2J+1)$ of the levels involved, and we might expect the combination $(5s^2\ 5p^3)\ {}^4S^\circ_{1½}-5s^2\ 5p^2\ 6s)\ {}^4P_{2½}$ with wavelength 2068.33 A to represent the strongest Sb I line [33]. According to our intensity estimates, however, 2068.33 A appears to be much weaker than 2311.47 A. Increased excitation energy and decreased photographic sensitivity both conspire against the former and favor the latter, so that without quantitative measurement it is not possible to fix the intensity ratio of these two lines.

Table 1 shows at a glance the general features of the first spectrum of antimony, intense emission in the ultraviolet, weak radiation in the visible, and relative richness in the infrared. Since the distribution of lines and of intensity in any atomic spectrum is a consequence of the atomic-energy states associated with various configurations of the valence electrons, it will be of interest to discuss these properties of antimony atoms.

2. TERM STRUCTURE OF THE Sb I SPECTRUM

Antimony has atomic number 51, and the atoms have electronic structures as follows: $1s^2\,2s^2\,2p^6\,3s^2\,3p^6\,3d^{10}\,4s^2\,4p^6\,4d^{10}\,5s^2\,5p^3$. The first spectrum of antimony is mainly accounted for by the three outermost valence electrons, various configurations of which give rise to theoretical spectral terms [34] shown in table 2. In addition to the terms indicated in table 2, it is probable that the even terms $^4P_{0\frac{1}{2}}$, $^4P_{1\frac{1}{2}}$, $^4P_{2\frac{1}{2}}$, $^2P_{0\frac{1}{2}}$, $^2P_{1\frac{1}{2}}$, $^2D_{1\frac{1}{2}}$, $^2D_{2\frac{1}{2}}$, and $^2S_{0\frac{1}{2}}$ given by the electron configuration $5s\,5p^4$ may appear in the Sb I spectrum, since terms of this character have been identified by Bowen [35] in the analogous N I spectrum.

TABLE 2.—*Theoretical terms of the* Sb I *spectrum*

Electron configurations	Spectral terms		
$5s^2\,5p^3$	$^4S_{1\frac{1}{2}}$, $^2D_{1\frac{1}{2}}$, $^2D_{2\frac{1}{2}}$ $^2P_{0\frac{1}{2}}$, $^2P_{1\frac{1}{2}}$		
	Convergence limit, $5p^3\,^4P_{0,1,2}$(Sb II)	Convergence limit, $5p^3\,^1D_2$(Sb II)	Convergence limit, $5p^3\,^1S_0$(Sb II)
$5s^2\,5p^2\,ns$	$^4P_{0\frac{1}{2}}$, $^4P_{1\frac{1}{2}}$, $^4P_{2\frac{1}{2}}$, $^2P_{0\frac{1}{2}}$, $^2P_{1\frac{1}{2}}$	$^2D_{1\frac{1}{2}}$, $^2D_{2\frac{1}{2}}$	$^2S_{0\frac{1}{2}}$
$5s^2\,5p^2\,np$	$^4S^0_{1\frac{1}{2}}$, $^4P^0_{0\frac{1}{2}}$, $^4P^0_{1\frac{1}{2}}$, $^4P^0_{2\frac{1}{2}}$, $^4D^0_{0\frac{1}{2}}$, $^4D^0_{1\frac{1}{2}}$, $^4D^0_{2\frac{1}{2}}$, $^4D^0_{3\frac{1}{2}}$, $^2S^0_{0\frac{1}{2}}$, $^2P^0_{0\frac{1}{2}}$, $^2P^0_{1\frac{1}{2}}$, $^2D^0_{1\frac{1}{2}}$, $^2D^0_{2\frac{1}{2}}$	$^2P^0_{0\frac{1}{2}}$, $^2P^0_{1\frac{1}{2}}$, $^2D^0_{1\frac{1}{2}}$, $^2D^0_{2\frac{1}{2}}$, $^2F^0_{2\frac{1}{2}}$, $^2F^0_{3\frac{1}{2}}$	$^2P^0_{0\frac{1}{2}}$, $^2P^0_{1\frac{1}{2}}$
$5s^2\,5p^2\,nd$	$^4P_{0\frac{1}{2}}$, $^4P_{1\frac{1}{2}}$, $^4P_{2\frac{1}{2}}$, $^4D_{0\frac{1}{2}}$, $^4D_{1\frac{1}{2}}$, $^4D_{2\frac{1}{2}}$, $^4D_{3\frac{1}{2}}$, $^4F_{1\frac{1}{2}}$, $^4F_{2\frac{1}{2}}$, $^4F_{3\frac{1}{2}}$, $^4F_{4\frac{1}{2}}$, $^2P_{0\frac{1}{2}}$, $^2P_{1\frac{1}{2}}$, $^2D_{1\frac{1}{2}}$, $^2D_{2\frac{1}{2}}$, $^2F_{2\frac{1}{2}}$, $^2F_{3\frac{1}{2}}$	$^2S_{0\frac{1}{2}}$, $^2P_{0\frac{1}{2}}$, $^2P_{1\frac{1}{2}}$, $^2D_{1\frac{1}{2}}$, $^2D_{2\frac{1}{2}}$, $^2F_{2\frac{1}{2}}$, $^2F_{3\frac{1}{2}}$, $^2G_{3\frac{1}{2}}$, $^2G_{4\frac{1}{2}}$	$^2D_{1\frac{1}{2}}$, $^2D_{2\frac{1}{2}}$

The first regularities among antimony arc lines were discovered in 1894 by Kayser and Runge [2], who found 12 pairs of ultraviolet lines with the wave-number difference 2069 cm^{-1}, 5 pairs separated 6543 cm^{-1} and 5 pairs separated 1342 cm^{-1}. These three constant differences measure the energy differences between four metastable states from highest to lowest (the ground state being 8512 cm^{-1} lower still), but a third of a century elapsed before the quantum interpretation of these levels could be given. An attempt by van Lohuizen [36] in 1913 to arrange antimony lines in spectral series appears to be artificial. Further progress in the classification of Sb I lines was made in 1923 by Ruark et al. [12], who added the deepest level, and fixed 25 high levels by means of 80+ combinations.

The first quantum interpreations of Sb I levels were made practically simultaneously by McLennan and McLay [37] and by Malurkar [38]. Both conjectured the first 5 levels to be $^4S_{1\frac{1}{2}}$, $^2D_{1\frac{1}{2}}$, $^2D_{2\frac{1}{2}}$, $^2P_{0\frac{1}{2}}$, $^2P_{1\frac{1}{2}}$ (arising from the electron configuration $5s^2 5p^3$) and the next 5 levels as $^4P_{0\frac{1}{2}}$, $^4P_{1\frac{1}{2}}$, $^2P_{0\frac{1}{2}}$, $^4P_{2\frac{1}{2}}$, $^2P_{1\frac{1}{2}}$ (the lowest from $5s^2 5p^2 6s$). Malurkar also suggested identification of 15 higher levels but not without much arbitrariness. A step backward seems to have been made in 1930 by Charola [17], who claims to have classified 64 Sb lines and discovered 25 new levels. His interpretation of 11 levels also in Malurkar's list is totally different, and the 14 remaining levels appear to be unreal.

Positive information about the nature of Sb I levels was not at hand until 1929, when the Zeeman-effect investigation by Löwenthal [21] supplied absolute values of g and j for 14 levels. Departures

from the g's representative of LS-couping are found even among the low levels, and a great deal of g-sharing may be expected among higher levels from various configurations. Löwenthal also established 11 levels due to $5s^2\ 5p^2\ 6p$ from infrared wavelength data then available.

TABLE 3.—*Levels and terms of* Sb I

Level number	Level value	Quantum number, j	Splitting factor, g	Electron configuration	Term symbol	Level number	Level value	Quantum number, j	Splitting factor, g	Electron configuration	Term symbol
1°	*0.0*	1½	1.967	$5s^2\ 5p^3$	$^4S_{1½}$	32	63826.4	0½			
2°	*8518.1*	1½	0.889	$5s^2\ 5p^3$	$^2D_{1½}$	20°	*63900.3*	0½			
3°	*9854.1*	2½	1.205	$5s^2\ 5p^3$	$^2D_{2½}$	33	64213.8	2½			
4°	*16395.6*	0½	0.688	$5s^2\ 5p^3$	$^2P_{0½}$	34	64221.4	1½			
5°	*18464.5*	1½	1.277	$5s^2\ 5p^3$	$^2P_{1½}$	35	64432.9	1½			
						21°	*64512.3*	2½			
1	43249.4	0½	2.332	$5s^2\ 5p^3(^2P_0)6s$	$^4P_{0½}$	36	64514.2	2½			
2	45945.4	1½	1.713	$5s^2\ 5p^3(^2P_1)6s$	$^4P_{1½}$	37	64769.5	0½			
3	46991.1	0½	1.004	$5s^2\ 5p^3(^2P_1)6s$	$^2P_{0½}$	38	64843.2	0½			
4	48332.5	2½	1.547	$5s^2\ 5p^3(^2P_2)6s$	$^4P_{2½}$	22°	*64878.9*	2½			
5	49391.1	1½	1.277	$5s^2\ 5p^3(^2P_2)6s$	$^2P_{1½}$						
						23°	*64957.0*	3½			
6°	*52612.5*	1½				24°	*64984.4*	1½			
6	53443.3	2½				39	65144.8	2½			
7	53528.3	1½				40	65243.0	1½			
7°	*54196.9*	1½				41	65257.8	0½			
8	55120.7	2½									
						42	65404.2	1½			
8°	*55154.4*	1½				25°	*65460.3*	2½			
9	55135.2	2½				26°	*65467.5*	3½			
9°	*55168.3*					27°	*65479.6*	2½			
10	55233.2	1½	0.991	$5s^2\ 5p^3(^1D_2)6s$	$^2D_{1½}$	28°	*65568.6*	2½			
10°	*55252.4*	2½									
						43	65653.2	0½		$5s^2\ 5p^3(^1S_0)6s$	$^2S_{0½}$
11	55728.3	2½	1.277	$5s^2\ 5p^3(^1D_2)6s$	$^2D_{2½}$	44	66009.5				
11°	*55864.8*	1½				29°	*66029.0*	2½			
12°	*55998.8*	1½				45	66113.0	1½		$5s^2\ 5p^3(^2P_1)8s$	$^4P_{1½}$
12	56152.1	1½	1.302			46	66354.0	0½			
13	56699.0	0½									
						47	66536.0	2½			
14	56733.4	1½	(1.311)			48	66743.7	3½			
15	57287.2					49	66828.6	1½			
13°	*57410.3*	2½				30°	*66837.1*	2½			
16	57597.3	0½		$5s^2\ 5p^3(^2P_0)7s$	$^4P_{0½}$	50	66967.3	3½			
14°	*58075.5*	1½									
						51	67052.6	1½			
17	58132.9	0½				52	67427.7	0½			
15°	*58589.5*	1½				53	67794.6				
16°	*58652.9*	0½				54	67840.3	1½			
18	58746.6	1½				55	68045.8				
17°	*58835.5*	2½									
						31°	*68069.9*	0½			
19	58863.4	2½				56	68141.5	1½			
20	59737.9	0½				57	68349.0				
21	60404.1	2½				58	68991.0	2½			
22	60580.8	1½				59	69893.3	0½			
23	60964.7	1½		$5s^2\ 5p^3(^2P_1)7s$	$^4P_{1½}$						
						60	70880.3	2½		$5s^2\ 5p^3(^1D_2)7s$	$^2D_{2½}$
18°	*61000.0*	0½					68503			$5s^2\ 5p^3(^2P_1)9s$	$^4P_{1½}$
24	61386.3	0½		$5s^2\ 5p^3(^2P_1)7s$	$^2P_{0½}$		68652			$5s^2\ 5p^3(^2P_2)8s$	$^4P_{2½}$
25	61631.2	2½					71089			$5s^2\ 5p^3(^2P_2)9s$	$^4P_{2½}$
26	61808.8	1½									
27	62502.2	2½									
28	62960.0	0½		$5s^2\ 5p^3(^2P_0)8s$	$^4P_{0½}$						
29	63193.3	1½									
30	63516.6	2½		$5s^2\ 5p^3(^2P_2)7s$	$^4P_{2½}$						
31	63649.6	2½									
19°	*63660.4*										

Being based on a more complete, accurate, and homogeneous description of the Sb I spectrum, the present investigation has resulted in the rejection of certain former levels, correction of the values of others, and the establishment of a considerable number of new levels. In addition to the 5 lowest odd levels ($5p^3$), the new ultraviolet data have revealed 60 levels from 43249 to 70880 cm^{-1} above the ground

state. These are even levels from configurations $5s^2\,5p^2\,ns$, $5s^2\,5p^2\,nd$, and probably $5s\,5p^4$, but on account of expected large separations of levels and consequent overlapping of terms, it is doubtful if L-values can be assigned to many of these. From the infrared data, we have obtained 31 odd levels with values between 52612 and 66907 cm^{-1}. These undoubtedly arise from the electron configuration $5p^2\,np$ and possibly $5p^2\,nf$, but here again the assignment of L-values probably has little meaning. It will be noticed that these odd levels are completely surrounded and interlaced by the even levels with which they combine to produce infrared radiations. Since the present limit of photographic observation is about 8000 cm^{-1}, only fringe combinations of these even and odd levels have been recorded, and a large number of combinations must exist in the unexplored infrared. The fact that only a portion of these combinations is within reach of present observations makes it impossible to fix unambiguously all the J-values of the established odd levels.

All of the known atomic energy levels of Sb I are collected in table 3 and are based on $^4S°_{1½}=0$. Since it is not possible to assign definite L-values to all of these (for reasons stated above), we have numbered the even and odd levels separately in the order of their magnitude, written the odd values in italics, and added the odd sign (°) to their numerical symbols. Table 3 does not include five provisional odd levels (*63798.1*, *64728.0*, *66541.3*, *67108.0*, *67876.6*) appearing in table 1, because each of these is based on only two combinations.

3. SPECTRAL SERIES AND IONIZATION POTENTIAL

The ultraviolet lines of Sb I are of special interest because it is among these that spectral series must be sought for the purposes of determining the spectroscopic ionization potential of Sb atoms and of tracing the convergence of term sequences in one spectrum to limits in the next. Table 4 shows all the combinations given by classified ultraviolet Sb lines, the low odd levels appearing at the head and the even levels at the left margin. The even levels, as stated before, arise from electron configurations $5s^2\,5p^2\,ns$, $5s^2\,5p^2\,nd$, and $5s5p^4$. Terms given by the series s electron ($6s$, $7s$, $8s$, ____) should fit a Ritz formula of the type

$$\nu=L-R/\left(n+a+\frac{b}{n^2}\right)^2$$

from which determinations of the limits (L) could be obtained. Each configuration of the type $5p^2\,ns$ gives rise to eight levels ($^4P_{0½}$, $^4P_{1½}$, $^4P_{2½}$, $^2P_{0½}$, $^2P_{1½}$, $^2D_{1½}$, $^2D_{2½}$, $^2S_{0½}$), which converge in an obvious manner toward five limits in the Sb II spectrum ($^3P_0$, $^3P_1$, $^3P_2$, $^1D_2$, $^1S_0$) when the s electron is removed by ionization. The structure of the Sb II spectrum has been partially analyzed by Dhavali [39], Lang and Vestine [40], and Krishnamurty [41]. The low Sb II terms from $5p^2$, according to Lang and Vestine [40], have the following values: $^3P_0=0$, $^3P_1=3055$, $^3P_2=5659$, $^1D_2=12791$, $^1S_0=23906$ cm^{-1}. Guided by these intervals, we have provisionally interpreted the following Sb I levels: $^2D_{1½}=55233.1$, $^2D_{2½}=55728.4$, and $^2S_{0½}=65653.2$, thus completing the assignment of levels to the configuration $5p^2\,6s$.

TABLE 4.—Sb I *combinations,* $5s^2\,5p^3 - 5s^2\,5p^2$ *(ns, nd)*

Level number		1°	2°	3°	4°	5°
Value		*0.0*	*8512.1*	*9854.1*	*16395.6*	*18464.5*
Level number	Value					
1	43249.4	43249.2(2500*R*)	34737.2(1000*R*)		26854.0(200*R*)	24785.1(200)
2	45945.4	45945.4(1500*R*)	37433.1(300*r*)	36091.1(400*R*)	29549.8(100)	27481.1(250)
3	46991.1	46991.0(100*R*)	38478.9(1500*R*)		30595.6(700*r*)	28526.8(50)
4	48332.5	48332.7(1000*R*)	39820.1(100)	38478.3(500*R*)		29868.0(5)
5	49391.1	49391.1(50)	40878.9(400*r*)	39536.9(2000*R*)	32995.6(500*r*)	30926.7(600*r*)
6	53443.3	53443.1(300*R*)	44931.2(120*r*)	43589.2(150*r*)		34978.9(20)
7	53528.3	53528.3(50*r*)	45016.2(150*r*)	43674.1(120)	37132.7(120)	35063.8(100)
8	55120.7	55120.7(80*r*)	46608.4(100*R*)	45266.5(300*r*)		36656.4(80)
9	55135.2		46623.2(10)	45281.2(20)		36670.3(4)
10	55233.2	55233.4(50*r*)	46721.0(100*R*)	45379.0(10)	38837.5(150)	36768.7(150*r*)
11	55728.3		47216.1(40)	45874.2(250*r*)		37264.0(200*r*)
12	56152.1	56152.3(100*r*)	47639.9(50*r*)	46298.0(40)	39756.4(40)	37687.7(200*r*)
13	56699.0	56699.3(40*r*)	48186.6(4)		40303.3(150)	38234.5(30)
14	56733.4	56731.8?(40*r*)[a]	48221.3(40)	46879.3(2)	40337.7(400)	38268.9(300*r*)
15	57287.2	57287.2(9)	48775.0(150*R*)			38822.9(5)
16	57597.3	57597.4(100*r*)	49085.1(9)		41201.7(250)	39132.7(80)
17	58132.9	58133.1(4)	49620.8(20)		41737.1(100)	39668.4(50)
18	58746.6	58746.8(20)	50234.3(40)	48892.8(25)	42350.9(80)	40282.1(40)
19	58863.4	58863.4(50)	50351.2(60)	49009.3(70*r*)[a]		40398.9(80)
20	59737.9	59737.9(10)	51225.6(10)		43343.1(300)[a]	41273.4(150)
21	60404.1	60403.9(10*r*)	51892.0(100*r*)	50550.2(30)		41939.8(300*h*)
22	60580.8	60580.4(3)	52069.0(10)	50726.9(20)	44185.0(300*r*)	42116.0(400*h*)
23	60964.7	60963.7(15)	52453.0(7)	51110.6(20)		42500.2(50)
24	61386.3	61386.2(10)	52874.2(70)		44990.9(100)	42921.8(50)
25	61631.2	61631.4(8)	53119.2(150*r*)	51777.0(40)		43166.6(150)
26	61808.8	61808.5(10)	53296.7(20)	51955.1(8)	45413.1(200*r*)	43343.1(300)[a]
27	62502.2	62501.6(80*R*)	53990.4(20)	52648.5(70)		44037.8(80)
28	62960.0	62959.6(8)	54448.1(20)		46564.5(15)	
29	63193.3	63192.8(40*R*)	54681.3(10)	53339.0(40)	46798.4(5)	44728.8(4)
30	63516.6	63515.9(30*R*)	55004.9(3)	53662.5(30)		45052.1(5)
31	63649.6	63649.7(15)	55137.4(20)	53795.5(60)		45185.2(20)
32	63826.4	63826.0(15*r*)	55314.6(8)		47430.9(20)	45361.8(10)
33	64213.8	64214.1(30)	55701.6(10)	54359.9(4)		45749.1(20)
34	64221.4	64220.7(10)	55709.4(3)	54367.6(7)	47825.9(30)	45758 (5)
35	64432.9	64432.6(3)	55920.9(100*r*)	54578.9(40)	48037.3(10)	45968.5(10)
36	64514.2		56002.3(15)	54659.7(100)		46049.8(15)
37	64769.5	64768.5(20*r*)	56258.8(20)[a]		48373.8(7)	46305.1(50)
38	64843.2		56331.4(20)		48447.4(50)	46378.7(20)
39	65144.8	65144.0(80*R*)	56632.8(100)	55290.8(25)		46680.4(20)
40	65243.0	66242.6(120*R*)	56731.8(40*r*)[a]	55389.4(30)	48846.5 (20)	46778.7(50*r*)
41	65257.8	65258.0(15*r*)	56746.0(20)		48861.8(2)	46793 (3)
42	65404.2			55550.0(150)	49009.3(70*r*)[a]	
43	65653.2	65653.4(4)	57140.9(15)		49257.5(60*r*)	47188.7(80*r*)
44	66009.5		57497.4(20)		49613.9(3)	
45	66113.0	66112.6(50*R*)		56258.8(20)[a]		47649.0(10)
46	66354.0		57841.6(15)		49958.5(3)	47889.6(25)
47	66536.0		58023.8(150*r*)	56681.9(15)		48071.7(100)
48	66743.3			56889.6(50)		
49	66828.6		58316.5(2)	56974.2(10)	50433.2(15*h*)	
50	66967.3			57113.2(15)		
51	67052.6	67052.9(40)		57198.4(6*h*)	50656.8(5)	48590.3?(8*h*)
52	67427.7	67427.7(5)	58915.7(2)		51032.1(2)	
53	67794.6	67794.8(*R*10)	59282.4(20*h*)			
54	67840.3	67840.3(*R*3)		57985.8(2)	51445.1(10)	
55	68045.8	68045.7(*R*5)	59533.7(*R*5)			
56	68141.5	68141.2(*R*10)		58287.3(2)		49677.5(20*h*)
57	68349.0	68349.0(*R*10)	59836.9(5)			50526.7(20*h*)
58	68991.0	68991.2(*R*5)		59135.9(30*h*)		51429.2(3)
59	69893.3	69892.9(10)	61380.9(10)		53498.0(5)	52415.8(5*h*)
60	70880.3	70880.8(*R*5)		61025.8(8)		

[a] Doubly classified.

Reference to Rydberg's interpolation table indicated that the lines with wave numbers 43249, 57597, and 62960 cm^{-1} might represent the series $5s^2\ 5p^3\ {}^4S^\circ_{1½}-5s^2\ 5p^2\ ({}^3P_0)ns\ {}^4P_{0½}$. The Ritz formula

$$\nu=70064-109737/\left(n-4.18902+\frac{7.63201}{n^2}\right)^2,\ n=6,7,8$$

represents these three lines without error, but no line is observed for $n=9$, probably because the intensity decrement (2500, 100, 8) is too great in this series. This same series was arrived at independently by Professor Russell, who employed the method of comparison with spectra of neighboring elements. Good series are known for all the spectra from Ag I to Cs I, except Sb I and I I. For these spectra, table 5 gives the effective quantum numbers, $n^*=\sqrt{R/T}$, corresponding to terms of highest L- and J-values converging to the lowest limit in the second spectrum.

TABLE 5.—*Effective quantum numbers n* in spectra* Ag I *to* Cs I

Spectrum	Ag I	Cd I	In I	Sn I	Sb I	Te I	I I	Xe I	Cs I
Term	$^2S_{0½}$	$^1S_1$	$^2S_{0½}$	$^3P_1$	$^4P_{0½}$	$^3S_1$	$^4P_{2½}$	$^2P_2$	$^2S_{0½}$
Electron ↓									
6*s*	2.432	2.283	2.219	2.128	.....	1.965	.....	1.889	1.869
7*s*	3.450	3.317	3.254	3.168	.....	.....	.....	.....	2.920
8*s*	4.457	4.328	4.266	4.229	.....	4.036	.....	3.951	3.935
9*s*	5.460	5.334	5.271	5.239	.....	5.050	.....	4.974	4.941
10*s*	6.464	6.337	6.274	6.299	.....	6.051	.....	5.975	5.944
11*s*	7.467	7.339	7.283	7.299	.....	7.055	.....	6.975	6.947

By interpolation, the 6*s* value of n^* for Sb I is found to be about 2.036. The corresponding term, $T=R/n^{*2}$, has a numerical value of $109737/(2.036)^2=26473$, and if this is added to the wave number 43249 cm^{-1}, representing the resonance line, a value of 69722 is obtained for the limit ($^3P_0$ of Sb II). This differs by less than 0.5 percent from the limit contained in the Ritz formula given above. Further series assignments were then suggested by the various limits in the Sb II spectrum to which such series are expected to converge. Complete data for the proposed series of Sb I are shown in table 6.

The Ritz formula,

$$\nu=72721-109737/\left(n-3.85951-\frac{4.17719}{n^2}\right),\ n=6,\ 7,\ 8,\ 9,$$

reproduces the series $5s^2\ 5p^3\ {}^4S^\circ_{1½}-5s^2\ 5p^2({}^3P_1)ns\ {}^4P_{1½}$ perfectly for three members but gives an observed-calculated residual of 20 cm^{-1} for $n=9$. If the Sb II interval, $^3P_0-{}^3P_1=3055$ cm^{-1}, is subtracted from the limit, 69666 cm^{-1} is derived as a value of $^3P_0$. Similarly, the formula

$$\nu=75206-109737/\left(n-3.81637-\frac{5.86271}{n^2}\right),\ n-6,\ 7,\ 8,\ 9,$$

represents without error the first three members of the $5s^2\ 5p^3\ {}^4S^\circ_{1½}-5s^2\ 5p^2({}^3P_2)ns\ {}^4P_{2½}$ series, but gives a residual of 84 cm^{-1} for $n=9$. Subtraction of the Sb II interval, $^3P_0-{}^3P_2=5659$ cm^{-1}, from the limit, gives a value of 69547 cm^{-1} for $^3P_0$.

TABLE 6.—Sb I *series and effective quantum numbers*

Limits	Electron	Lines	Terms	Effective quantum numbers $n^*=\sqrt{R/T}$
cm^{-1}		cm^{-1}	cm^{-1}	
$^3P_0=69700$	6*s*	43249	$^4P_{0½}=26451$	2.0368
	7*s*	57597	=12103	3.0112
	8*s*	62960	=6740	4.0350
$^3P_1=72755$	6*s*	45945	$^4P_{1½}=26810$	2.0232
	7*s*	60965	=11790	3.0508
	8*s*	66113	=6642	4.0647
	9*s*	68503	=4252	5.0802
	6*s*	46991	$^3P_{0½}=25764$	2.0638
	7*s*	61386	=11369	3.1068
$^3P_2=75359$	6*s*	48332	$^4P_{2½}=27027$	2.0150
	7*s*	63517	=11842	3.0442
	8*s*	68652	=6707	4.0450
	9*s*	71089	=4270	5.0695
	6*s*	49391	$^3P_{1½}=25968$	2.0557
$^1D_2=82491$	6*s*	55233	$^3D_{1½}=27258$	2.0065
	6*s*	55728	$^3D_{2½}=26763$	2.0250
	7*s*	70880?	=11611?	3.0742?
$^1S_0=93606$	6*s*	65653	$^3S_{0½}=65653$	1.9814

The average of the three values of $^3P_0$ indicated by the above series is 69759 cm^{-1}. However, the second series appears to be least perturbed, and its value of $^3P_0$ (=69666) agrees very closely with 69722 obtained from the resonance line and interpolated n^*. We have, therefore, adopted the rounded mean of these two values as the most probable magnitude of $^3P_0=69700$ cm^{-1}. The *principal ionization potential* of antimony is then $69700\times1.2395\times10^{-4}=8.64$ volts. This is a measure of the energy required to move a valence electron from its normal state in a neutral Sb atom to the lowest energy state ($^3P_0$) of the Sb^+ ion. Ionization to the higher (metastable) states will require greater energy, the maximum being $(69700+23906)\times1.2395\times10^{-4}=11.60$ volts, which is necessary for transferring a valence electron from the normal state of Sb to the $^1S_0$ state of Sb^+. In fact, the only levels of Sb I which, according to Hund's theory, go to the $^3P_0$ state of Sb II are $^4P_{0½}$ with an *s*-electron and $^4F_{1½,2½}$ with a *d*-electron. All other types of Sb I terms seek metastable states in Sb^+ ions, and this accounts for the fact that Sb I lines have actually been observed with wave numbers exceeding 69700 cm^{-1}, the principal ionization limit.

The authors express their indebtedness to Professor Shenstone for the extreme ultraviolet spectrograms, and to Professor Russell for the data in table 5 and for assistance in selecting the series terms shown in table 6.

IV. REFERENCES

[1] H. Kayser, Handbuch der Spectroscopie **6,** 426 (S. Hirzel Leipzig, 1912).
[2] H. Kayser and C. Runge, Abhandl. Berlin Akad. (1893); Weidem. Ann. **52,** 93 (1894).
[3] H. Schippers, Z. wiss. Phot. **11,** 235 (1912).
[4] F. M. Walters, Jr., BS Sci. Pap. **17,** 161 (1921) S411.
[5] H. M. Randall, Astrophys. J. **34,** 1. (1911).
[6] H. Lehmann, Ann. Physik **39,** 53 (1912).
[7] T. Takamine and S. Nitta, Mem. Coll. Sci. Kyoto Imp. Univ. **2,** 117 (1917).
[8] J. C. McLennan, J. F. T. Young, and H. J. C. Ireton, Proc. Roy. Soc. (London) [A] **98,** 95 (1920).
[9] L. and E. Bloch, J. phys. radium **8,** 217 (1937).
[10] J. C. Dobbie and J. J. Fox, Proc. Roy. Soc. (London) [A] **98,** 147 (1920).
[11] W. Grotrian, Z. Physik **18,** 169 (1923).
[12] A. E. Ruark, F. L. Mohler, P. D. Foote, and R. L. Chenault, BS Sci. Pap. **19,** 463 (1920) S490.
[13] A. L. Narayan and K. R. Rao, Phil. Mag. [6] **50,** 645 (1925).
[14] J. C. McLennan and A. B. McLay, Trans. Roy. Soc. Can. **19,** 89 (1925).
[15] J. G. Frayne and A. W. Smith, Phil. Mag. [7] **1,** 732 (1926).
[16] R. V. Zumstein, Phys. Rev. **29,** 209 (1927).
[17] F. Charola, Physik. Z. **31,** 457 (1930).
[18] E. O. Hulburt, Phys. Rev. **24,** 129 (1924).
[19] M. C. W. Buffam and H. J. C. Ireton, Trans. Roy. Soc. Can. **19,** 113 (1925).
[20] P. A. van der Harst, Proc. Acad. Sci. Amsterdam. **22,** 300 (1920).
[21] H. Löwenthal, Z. Physik, **57,** 822 (1929).
[22] A. G. Shenstone, Trans. Roy. Soc. (London) [A] **237,** 453 (1938).
[23] W. F. Meggers and K. Burns, BS Sci. Pap. **18,** 185 (1922) S442.
[24] Eastman Kodak Co., Photographic Plates for use in Spectroscopy and Astronomy (1940).
[25] Proc. Sixth Summer Conference on Spectroscopy, p. 114, (John Wiley & Sons, New York, N. Y., 1939).
[26] K. Burns and F. M. Walters, Jr., Pub. Allegheny Observatory, Univ. Pittsburgh, **6,** 159 (1929); **8,** 39 (1931); **8,** 27 (1931).
[27] J. C. Boyce and H. A. Robinson, J. Opt. Soc. Am. **26,** 133 (1936).
[28] W. F. Meggers, J. Research NBS **14,** 33 (1935) RP755; W. F. Meggers and C. J. Humphreys, J. Research NBS **18,** 543 (1937) RP992.
[29] H. Kayser, Tabelle der Schwingungszahlen (Julius Springer, Berlin, 1927).
[30] W. F. Meggers and C. G. Peters, Bul. BS **14,** 697 (1918) S327.
[31] Trans. Int. Astron. Union **6,** 100 (1938).
[32] W. F. Meggers and B. F. Scribner, J. Research NBS **13,** 657 (1934) RP732.
[33] W. F. Meggers, J. Opt. Soc. Am. **31,** 44 (1941).
[34] F. Hund, Linienspektren und Periodisches System der Elemente (Julius Springer, Berlin, 1927).
[35] I. S. Bowen, Phys. Rev. **29,** 231 (1927).
[36] T. van Lohuizen, Z. wiss. Phot. **11,** 397 (1913).
[37] J. C. McLennan and A. B. McLay, Trans. Roy. Soc. Can. **21,** 63 (1927).
[38] S. L. Malurkar, Proc. Cambr. Phil. Soc. **24,** 85 (1927).
[39] D. G. Dhavali, Proc. Roy. Soc. (London) [A] **131,** 109 (1931).
[40] R. J. Lang and E. H. Vestine, Phys. Rev. **42,** 233 (1932).
[41] S. G. Krishnamurty, Indian J. Phys. **10,** 83 (1936).

WASHINGTON, January 19, 1942.

U. S. Department of Commerce National Bureau of Standards

RESEARCH PAPER RP1465

Part of Journal of Research of the National Bureau of Standards, Volume 28, April 1942

STRUCTURAL CHANGES IN THE BONDING LAYER OF SOFT-SOLDERED JOINTS IN COPPER PIPE LINES ON LONG-CONTINUED HEATING

By William H. Swanger and Arthur R. Maupin[1]

ABSTRACT

In the course of previous investigations [1, 2][2] to establish the merits of soldered joints in copper-tube lines for domestic plumbing and other purposes, it became evident that in the evaluation of such joints consideration must be given to possible deterioration with time of the bond of the soldered joint if the service involves use at elevated temperatures. Joints made with solder containing tin were found to be susceptible to such a change, under favorable circumstances, whereas many lead-base solders were not. By means of metallographic studies of specimens cut from soldered joints held at elevated temperature for long periods, the nature of the microstructural change was established and correlated with the lowering of the bonding properties of the soldered joint. Essentially, this consists in the formation of a bonding layer adjacent to the copper base by alloying, by diffusion, of the tin of the solder and the adjacent copper. Microhardness determinations showed this constituent to be much harder than the initial solder and also harder than the copper base. Evidence of brittleness was also found. Most tin-free lead-base solders, including lead-silver solder, were found not to be susceptible of this change. Lead-cadmium solder was an exception.

CONTENTS

	Page
I. Introduction	479
II. The soldered joint—construction and use	480
III. Metallographic study of soldered joints—results and discussion	481
1. General discussion	481
2. Solders containing tin	482
(a) (50–50) tin-lead	482
(b) (60–39–1) lead-tin-antimony and (95–5) lead-tin	484
(c) (95–5) tin-antimony solder	484
3. Lead-base tin-free solders	485
(a) Lead-silver	485
(b) Lead-cadmium-zinc	485
(c) High-purity lead	485
IV. Conclusions	485
V. References	487

I. INTRODUCTION

Previous investigations [1, 2] on the use of soft-soldered joints in copper-pipe lines for domestic plumbing and for other purposes have shown that strength measurements at room and at elevated tempera-

[1] Research Associate at the National Bureau of Standards, representing the Copper & Brass Research Association.

[2] Figures in brackets indicate the literature references at the end of this paper.

tures do not yield sufficient information on which complete evaluation of the permanence of such joints in service can be based. In addition to the information obtained by long-time loading tests carried out at the temperatures expected in service, consideration must be given to the possible deterioration with time of the "bond" between the solder film and the copper in the joints. This is especially necessary if the service conditions involve long periods at temperatures considerably above normal atmospheric temperature, though below the lower limit of the melting range of the solder.

The previous study has shown that when used on copper and copper-base alloys, soft solders containing tin as an essential constituent are susceptible of deterioration of the "bond", at temperatures approaching 250° F, involving loss of strength and other undesirable changes [1]. Tin-alloy solders, therefore, should not be recommended for joining copper that is to be used for extended periods at temperatures above 250° F. Lead-base solders, free from tin, were found not to be susceptible of such deteriorations of the bond on copper. Within the necessary strength limitations [2], joints made with the lead-base solders investigated can be used with safety at temperatures up to 325° F.

In order to determine the nature of the changes which occur in the solder films, a metallographic study was made of these joints after exposing them to the appropriate temperatures for various periods of relatively long duration.

II. THE SOLDERED JOINT—CONSTRUCTION AND USE

Although the work described in this report was restricted to soldered sleeve joints of the type used in copper-tube plumbing lines, it is obvious that the results are representative of all joints made with the same solders on copper as the base material. Presumably also the results are typical of similar soldered joints on various alloys of which copper is the predominating component. The results of some tests on soldered joints in brass are confirmatory of this.

Figure 1 shows the outward appearance of a soldered sleeve joint in copper tubing, together with a longitudinal section to show the location of the solder film.

In making any kind of soldered joint, an initially clean surface is necessary. Removal of the surface tarnish film, grease, or other contamination by abrasion or scraping, so as to expose bright metal, is common practice. Use of a flux at the soldering temperature is necessary. In the present work zinc chloride or a mixture of zinc and ammonium chlorides was used. These fluxes are molten at the soldering temperature and exert a further cleansing action on the base metal and also prevent oxidation of base metal surface and solder by blanketing them from the air. The "wetting" or spread of the solder on the surface and the ability of the molten solder to fill by capillary action the crevice between the surfaces to be joined is also promoted by the flux. In fact, if the fluxing action is not obtained, the solder will not spread out in a thin film but will tend to coalesce on the surface or fail to penetrate a crevice by capillary action.

Wetting of the surface occurs most readily when there is some alloying between a component of the solder and the metal with which it is in contact. Alloying between copper and the tin constituent of

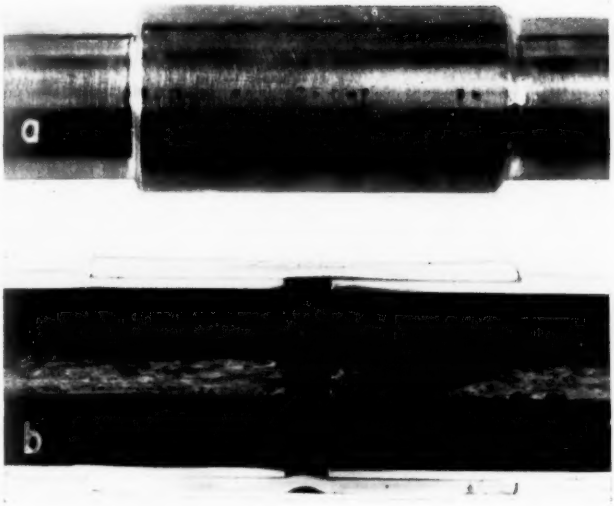

FIGURE 1.—*Soldered sleeve joint in copper-tube plumbing line,* ×1.

(a) External appearance; (b) longitudinal section showing the solder film.

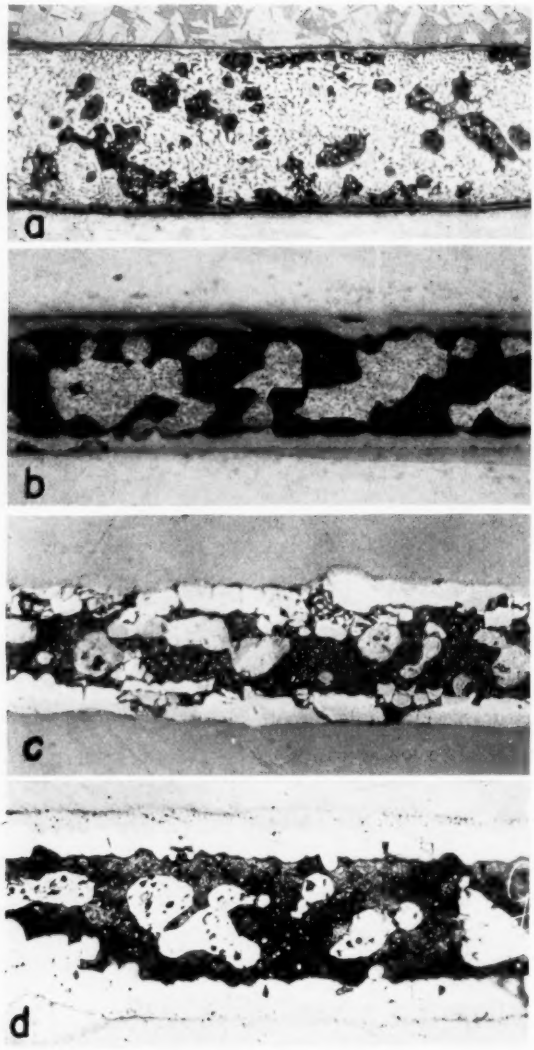

FIGURE 3.—*Structural changes in the solder film in a copper-tube joint,* (50–50) *tin-lead solder,* ×250.

(a) Initial structure of the solder film, consisting of the tin-lead eutectic embedded in which are dendrites of the excess lead, etched. A thin bonding layer was formed by alloying of tin from the solder with the copper base; (b) solder film in a joint maintained at 250° F for 7,500 hours under a tensile shear stress of 70 lb/in.², unetched. Note the increased thickness of the bonding-alloy layer (Cu_3Sn) and the pronounced coalescence of the structural constituents within the solder film; (c) solder film in a joint maintained for 12,000 hours at 250° F under a tensile shear stress of 70 lb/in.² for first 5,000 hours, and 90 lb/in.² for 7,000 hours, unetched. Note marked increase in the alloy (Cu_3Sn) layer and its cracked condition; (d) solder film in a joint maintained for 28,000 hours at 250° F under a tensile shear stress of 70 lb/in.² for 5,000 hours; 90 lb/in.² for 7,000 hours; and zero stress, 16,000 hours; unetched. Note the duplex structure of the alloy layer; the white constituent is Cu_3Sn.

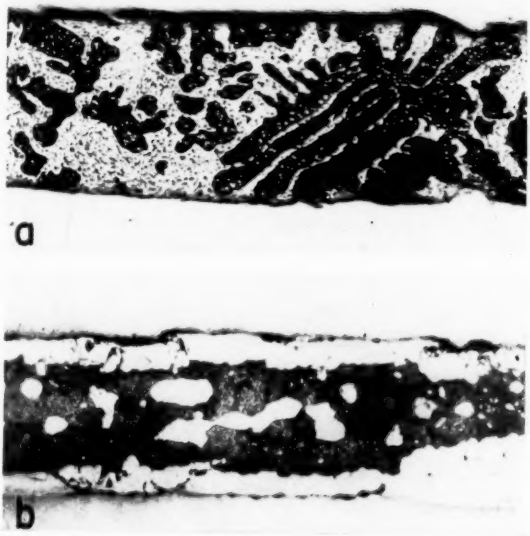

FIGURE 4.—*Structural changes in the solder film in a copper-tube joint, (60–39–1) lead-tin-antimony solder,* ×250.

(a) Initial structure of solder film, unetched; this is comparable with the structure shown in figure 3 (a). (b) solder film in a joint maintained at 250° F for 12,500 hours under a tensile shear stress of 90 lb/in.², unetched. Compare with figure 3 (c).

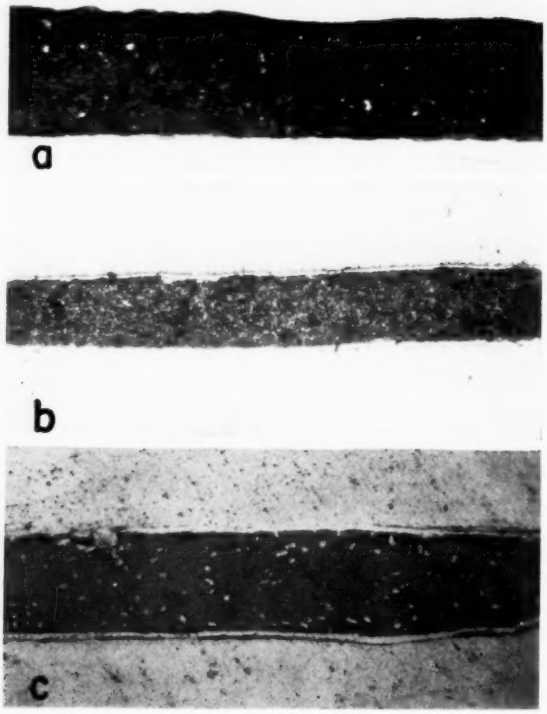

FIGURE 5.—*Structural changes in the solder film in copper-tube joint, (95–5) lead-tin solder, unetched,* ×250.

(a) Initial structure of solder film; (b) solder film in a joint maintained at 250° F for 7,200 hours under a tensile shear stress of 180 lb/in². Some trace of a bonding-alloy layer can be seen; (c) solder film in a joint maintained at 325° F for 6,800 hours under a tensile shear stress of 160 lb/in². Note the bonding-alloy layer and the coalescence within the solder film.

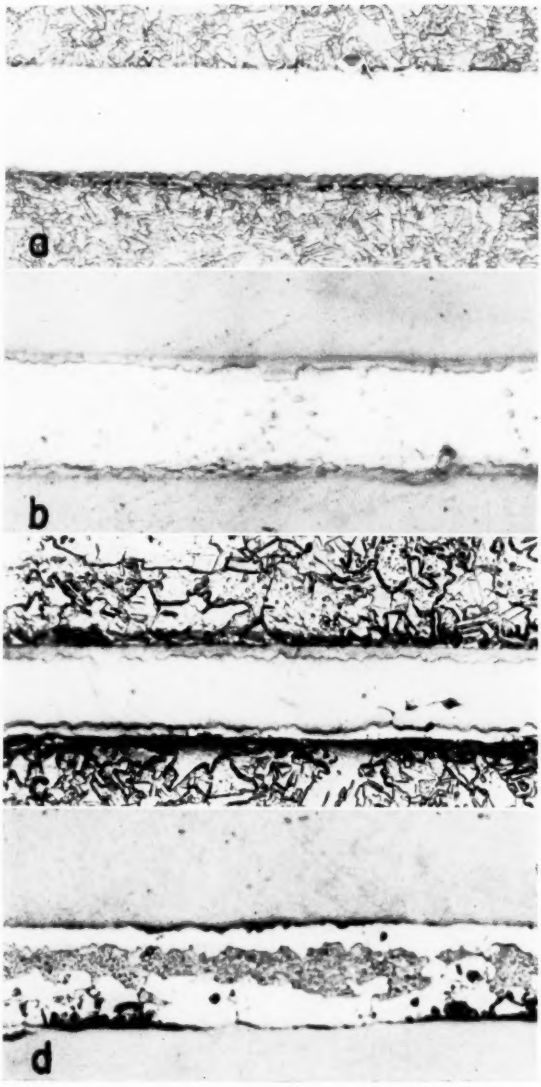

FIGURE 6.—*Structural changes in the solder film in a copper-tube joint, (95–5) tin-antimony solder,* ×250.

(a) Initial structure of solder film; note the bonding alloy layer, presumably not simple Cu_3Sn; etched; (b) solder film in a joint maintained at 250° F for 6,000 hours under a tensile shear stress of 175 lb/in.^{2} for 2,200 hours and 80 lb/in.^{2}, 3,800 hours, unetched. Note increase in the bonding layer; (c) solder film in a joint maintained at 250° F for 9,100 hours under a tensile shear stress of 80 lb/in.^{2}, etched; (d) solder film in a joint maintained at 325° F for 7,500 hours under a tensile shear stress of 153 lb/in.^{2}, unetched. Compare figure 3 (c).

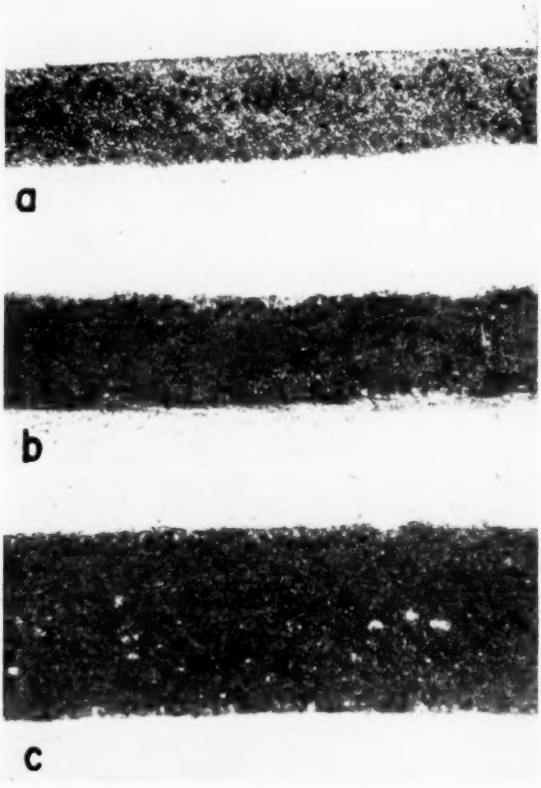

FIGURE 7.—*Structural changes in the solder film in a copper-tube joint, (95–5) lead-silver solder, unetched,* ×250.

(a) Initial structure of solder film; (b) solder film in a copper-tube joint maintained at 250° F for 13,200 hours under a tensile shear stress of 220 lb/in². Note coalescence of the silver constituent within the solder; (c) solder film in a copper-tube joint maintained at 325° F for 12,500 hours under a tensile shear stress of 105 lb/in². Note increased coalescence of the silver constituent of the solder.

FIGURE 8.—*Structural changes in the solder film in a copper-tube joint, (85.4–14.3–0.3) lead-cadmium-zinc solder, unetched,* ×250.

(a) Initial structure of the solder film; no bonding layer was detected; (b) solder film in a joint maintained at 325° F for 5,000 hours under a tensile shear stress of 90 lb/in². Note the pronounced development of the bonding-alloy layer, $CdCu_2$.

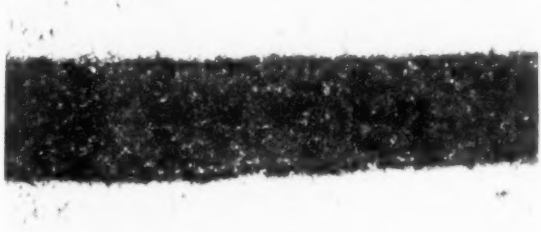

FIGURE 9.—*Initial structure of lead-solder film in a copper-tube joint, etched,* ×250.

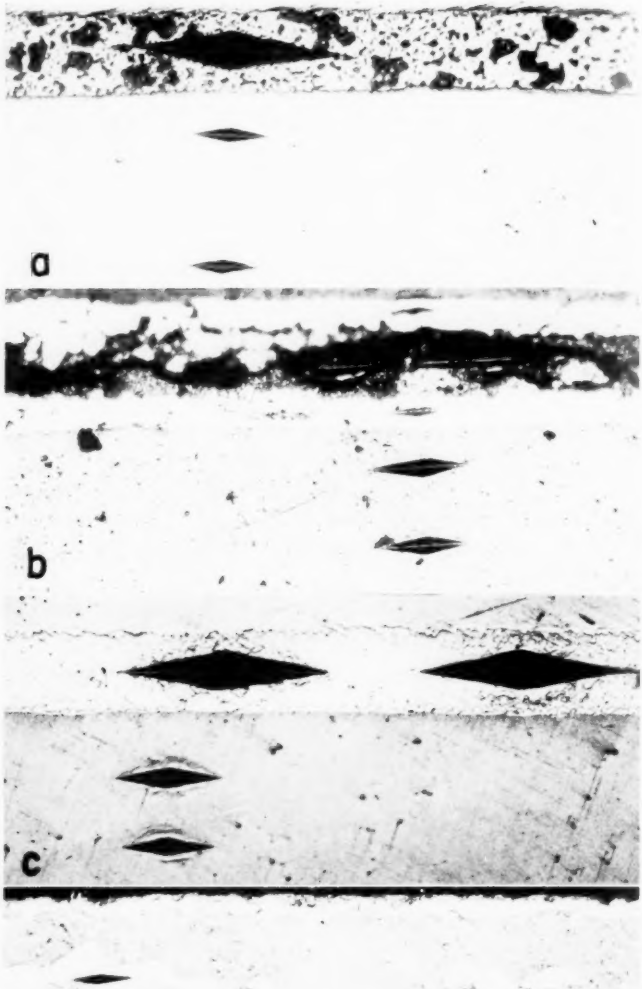

FIGURE 10.—*Indentations in the constituent parts of soldered copper-tube joints produced by the Knoop hardness indenter with 25-g load,* ×250.

(a) Initial condition of a solder film of (50–50) tin-lead solder. Indentation hardness; solder, 14; copper base, 102; (b) solder film similar to (a) after 12,000 hours at 250° F. Indentation hardness; center of solder film, 15; bonding-alloy layer, 196; copper base, 110; (c) initial condition of a solder film of (95–5) tin-antimony solder. Indentation hardness; solder, 22; copper base, 113; (d) solder film similar to (c) after 7,500 hours at 325° F. Indentation hardness; center of solder film, 19; bonding-alloy layer, 165; copper base, 99. Note the shatter cracks in the bonding layer adjacent to the indentations.

tin-base solders occurs readily if the solder is molten and the copper is clean and at the proper soldering temperature. It can also occur, but at a much slower rate, after the solder has solidified, provided the soldered joint is maintained for a long time at a sufficiently high temperature.

III. METALLOGRAPHIC STUDY OF SOLDERED JOINTS—RESULTS AND DISCUSSION

1. GENERAL DISCUSSION

Soldered sleeve joints of the kind shown in figure 1 were used to supply the specimens for metallographic examination. The joined

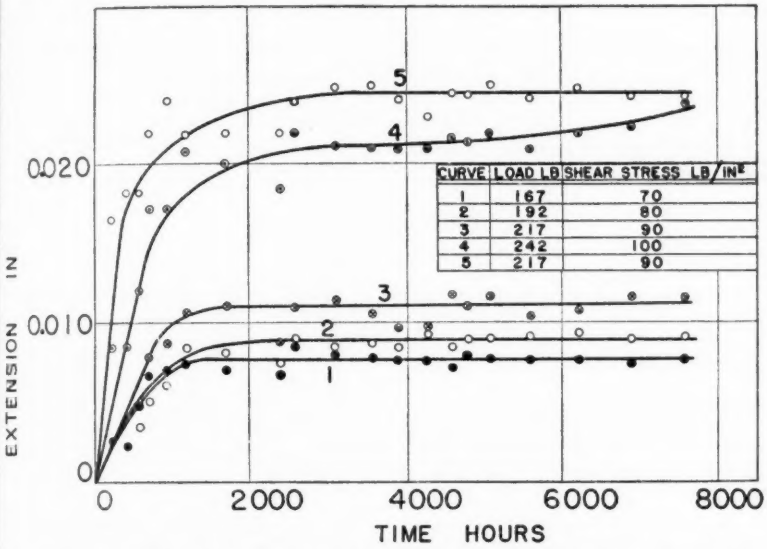

FIGURE 2.—*Extension-time curves of joints soldered with (50–50) tin-lead solder maintained at 250° F for 7,500 hours.*

Curve 5 for cast-brass (85–5–5–5) coupling; others for copper couplings; diametral clearance, 0.004 inch.

tubular specimens were maintained for long periods, usually under tensile load, at the temperature whose effect was being considered. The loading conditions are given in the legend for the corresponding micrograph in the succeeding figures. In some cases, after a specimen had been cut from the joint, the heating of the joint was continued under no load.

The solders used in making the joints were those reported in the previous studies [1, 2]. The nominal percentage compositions of the solders containing tin were (50–50) tin-lead, (95–5) tin-antimony, (60–39–1) lead-tin-antimony, and (95–5) lead-tin. The tin-free lead-base solders used were (85.4–14.3–0.3) lead-cadmium-zinc, (95–5) lead-silver, and high-purity lead.

In figure 2 are given time-extension curves of a series of jointed specimens made with (50–50) tin-lead solder maintained for long periods at 250° F under suitable tensile loads to produce the designated shear stresses. Two phenomena are outstanding in these

curves. During the initial stage of heating, approximately 1,000 hours, extension occurred in each of the joints, the extension increasing as the shear stress was increased. With increasing heating period, the resistance of the joint to extension at all of the applied stresses increased, so that after 2,000 hours' heating (approximately) the extension rate was negligible and remained so for the remainder of the 7,800 hours' heating period. It is evident that a change occurred within the joint, presumably in the soldered film, during the initial heating and that this change was nearly completed after 2,000 hours. At the conclusion of the test, the strength of the joint was measured by a short-time tensile test. The load required to fracture a joint was approximately seven-tenths of that needed for a freshly soldered joint.

To obtain further information on the change produced in a soldered joint by heat, comparison jointed specimens were held at 600° F (approximately) several hours, after which creep (extension with time) tests at room temperature were made. The observed extension was only half that of joints not subjected to this initial heating. Furthermore, the breaking strength of the joints (short-time test method) which had been heated to 600° F before being tested at room temperature was only three-fourths that of joints made in the same manner but not subjected to the preliminary heating at 600° F.

2. SOLDERS CONTAINING TIN

(a) (50–50) TIN-LEAD

The binary lead-tin alloys form a simple eutectic system with the eutectic composition at 63 percent of tin. The microstructure of (50–50) lead-tin solder therefore consists of the eutectic and some excess lead, with the eutectic constituting about 85 percent of the entire structure. Structural changes of two kinds might be expected to occur when (50–50) lead-tin solder is maintained at an elevated temperature in intimate contact with copper, as in a soldered joint: (a) within the solder film, coalescence of the structural constituents; and (b) at the copper interface, progressive alloying of the tin and copper as a result of mutual diffusion. Figure 3 illustrates microstructural changes of both kinds. The structure in figure 3 (*a*) is typical of the freshly soldered joint. The middle portion of the solder film, which is the structure of the unaltered solder, is characterized by the excess lead, occurring as dendrites, in a eutectic matrix. Adjacent to the copper, a thin alloy layer, the "bonding" alloy, is formed by the alloying of the tin of the molten solder and the copper. Continued heating at a moderately elevated temperature, 250° F (fig. 3, *b*), results in pronounced coalescence of the constituents within the solder film and an increase in thickness of the bonding-alloy layer. Presumably also, composition changes toward the middle of the solder film occurred as a result of inward diffusion of copper, which, however, is not detectable in the microstructure. With long-continued heating, the structural change becomes more pronounced, particularly in the copper-bearing alloy layer. This layer, at first at least, probably consists chiefly of the intermetallic compound Cu_3Sn. Another constituent of the copper-tin system, of higher copper content, was observed in some joints which had been heated for very long periods (fig. 3, *d*). It is also faintly visible in figure 3 (*c*).

A study of the relative hardness of the various portions of the soldered joint was made with a pyramidal diamond indenter [3].

Measurements were made on the solder film in its original condition, figure 3 (*a*), and on the bonding-alloy layers and coalesced constituents of the films after 7,500 and 12,000 hours at 250° F (fig. 3, *b* and *c*). An indenting load of 25 g was used and the indentation numbers tabulated (table 1) were calculated from the lengths of the indentations by the method of Knoop, Peters, and Emerson [3]. It was not possible to make indentations separately on the two bonding-alloy layers shown in figure 3 (*d*) because of their small widths. Brinell and Vickers numbers were also determined on the copper tubing to show the relationship between these and the Knoop numbers. While these same relationships do not necessarily hold for estimating Brinell and Vickers numbers equivalent to the Knoop numbers obtained on the constituents in the solder films, it is believed that the comparisons on the copper serve as a fair approximation.

TABLE 1.—*Hardness of constituent parts of soldered copper tube sleeve joints (Knoop pyramidal diamond microindenter, 25-g load)*

Nominal composition of solder (percent)	Condition	Location	Knoop indentation hardness number [1]
(50-50) lead-tin	Original	Center of solder film (fig. 10, a).	14
Do	12,000 hours at 250° F.	Center of solder film (fig. 10, b).	15
Do	do	Bonding-alloy layer (fig. 10, b).	196
(60-39-1) lead-tin-antimony	Original	Center of solder film	12
Do	12,000 hours at 250° F	do	14
Do	do	Bonding-alloy layer	198
(95-5) tin-antimony	Original	Center of solder film (fig. 10, c).	22
Do	7,500 hours at 325° F	Center of solder film (fig. 10, d).	1 9
Do	do	Bonding-alloy layer (fig. 10, d).	16 5
(85.4-14.3-0.3) lead-cadmium-zinc	Original	Center of solder film	1
Do	5,000 hours at 325° F	do	16
Do	do	Bonding-alloy layer	173 5

[1] The average Knoop indentation hardness number of the copper tubing, 8 specimens, transverse sections, was 107±8. The Brinell hardness number, 15-kg load, 1/16-inch ball, of copper tubing (99 Knoop indentation) was 101; (115 Knoop indentation) 114. The Vickers hardness number, 15-kg load, 136° square base pyramid, of same specimens was 107 and 120, respectively.

The hardness of the coalesced particles of tin-lead eutectic (fig. 3, *c*) as was expected was not significantly different from that of the solder in its original condition in the film (fig. 3, *a*) in which the eutectic was more uniformly dispersed. Both have essentially the same constitution. The hardness numbers obtained on the thin film have the same general magnitude as those obtained on tin-lead alloys in more massive form. The results may be considered as indicating also that no significant amount of copper had diffused as far as the middle of the film.

The hardness of the bonding-alloy layers adjacent to the copper is surprisingly high, being of the order of that of structural steels having a tensile strength of about 100,000 lb/in.^{2} These layers are considered to consist essentially of the copper-tin intermetallic compound. It is characteristic of intermetallic compounds of this kind that their hardness is much greater than that of any of the constituent metals. The shattered condition of the hard layers (fig. 3, *c*) is evidence that brittleness accompanies the greatly increased hardness.

Increased shear strength would also be expected in the hard, brittle layers and could account for the observed increase in the resistance of the joints to extension under tensile loads. Such joints, when pulled apart, whether in a short- or a long-time test, failed without appreciable extension as the load was increased to the rupturing point. Freshly made joints, in similar tests, showed increasing extension with increase in load practically to the breaking point.

(b) (60–39–1) LEAD-TIN-ANTIMONY AND (95–5) LEAD-TIN

The structural changes which were observed in the (60–39–1) lead-tin-antimony solder films (fig. 4) and in the (95–5) lead-tin solder (fig. 5) were of the same general nature as those described above. In the (95–5) lead-tin solder, however, the alloy layers were not nearly so thick and well developed, probably because of the relatively low tin content of the alloy.

Indentation-hardness tests could not be made on the thin, poorly developed bonding-alloy layer of the solder film of the (95–5) lead-tin solder. On the middle of the (60–39–1) lead-tin-antimony solder film in a freshly made joint, a Knoop indentation number of 12 was obtained (table 1). On the bonding-alloy layers, from a joint held at 250° F for 12,000 hours, the Knoop number was 198. These results agreed closely with those obtained on (50–50) tin-lead solder.

(c) (95–5) TIN-ANTIMONY SOLDER

The structural change in the (95–5) tin-antimony solder (fig. 6), although of the same general nature as those in the tin-lead solders, proceeded at a lower rate, and the bonding-alloy layer was distinctly different in some of its characteristics from the bonding-alloy layer in the lead-tin solder. Comparison of the micrographs in figure 3 with those in figure 6 of specimens treated at the same temperature, 250° F, illustrates the slower rate of alloy formation in the tin-antimony solder. The specimen of this solder treated at 325° F had essentially the same appearance as the specimens of lead-tin solder treated at 250° F.

The tin-antimony equilibrium diagram is rather complex. However, so far as the (95–5) tin-antimony solder is concerned, it is very simple, since tin is capable of holding approximately 9 percent of antimony in solid solution. The temperature interval within which the (95–5) solid solution is partially molten is relatively very narrow. Coalescence within the solid solution on continued heating is not to be expected until its composition has been substantially changed by diffusion of copper into it (fig. 6, *b*).

In the middle of the film of (95–5) tin-antimony solder in a freshly made joint, a Knoop number of 22 was obtained, showing that this solder is harder than the tin-lead solders (table 1). This result is in agreement with the higher strength at room temperature shown by joints made with this solder [1, 2].

In the diffusion zone bordering the film of (95–5) tin-antimony solder in a joint held at 325° F for 5,000 hours (fig. 6, *d*), a Knoop number of 200 was obtained, the same as in the corresponding diffusion zone of the tin-lead solders. These zones also probably consist of copper-tin intermetallic compound, possibly altered somewhat by antimony. This was indicated by a shattering effect when the indentations (fig. 10, *b*) were made.

3. LEAD-BASE TIN-FREE SOLDERS

(a) LEAD-SILVER

The solders of this group differed among themselves in their response to long-continued heating. The (95–5) lead-silver solder exhibited no marked tendency toward alloy formation with the adjacent copper, which was found to be so characteristic of the lead-tin solders.

Lead and silver form a simple eutectic series of binary alloys. The silver content of the eutectic is 2.3 percent and the eutectic temperature, 304° C (579° F). On long-continued heating, coalescence of the eutectic occurs, and the silver constituent becomes a more prominent feature of the microstructure (fig. 7).

(b) LEAD-CADMIUM-ZINC

The lead-cadmium alloy system is a simple eutectic one. The two constituent metals are soluble in each other to a limited extent. The eutectic of these solid solutions corresponds to a cadmium content of 17.4 percent by weight, the eutectic temperature being 240° C (464° F). The solder used (14 percent of cadmium), therefore, consists structurally of a eutectic matrix in which the excess constituent, lead, is embedded (fig. 8, *a*). The small amount of zinc (0.3 percent) is not considered to affect the properties of the finished joint. The changes observed in the microstructure of the solder films on copper after long-continued heating were similar to those described for the solders containing tin. Coalescence of the eutectic constituents is to be expected and is shown in figure 8 (*b*). A well-developed bonding-alloy layer also was developed as a result of the diffusion between the cadmium and copper, although a distinctly higher temperature was required. Presumably, the constituent in this layer is the intermetallic compound Cd_3Cu_2.

Indentation-hardness tests on the middle of the solder film of a freshly made joint showed a Knoop number of 15, which is at the same hardness level as that of tin-lead solders similarly tested (table 1). In a joint made with the same solder and held at 325° F for 5,000 hours, a Knoop number less than 13 was obtained in the middle of the solder film, indicating that coalescence of the eutectic constituents had resulted in a softening effect. In the diffusion zone near the bond, a Knoop number of 175 was obtained, which shows a hardness significantly lower than that of the copper-tin compound formed in the tin-alloy solders.

(c) HIGH-PURITY LEAD

As would be expected, high-purity lead when used as a solder on copper had no detectable alloying action, either in a freshly made joint or in the joints held for long periods of time at temperatures up to 325° F (fig. 9).

IV. CONCLUSIONS

1. Investigations previously reported have clearly shown the reliability of soldered sleeve joints in copper-tube lines used in domestic plumbing and for various other purposes. A limitation on the maximum temperature for elevated temperature service appeared necessary, however, especially for joints made with solder containing tin.

2. Joints made with solder containing tin were considered to be entirely satisfactory for service in which the temperatures did not ex-

ceed 250° F. Some lead-base solders, containing no tin, were considered reliable for use at somewhat higher temperatures, 325° F being the maximum.

3. A criterion for the complete evaluation of soldered joints of the type discussed here for extended use at elevated temperature is not furnished by strength measurements alone. The possibility of bond deterioration under long-continued heating must be considered also.

4. Creep, or time-extension, tests at a constant elevated temperature of joints made with (50–50) lead-tin solder showed an initial period, approximately 1,000 hours, during which extension within the soldered joint normally occurred, the magnitude of the extension being determined by the shear stress acting in the joint. However, this initial behavior was followed by a very great increase in creep resistance in the joint, and during the remainder of the period at the elevated temperature substantially no extension occurred. Such joints showed a marked decrease in strength, as determined subsequently at room temperature by short-time tensile tests.

5. To determine the nature of the change in the solder underlying this behavior of the joint, a metallographic study of the microstructure of soldered sleeve joints in copper tubing was made. Joints made with solders containing tin and maintained for long periods at 250° F showed coalescence of the microstructural constituents and progressive formation of a layer of a new constituent adjacent to the copper. This is evidently the intermetallic compound, designated as the "bonding-alloy layer" and consisting of Cu_3Sn, which results from alloying of the tin with copper by diffusion.

6. Hardness measurements of the bonding-alloy layer by the Knoop microindentation method showed it to be very much harder than the solder, the indentation harness numbers for (50–50) lead-tin solder and alloy layer being in the approximate ratio 14:196. The indentation hardness of the bonding alloy varied somewhat for the different solders but was always higher than that of the copper, which averaged 107. Fragmentation of the bonding-alloy layer was observed to occur in some cases as a result of the indentation hardness tests. The thickness of the hard, brittle bonding-alloy layer was dependent upon the initial tin content of the solder.

7. Tin-antimony solder used in sleeve joints, when maintained at an elevated temperature, behaved in essentially the same manner as tin-lead solder. The resulting bonding-alloy layer possessed the same general characteristics, although the hardness was somewhat lower than that of the bonding layer in the lead-tin solder film.

8. The lead-cadmium alloy showed a progressive growth of a bonding-alloy layer at elevated temperature which did not differ markedly in its characteristics from the corresponding constituent in the lead-tin solder films.

9. Pronounced coalescence of the structural constituents occurred in the lead-silver solder maintained at elevated temperature, but substantially no increase in the bonding layer was detected. No evidence of alloying with the copper base was observed in the lead-solder joints after long-continued heating.

The authors gratefully acknowledge their indebtedness to a number of their associates in the Division of Metallurgy, National Bureau of Standards, and particularly to H. K. Herschman for carrying out the hardness determinations, and to T. D. Brown for his assistance in the metallographic studies of the lead-base solders.

V. REFERENCES

[1] A. R. Maupin and W. H. Swanger, *Strength of soft-soldered joints in copper tubing*, Building Materials and Structures (1938) NBS Rep. BMS58.

[2] A. R. Maupin and W. H. Swanger, *Strength of sleeve joints in copper tubing made with various lead-base solders*, Building Materials and Structures (1942) NBS Rep. BMS83.

[3] F. Knoop, C. G. Peters, and W. B. Emerson, *A sensitive pyramidal-diamond tool for indentation measurements*, J. Research NBS **23,** 39 (1939) RP1220.

[4] S. J. Nightingale, *The jointing of metals, Part I. Soft solders and soldered joints*, Brit. Non-Ferrous Metals Research Assn., Research Reports, No. C 234/214 (Dec. 1936).

[5] R. Chadwick, *The influence of surface alloying on the strength of soft soldered joints*, J. Inst. Metals **62,** 277 (1938).

WASHINGTON, January 28, 1942.

U. S. DEPARTMENT OF COMMERCE NATIONAL BUREAU OF STANDARDS

RESEARCH PAPER RP1466

Part of Journal of Research of the National Bureau of Standards, Volume 28, April 1942

ELECTRICAL CONDUCTION IN THE GLASS INSULATION OF RESISTANCE THERMOMETERS

By Harold J. Hoge

ABSTRACT

At temperatures above 350° C, electrical conduction may become troublesome in the glass through which the leads of certain types of resistance thermometers are sealed. It was found that conduction in these seals is rapidly reduced by polarization of the glass, and that the error in temperature measurement resulting from conduction in the glass may be considerably reduced by adopting a measuring schedule which takes full advantage of this polarization.

One type of glass was investigated under experimental conditions which prevented polarization. At 445° C this glass had a volume resistivity of approximately 21,000 ohm-cm. The temperature dependence of the resistance could be represented very roughly by $1/r = Ae^{-\epsilon/kT}$, with ϵ having a value of the order of 0.8 electron volt.

CONTENTS

	Page
I. Introduction	489
II. Experimental results	490
III. Supplementary observations	495
IV. References	498

I. INTRODUCTION

The form of platinum resistance thermometer which consists of a Meyers-type coiled filament enclosed in a small platinum case was first used by Southard and Milner [1].[1] The coil is sealed inside the platinum case with a soft glass seal, as shown in figure 1.

Although this type of thermometer is not ordinarily used above 100° C, it is calibrated in the usual way [2] at the sulfur, steam, oxygen, and ice points. At the sulfur point (444.60° C) the soft glass is noticeably conducting, the conduction taking place between the two pairs of leads which pass through the glass and connect the thermometer with the bridge or potentiometer. For most of our thermometers the electromotive force between the two pairs of leads at the sulfur point is of the order of 0.075 v, the measuring current being 1 ma and the resistance at this temperature approximately 75 ohms. The conduction decreases as the temperature is lowered, and is not appreciable below 300° C. It might pass unnoticed except for the very rapid polarization of the glass, which causes the measured resistance to increase as soon as the electromotive force is applied to the specimen. After the current has flowed for a few minutes, the rate of increase of

[1] Figures in brackets indicate the literature references at the end of this paper.

resistance becomes negligible, indicating that the current in the glass is approaching a limiting value.

The present investigation was undertaken to see whether or not the remaining current in the glass was large enough to cause appreciable error in temperature measurements. Three seals, as nearly as possible like those in figure 1, were made, but with the thermometer coil omitted to make it possible to measure the resistance of the glass directly. A number of preliminary experiments on more roughly constructed seals had shown that, in general, the resistance of any specimen depended on its past thermal and electrical history. Accordingly, the

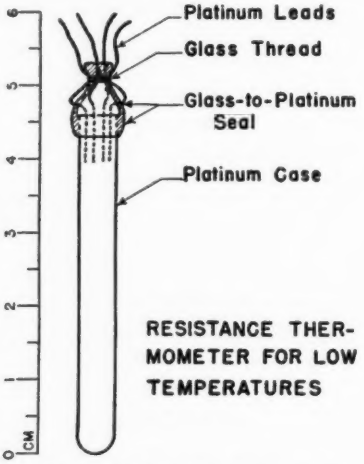

FIGURE 1.—*Scale drawing of a thermometer.*

The platinum leads are 0.2 mm in diameter. The platinum case has an inside diameter of 5 mm and weighs approximately 0.51 g/cm of length. The bottom is spun to a hemispherical form and the center welded. After the thermometer is filled with helium and sealed off, the glass tip is flattened to provide a shoulder so that the leads may be tied down with glass thread.

three seals were subjected to identical test schedules. No electromotive forces were applied to any of them prior to the measurements reported.

II. EXPERIMENTAL RESULTS

The first group of experiments was made with an apparatus which did not duplicate exactly the conditions of use in resistance thermometry, but provided somewhat greater sensitivity and flexibility. These experiments showed the general nature of the conduction phenomena and the relative merits of the three types of glass. They are most readily explained by reference to figure 2. A seal was placed in a small furnace and connected to the measuring equipment. Prior to the time $t=0$ the furnace and seal were held at a temperature of approximately 147° C, but at this time the furnace current was suddenly raised to a higher value. The resulting rise in temperature of the seal was indicated by a Chromel-Alumel thermocouple, whose electromotive force is given by the lowest curve of figure 2.

A 2,100-ohm resistance was connected in series with the seal. Measurement of the potential drop across part of this allowed the current through the seal to be computed, while the remainder of the resist-

ance served as a partial protection to the galvanometer in case of a short circuit in the seal. At regular intervals an electromotive force of 0.075 v was applied to the seal and the galvanometer deflection noted after 4½ seconds, which was the time required to reach maximum deflection. Connections to the seal were reversed before each succeeding application of the electromotive force, to reduce the effects of polarization. The current through the seal in arbitrary units (millimeters galvanometer deflection) is plotted in the upper curves

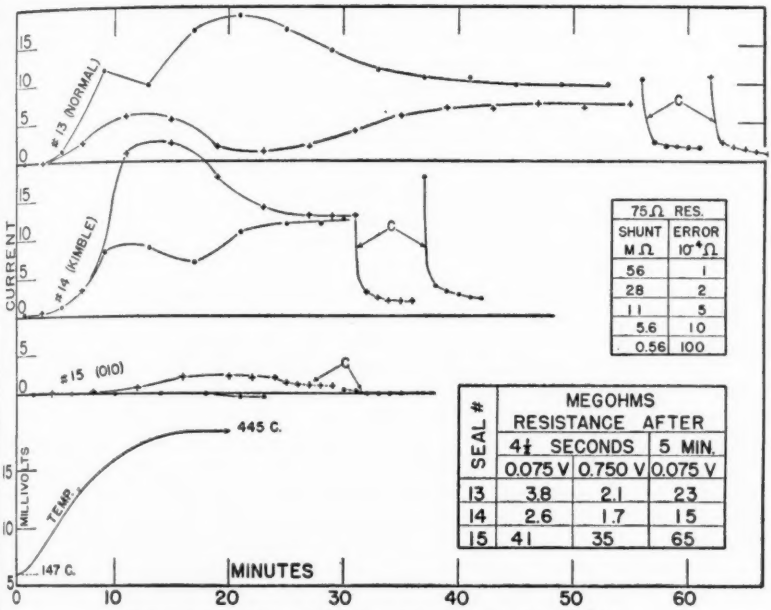

FIGURE 2.—*Data and curves for seals 13, 14, and 15.*

The current flowing through each seal was measured at intervals while the temperature was being raised. The six upper curves show the magnitude of *this* current in terms of galvanometer deflections, while the corresponding temperature may be obtained from the lowest curve, which shows the electromotive force developed by a Chromel-Alumel thermocouple placed in the furnace beside the test specimen.

The table of values at the lower right-hand corner gives the effective resistance of each seal at 445° C under various conditions of measurement. The upper table shows the magnitude of the error which will result if the thermometer has a resistance of 75 ohms, for various values of the effective resistance of the shunt (glass seal).

of figure 2, where dots and crosses refer respectively to the two directions of application of electromotive force to the seal. The applied electromotive force was measured by means of a potentiometer. As electromotive forces as high as 9 v were sometimes employed, the range of the potentiometer was extended by means of a volt box.

The existence of electromotive forces in the seals themselves is indicated by the fact that the currents in the two directions were not equal. The differences tended to disappear as the measurements continued. When an approximately steady state had been reached, the ordinates of the two curves for each seal were averaged and the current passing through the seal was computed. Dividing the applied electromotive force by this current yields the values in column 2 of the lower table of figure 2. All the values in this table were obtained at a seal temperature of 445° C. The current passing through a seal is a function both

of the ordinary resistance of the seal, and of the electromotive forces in the seal which result from the previous passage of current, each of which changes with the conditions of measurement. Hence the values in the lower table of figure 2 are not to be considered as resistances in the ordinary sense but rather as "effective resistances," which are nothing more than the quotient of the applied electromotive force by the current observed under the given conditions of measurement.

Data for the parts of the curves marked *C* were taken in a different way. Here the electromotive force was applied in the same direction and continuously for 5 minutes, galvanometer deflections being recorded at 1-minute intervals. Then the electromotive force was reversed and the current allowed to flow continuously for 5 minutes in the other direction. The two final values of the ordinate were averaged and used to obtain the effective resistance given in column 4 of the above-mentioned table. The values given in column 3 of this table were obtained in the same way as those in column 2, but the corresponding data are not plotted in the figure.

The effect of polarization is plainly evident from columns 2 and 4. By allowing the current to flow for 5 minutes rather than for only 4½ seconds, the effective resistances of the three seals at 445° C were increased by factors of 6.1, 5.8, and 1.6, respectively.

Seal 13 was of Corning normal bulb glass, which has been found to be satisfactory mechanically for the construction of thermometers. The other glasses had not been previously used. Seal 14 was made from a Kimble glass used in the construction of standard cells. The glass from which seal 15 (code No. 010) was made was kindly furnished us by H. R. Lillie, of the Corning Glass Works. One of the seals (No. 15) developed several small cracks some weeks after it was tested. As this seal had been the most satisfactory electrically of the three tested, it was thought desirable to make further tests to see whether the cracking could be prevented by careful annealing. Four similar seals were prepared, and placed in an annealing furnace. This was heated to approximately 525° C, then cooled fairly rapidly to 500° C. From this point down to 340° C the temperature was reduced slowly, by lowering the setting of the thermoregulator in 0.2–mv (5-degree) steps, at intervals of not less than 10 minutes.

These seals remained at room temperature for 2½ months without developing any cracks. They were then subjected to rapid heating and cooling, but were not, however, carried above the sulfur point (445° C). No cracks have developed as a result of this treatment, and we may conclude that seals made of this glass will, if carefully annealed, stand up under conditions as severe as those experienced in a sulfur-point calibration. If during the annealing of the platinum coil the thermometer is heated to a temperature much above 445° C, slow cooling may be necessary to avoid danger of breaking the seal.

From figure 2 it can readily be concluded that 4½ seconds is too short a time to allow the current to flow, if it is desired to take full advantage of the increase in effective seal resistance caused by polarization. Just how long it will be profitable to wait cannot be accurately predicted from the curves *C*, however, because of the dependence of the behavior of a seal on its past history. The rate at which the current through a seal diminishes with time is influenced by its initial condition of polarization, and this will depend in practice on the measuring schedule adopted.

To approximate the conditions of actual resistance thermometry, a circuit was employed in which the seal placed in a furnace at 445° C could be connected as a shunt across a 100-ohm standard resistor, which formed one arm of a Wheatstone bridge. The suitability of various mesauring schedules was investigated by determining the reduction in apparent resistance of the 100-ohm standard which resulted from the presence of the shunt.

In one set of measurements the battery key was closed for a certain length of time and then opened for the same length of time, and the seal error investigated as a function of this interval. The shunting effect of the seal decreased with increasing interval rapidly at first, but beyond a period of ½ minute on and ½ minute off the decrease in error was small. Unless the galvanometer zero is unusually stable, it should not ordinarily be worth while to increase the on and off intervals to more than 45 seconds each.

In another series of measurements the total period was held constant at 1½ minutes, while the relative lengths of the on and off periods were varied. The most desirable operating conditions were found to be in the neighborhood of 50 percent on and 50 percent off, but the minimum is rather broad.

The measurements described in the preceding paragraphs of this section were made without reversal of the current in the bridge. Many investigators balance their bridges not by opening and closing the battery circuit but by reversing the direction of the current, since the reversal gives double the deflection produced by simply reducing the current to zero. The method of reversal can be used, and the errors due to the glass seals are substantially the same as with the on-off method, when the time between reversals is made equal to the time on or off. If the temperature of a resistance thermometer is changing, as it will in a sulfur bath while the barometer is rising or falling, the on-off method of balancing will usually be found more convenient.

In a previously published abstract [3] it was recommended that the electromotive force be always applied to the seal in the same direction. This recommendation was based on the observed fact that the current falls less rapidly to its limiting value in a seal which has been previously polarized by passage of current in the opposite direction than when the current has previously flowed in the same direction. In spite of this fact the current-reversal method of balancing gave seal errors no larger than the on-off method. The probable explanation is the following: The galvanometer of a bridge which is in balance will be deflected in a certain direction when one arm is shunted by a glass seal, because of the passage of current through the seal. If the applied electromotive force is removed, by opening the battery key, the seal will discharge itself, and the galvanometer zero will be displaced in the opposite direction by the current from the seal. Hence the total effect of the seal on the balance of the bridge is the sum of two separate effects, when balance is obtained by the on-off method. When balance is obtained by current reversal, however, the entire effect of the seal is simply that of the current passing through it at the time readings are taken. With on and off intervals equal to the interval between reversals, an "on" current following an off period will indeed fall to a lower value than one which follows a current reversal; but because of the effect of the seal in displacing the galva-

nometer zero during the off period, this does not necessarily mean that the on-off method is preferable to the method of reversals.

Seal 14, when measured with on and off intervals of 30 seconds each, caused an error equal to that of a 20-megohm shunt. When measured with current reversal at 30-second intervals, the same seal caused approximately the same error. A sufficient number of readings was taken in each case to insure the presence of a steady state.

The effective resistance found for the seal with current reversals at 30-second intervals is larger than the effective resistance shown in figure 2 for the same seal with one cycle of current reversals at 5-minute intervals (curves *C*). The difference is doubtless due to differences in the condition of the seal in the two cases, although because of the greater polarization which takes place in the longer interval, it should not be assumed that current reversal at 30-second intervals would yield curves identical with the initial portions of the curves for 5-minute intervals.

When resistance measurements are made with a Mueller bridge, lead resistance is eliminated by interchanging lead connections. This normally reverses the electromotive force applied to the thermometer and will interrupt an otherwise uniform measuring schedule. This may be of no consequence if plenty of time can be taken for the measurement, but if it is necessary to go from "N" to "R" rapidly, it is desirable to place a reversing switch in the battery circuit and to operate this switch whenever the commutator is changed from "N" to "R" or vice versa. The direction of the flow of current in the seal will then be independent of the position of the commutator. If a four-pole double-throw switch is available, it is advantageous to use two poles for reversing the battery connections and the other two for simultaneously reversing the galvanometer connections. This will preserve the sense of the galvanometer deflections in their relation to the unbalance of the bridge.

It is realized that rather elaborate precautions have been outlined in order to eliminate errors equivalent to a few thousandths, or at most hundredths, of a degree. Such precautions would hardly be justified in routine measurements, but since they will ordinarily be required only at the time of making a sulfur-point calibration, it is thought that some investigators may wish to make use of them.

The upper table of figure 2 indicates what values of effective seal resistance may be tolerated. A platinum resistance thermometer having an ice-point resistance of between 25 and 30 ohms will have a sulfur-point resistance of the order of 75 ohms. If under the conditions of measurement the seal acts as a shunt having the resistance given in the first column of this table, the true resistance of the thermometer will be lowered by the amount given in the second column. Since for this type of thermometer dt/dR is roughly 10 degrees per ohm, the values in the last column are also approximately equal to the resulting error in thousandths of a degree.

The accuracy required in a sulfur-point calibration depends on the temperature interval in which the thermometer will subsequently be used. Suppose an error equivalent to 10 millidegrees is made in the sulfur-point calibration. Then the maximum resultant error [4] in the range −182.97° to 0° C is slightly less than 1 millidegree (near −120° C). In the range 0° to 100° C the maximum resultant error (near 50° C) is less than 0.2 millidegree.

III. SUPPLEMENTARY OBSERVATIONS

The experimental results given in section II (and fig. 2) of this paper have been explained in terms of an increase of polarization of the glass caused by the passage of current. There is a great deal of experimental evidence in the literature showing that the electric current in glass is ordinarily carried by sodium ions, and that polarization results from a depletion of sodium ions in the layer of glass near the anode. Schtschukarew and Müller [5], among others, have shown that resistivity values reproducible both from sample to sample and from time to time may be obtained by using electrodes capable of supplying sodium ions to the glass. Robinson [6] has also demonstrated the necessity of avoiding polarization if true values of the resistivity of glass are to be obtained.

It was thought worth while to measure the resistivity of one of the types of glass used for glass seals under conditions where polarization would be largely avoided. The experimental arrangement used for this purpose is shown schematically in figure 3, together with the results obtained. The high temperatures involved made it impossible to use the sodium-amalgam electrodes which are ordinarily employed, so a sodium-tin alloy (roughly 3Na:97Sn by weight) was used. As this alloy must be protected from the air, it was used only for the anode, while pure tin served for the cathode. The inside tube of the apparatus was made of the glass to be tested, which was Corning normal bulb glass, the same as that used in seal 13.

The curve at the left of the diagram was obtained by varying the applied electromotive force while the temperature was held constant at 445° C. Because the two electrodes were of different composition, an electromotive force was produced, with pure tin positive relative to the alloy. As shown by the first point on the curve, it was necessary to oppose the electromotive force of this cell by one of approximately 1.4 v to obtain zero current in an external circuit. As the opposing electromotive force was removed and replaced by one in the opposite direction, the current rapidly increased, while the effective electromotive force of the "cell" became much smaller. This is evident from the shape of the curve when it is recalled that if the cell developed no electromotive force, the curve would pass through the origin. The actual resistance of the specimen at 445° C was 432 ohms, which corresponds to a volume resistivity of the glass of approximately 21,000 ohm-cm.

From the lower table of figure 2 we find that the effective resistance of a seal made from this type of glass ranged from 2.1 to 23 megohms, depending on the conditions of measurement. By employing these figures and estimates of the dimensions of the seal, calculations of the "effective resistivity" of the glass may be made. Such calculations yielded values from 8 to 90 times larger than the 21,000 ohm-cm found when polarization was avoided. The difference is to be attributed primarily to the effect of polarization. The term "effective resistance" has been applied to the quotient of the applied electromotive force by the observed current, to distinguish it from the true resistance in the absence of polarization.

A number of preliminary experiments performed on seals 1 to 12 also indicated that polarization is more important than resistivity of

446682—42——7

the glass in determining the effective resistance. These seals consisted simply of two or more electrodes sealed into a small specimen of glass, and were measured under conditions less carefully controlled than those reported for seals 13, 14, and 15. Nevertheless it was plainly evident that the effective resistance was markedly affected by the material of the electrodes, and by the area in contact with the glass. Most of these seals had platinum electrodes, but one having constantan electrodes and another with silver electrodes had much lower effective resistances than the rest. In view of what is known about polarization, this is not surprising, for silver and copper will replace sodium in glass by electrolysis, while platinum will not [7]. Both the silver and the constantan discolored the glass somewhat when sealed in.

It is, of course, well known that a seal which has been polarized by the passage of current will serve as a source of electromotive force. In one of the preliminary experiments it was found that the initial charging by passage of current is not always necessary. In this experiment galvanometer deflections were produced by a freshly made seal to which no external electromotive force had ever been applied. The deflections corresponded to an electromotive force of the order of 0.1 v. Initial charges or polarization of this type could easily account for the directional dependence of the effective resistance found for seals 13, 14, and 15 (difference between corresponding curves of dots and crosses in fig. 2). The seal whose initial charge was investigated showed a much larger electromotive force during its initial heating than on subsequent occasions. No appreciable electromotive force was detected below about 300° C.

The apparatus shown in figure 3 was also used to obtain the temperature-dependence of the resistance of a specimen of glass. The dependence is shown by the semilog plot at the upper right in this figure. Both of the curves in figure 3 refer to the same specimen of Corning normal bulb glass. According to the theory of ionic conduction in solids [8, p. 235–241; and 9, p. 547–558], the passage of current is associated with the motion through the material of lattice imperfections, which may be either interstitial ions, vacancies at regular lattice points, or both. The current, which for ordinary field strengths should be proportional to the field, is also proportional to the number of lattice imperfections present and to the rate at which these imperfections wander through the material as a result of thermal agitation. Both of the two latter factors should vary exponentially with temperature. If E is the *net* energy required to form a lattice imperfection, and U is the height of the potential barrier to be surmounted when an imperfection moves from one position of equilibrium to another, the conductance should be proportional to

$$\exp-(\tfrac{1}{2}E+U)/kT.$$

Putting $\epsilon \equiv (\tfrac{1}{2}E+U)$ the resistance of a specimen should be given by

$$1/r = Ae^{-\epsilon/kT}.$$

The extent to which one is justified in applying a theory of this kind to glass is open to question. Since there is no long-range order in glass and only a limited amount of short-range order [10, 11], one might expect that the quantities U and E would not be sharply defined. However, it is of interest to see that the observed resistance of the glass does show a roughly exponential temperature-dependence.

Taking logarithms of the equation above, we obtain

$$\log r = -\log A + \frac{\epsilon}{2.303k}\left(\frac{1}{T}\right);$$

and by plotting log r against $1/T$, we should be able to obtain ϵ from the slope. The experimental curve of figure 3 decreases in slope as the temperature increases. For comparison the dotted straight line, which has a slope corresponding to $\epsilon = 0.8$ electron-volt, was drawn. This can be seen to be roughly equal to the mean slope of the experi-

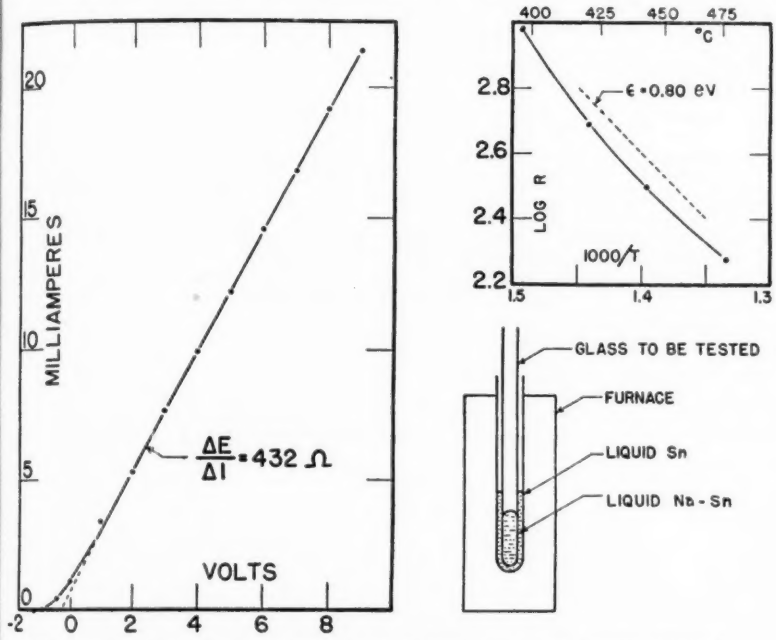

FIGURE 3.—*Arrangement to eliminate polarization, and results obtained.*

The curve at the left gives the variation of current with applied electromotive force, and shows that the "cell" develops an open-circuit electromotive force at 445° C, of the order of 1.4 v. Pure tin is positive relative to the alloy, which had a composition of roughly 3Na:97Sn by weight.

The curve at the upper right shows the temperature-dependence of the resistance of the glass when the electromotive force was held constant. The dotted line represents a slope corresponding to $\epsilon = 0.8$ electron-volt in the equation $1/r = Ae^{-\epsilon/kT}$.

mental curve. A suitable temperature-dependence of U or E could account for the observed curvature, or the curvature may be associated with the lack of sharply defined values of these quantities. According to Seitz [9, p. 549], the coefficient A is proportional to T^2. The temperature variation in this factor is much less important than in the exponential factor. If A is assumed to vary as T^2, the value obtained for ϵ in figure 3 is reduced by about 20 percent, without noticeable reduction in the curvature of the graph.

The author acknowledges valuable discussions with Frank Wenner, of the Resistance Measurements Section.

IV. REFERENCES

[1] J. C. Southard and R. T. Milner, *Low temperature specific heats. II. The calibration of the thermometer and the resistance of* Pt, Pt—10% Rh, *and constantan between −259 and −190°.* J. Am. Chem. Soc. **55,** 4384–4391 (1933).

[2] George K. Burgess, *The international temperature scale,* BS J. Research **1,** 635–640 (1928) RP22.

[3] Harold J. Hoge, *Electrical conduction in the glass insulation of resistance thermometers,* Phys. Rev. **59,** 921 (1941) [abstract].

[4] E. F. Mueller, *Precision Resistance Thermometry.* Temperature, its Measurement and Control in Science and Industry, p. 162–179 (Reinhold Pub. Corp., New York, N. Y., 1941).

[5] S. A. Schtschukarew and R. L. Müller, *Investigation of the electrical conductivity of glasses. System* $B_2O_3+Na_2O$. Z. physik. Chem. **A150,** 439–475 (1930).

[6] Denis M. Robinson, *The unpolarized resistivity of glass.* Physics, **2,** 52–59 (1932).

[7] George W. Morey, The Properties of Glass, ch. 17 (Reinhold Pub. Corp., New York, N. Y. 1938).

[8] Millard F. Manning and Maurice E. Bell, *Electrical conduction and related phenomena in solid dielectrics.* Rev. Mod. Phys. **12,** 215–256 (1940).

[9] Frederick Seitz, The Modern Theory of Solids (McGraw-Hill Book Co., New York, N. Y., 1940).

10] B. E. Warren and J. Biscoe, *Fourier Analysis of X-ray patterns of soda-silica glass.* J. Am. Ceramic Soc. **21,** 259–265 (1938).

[11] J. Biscoe, M. A. A. Druesne, and B. E. Warren, *X-ray study of potash-silica glass.* J. Am. Ceramic Soc. **24,** 100–102 (1941).

WASHINGTON, February 13, 1942.

U. S. Department of Commerce National Bureau of Standards

RESEARCH PAPER RP1467

Part of Journal of Research of the National Bureau of Standards, Volume 28, April 1942

TENSILE AND COMPRESSIVE PROPERTIES OF SOME STAINLESS-STEEL SHEETS

By C. S. Aitchison, Walter Ramberg, L. B. Tuckerman, and Herbert L. Whittemore

ABSTRACT

Tensile and compressive tests were made on specimens from chromium-nickel (17-7 and 18-7) stainless-steel sheets, with cold-reductions from zero percent (annealed) to 50 percent, and thicknesses from 0.01 to 0.06 in. The tensile yield strengths ranged from 34 to 200 kips/in². The effect of a stress-relieving treatment at 300° C for 24 hours was investigated for one of the compositions.

The tensile tests were made on standard specimens. The compressive tests were made by the pack method developed at the National Bureau of Standards and by the cylinder method developed by Russell Franks, of the Union Carbide & Carbon Research Laboratories. Tests were made on both longitudinal and transverse specimens from each sheet.

The results are given in tables and stress-strain curves to facilitate application in the design of light-weight structures from these materials. The effect of the degree of cold-reduction and of the stress-relieving treatment on the shape of the stress-strain curves and on the tensile and compressive properties is discussed.

CONTENTS

	Page
I. Introduction	499
II. Material	500
III. Method of testing	501
1. Tensile tests	501
2. Pack compressive tests	501
3. Cylinder compressive tests	502
IV. Results and discussion	502
V. Conclusions	504
VI. References	505

I. INTRODUCTION

There is a definite trend in structural design to use less material and so design the members that they are more efficient under load. Although this trend is noticeable in stationary structures, it is particularly marked in mobile structures, such as aircraft, where reduction in weight contributes directly to increased pay load, increased cruising range, and higher speed.

Stainless steel, available in sheets of a wide range of thickness, has, when cold-worked, a high strength-weight ratio, and since it is quite highly resistant to corrosion, little, if any, loss of strength results during its service life.

To make the most efficient use of a material, particularly where thin sheets are employed, the designer must have accurate and reliable data on the tensile and compressive properties. Many aircraft members are subjected to high compressive stress—obviously compression members should not fail at loads below those required to produce tensile failure in some other part of the structure.

To provide data on the tensile and compressive properties of stainless-steel sheets, the following manufacturers sponsored an investigation at the National Bureau of Standards under the Research Associate Plan [1]: [1]

Allegheny Ludlum Steel Corporation.
American Rolling Mill Co.
American Steel & Wire Co.
Carnegie-Illinois Steel Corporation.
Crucible Steel Company of America.
Electro Metallurgical Co.
International Nickel Co.
Republic Steel Corporation.
Rustless Iron & Steel Corporation.

The members of the sponsors' committee representing the manufacturers were:

Milton Male, chairman, United States Steel Corporation.
L. S. Bergen, Crucible Steel Company of America.
V. B. Browne, Allegheny Ludlum Steel Corporation.
A. L. Feild, Rustless Iron & Steel Corporation.
Russell Franks, Union Carbide & Carbon Research Laboratories.
H. J. French, International Nickel Co.
T. F. Olt, American Rolling Mill Co.
E. C. Smith, Republic Steel Corporation.

The purpose of this investigation was to determine the tensile and compressive properties of stainless-steel sheets of two chemical compositions which are commercially available and particularly suitable for aircraft structures. Compressive tests were to be made on flat sheet by the pack method [2] developed at the National Bureau of Standards and on sheet rolled into cylinders by the cylinder method [3] developed by Franks and Binder.

II. MATERIAL

The stainless steel used in this investigation was obtained from two of the cooperating manufacturers. In this report the heat of steel from one manufacturer will be called "17–7 sheet" and the heat from the second manufacturer "18–7 sheet." The chemical compositions, given in table 1, were furnished by the manufacturers.

The sheets were cold-rolled to the nominal thickness after the final anneal in order to increase the mechanical properties. "Cold-reduction" is defined as the percentage decrease in thickness after the final anneal. The thickness and the cold-reduction for the 17–7 sheets are given in table 2 and for the 18–7 sheets in table 3. For identification, the sheets were numbered consecutively as they were received.

[1] Numbers in brackets indicate the literature references at the end of this paper.

III. METHOD OF TESTING

1. TENSILE TESTS

From each 17–7 sheet, two tensile specimens were taken longitudinally and two transversely to the direction in which the sheets had been rolled. One specimen of each was stress-relieved by heating to 300° C for 24 hours, followed by air-cooling. From each 18–7 sheet, one tensile specimen was taken longitudinally and one transversely. None of the specimens of the 18–7 sheet was stress-relieved. The specimens were ASTM standard test specimens [4], ½ in. wide and 2-in. gage length. The cross-sectional area of each specimen was computed from its measured thickness and width.

The specimens were tested in a Baldwin-Southwark testing machine having a fluid-support, a Tate-Emery load-indicating mechanism, and scale ranges of 1, 10, and 20 kips.[2] Templin grips were used to hold the specimens.

The strain was measured by a pair of Tuckerman 2-in. optical strain gages, having 0.4-in. knife-edges and lozenges. Each division of the vernier scale for these gages corresponded to a strain of 0.000004. The readings were estimated to one-half a division. The strain gages were attached to opposite faces of the reduced section when the specimen was under an initial load, not exceeding 4.2 kips/in^2.

For stresses up to the yield strength, the loading rate was about (2 kips/in.^{2})/min. The speed of testing from yield strength to failure corresponded to a movement of the testing-machine head of 0.03 in./min. The value of initial strain, corresponding to the stress at the initial load, was obtained by a least-square extrapolation to zero stress.

Marks were spaced ¼ in. apart in the gage length, and the elongation was measured in accordance with AST Mspecifications [4].

2. PACK COMPRESSIVE TESTS

Pack compressive tests were made on both longitudinal and transverse specimens taken from all sheets having a thickness of 0.020 in. or greater. These tests were not made on the 0.010-in. sheet nor on any sheets which had been stress-relieved. Each pack consisted of several specimens taken from the same sheet and in the same direction. The specimens for the packs from 0.020-, 0.035-, and 0.040-in. sheet were cemented together with fused shellac, but the specimens from the 0.060-in. sheet were not cemented together. The fusing temperature was not higher than 66° C and the fusing time not more than 8 hours. The number of specimens and the lengths of the packs are given in tables 4 and 5. There was a steel clamp at each end of each pack.

For the packs tested in the subpress (see tables), the middle specimen was about 0.03 in. wider than the others. For all the other packs, all the specimens were of the same width to facilitate machining.

The cross-sectional area of each pack was determined by the weight method [5]. The length was measured before and the weight and density determined after the pack was tested and the shellac removed.

[2] A kip is 1,000 lb.

The packs were loaded in Baldwin-Southwark testing machines having fluid-supports, Tate-Emery load-indicating mechanisms, and scale ranges of 6, 24, and 120, or 1, 10, and 20 kips. They were tested between hardened and ground steel blocks. To apply the load uniformly, a shim of plaster of paris was cast between the upper block and the head of the testing machine.

The strain was measured by a pair of 1-in. Tuckerman optical strain gages, having 0.2 in. knife-edges and lozenges. Each division of the vernier scale of these gages corresponded to a strain of 0.000004. The readings were estimated to one-half a division. The strain gages were attached to the middle of the opposite edge faces when the pack was under the initial load, not exceeding 2.3 kip/in^2.

The rate of loading was about (2 kips/in.^{2})/min. The value of strain corresponding to the stress at the initial load was obtained by a least-square extrapolation to zero stress.

3. CYLINDER COMPRESSIVE TESTS

The specimens for the cylinder compressive tests were taken both longitudinally and transversely from all sheets except those having a thickness of 0.060 in. The specimens were rolled to shape and the axial butt joints soldered under the direction of Russell Franks at the Union Carbide and Carbon Research Laboratories.

Additional longitudinal and transverse cylinders from 17–7 sheets were given a stress-relieving treatment, before they were soldered, by heating at 300° C for 24 hours followed by air-cooling.

The dimensions of the cylinders are given in tables 4 and 5. The bases of the cylinders were plane and were parallel within 0.0004 in. The ends of the cylinders were restrained against crinkling by annular castings of Wood's metal having a thickness of about ¼ in. along the length of the cylinder. A clearance was maintained between the end face of the casting and the end face of the cylinder, to assure that the compressive load would act only on the cylinder. The cross-sectional area was determined by the weight method [5] after the specimens were machined but before they were rolled into cylinders.

The procedure for loading and measuring strain was the same for the cylinders as for the packs. The strain gages were attached to opposite elements of the outside cylindrical surface when the cylinder was under the initial load. Each of those elements was about an equal distance from the butt joint.

IV. RESULTS AND DISCUSSION

The stress-strain curves for each specimen are shown in figures 1 to 55. Figure 56 shows the individual points for the 18–7, 0.060-in. sheet having 47.7 percent cold-reduction (fig. 55) to indicate the order of agreement between the points and the curves drawn through them. The other stress-strain curves are drawn without indicating the individual points in order to facilitate the ease of obtaining tangent moduli. They are all plotted to the same scales, and a straight-line projection of these curves in all cases would pass through the origin at zero stress and zero strain. The slope of the straight line was determined from the low-load data by the method of least squares,

which, although requiring a certain amount of computation, is less dependent upon judgment than is the drawing of a line through the points. The reason for obtaining this low-load (or initial) slope is that it permits the determination of the yield-strength value (offset=0.2 percent) for each specimen individually.

The tensile and compressive properties of the specimens are given in tables 4 and 5. For all sheets, except those that were stress-relieved, both the longitudinal and the transverse tensile strengths were significantly greater for the 18–7 stainless steel than for the 17–7 stainless steel with comparable cold-reduction. The elongations for the longitudinal specimens were consistently somewhat less for the 18–7 material than for the 17–7, but the elongations for the transverse specimens were nearly the same. There were no consistent differences between the yield strengths. In considering the elongations, it should be noted that the rates of loading are much lower than those customary in commercial practice and that, consequently, the elongations generally will be higher than those obtained commercially. For example, an increase in the rate of movement of the testing machine head from 0.03 to 0.10 in./min lowered the elongation of a representative sample from 32.0 to 15.5 percent.

Certain differences were found in the shape of the stress-strain curves, depending upon the orientation of the specimens in the sheet and the nature of the loading; that is, tension or compression. For the annealed sheets (zero cold-reduction), the tensile and pack compressive stress-strain curves were almost the same. The ordinates of each cylinder compressive stress-strain curve were in all cases larger than the corresponding ordinates of both the tensile and pack compressive stress-strain curves. This was shown by the cylinder compressive yield strengths, which exceeded the pack compressive yield strengths by more than 14 percent.

For the cold-reduced sheets, regardless of thickness, the tensile stress-strain curves for the longitudinal specimens and for the transverse specimens were significantly different in shape. However, the tensile yield strengths for the longitudinal specimens were about the same as for the transverse specimens. There were large differences in shape between the compressive stress-strain curves for the longitudinal packs, or cylinders, and for the transverse packs, or cylinders. These differences were greater with increased cold-reduction.

For the cold-reduced sheets, the ordinates of the compressive stress-strain curves for *transverse* packs, or cylinders, were significantly larger than the corresponding ordinates of the tensile curves for either the longitudinal or transverse specimens. However, the ordinates of the compressive stress-strain curves for the *longitudinal* packs, or cylinders, were markedly smaller than the corresponding ordinates of the tensile curves for either the longitudinal or the transverse specimens.

For the cold-reduced sheets, the compressive yield strengths for the transverse cylinders and for the transverse packs were nearly the same. However, the compressive yield strengths for the longitudinal cylinders exceeded those for the longitudinal packs by more than 7 percent.

The stress-strain curves for stress-relieved specimens from the cold-reduced sheets were significantly different in shape from the curves from corresponding specimens which were not stress-relieved. The

curves for the stress-relieved specimens did not change in slope as rapidly over the lower portion of the curve but, particularly for cold-reductions up to 20 percent, changed more rapidly over the upper portion of the curve in the neighborhood of the yield strength.

The curves of strengths and elongations plotted against cold-reductions (figs. 57 to 66) were not smooth, but they were remarkably regular considering that they were obtained from only one specimen for each cold-reduction. They suggest an approximate relationship between strength or elongation and cold-reduction independent of thickness. They show that the strengthening effect of cold-reduction is much greater on the yield strength than upon the tensile strength and that this effect is more pronounced in compression for transverse packs or cylinders than for longitudinal packs or cylinders.

For the 17–7 sheets, the tensile strengths for stress-relieved specimens were nearly the same as those for the specimens not stress-relieved. However, the elongations for the former were significantly greater than for the latter. For cold-reductions less than 20 percent, stress-relieving had very little effect on the tensile yield strength. For cold-reductions greater than 20 percent, stress-relieving significantly increased the tensile yield strengths. Stress-relieving caused no difference in compressive yield strength for transverse cylinders when the cold-reduction was small. At 20-percent cold-reduction, however, the yield strength of stress-relieved transverse cylinders was significantly greater than that of the nonstress-relieved cylinders, and the difference increased with the degree of cold-reduction.

V. CONCLUSIONS

The stress-strain graphs and the tensile and compressive properties of 17–7 and 18–7 stainless steel sheets, with longitudinal tensile yield strengths from 34 to 200 kips/in.^{2} (corresponding to a range of sheets from annealed to 50-percent cold-reduction) and with thicknesses from 0.01 to 0.06 in., justify the following conclusions:

1. For annealed sheet, the stress-strain curves and the yield strengths from both tensile and pack compressive tests were about the same. The ordinates of the compressive stress-strain curves for either longitudinal or transverse cylinders were in all cases larger than the corresponding ordinates for tensile or pack compressive stress-strain curves.

2. For cold-reduced sheet, the tensile stress-strain curves for longitudinal specimens differed in shape from the tensile stress-strain curves for transverse specimens but the yield strengths for the longitudinal and transverse specimens were about the same.

3. For cold-reduced sheet, the compressive stress-strain curves for the longitudinal packs, or cylinders, and for the transverse packs, or cylinders, differed widely in shape. The yield strengths for the longitudinal packs, or cylinders, were markedly less than those for the transverse packs, or cylinders.

4. For cold-reduced sheet, the ordinates of the compressive stress-strain curves for transverse packs, or cylinders, were significantly larger than the corresponding ordinates of the tensile stress-strain curves for either longitudinal or transverse specimens. But the ordinates of the compressive stress-strain curves for longitudinal packs, or cylinders, were appreciably smaller than the corresponding ordinates

of the tensile stress-strain curves for either longitudinal or transverse specimens.

5. With comparable cold-reduction, the tensile strengths and the tensile and compressive yield strengths were about the same for all thicknesses of sheet investigated.

6. Stress-relieving increased the tensile and compressive yield strengths in both longitudinal and transverse directions. This effect was more marked the greater the amount of cold-reduction.

The authors express their appreciation to R. W. Gerby, G. E. Marquis, and W. H. Mather for their work in carrying out the tests and their helpful comments and suggestions.

VI. REFERENCES

[1] Research associates at the Bureau of Standards, NBS Circular C296 (1926).
[2] C. S. Aitchison and L. B. Tuckerman, The "Pack" Method for Compressive Tests of Thin Specimens of Materials Used in Thin-Wall Structures, NACA Rep. 649 (1939).
[3] Russell Franks and W. O. Binder, *The stress-strain characteristics of cold-rolled austenitic stainless steels in compression as determined by the cylinder test method*, Proc. ASTM **41,** 629 (1941).
[4] Tentative Methods of Tension Testing of Metallic Materials, E8–40T. ASTM Standards, 1940 supplement, pt. 1, Metals, p. 453.
[5] James A. Miller, *Determination of cross-sectional areas of structural members*, J. Research NBS **23,** 329 (1939) RP1237.

TABLE 1.—*Chemical compositions of sheet*

[Analysis as determined by the producers]

Elements	17–7 sheet	18–7 sheet
	Percent	*Percent*
Carbon	0.12	0.11
Manganese	1.26	.56
Phosphorus	0.015	.014
Sulfur	.009	.015
Silicon	.36	.272
Chromium	17.44	17.90
Nickel	7.18	6.72

TABLE 2.—*Thickness and cold-reduction of 17–7 sheets*

Sheet number	Thickness, nominal	Cold-reduction [1]
	Inch	*Percent*
225	0.01	0.0
214	.01	8.2
219	.01	18.0
221	.01	28.0
223	.01	37.0
218	.02	0.0
216	.02	8.2
204	.02	18.0
202	.02	30.5
200	.02	37.5
197	.04	0.0
211	.04	9.2
209	.04	23.6
207	.04	28.5
205	.04	38.8

[1] Values reported by the producer.

TABLE 3.—*Thickness and cold-reduction of 18–7 sheet*

Sheet number	Thickness, nominal	Cold-reduction [1]	Sheet number	Thickness, nominal	Cold-reduction [1]
	Inch	*Percent*		*Inch*	*Percent*
51	0.01	0.0	36	0.035	0.0
50	.01	12.0	25	.035	7.5
52	.01	19.6	26	.035	7.5
53	.01	31.5	27	.035	19.6
54	.01	40.0	86	.035	29.2
59	.01	50.0	37	.035	39.7
55	.01	52.5	38	.035	47.0
57	.02	0.0	39	.035	47.0
68	.02	.0	41	.06	0.0
58	.02	5.3	7	.06	6.7
69	.02	5.3	8	.06	18.1
44	.02	18.3	11	.06	30.5
45	.02	18.3	29	.06	36.9
46	.02	29.8	13	.06	47.7
47	.02	29.8			
56	.02	37.5			
66	.02	37.5			
48	.02	50.0			
49	.02	50.0			
35	.035	0.0			

[1] Values reported by the producer.

TABLE 4.—*Results of tensile and compressive tests on 17–7 stainless stee*

Cold-reduction	Tension						Pack compression					Cylinder compression				
	Specimen number	Slope of straight line [1]	Yield strength;[2] offset = 0.2%	Tensile strength	Elongation in 2 in.	Remarks[3]	Pack number	Length	Number of specimens in pack	Slope of straight line [1]	Yield strength;[2] offset = 0.2%	Cylinder number	Length	Outside diameter, nominal	Slope of straight line [1]	Yield strength;[2] offset = 0.2%
0.010 IN. THICK, AS-ROLLED, LONGITUDINAL																
Percent		*Kips/in.²*	*Kips/in.²*	*Kips/in.²*	%			*Inches*		*Kips/in.²*	*Kips/in.²*		*Inches*	*Inches*	*Kips/in.²*	*Kips/in.²*
0.0	225-B1L	29,100	39.0	136.3	72.0	d (71.0)	None					225-CX3L	1.749	0.40	28,900	43.7
8.2	214-B1L	27,400	77.9	155.6	60.0	d (58.0)	do					214-CX3L	1.744	.40	26,100	60.5
18.0	219-B2L	28,500	103.8	167.3	49.0	b	do					219-CX3L	1.750	.40	27,700	73.7
28.0	221-B1L	27,300	133.1	174.7	46.0	b	do					221-CX3L	1.745	.40	25,700	90.2
37.0	223-B2L	26,500	150.3	187.5	40.0	c	do					223-CX3L	1.753	.40	26,400	98.3
0.010 IN. THICK, AS-ROLLED, TRANSVERSE																
0.0	225-B1T	29,100	38.5	120.9	53.0	b	None					225-CX3T	1.746	0.40	33,200	42.6
8.2	214-B1T	28,500	76.7	152.7	53.5	b	do					214-CX3T	1.750	.40	30,000	81.5
18.0	219-B1T	28,400	100.8	161.9	40.5	b	do					219-CX3T	1.752	.40	30,500	104.4
28.0	221-B1T	29,000	121.0	176.9	42.0	c	do					221-CX3T	1.740	.40	29,400	137.8
37.0	223-B1T	28,900	138.8	186.4	39.0	d (35.5)	do					223-CX3T	1.746	.40	28,600	150.0
0.010 IN. THICK, STRESS-RELIEVED, LONGITUDINAL																
0.0	225-Y3L	30,300	39.2	135.5	84.5	c	None					225-CX4L	1.749	0.40	29,700	43.5
8.2	214-Y3L	28,800	78.2	149.7	67.0	c	do					214-CX4L	1.744	.40	28,100	71.6
18.0	219-Y4L	28,400	108.4	162.9	54.0	c	do					219-CX4L	1.747	.40	31,500	89.7
28.0	221-Y3L	27,900	141.5	174.4	53.0	b	do					221-CX4L	1.750	.40	28,600	109.7
37.0	223-Y4L	29,400	171.7	198.2	37.0	b	do					223-CX4L	1.749	.40	29,200	123.4

[1] Obtai ned by least-square fit to lower portion of stress-strain graph.
[2] Using straight line with slope given in previous column.
[3] Letters describe location of fracture in accordance with section 24 and figure 19, page 462 of ASTM Specification E8-40T. Numbers in parentheses are alternate elongation values determined from sum of the distances *A* to *F* and *B* to *E* shown in that figure.

TABLE 4.—*Results of tensile and compressive tests on 17–7 stainless steel*—Continued

Cold-reduction	Tension						Pack compression					Cylinder compression				
	Specimen number	Slope of straight line [1]	Yield strength;[2] offset = 0.2%	Tensile strength	Elongation in 2 in.	Remarks[3]	Pack number	Length	Number of specimens in pack	Slope of straight line [1]	Yield strength;[2] offset = 0.2%	Cylinder number	Length	Outside diameter, nominal	Slope of straight line [1]	Yield strength;[2] offset = 0.2%
							0.010 IN. THICK, STRESS-RELIEVED, TRANSVERSE									
Percent		*Kips/in.*	*Kips/in.*	*Kips/in.*	%			*Inches*		*Kips/in.*	*Kips/in.*		*Inches*	*Inches*	*Kips/in.*	*Kips/in.*
0.0	225–Y3T	29,400	39.0	135.9	81.5	c	None					225–CX4T	1.750	0.40	26,900	42.9
8.2	214–Y3T	28,000	77.7	148.6	67.5	b	do					214–CX4T	1.750	.40	26,600	80.3
18.0	219–Y3T	29,000	109.5	161.0	55.0	b	do					219–CX4T	1.750	.40	29,400	112.7
28.0	221–Y4T	28,800	139.8	176.6	58.0	c	do					221–CX4T	1.749	.40	29,900	146.6
37.0	223–Y3T	29,600	156.5	189.2	41.5	c	do					223–CX4T	1.754	.40	31,300	170.4
							0.020 IN. THICK, AS-ROLLED, LONGITUDINAL									
0.0	218–B2L	29,000	36.7	136.4	77.0	b	218–CN2L	2.502	21	27,400	37.9	218–CX1L	1.998	0.80	32,400	43.3
8.2	216–B2L	28,600	78.3	158.0	55.0	b	216–CN1L	2.501	21	28,400	49.4	216–CX3L	1.995	.80	27,700	64.0
18.0	204–B2L	27,600	111.0	167.7	43.5	b	204–CN1L	2.501	21	28,600	67.2	204–CX1L	1.997	.80	28,700	77.7
30.5	202–B2L	27,800	129.8	175.7	47.0	b	202–CN1L	2.501	21	28,200	75.4	202–CX1L	1.998	.80	26,800	90.6
37.5	200–B2L	26,700	151.9	185.3	37.0	b	200–CN1L	2.501	21	27,600	83.8	200–CX1L	1.998	.80	27,900	96.7
							0.020 IN. THICK, AS-ROLLED, TRANSVERSE									
0.0	218–B2T	29,000	36.7	134.9	76.0	d (73.5)	218–CN1T	2.500	21	28,500	37.5	218–CX3T	2.000	0.80	31,800	42.4
8.2	216–B2T	28,500	84.0	153.8	45.0	d (43.5)	216–CN1T	2.501	21	29,200	91.1	216–CX3T	2.000	.80	28,600	88.9
18.0	204–B2T	28,000	106.9	167.0	54.0	b	204–CN1T	2.501	21	28,600	117.3	204–CX1T	1.997	.80	28,100	114.8
30.5	202–B2T	28,500	123.9	179.4	38.0	b	202–CP3T [4]	2.497	9	28,900	140.0	202–CX1T	1.999	.80	28,900	139.2
37.5	200–B2T	29,300	143.0	188.2	35.5	b	200–CP2T [4]	2.501	9	29,800	165.0	200–CX1T	2.000	.80	28,800	165.0
							0.020 IN. THICK, STRESS-RELIEVED, LONGITUDINAL									
0.0	218–Y4L	29,100	36.2	133.3	85.5	c	None					218–CX2L	1.996	0.80	32,800	41.7
8.2	216–Y4L	28,100	80.4	153.8	62.5	b	do					216–CX2L	2.002	.80	28,900	77.5
18.0	204–Y3L	28,200	116.4	163.3	52.0	b	do					204–CX2L	2.002	.80	31,100	98.0
30.5	202–Y3L	27,300	140.0	174.0	47.0	c	do					202–CX2L	2.002	.80	29,000	113.0
37.5	200–Y4L	27,000	160.4	180.8	39.5	b	do					200–CX4L	2.001	.80	27,400	134.5

37.5	200–Y4L	27,000	160.4	180.8	39.5	b	....do					200–CX4L	2.001	.80	27,400	134.5

0.020 IN. THICK, STRESS-RELIEVED, TRANSVERSE

0.0	218–Y4T	28,400	36.0	136.2	86.5	b	None					218–CX2T	2.000	0.80	35,600	42.0
8.2	216–Y4T	28,800	83.1	148.0	69.0	c	....do					216–CX2T	2.000	.80	29,000	86.8
18.0	204–Y3T	28,200	112.1	155.8	62.0	b	....do					204–CX2T	1.977	.80	29,800	117.8
30.5	202–Y3T	28,800	136.0	172.0	46.5	b	....do					202–CX2T	1.961	.80	29,600	146.7
37.5	200–Y4T	29,200	158.6	187.9	36.5	c	....do					200–CX3T	1.993	.80	29,400	176.4

0.040 IN. THICK, AS-ROLLED, LONGITUDINAL

0.0	197–B1L	29,900	37.7	127.7	87.0	c	197–CN1L	2.501	9	30,400	38.8	197–CX1L	1.999	1.53	30,100	45.0
9.2	211–B1L	28,700	83.9	160.0	61.0	c	211–CN1L	2.503	9	29,500	59.1	211–CX1L	1.993	1.53	31,200	68.6
23.6	209–B1L	27,600	113.1	162.0	49.0	c	209–CN1L	2.491	9	28,400	72.3	209–CX1L	2.002	1.53	29,200	83.3
28.5	207–B1L	26,500	135.5	182.2	45.0	d (42.0)	207–CN1L	2.500	9	27,800	83.1	207–CX1L	2.002	1.53	28,500	94.8
38.8	205–B1L	26,200	156.7	191.4	32.0	c	205–CN1L	2.501	9	26,700	88.9	205–CX1L	2.000	1.53	26,800	107.3

0.040 IN. THICK, AS-ROLLED, TRANSVERSE

0.0	197–B1T	27,800	37.9	133.1	82.5	b	197–CN1T	2.500	9	29,400	38.5	197–CX1T	2.002	1.53	27,900	44.1
9.2	211–B1T	27,500	89.2	159.6	61.0	b	211–CN1T	2.502	9	28,300	96.1	211–CX1T	1.998	1.53	29,800	94.1
23.6	209–B1T	27,800	110.6	166.7	51.0	b	209–CN1T	2.502	9	28,800	122.7	209–CX1T	1.993	1.53	29,600	120.9
28.5	207–B1T	28,200	129.3	180.8	35.0	c	207–CN1T	2.501	9	29,800	144.5	207–CX1T	1.974	1.53	28,900	144.4
38.8	205–B2T	29,200	156.6	197.3	21.0	b	205–CN1T	2.502	9	30,200	175.1	205–CX1T	2.001	1.53	30,500	174.9

0.040 IN. THICK, STRESS-RELIEVED, LONGITUDINAL

0.0	197–Y4L	30,200	38.1	132.3	87.0	d (84.5)	None					197–CX2L	2.002	1.53	30,700	43.8
9.2	211–Y3L	28,700	88.3	153.4	64.5	b	....do					211–CX2L	2.000	1.53	31,200	83.7
23.6	209–Y3L	28,900	121.3	160.1	55.5	b	....do					209–CX2L	2.000	1.53	29,000	104.5
28.5	207–Y3L	27,000	145.6	175.5	44.5	b	....do					207–CX2L	2.000	1.53	29,100	121.7
38.8	205–Y3L	28,100	170.0	201.8	18.0	b	....do					205–CX2L	2.000	1.53	27,600	145.5

0.040 IN. THICK, STRESS-RELIEVED, TRANSVERSE

0.0	197–Y4T	28,600	37.5	127.5	82.5	c	None					197–CX2T	1.997	1.53	29,100	43.4
9.2	211–Y4T	28,200	90.3	153.2	65.5	c	....do					211–CX2T	2.000	1.53	29,000	92.6
23.6	209–Y4T	28,700	118.1	158.9	63.0	c	....do					209–CX2T	1.997	1.53	29,800	124.6
28.5	207–Y3T	29,200	139.2	173.6	38.5	b	....do					207–CX2T	1.999	1.53	32,900	160.4
38.8	205–Y3T	30,100	171.2	206.4	9.5	b	....do					205–CX2T	1.994	1.53	29,900	193.5

[1] [2] [3] See footnotes 1, 2, and 3, p. 507.
[4] One-half-inch-wide pack tested in subpress, lateral support, 39 pins on each side, 3/16-in. spacing.

TABLE 5.—*Results of tensile and compressive tests on 18–7 stainless steel*

Cold-reduction	Tension						Pack compression					Cylinder compression				
	Specimen number	Slope of straight line [1]	Yield strength;[1] offset =0.2%	Tensile strength	Elongation in 2 in.	Remarks[1]	Pack number	Length	Number of specimens in pack	Slope of straight line [1]	Yield strength;[2] offset =0.2%	Cylinder number	Length	Outside diameter, nominal	Slope of straight line [1]	Yield strength;[2] offset =0.2%
0.010 IN. THICK, AS-ROLLED, LONGITUDINAL																
Percent		*Kips/in.*[1]	*Kips/in.*[1]	*Kips/in.*[1]	*Percent*			*Inches*		*Kips/in.*[1]	*Kips/in.*[1]		*Inches*	*Inches*	*Kips/in.*[1]	*Kips/in.*[1]
0.0	51–B1L	28,600	36.7	153.6	60.5	c	None					51–CX1L	1.743	0.40	32,100	44.4
12.0	50–B1L	26,500	74.3	170.0	47.5	b	do					50–CX1L	1.742	.40	30,400	59.7
19.6	52–B1L	27,400	102.6	182.6	35.5	b	do					52–CX1L	1.748	.40	28,700	74.5
31.5	53–B1L	26,700	149.7	204.0	28.5	b	do					53–CX1L	1.749	.40	26,900	100.9
40.0	54–B2L	26,300	174.5	211.9	25.0	b	do					54–CX1L	1.725	.40	29,900	109.0
50.0	59–B2L	25,800	216.0	231.7	11.0	b	do					59–CX1L	1.746	.40	26,000	142.2
52.5	55–B1L	26,400	246.4	261.0	3.0	b	do					55–CX1L	1.750	.40	26,300	166.8
0.010 IN. THICK, AS-ROLLED, TRANSVERSE																
0.0	51–B2T	28,400	36.4	154.4	60.0	b	None					51–CX1T	1.732	0.40	31,600	41.5
12.0	50–B2T	27,400	72.5	167.2	47.0	b	do					50–CX1T	1.751	.40	28,800	79.4
19.6	52–B1T	27,800	100.2	180.1	37.5	b	do					52–CX1T	1.743	.40	31,500	112.1
31.5	53–B1T	28,200	136.7	201.5	22.5	b	do					53–CX1T	1.748	.40	28,300	163.8
40.0	54–B2T	28,900	154.4	217.7	21.5	c	do					54–CX1T	1.728	.40	29,900	180.7
50.0	59–B1T	30,400	197.0	244.8	11.0	d(9.0)	do					59–CX1T	1.746	.40	30,200	231.6
52.5	55–B1T	30,700	218.5	285.1	4.5	b	do					55–CX1T	1.744	.40	31,100	248.2
0.020 IN. THICK, AS-ROLLED, LONGITUDINAL																
0.0	68–B1L	28,400	36.2	152.1	63.0	b	57–C2L	3.501	31	29,500	36.7	57–CX1L	1.994	0.80	30,700	43.8
5.3	69–B2L	27,800	80.4	169.9	49.0	b	58–C1L	3.500	31	28,500	47.4	58–CX1L	1.993	.80	26,400	66.8
18.3	45–B1L	26,600	115.5	186.3	32.5	b	44–C2L	3.497	31	27,800	82.0	45–CX1L	1.992	.80	26,300	87.8
29.8	47–B2L	27,000	138.7	198.9	28.0	b	46–C2L	3.498	31	27,400	94.3	47–CX1L	1.996	.80	26,700	101.7
37.5	66–B2L	26,300	152.6	205.1	25.0	b	66–CP4L[7]	2.500	7	27,000	104.7	56–CX1L	1.994	.80	25,700	129.4
50.0	49–B1L	26,300	201.6	236.8	27.5	c	49–CN1L	2.502	21	26,400	135.1	49–CX1L	1.998	.80	24,800	147.8
0.020 IN. THICK, AS-ROLLED, TRANSVERSE																
0.0	68–B1T	28,000	35.8	153.1	62.0	b	57–C1T	3.502	31	29,800	37.8	57–CX1T	1.995	0.80	31,800	43.1
5.3	69–B2T	27,700	82.9	174.1	44.5	b	58–C1T	3.500	31	28,800	88.1	58–CX1T	1.995	.80	28,600	86.6
18.3	45–B2T	28,100	115.8	186.3	37.0	b	44–C1T	3.502	31	28,500	132.0	45–CX1T	1.996	.80	28,800	127.7
29.8	47–B2T	28,800	136.9	203.5	29.0	c	47–CP6T[7]	2.500	7	28,900	158.1	47–CX1T	1.996	.80	29,300	155.3
37.5	66–B2T	28,000	154.7	205.2	27.0	d(24.0)	66–CP4T[7]	2.500	7	29,000	173.5	56–CX1T	1.995	.80	29,000	174.1
0.035 IN. THICK, AS-ROLLED, LONGITUDINAL																
0.0	70–B1L	28,400	36.2	151.8	63.0	b	57–C3L	3.501	31	29,500	36.7	57–CX1L	1.994	0.80	30,700	43.8
5.3	71–B2L	27,800	80.4	169.9	49.0	b	58–C2L	3.500	31	28,500	47.4	58–CX1L	1.993	.80	26,400	66.8
18.3	72–B1L	26,600	115.5	186.3	32.5	b	44–C3L	3.497	31	27,800	82.0	45–CX1L	1.992	.80	26,300	87.8
29.8	73–B2L	27,000	138.7	198.9	28.0	b	46–C3L	3.498	31	27,400	94.3	47–CX1L	1.996	.80	26,700	101.7
37.5	74–B2L	26,300	152.6	205.1	25.0	b	66–CP5L[7]	2.500	7	27,000	104.7	56–CX1L	1.994	.80	25,700	129.4
50.0	75–B1L	26,300	201.6	236.8	27.5	c	49–CN2L	2.502	21	26,400	135.1	49–CX1L	1.998	.80	24,800	147.8
0.035 IN. THICK, AS-ROLLED, TRANSVERSE																
0.0	70–B1T	28,000	35.8	153.1	62.0	b	57–C2T	3.502	31	29,800	37.8	57–CX1T	1.995	0.80	31,800	43.1
5.3	71–B2T	27,700	82.9	174.1	44.5	b	58–C2T	3.500	31	28,800	88.1	58–CX1T	1.995	.80	28,600	86.6
18.3	72–B2T	28,100	115.8	186.3	37.0	b	44–C2T	3.502	31	28,500	132.0	45–CX1T	1.996	.80	28,800	127.7
29.8	73–B1T	28,800	136.9	203.5	29.0	c	47–CP3T[7]	2.500	7	28,900	158.1	47–CX1T	1.996	.80	29,300	155.3
37.5	74–B1T	28,000	154.7	205.2	27.0	d(24.0)	66–CP2T[7]	2.500	7	29,000	173.5	56–CX1T	1.995	.80	29,000	174.1

0.035 IN. THICK, AS-ROLLED, LONGITUDINAL

0.0	35–B2L	29,200	37.5	147.2	67.0	b	36–C1L	3.502	19	29,900	37.8	35–CX1L	1.979	1.46	31,200	45.1
7.5	26–B2L	29,300	55.4	154.9	54.5	b	25–C1L	3.502	19	30,000	40.1	25–CX1L	1.984	1.46	30,000	53.2
19.6	27–B2L	27,900	89.5	173.7	45.0	b	27–C2L	3.501	19	27,900	55.9	27–CX1L	1.982	1.46	28,200	77.3
29.2	86–B2L	26,800	148.2	198.5	34.0	d (30.0)	86–CN3L	2.501	10	26,800	94.8	86–CX1L	1,980	1.46	27,100	113.5
39.7	37–B2L	26,300	177.7	215.4	27.5	c	37–CN6L	2.500	10	27,100	105.5	37–CX1L	1.992	1.46	26,000	135.0
47.0	38–B2L	25,900	200.9	235.5	21.0	d (17.5)	39–C1L	3.501	19	26,700	133.5	38–CX1L	2.006	1.46	25,600	163.2

0.035 IN. THICK, AS-ROLLED, TRANSVERSE

0.0	35–B2T	29,500	37.7	148.4	65.0	b	36–C1T	3.501	19	29,800	38.2	35–CX1T	1.987	1.46	32,000	45.4
7.5	26–B2T	28,800	59.1	158.8	59.0	b	25–C2T	3.501	19	29,000	61.0	25–CX1T	1.986	1.46	28,600	61.3
19.6	27–B2T	28,100	91.8	172.1	49.0	c	27–C1T	3.501	19	29,400	101.2	27–CX1T	1.996	1.46	28,100	100.2
29.2	86–B2T	28,200	143.0	200.8	35.0	d (31.0)	86–CN2T	2.498	10	29,300	165.6	86–CX1T	1.990	1.46	29,200	172.1
39.7	37–B1T	29,400	167.0	219.6	19.0	c	37–C1T	3.501	19	29,200	189.1	37–CX1T	1.997	1.46	30,000	183.8
47.0	38–B2T	29,800	200.4	246.1	7.5	b	38–CS4T	1.801	19	31,600	229.5	38–CX1T	1.981	1.24	30,200	221.5

0.060 IN. THICK, AS-ROLLED, LONGITUDINAL

0.0	41–B1L	28,600	34.1	146.9	72.5	b	41–CN1L	2.485	5	31,400	35.3	None				
6.7	7–B2L	26,900	81.5	[4] 168.8	[4] 52.5	b	7–CN1L	2.488	5	27,600	57.8	do				
18.1	8–B2L	27,700	103.7	178.7	37.5	b	8–CN1L	2.463	5	27,700	69.4	do				
30.5	11–B2L	26,600	148.6	202.2	31.0	c	11–CN1L	2.479	5	27,200	97.4	do				
36.9	29–B1L	26,300	173.7	209.5	27.0	c	29–CN1L	2.486	5	26,900	104.3	do				
47.7	13–B1L	26,300	194.3	225.0	16.0	c	13–CN2L	2.474	5	26,600	125.1	do				

0.060 IN. THICK, AS-ROLLED, TRANSVERSE

0.0	41–B2T	28,500	34.1	[5] 142.6	[5] 72.0	b	41–CN1T	2.500	5	31,100	35.5	None				
6.7	7–B2T	28,300	88.3	[6] 166.2	[6] 56.0	b	7–CN1T	2.501	5	28,500	96.3	do				
18.1	8–B2T	28,200	105.2	179.3	43.0	c	8–CN1T	2.502	5	28,300	120.7	do				
30.5	11–B1T	28,600	141.4	206.0	32.0	c	11–CN1T	2.494	5	29,400	176.0	do				
36.9	29–B2T	28,700	153.8	215.9	24.0	c	29–CN1T	2.483	5	29,300	185.3	do				
47.7	13–B1T	29,600	185.3	234.0	10.0	b	13–CN1T	2.492	5	30,500	228.2	do				

[1] Obtained by least-square fit to lower portion of stress-strain graph.
[2] Using straight line with slope given in previous column.
[3] Letters describe location of fracture in accordance with section 24 and figure 19, page 462 of ASTM Specification E8–40T. Figures in parentheses are alternate elongation values determined from sum of the distances A to F and B to E shown in that figure.
[4] Loaded at 0.02 in./min.
[5] 41–B2T broke in grip; duplicate specimen (41–B1T) tested for tensile strength and elongation.
[6] 7–B2T broke outside of gage length, duplicate specimen (7–B1T) tested for tensile strength and elongation.
[7] One-half-inch-wide pack, tested in subpress, lateral support 39 pins on each side, $\frac{3}{16}$-in. spacing.

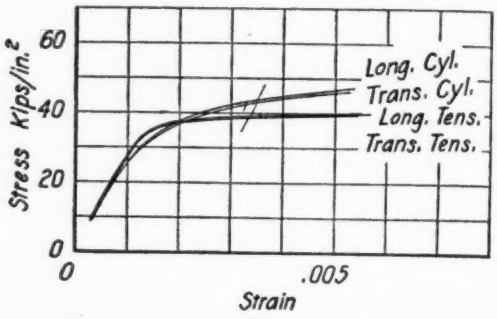

FIGURE 1.—*17–7, 0.01-inch sheet, annealed.*

Yield strength, offset = 0.2 percent

Test	Longitudinal	Transverse
	*Kips/in.*²	*Kips/in.*²
Tensile	39.0	38.5
Cylinder compressive	43.7	42.6

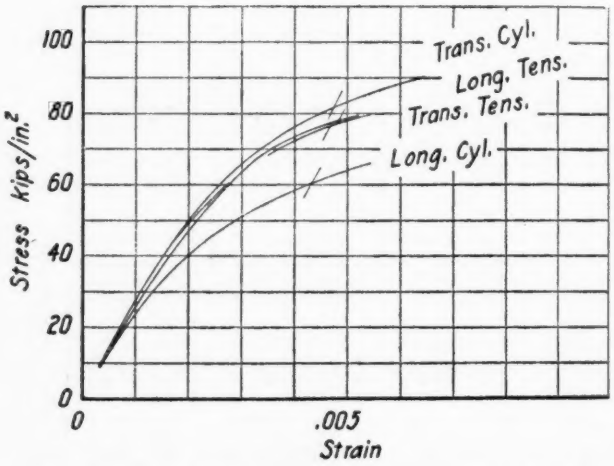

FIGURE 2.—*17–7, 0.01-inch sheet, 8.2 percent cold-reduced.*

Yield strength, offset = 0.2 percent

Test	Longitudinal	Transverse
	*Kips/in.*²	*Kips/in.*²
Tensile	77.9	76.7
Cylinder compressive	60.5	81.5

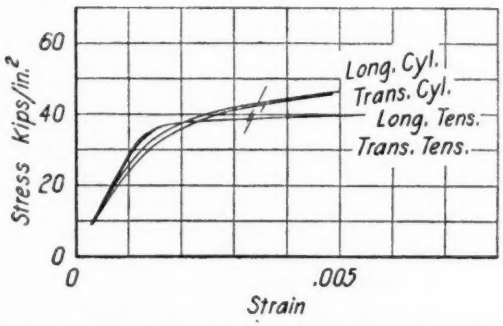

FIGURE 3.—*17–7, 0.01-inch sheet, annealed, stress-relieved.*

Yield strength, offset=0.2 percent

Test	Longitudinal	Transverse
	*Kips/in.*²	*Kips/in.*²
Tensile	39.2	39.0
Cylinder compressive	43.5	42.9

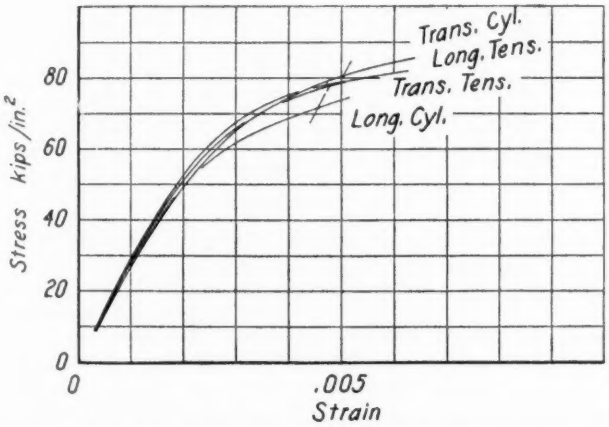

FIGURE 4.—*17–7, 0.01-inch sheet, 8.2 percent cold-reduced, stress-relieved.*

Yield strength, offset=0.2 percent

Test	Longitudinal	Transverse
	*Kips/in.*²	*Kips/in.*²
Tensile	78.2	77.7
Cylinder compressive	71.6	80.3

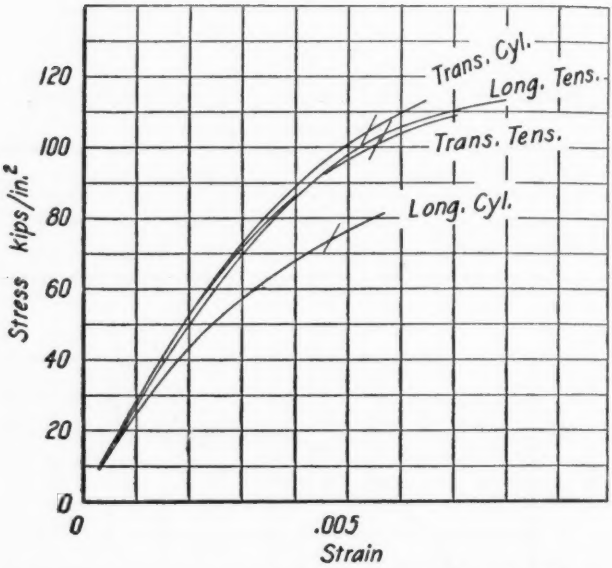

FIGURE 5.—*17–7, 0.01-inch sheet, 18.0 percent cold-reduced.*

Yield strength, offset=0.2 percent

Test	Longitudinal	Transverse
	Kips/in.²	*Kips/in.²*
Tensile	103.8	100.8
Cylinder compressive	73.7	104.4

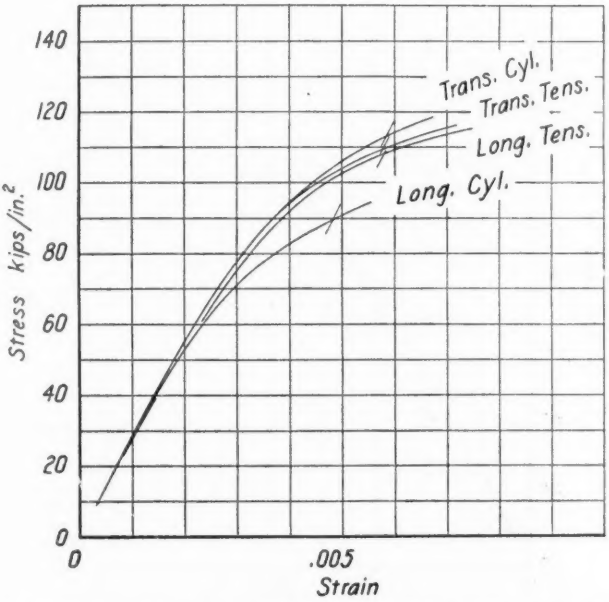

FIGURE 6.—*17–7, 0.01-inch sheet, 18.0 percent cold-reduced, stress-relieved.*

Yield strength, offset=0.2 percent

Test	Longitudinal	Transverse
	*Kips/in.*²	*Kips/in.*²
Tensile	108.4	109.5
Cylinder compressive	89.7	112.7

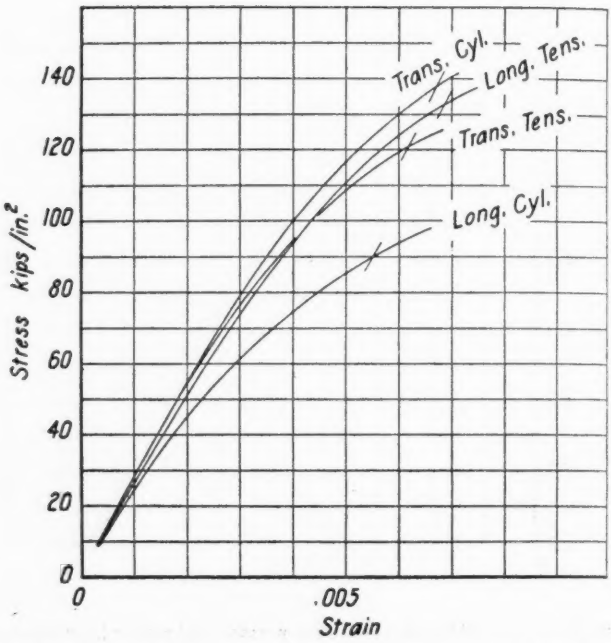

FIGURE 7.—*17-7, 0.01-inch sheet, 28.0 percent cold-reduced.*

Yield strength, offset=0.2 percent

Test	Longitudinal	Transverse
	Kips/in.²	*Kips/in.²*
Tensile	133.1	121.0
Cylinder compressive	90.2	137.8

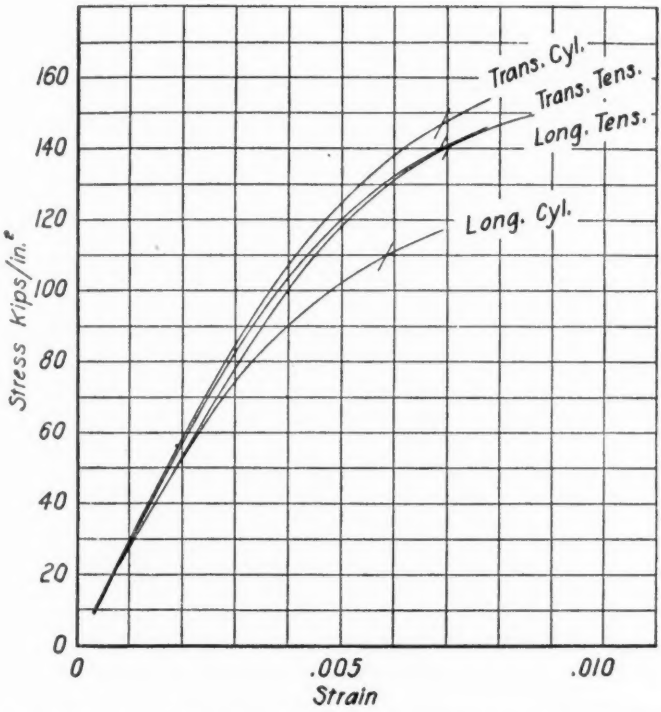

FIGURE 8.—*17–7, 0.01-inch sheet, 28.0 percent cold-reduced, stress-relieved.*

Yield strength, offset=0.2 percent

Test	Longitudinal	Transverse
	*Kips/in.*²	*Kips/in.*²
Tensile	141.5	139.8
Cylinder compressive	109.7	146.6

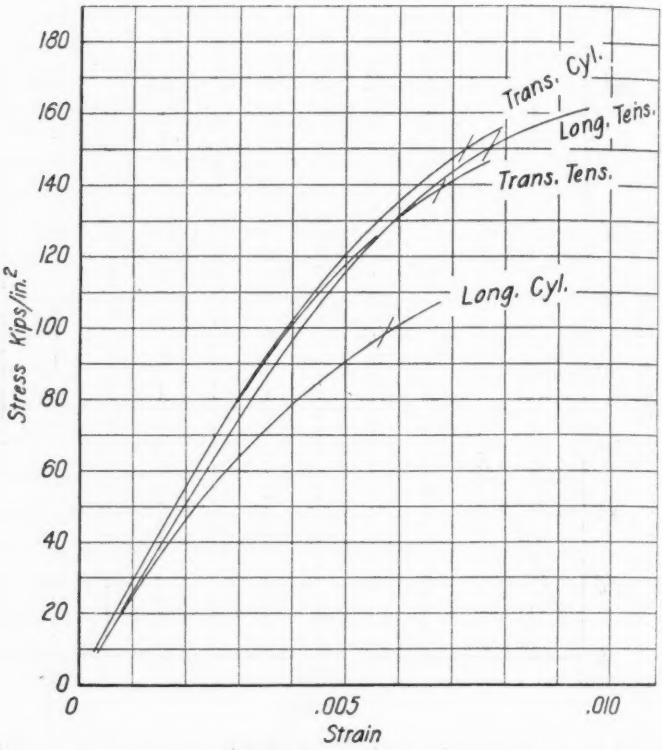

FIGURE 9.—*17–7, 0.01-inch sheet, 37.0 percent cold-reduced.*

Yield strength, offset=0.2 percent

Test	Longitudinal	Transverse
	Kips/in.²	*Kips/in.²*
Tensile	150.3	138.8
Cylinder compressive	98.3	150.0

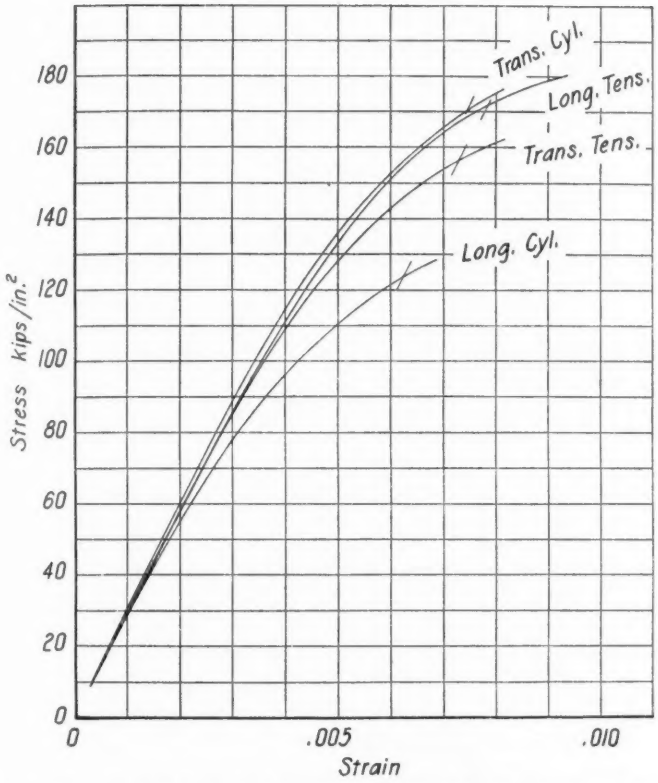

FIGURE 10.—*17–7, 0.01-inch sheet, 37.0 percent cold-reduced, stress-relieved.*

Yield strength, offset=0.2 percent

Test	Longitudinal	Transverse
	Kips/in.²	*Kips/in.²*
Tensile	171.7	156.5
Cylinder compressive	123.4	170.4

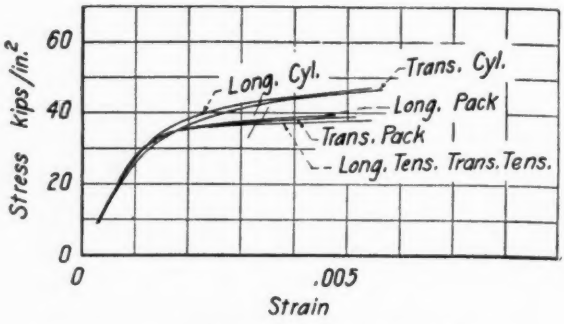

FIGURE 11.—*17–7, 0.02-inch sheet, annealed.*

Yield strength, offset=0.2 percent

Test	Longitudinal	Transverse
	Kips/in.²	*Kips/in.²*
Tensile	36.7	36.7
Pack compressive	37.9	37.5
Cylinder compressive	43.3	42.4

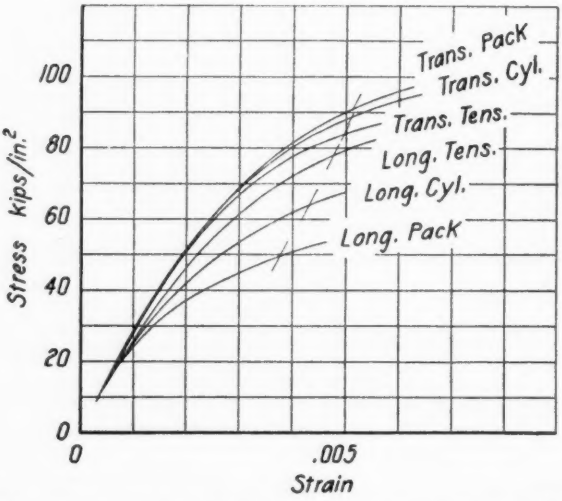

FIGURE 12.—*17–7, 0.02-inch sheet, 8.2 percent cold-reduced.*

Yield strength, offset=0.2 percent

Test	Longitudinal	Transverse
	Kips/in.²	*Kips/in.²*
Tensile	78.3	84.0
Pack compressive	49.4	91.1
Cylinder compressive	64.0	88.9

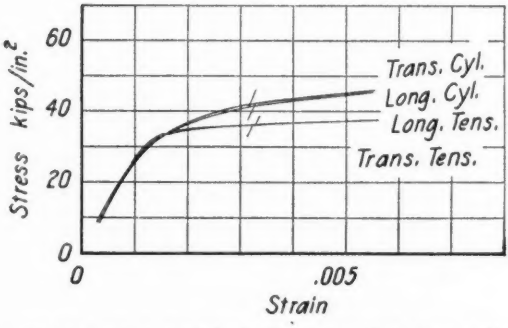

FIGURE 13.—*17–7, 0.02-inch sheet, annealed, stress-relieved.*

Yield strength, offset=0.2 percent

Test	Longitudinal	Transverse
	*Kips/in.*²	*Kips/in.*²
Tensile	36.2	36.0
Cylinder compressive	41.7	42.0

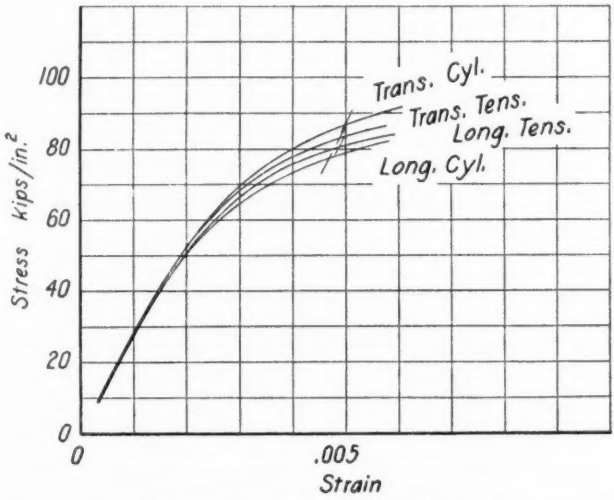

FIGURE 14.—*17–7, 0.02-inch sheet, 8.2 percent cold-reduced, stress-relieved.*

Yield strength, offset=0.2 percent

Test	Longitudinal	Transverse
	*Kips/in.*²	*Kips/in.*²
Tensile	80.4	83.1
Cylinder compressive	77.5	86.8

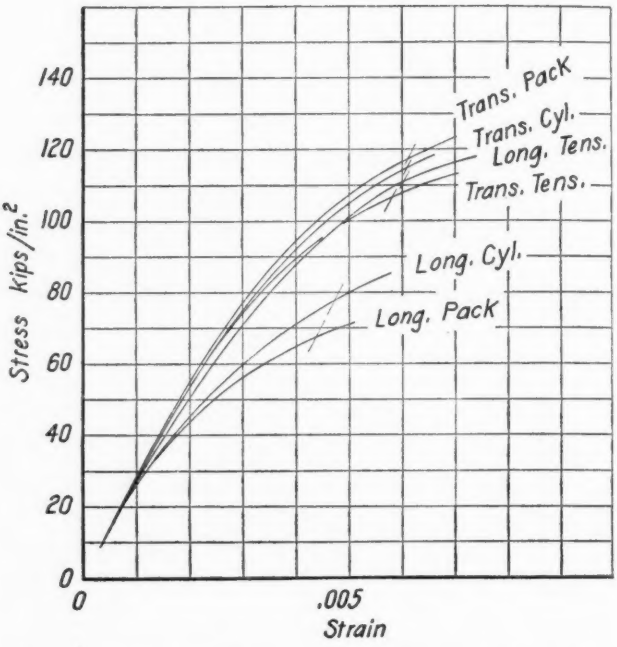

FIGURE 15.—*17-7, 0.02-inch sheet, 18.0 percent cold-reduced.*

Yield strength, offset=0.2 percent

Test	Longitudinal	Transverse
	Kips/in.²	*Kips/in.²*
Tensile	111.0	106.9
Pack compressive	67.2	117.3
Cylinder compressive	77.7	114.8

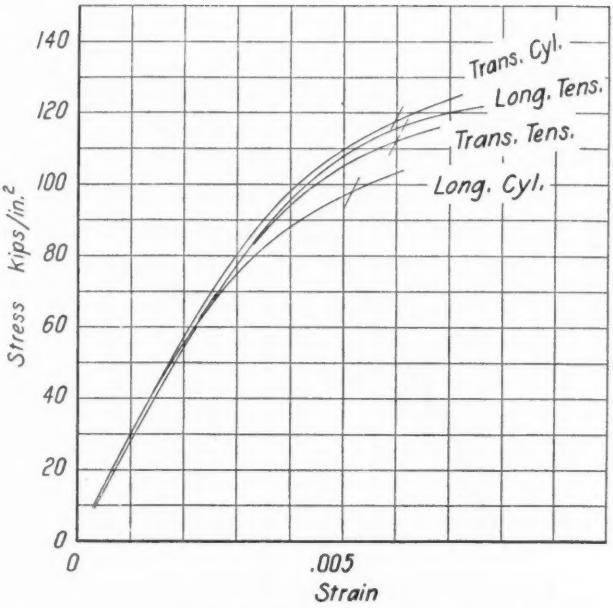

FIGURE 16.—*17–7, 0.02-inch sheet, 18.0 percent cold-reduced, stress-relieved.*

Yield strength, offset=0.2 percent

Test	Longitudinal	Transverse
	Kips/in.²	*Kips/in.²*
Tensile	116.4	112.1
Cylinder compressive	98.0	117.8

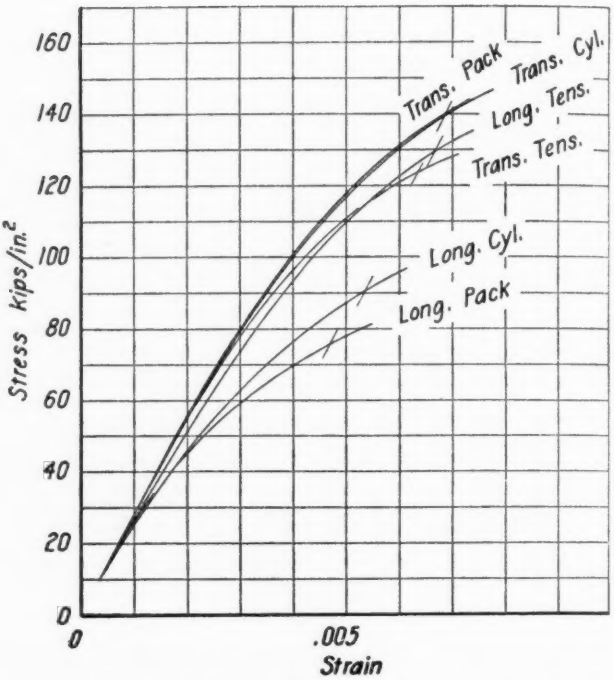

FIGURE 17.—*17–7, 0.02-inch sheet, 30.5 percent cold-reduced.*

Yield strength, offset=0.2 percent

Test	Longitudinal	Transverse
	*Kips/in.*²	*Kips/in.*²
Tensile	129.8	123.9
Pack compressive	75.4	140.0
Cylinder compressive	90.6	139.2

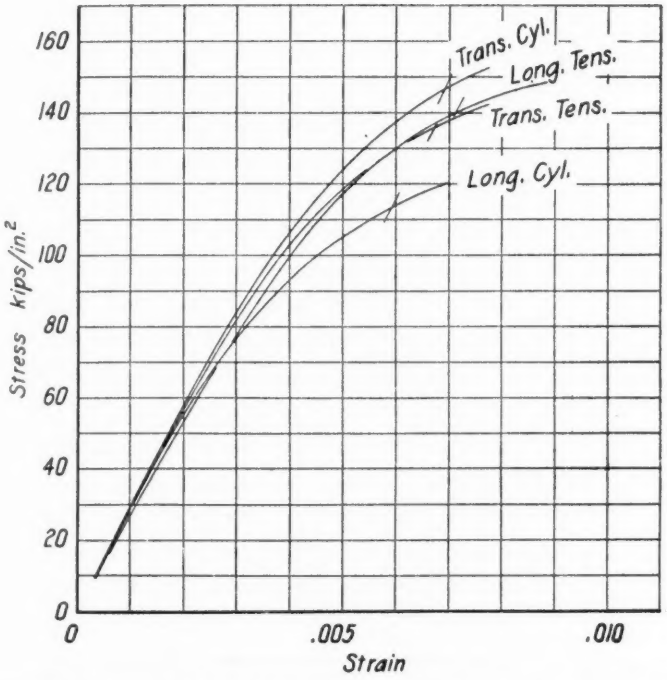

FIGURE 18.—*17–7, 0.02-inch sheet, 30.5 percent cold-reduced, stress-relieved.*

Yield strength, offset=0.2 percent

Test	Longitudinal	Transverse
	Kips/in.²	*Kips/in.²*
Tensile	140.0	136.0
Cylinder compressive	113.0	146.7

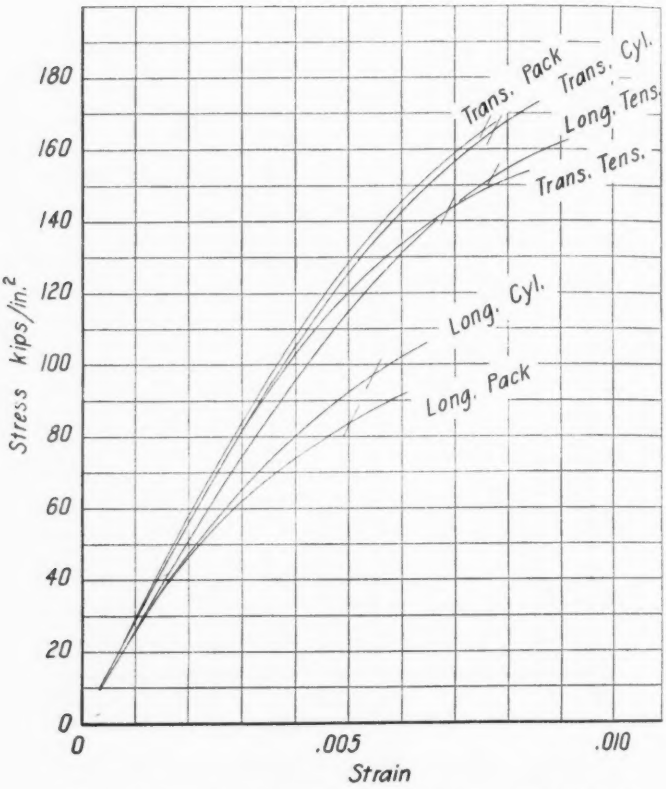

FIGURE 19.—*17–7, 0.02-inch sheet, 37.5 percent cold-reduced.*

Yield strength, offset=0.2 percent

Test	Longitudinal	Transverse
	Kips/in.²	*Kips/in.²*
Tensile	151.9	143.0
Pack compressive	83.8	165.0
Cylinder compressive	96.7	165.0

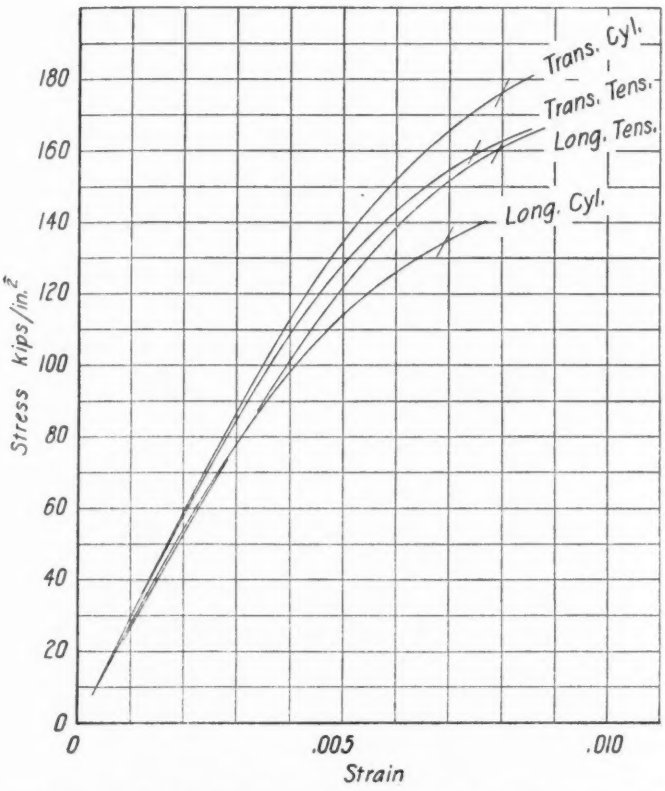

FIGURE 20.—*17–7, 0.02-inch sheet, 37.5 percent cold-reduced, stress-relieved.*

Yield strength, offset=0.2 percent

Test	Longitudinal	Transverse
	Kips/in.²	*Kips/in.²*
Tensile	160.4	158.6
Cylinder compressive	134.5	176.4

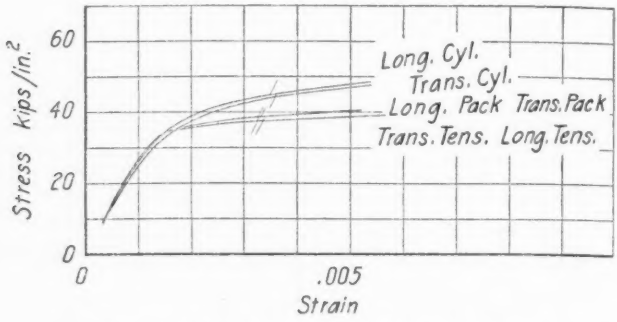

FIGURE 21.—*17–7, 0.04-inch sheet, annealed.*

Yield strength, offset=0.2 percent

Test	Longitudinal	Transverse
	Kips/in.²	*Kips/in.²*
Tensile	37.7	37.9
Pack compressive	38.8	38.5
Cylinder compressive	45.0	44.1

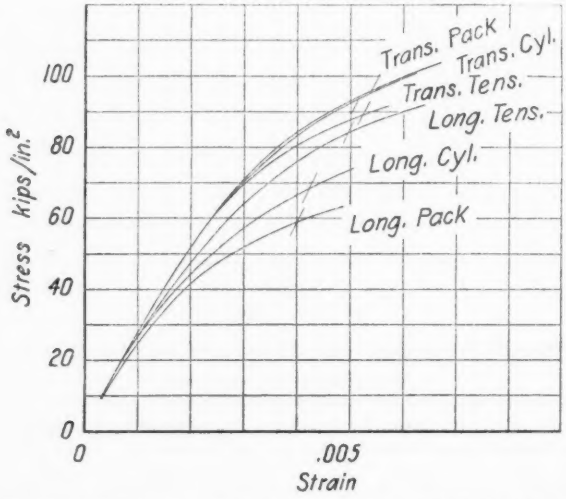

FIGURE 22.—*17–7, 0.04-inch sheet, 9.2 percent cold-reduced.*

Yield strength, offset=0.2 percent

Test	Longitudinal	Transverse
	Kips/in.²	*Kips/in.²*
Tensile	83.9	89.2
Pack compressive	89.1	96.1
Cylinder compressive	68.6	94.1

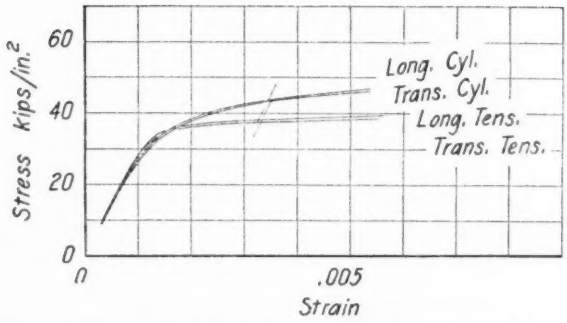

FIGURE 23.—*17–7, 0.04-inch sheet, annealed, stress-relieved.*

Yield strength, offset=0.2 percent

Test	Longitudinal	Transverse
	Kips/in.²	*Kips/in.²*
Tensile	38.1	37.5
Cylinder compressive	43.8	43.4

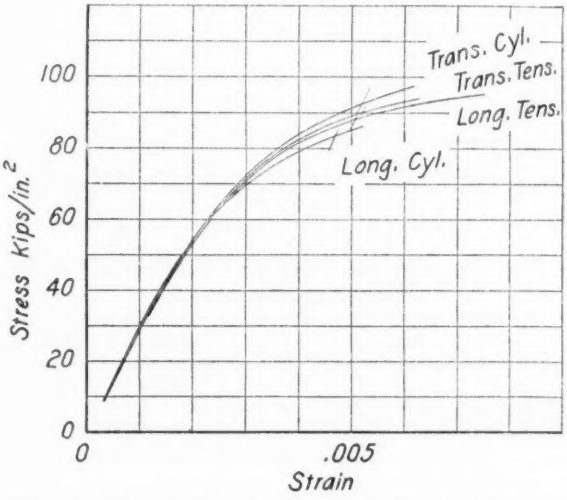

FIGURE 24.—*17–7, 0.04-inch sheet, 9.2 percent cold-reduced, stress-relieved.*

Yield strength, offset=0.2 percent

Test	Longitudinal	Transverse
	Kips/in.²	*Kips/in.²*
Tensile	88.3	90.3
Cylinder compressive	83.7	92.6

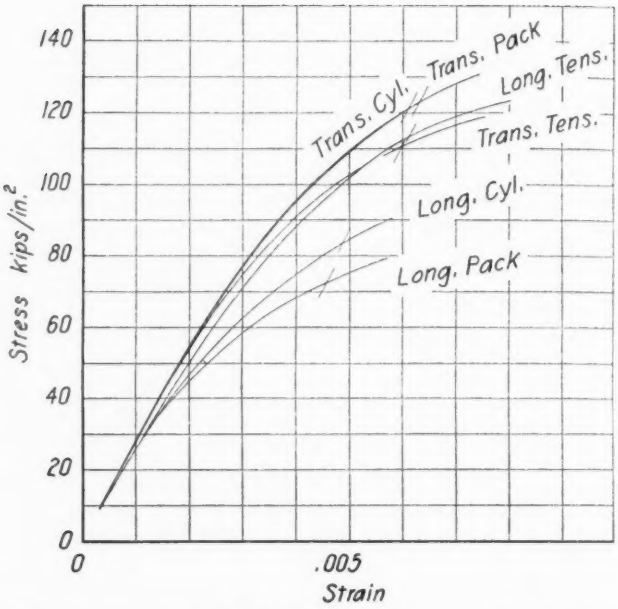

FIGURE 25.—*17–7, 0.04-inch sheet, 23.6 percent cold-reduced.*

Yield strength, offset=0.2 percent

Test	Longitudinal	Transverse
	Kips/in.²	*Kips/in.²*
Tensile	113.1	110.6
Pack compressive	72.3	122.7
Cylinder compressive	83.3	120.9

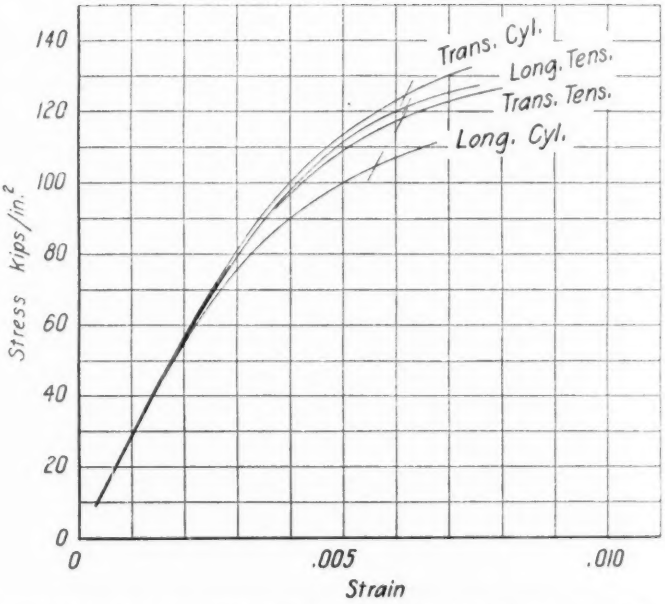

FIGURE 26.—*17–7, 0.04-inch sheet, 23.6 percent cold-reduced, stress-relieved.*

Yield strength, offset=0.2 percent

Test	Longitudinal	Transverse
	Kips/in.²	*Kips/in.²*
Tensile	121.3	118.1
Cylinder compressive	104.5	124.6

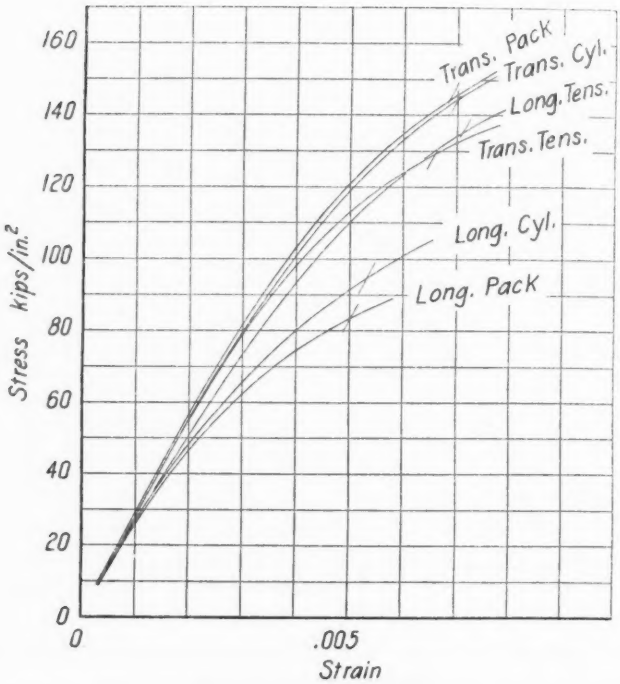

FIGURE 27.—*17–7, 0.04-inch sheet, 28.5 percent cold-reduced.*

Yield strength, offset=0.2 percent

Test	Longitudinal	Transverse
	Kips/in.²	*Kips/in.²*
Tensile	135.5	129.3
Pack compressive	83.1	144.5
Cylinder compressive	94.8	144.4

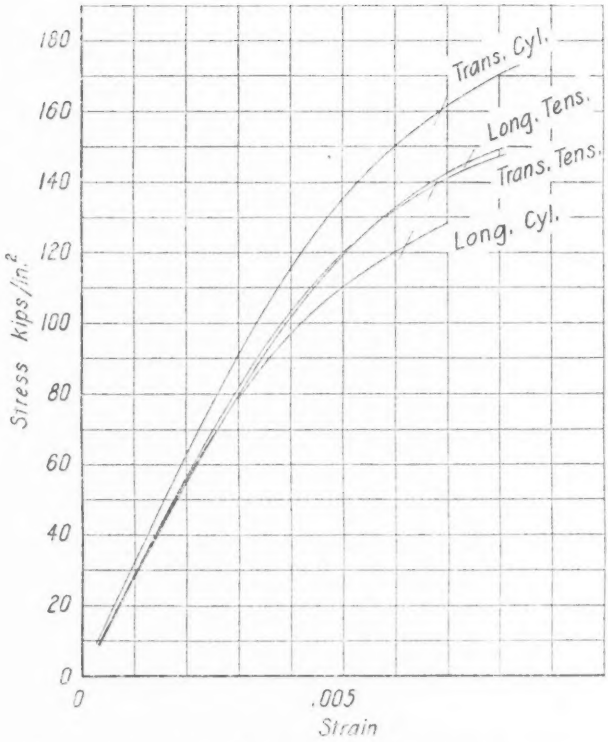

FIGURE 28.—*17–7, 0.04-inch sheet, 28.5 percent cold-reduced, stress-relieved.*

Yield strength, offset=0.2 percent

Test	Longitudinal	Transverse
	Kips/in.²	*Kips/in.²*
Tensile	145.6	130.2
Cylinder compressive	121.7	160.4

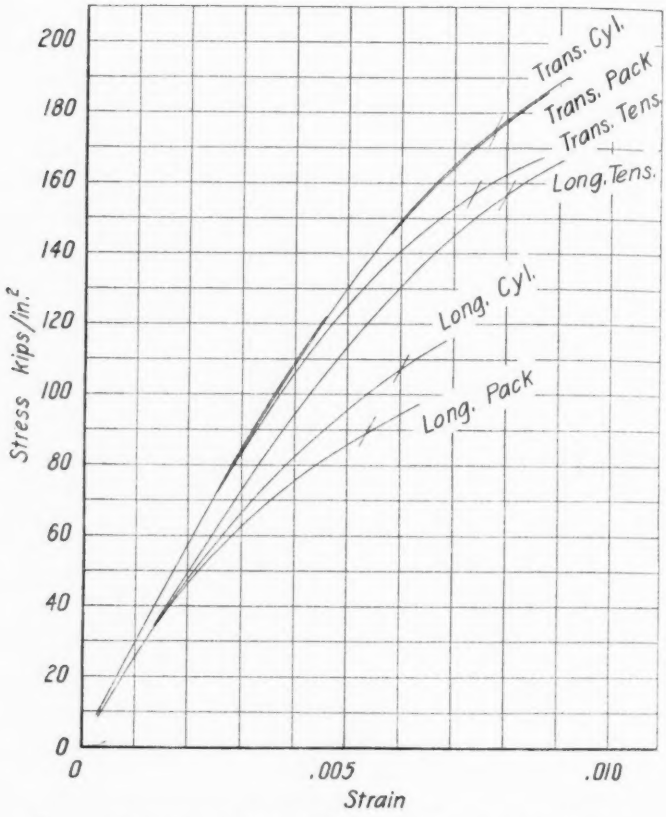

FIGURE 29.—*17–7, 0.04-inch sheet, 38.8 percent cold-reduced.*

Yield strength, offset=0.2 percent

Test	Longitudinal	Transverse
	*Kips/in.*²	*Kips/in.*²
Tensile	156.7	156.6
Pack compressive	88.9	175.1
Cylinder compressive	107.3	174.9

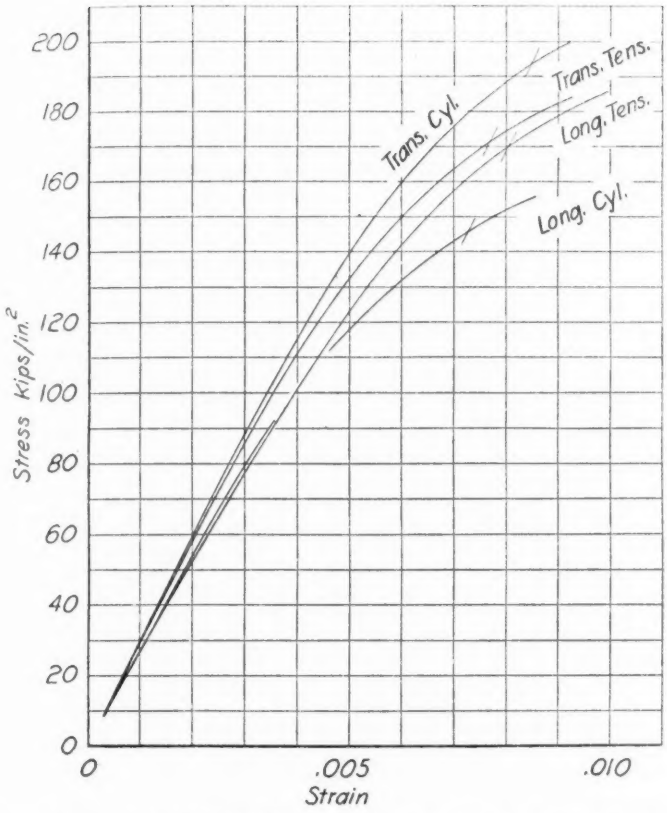

FIGURE 30.—*17–7, 0.04-inch sheet, 38.8 percent cold-reduced, stress-relieved.*

Yield strength, offset=0.2 percent

Test	Longitudinal	Transverse
	Kips/in.²	*Kips/in.²*
Tensile	170.0	171.2
Cylinder compressive	145.5	193.5

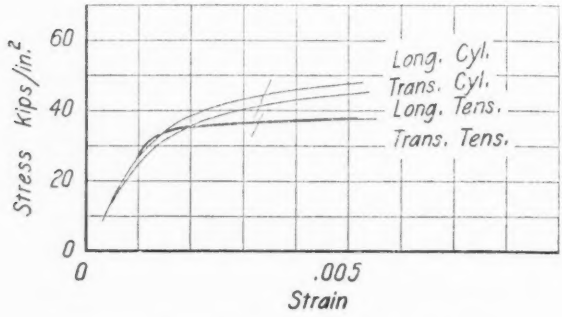

FIGURE 31.—*18–7, 0.01-inch sheet, annealed.*

Yield strength, offset=0.2 percent

Test	Longitudinal	Transverse
	Kips/in.²	*Kips/in.²*
Tensile	36.7	36.4
Cylinder compressive	44.4	41.5

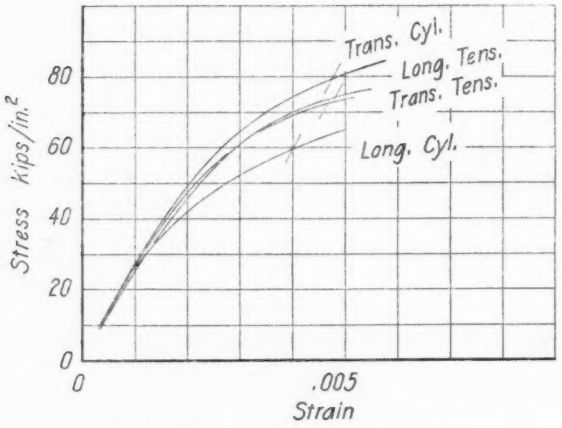

FIGURE 32.—*18–7, 0.01-inch sheet, 12.0 percent cold-reduced.*

Yield strength, offset=0.2 percent

Test	Longitudinal	Transverse
	Kips/in.²	*Kips/in.²*
Tensile	74.3	72.5
Cylinder compressive	59.7	79.4

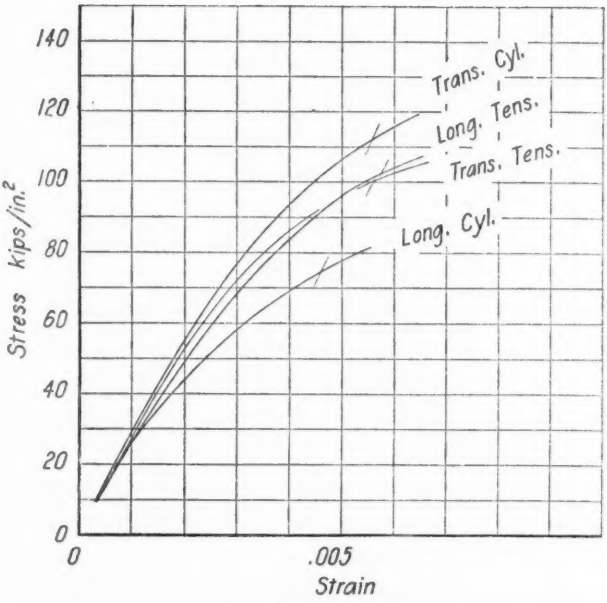

FIGURE 33.—*18–7, 0.01-inch sheet, 19.6 percent cold-reduced.*

Yield strength, offset=0.2 percent

Test	Longitudinal	Transverse
	Kips/in.²	*Kips/in.²*
Tensile	102.6	100.2
Cylinder compressive	74.5	112.1

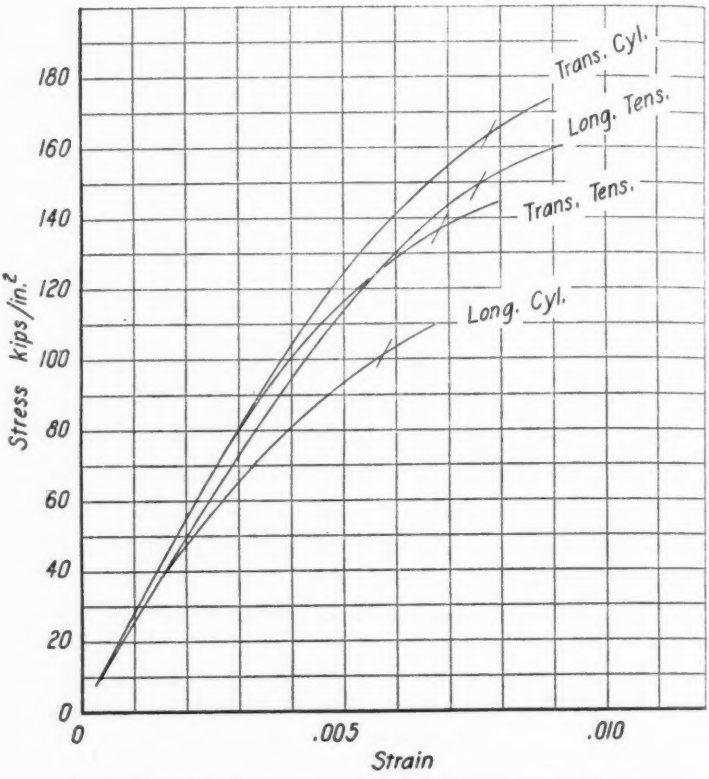

FIGURE 34.—*18–7, 0.01-inch sheet, 31.5 percent cold-reduced.*

Yield strength, offset=0.2 percent

Test	Longitudinal	Transverse
	*Kips/in.*²	*Kips/in.*²
Tensile	149.7	136.7
Cylinder compressive	100.9	163.8

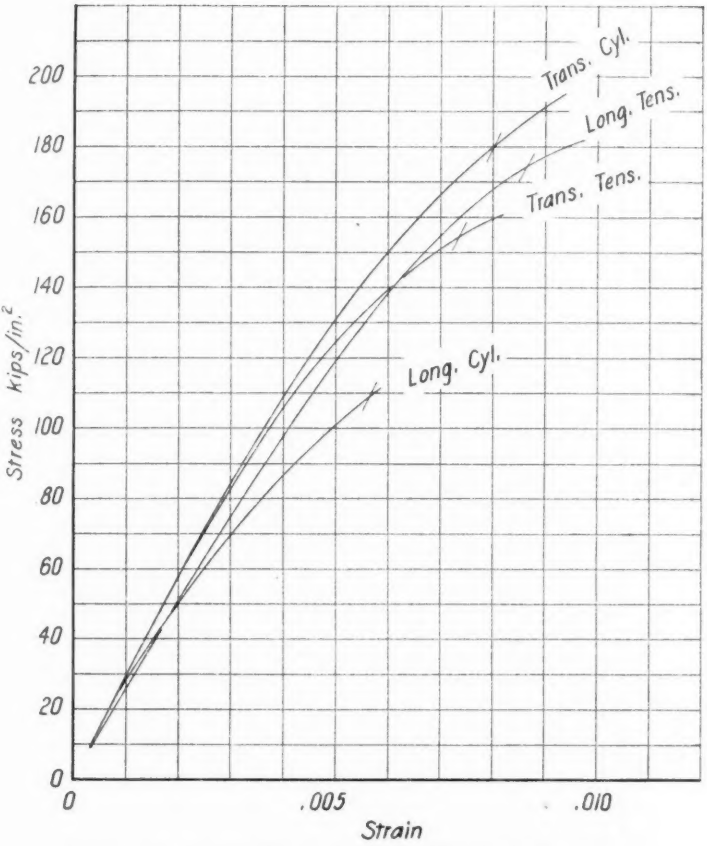

FIGURE 35.—*18–7, 0.01-inch sheet, 40.0 percent cold-reduced.*

Yield strength, offset=0.2 percent

Test	Longitudinal	Transverse
	Kips/in.²	*Kips/in.²*
Tensile	174.5	154.4
Cylinder compressive	109.0	180.7

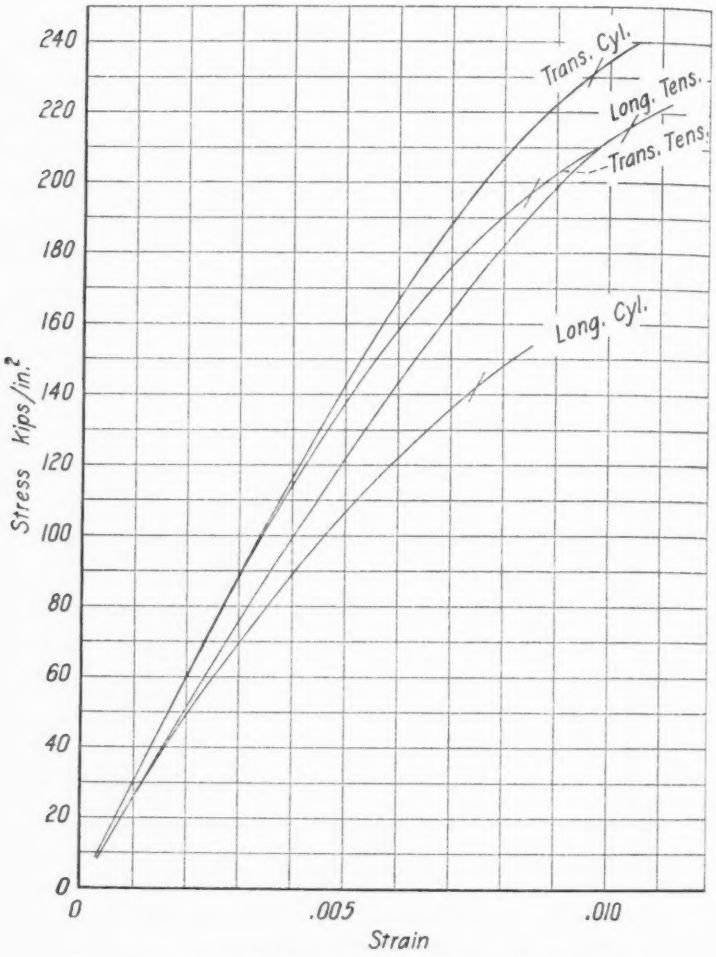

FIGURE 36.—*18–7, 0.01-inch sheet, 50.0 percent cold-reduced.*

Yield strength, offset=0.2 percent

Test	Longitudinal	Transverse
	Kips/in.²	*Kips/in.²*
Tensile	216.0	197.0
Cylinder compressive	142.2	231.6

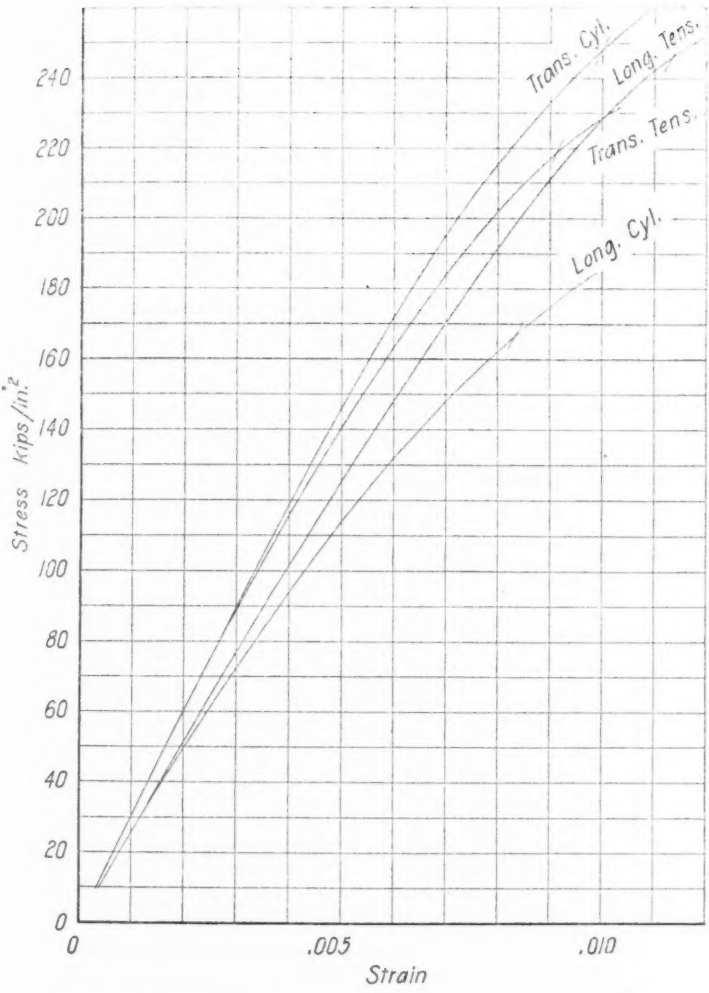

FIGURE 37.—*18-7, 0.01-inch sheet, 52.5 percent cold-reduced.*

Yield strength, offset=0.2 percent

Test	Longitudinal	Transverse
	*Kips/in.*²	*Kips/in.*²
Tensile	246.4	218.5
Cylinder compressive	166.8	248.2

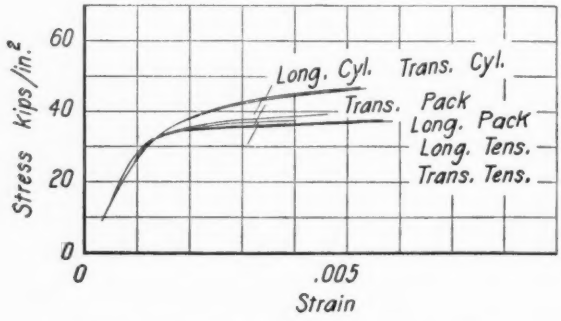

FIGURE 38.—*18–7, 0.02-inch sheet-annealed.*

Yield strength, offset=0.2 percent

Test	Longitudinal	Transverse
	Kips/in.²	*Kips/in.²*
Tensile	36.2	35.8
Pack compressive	36.7	37.8
Cylinder compressive	43.8	43.1

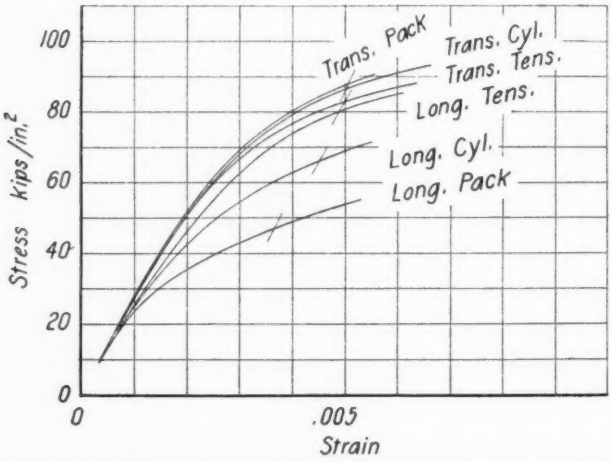

FIGURE 39.—*18–7, 0.02-inch sheet, 5.3 percent cold-reduced.*

Yield strength, offset=0.2 percent

Test	Longitudinal	Transverse
	Kips/in.²	*Kips/in.²*
Tensile	80.4	82.9
Pack compressive	47.4	88.1
Cylinder compressive	66.8	86.6

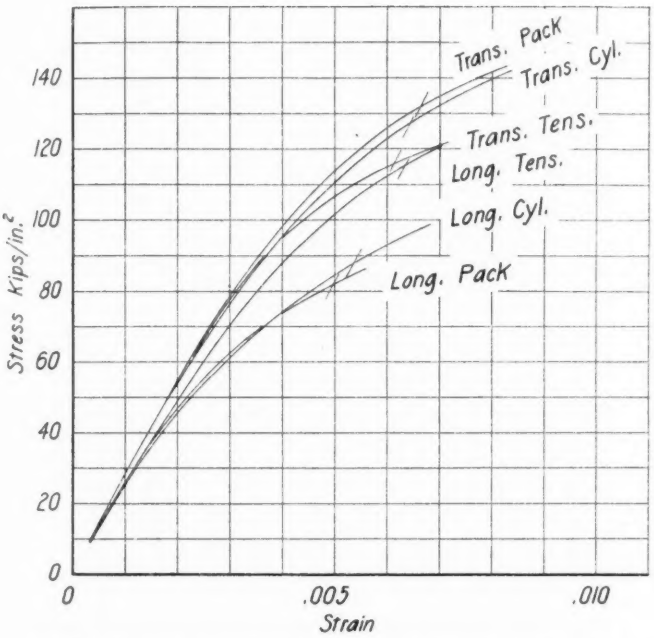

FIGURE 40.—*18–7, 0.02-inch sheet, 18.3 percent cold-reduced.*

Yield strength, offset=0.2 percent

Test	Longitudinal	Transverse
	Kips/in.²	*Kips/in.²*
Tensile	115.5	115.8
Pack compressive	82.0	132.0
Cylinder compressive	87.8	127.7

446682—42——10

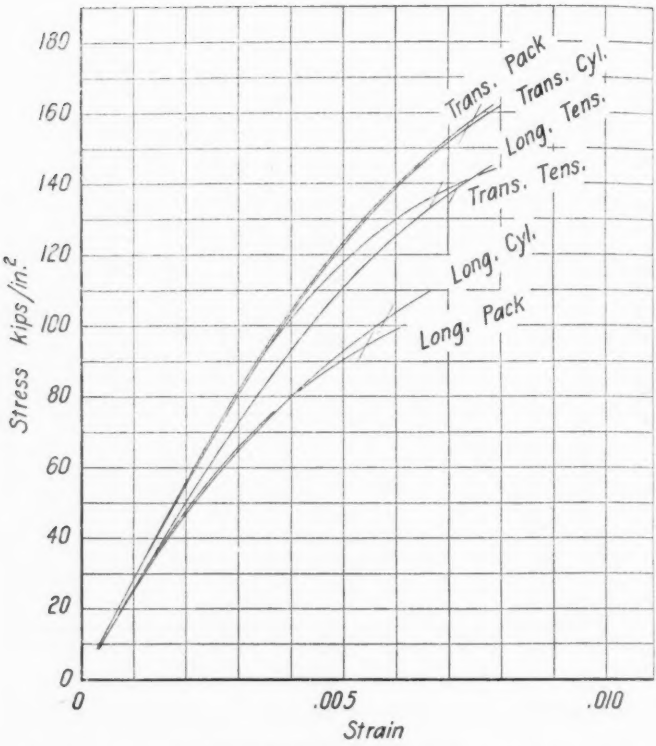

FIGURE 41.—*18–7, 0.02-inch sheet, 29.8 percent cold-reduced.*

Yield strength, offset=0.2 percent

Test	Longitudinal	Transverse
	Kips/in.²	*Kips/in.²*
Tensile	138.7	136.6
Pack compressive	94.3	158.1
Cylinder compressive	101.7	155.3

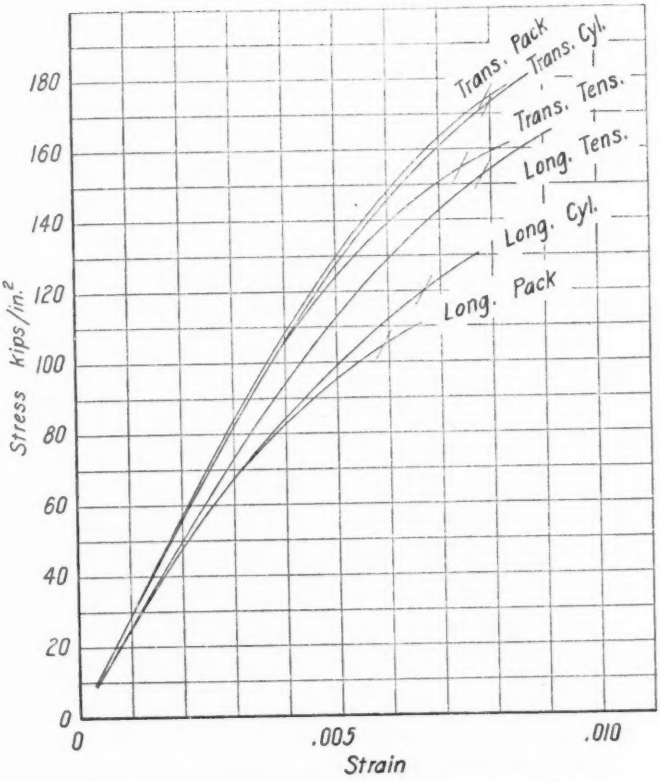

FIGURE 42.—*18–7, 0.02-inch sheet, 37.5 percent cold-reduced.*

Yield strength, offset=0.2 percent

Test	Longitudinal	Transverse
	Kips/in.²	*Kips/in.²*
Tensile	152.6	154.7
Pack compressive	104.7	173.8
Cylinder compressive	120.4	173.1

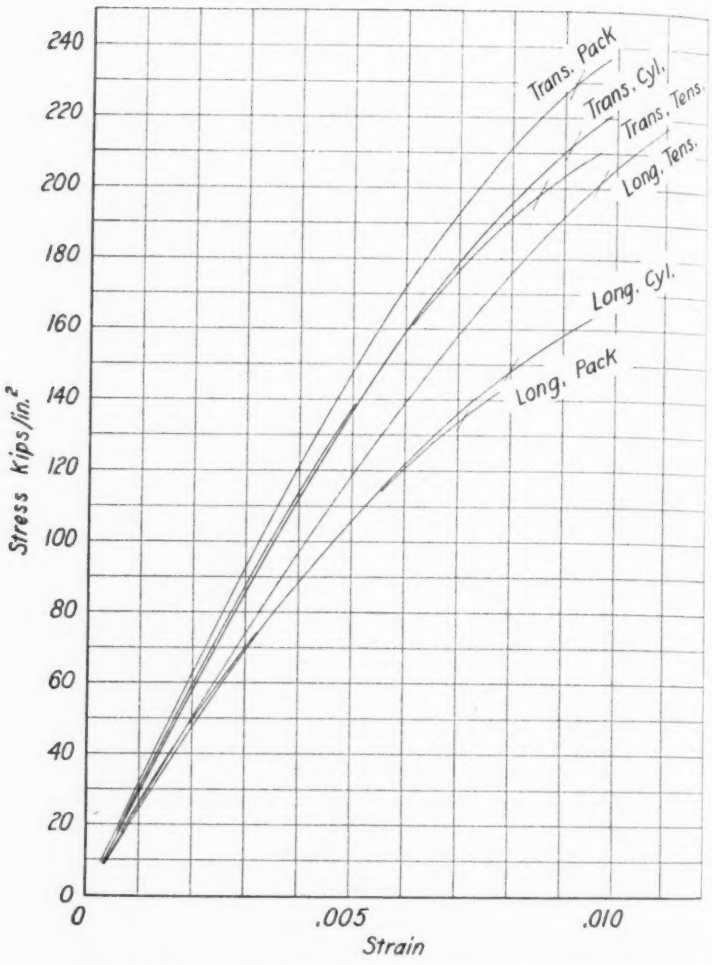

FIGURE 43.—*18–7, 0.02-inch sheet, 50.0 percent cold-reduced.*

Yield strength, offset=0.2 percent

Test	Longitudinal	Transverse
	Kips/in.²	*Kips/in.²*
Tensile	201.6	198.3
Pack compressive	135.1	228.8
Cylinder compressive	147.8	212.5

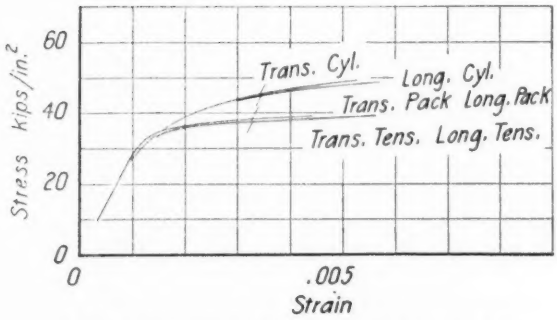

FIGURE 44.—*18–7, 0.035-inch sheet, annealed.*

Yield strength, offset=0.2 percent

Test	Longitudinal	Transverse
	Kips/in.²	*Kips/in.²*
Tensile	37.5	37.7
Pack compressive	37.8	38.2
Cylinder compressive	45.1	45.4

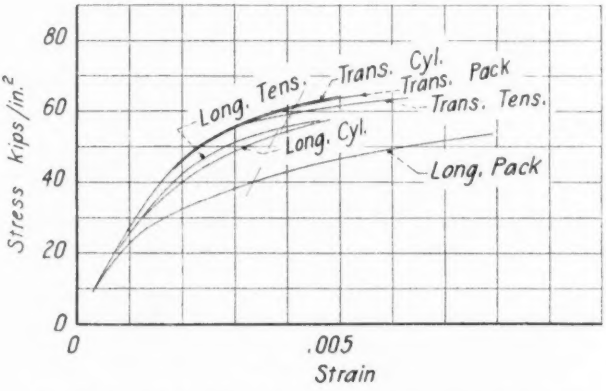

FIGURE 45.—*18–7, 0.035-inch sheet, 7.5 percent cold-reduced.*

Yield strength, offset=0.2 percent

Test	Longitudinal	Transverse
	Kips/in.²	*Kips/in.²*
Tensile	55.4	59.1
Pack compressive	40.1	61.0
Cylinder compressive	53.2	61.3

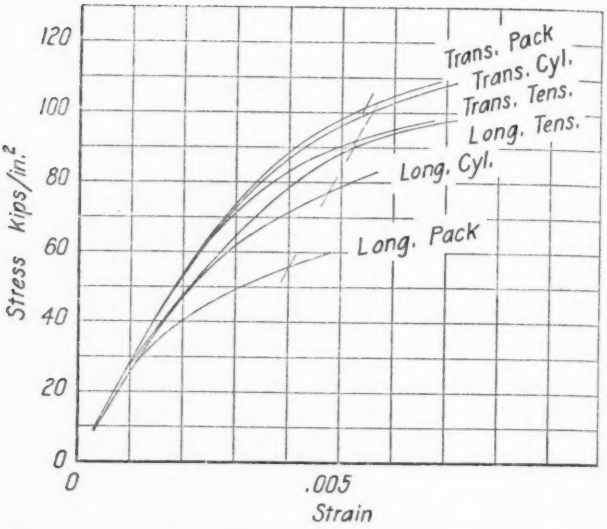

FIGURE 46.—*18–7, 0.035-inch sheet, 19.6 percent cold-reduced.*

Yield strength, offset = 0.2 percent

Test	Longitudinal	Transverse
	Kips/in.²	*Kips/in.²*
Tensile	89.5	91.8
Pack compressive	55.9	101.2
Cylinder compressive	77.3	100.2

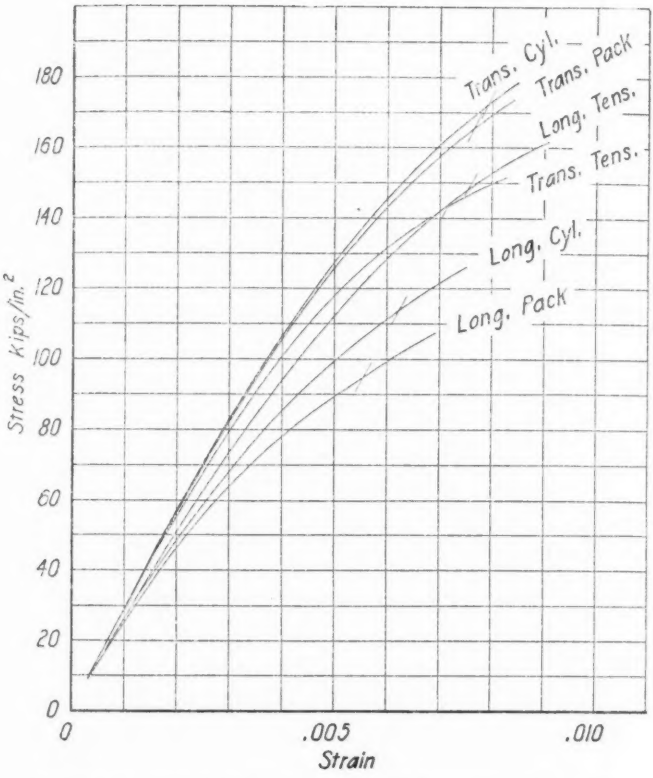

FIGURE 47.—*18–7, 0.035-inch sheet, 29.2 percent cold-reduced.*

Yield strength, offset=0.2 percent

Test	Longitudinal	Transverse
	Kips/in.²	*Kips/in.²*
Tensile	148.2	143.0
Pack compressive	94.8	165.6
Cylinder compressive	113.5	172.1

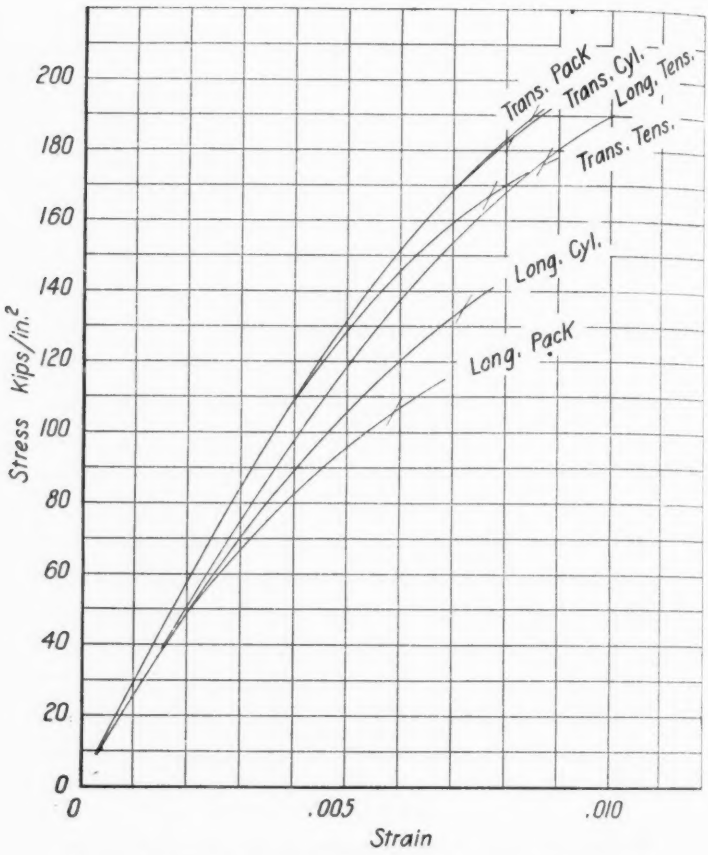

FIGURE 48.—*18–7, 0.035-inch sheet, 39.7 percent cold-reduced.*

Yield strength, offset=0.2 percent

Test	Longitudinal	Transverse
	Kips/in.²	*Kips/in.²*
Tensile	177.7	167.0
Pack compressive	105.5	189.1
Cylinder compressive	135.0	183.8

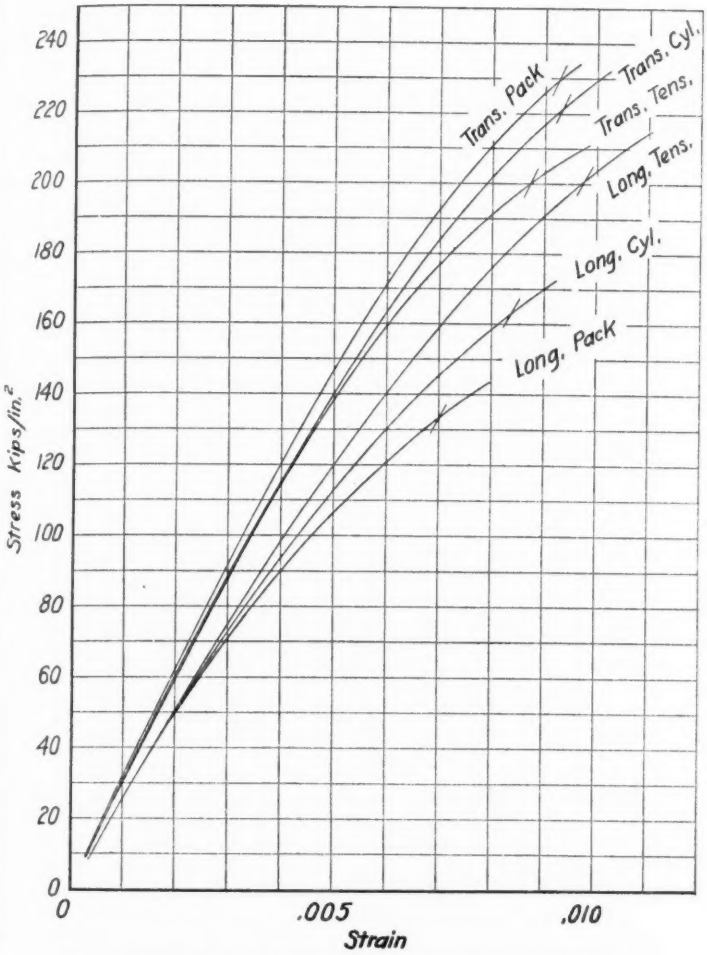

FIGURE 49.—*18–7, 0.035-inch sheet, 47.0 percent cold-reduced.*

Yield strength, offset=0.2 percent

Test	Longitudinal	Transverse
	Kips/in.²	*Kips/in.²*
Tensile	200.9	200.4
Pack compressive	133.5	229.5
Cylinder compressive	163.2	221.5

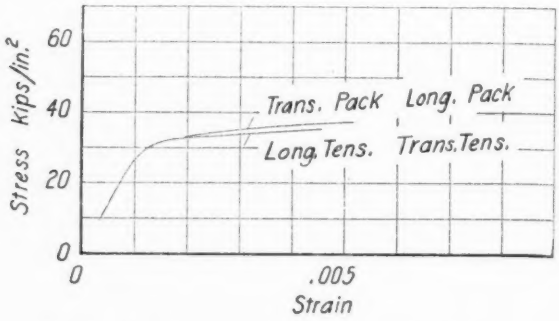

FIGURE 50.—*18–7, 0.06-inch sheet, annealed.*

Yield strength, offset=0.2 percent

Test	Longitudinal	Transverse
	Kips/in.²	*Kips/in.²*
Tensile	34.1	34.1
Pack compressive	35.3	35.5

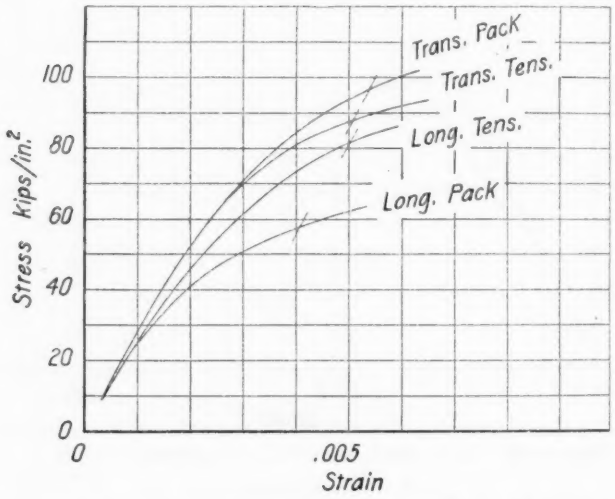

FIGURE 51.—*18–7, 0.06-inch sheet, 6.7 percent cold-reduced.*

Yield strength, offset=0.2 percent

Test	Longitudinal	Transverse
	Kips/in.²	*Kips/in.²*
Tensile	81.5	88.3
Pack compressive	57.8	96.3

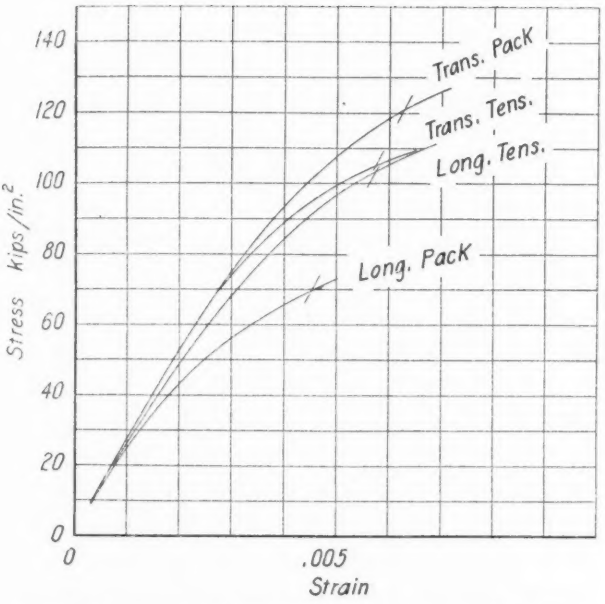

FIGURE 52.—*18-7, 0.06-inch sheet, 18.1 percent cold-reduced.*

Yield strength, offset = 0.2 percent

Test	Longitudinal	Transverse
	Kips/in.²	*Kips/in.²*
Tensile	103.7	105.2
Pack compressive	69.4	120.7

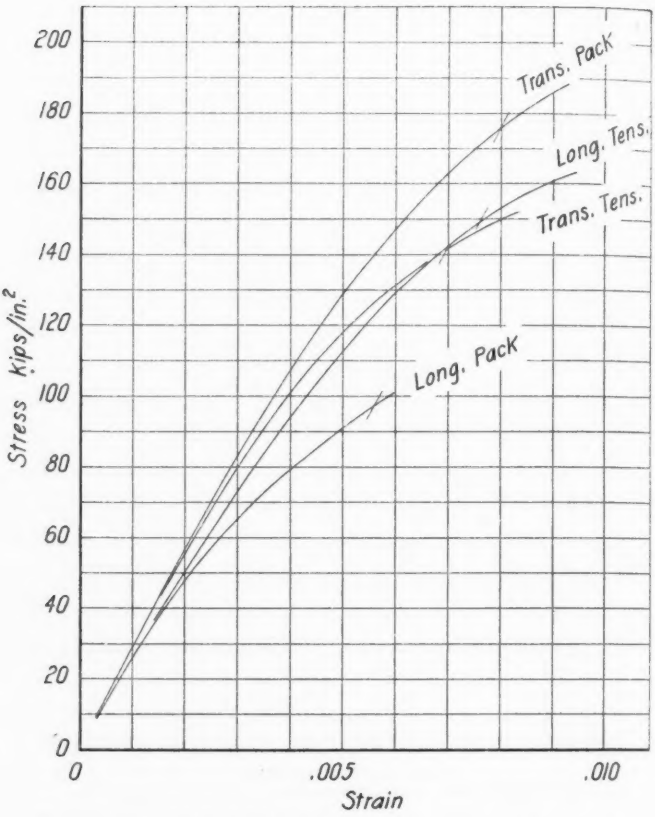

FIGURE 53.—*18–7, 0.06-inch sheet, 30.5 percent cold-reduced.*

Yield strength, offset=0.2 percent

Test	Longitudinal	Transverse
	*Kips/in.*²	*Kips/in.*²
Tensile	148.6	141.4
Pack compressive	97.4	176.0

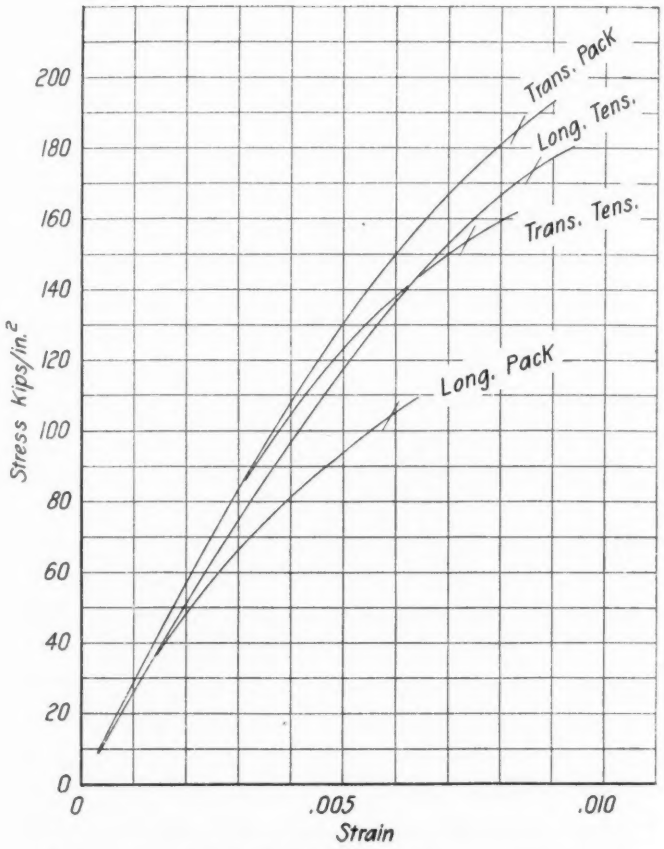

FIGURE 54.—*18-7, 0.06-inch sheet, 36.9 percent cold-reduced.*

Yield strength, offset=0.2 percent

Test	Longitudinal	Transverse
	Kips/in.²	*Kips/in.²*
Tensile	173.7	153.8
Pack compressive	104.3	185.3

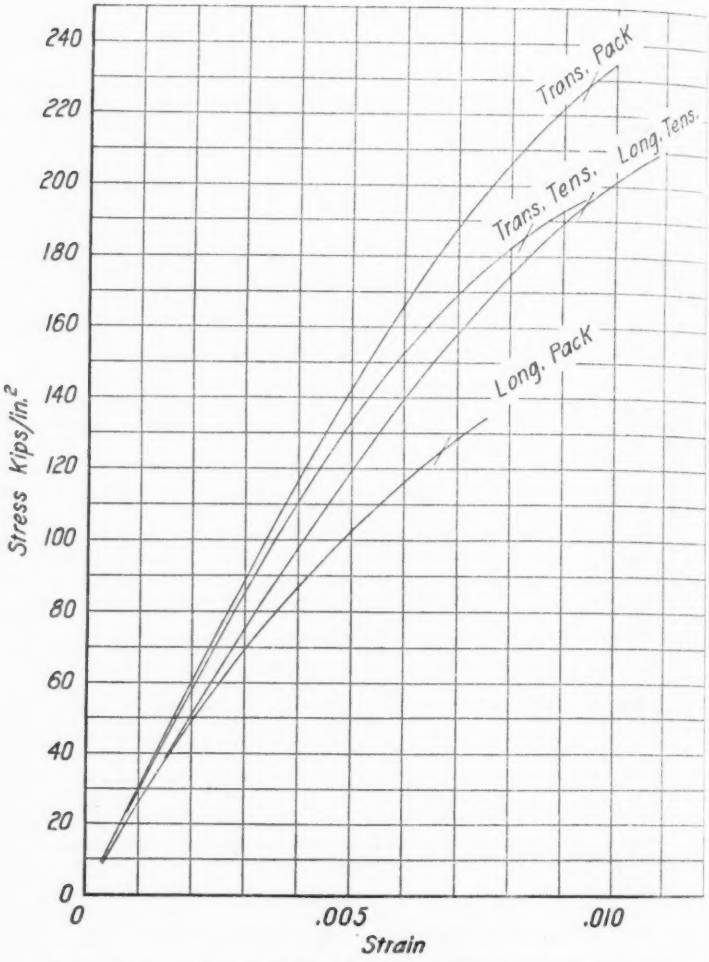

FIGURE 55.—*18-7, 0.06-inch sheet, 47.7 percent cold-reduced.*

Yield strength, offset=0.2 percent

Test	Longitudinal	Transverse
	Kips/in.²	*Kips/in.²*
Tensile	194.3	185.3
Pack compressive	125.1	228.2

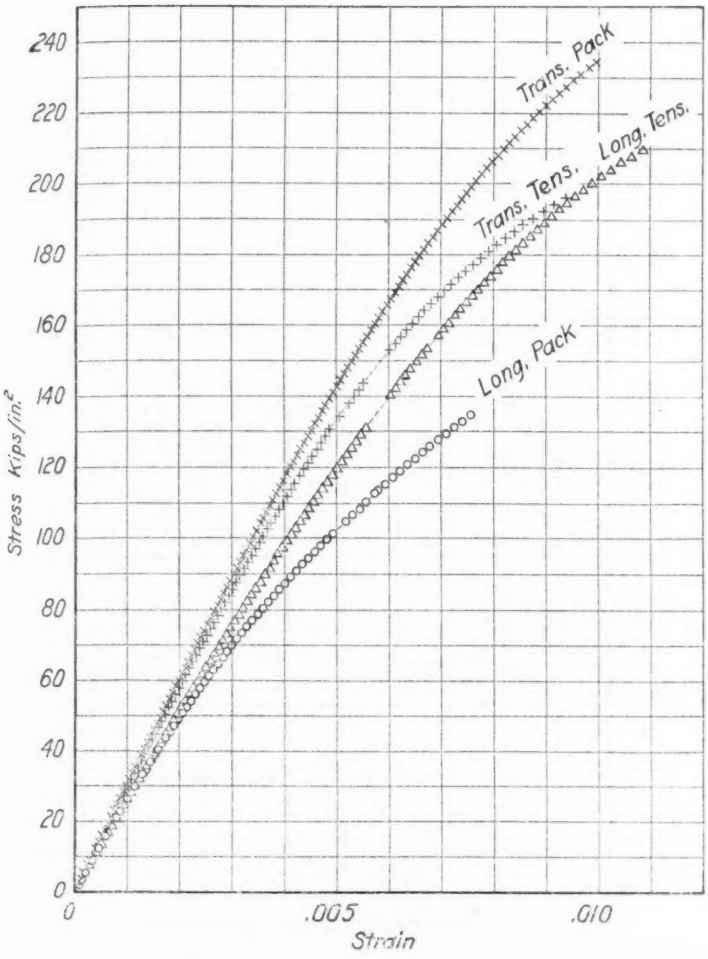

FIGURE 56.—*18–7, 0.06-inch sheet, 47.7 percent cold-reduced, individual points.*

Both strain gages were read simultaneously at increments of about 2.0 kips/in². Gaps in the readings were unavoidable, however, where occasional readings were missed or where, to avoid resetting the strain gage, both the tensile and compressive images were used.

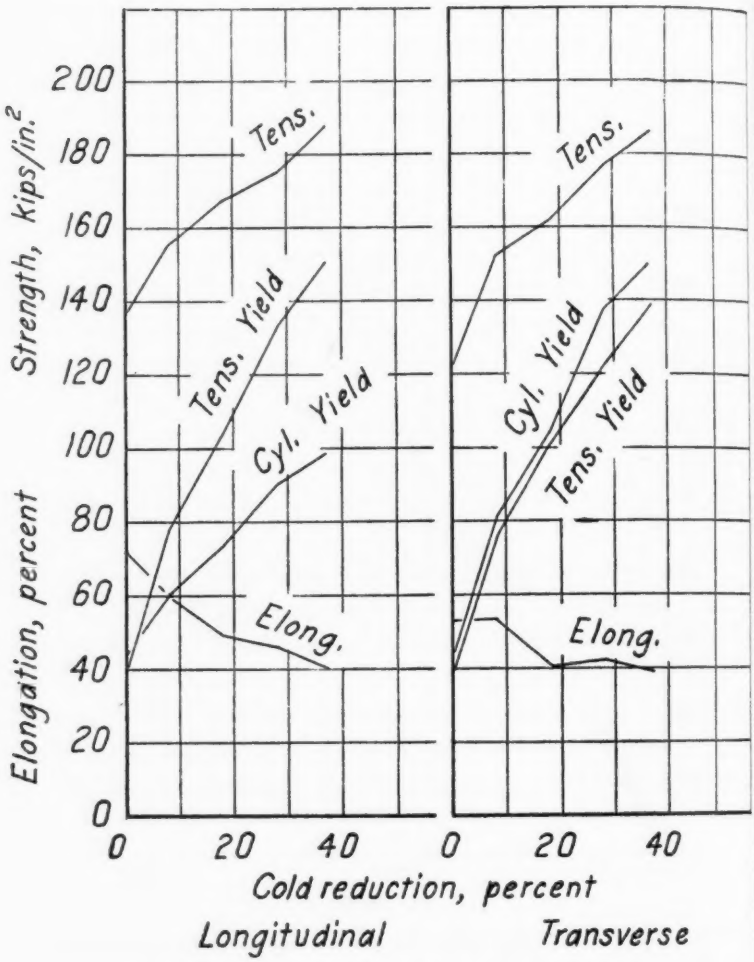

FIGURE 57.—*17-7, 0.01-inch sheet.*

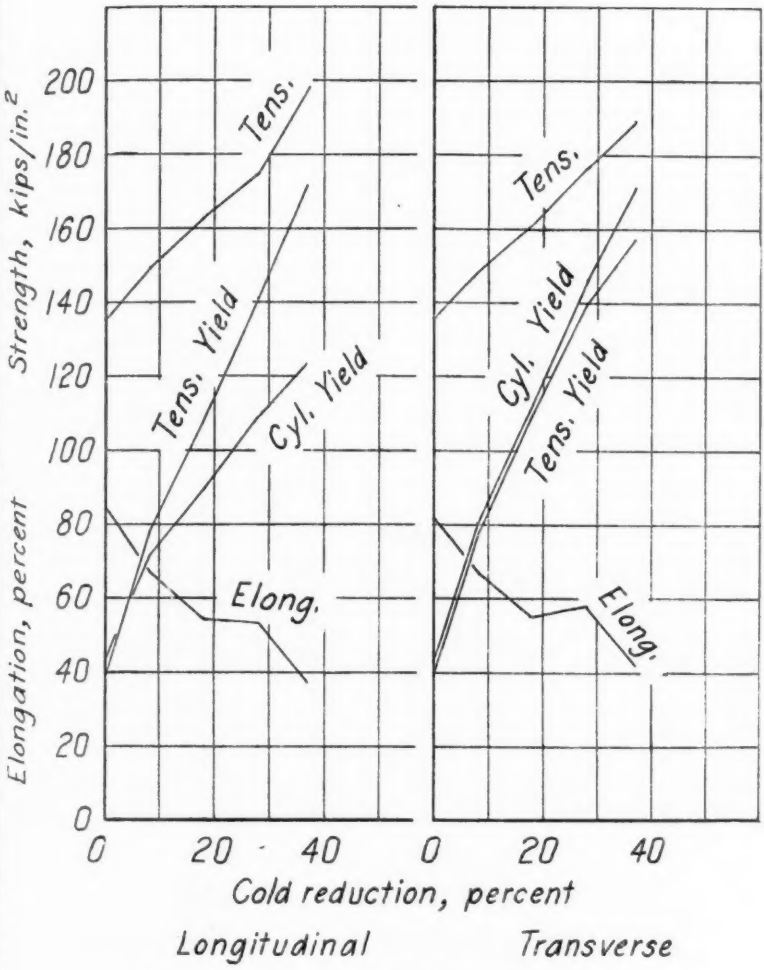

FIGURE 58.—*17–7, 0.01-inch sheet, stress-relieved.*

446682—42——11

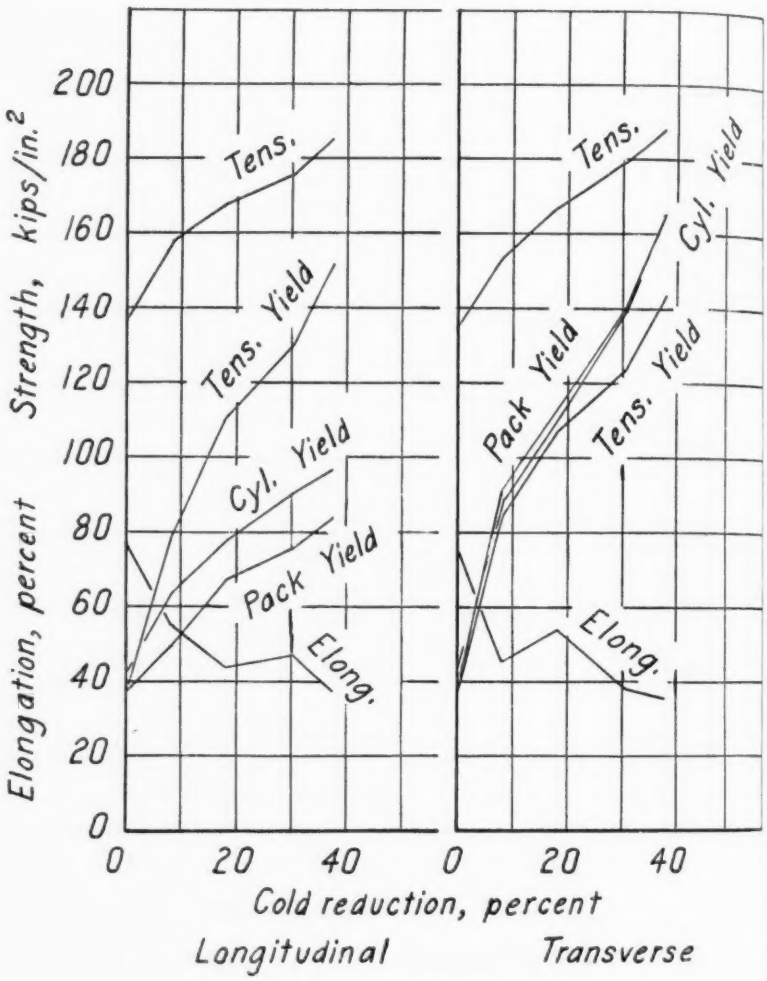

FIGURE 59.—*17-7, 0.02-inch sheet.*

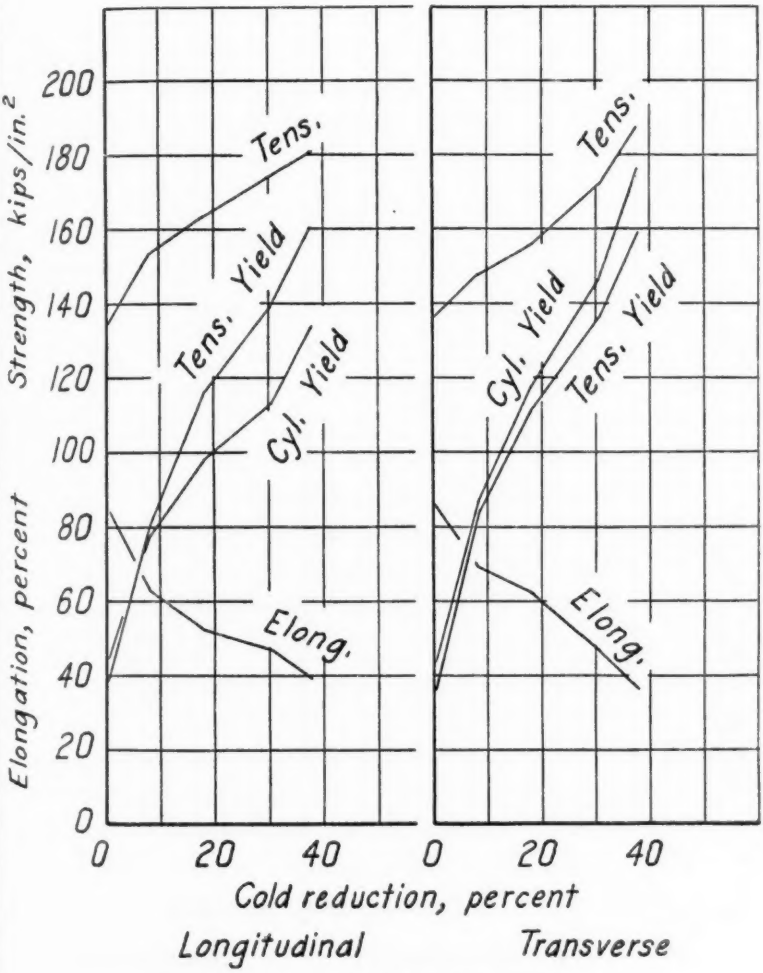

FIGURE 60.—*17-7, 0.02-inch sheet, stress-relieved.*

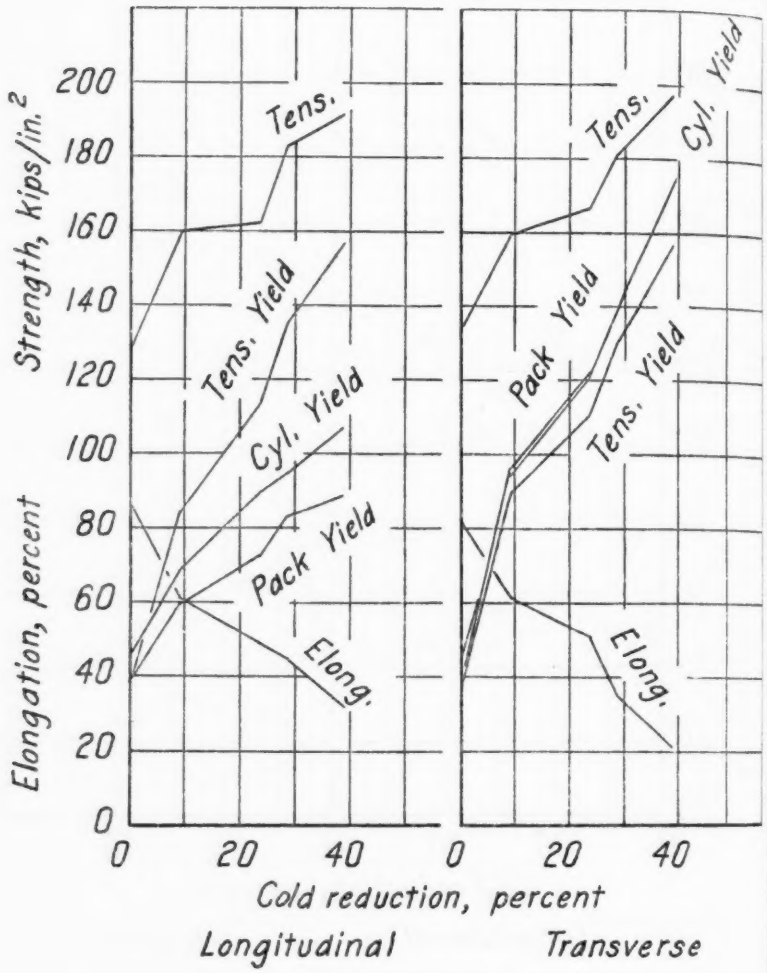

FIGURE 61.—*17-7, 0.04-inch sheet.*

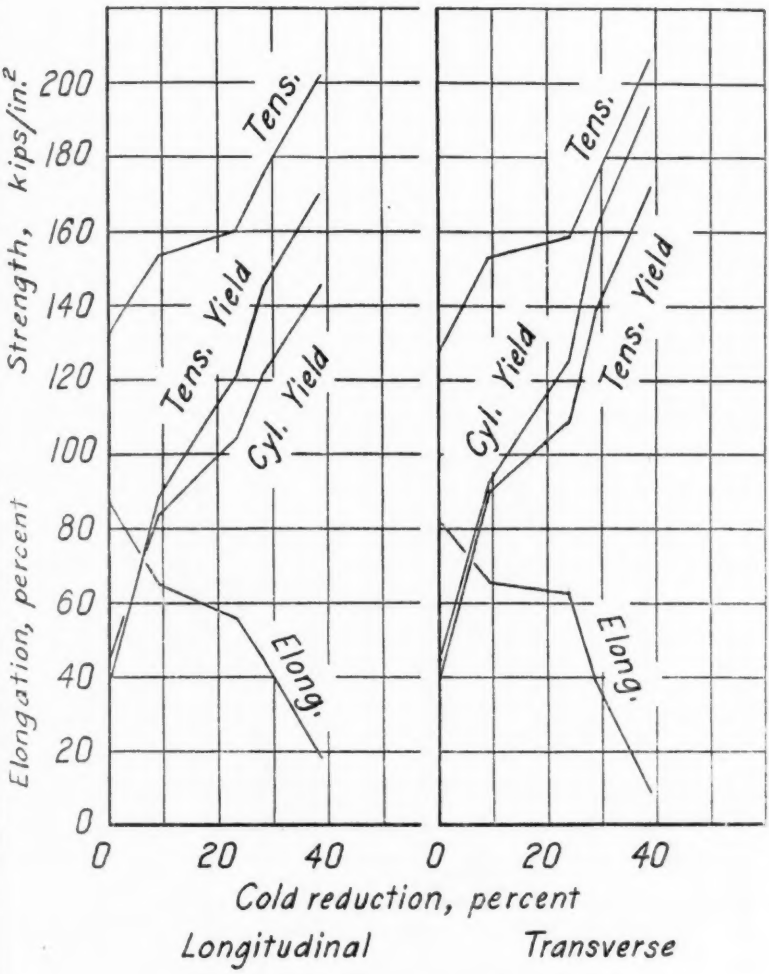

FIGURE 62.—*17–7, 0.04-inch sheet, stress-relieved.*

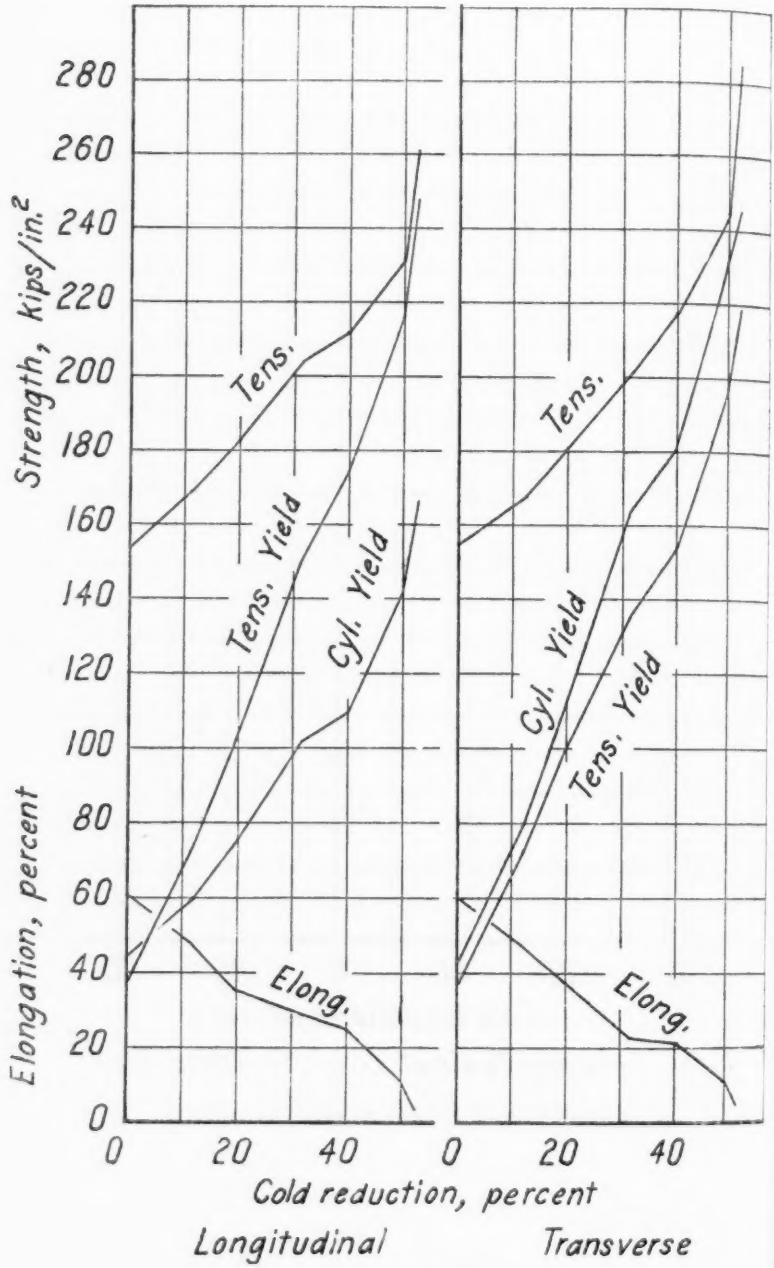

FIGURE 63.—*18–7, 0.01-inch sheet.*

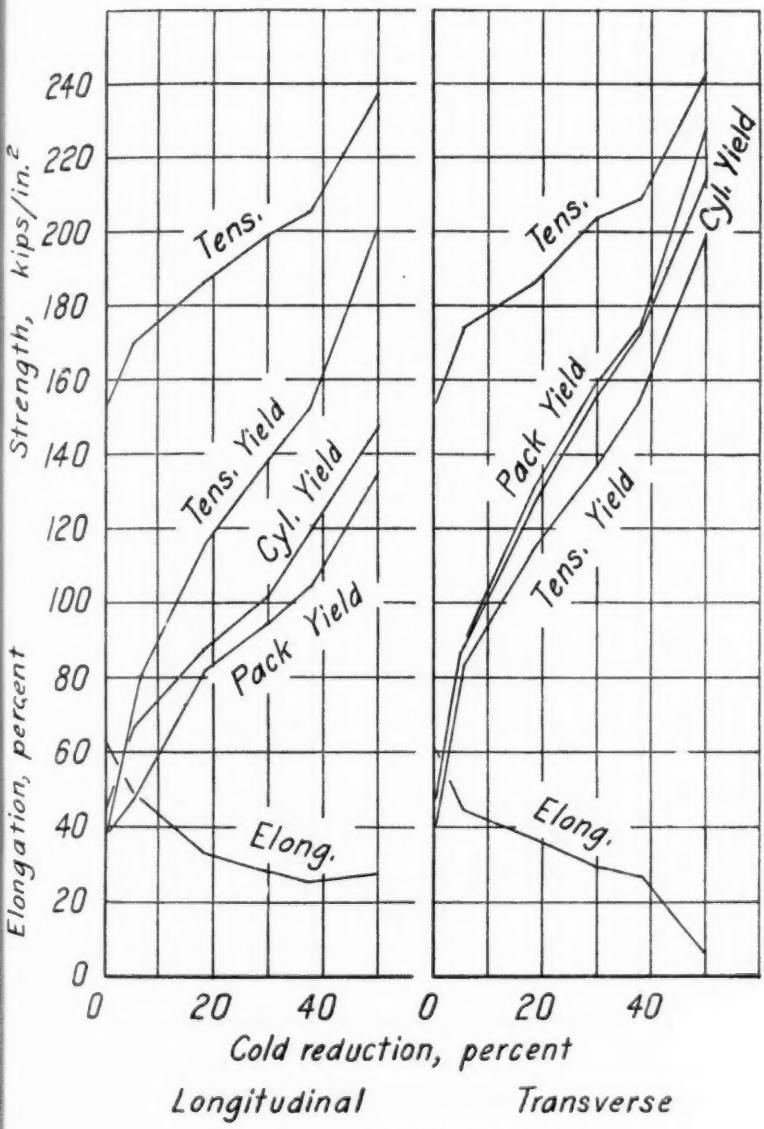

FIGURE 64.—*18–7, 0.02-inch sheet.*

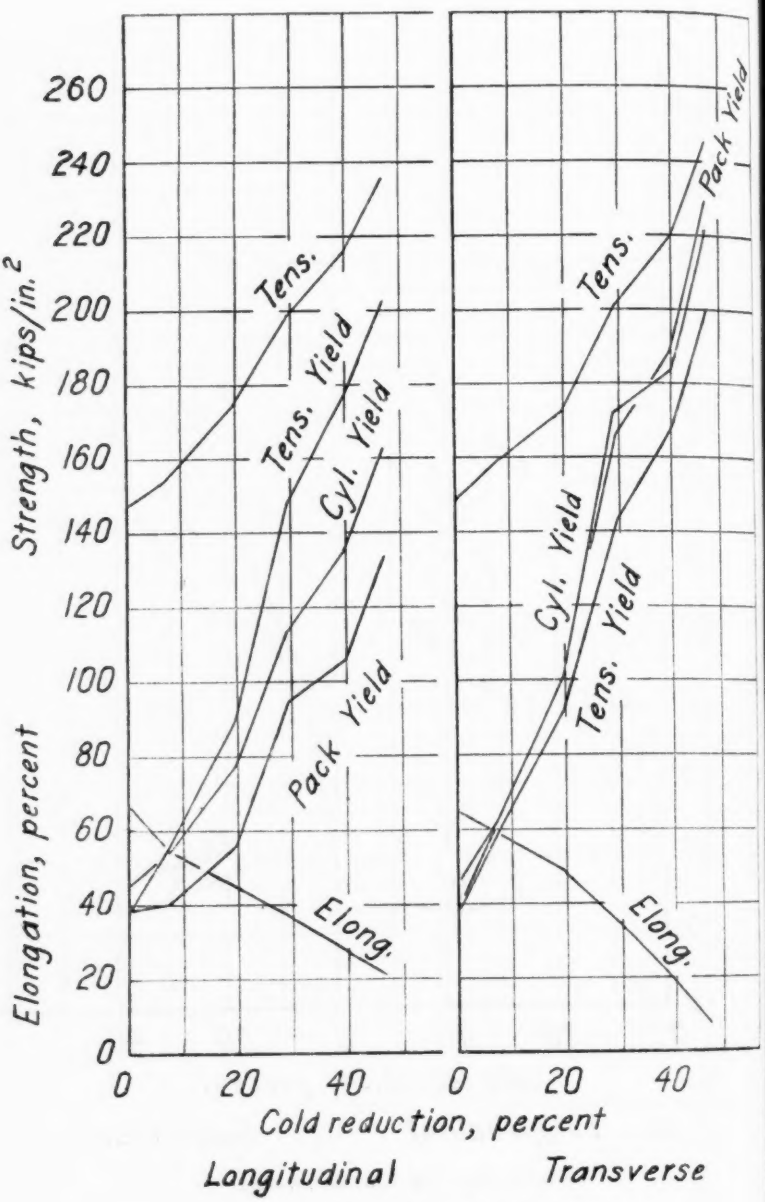

FIGURE 65.—*18-7, 0.035-inch sheet.*

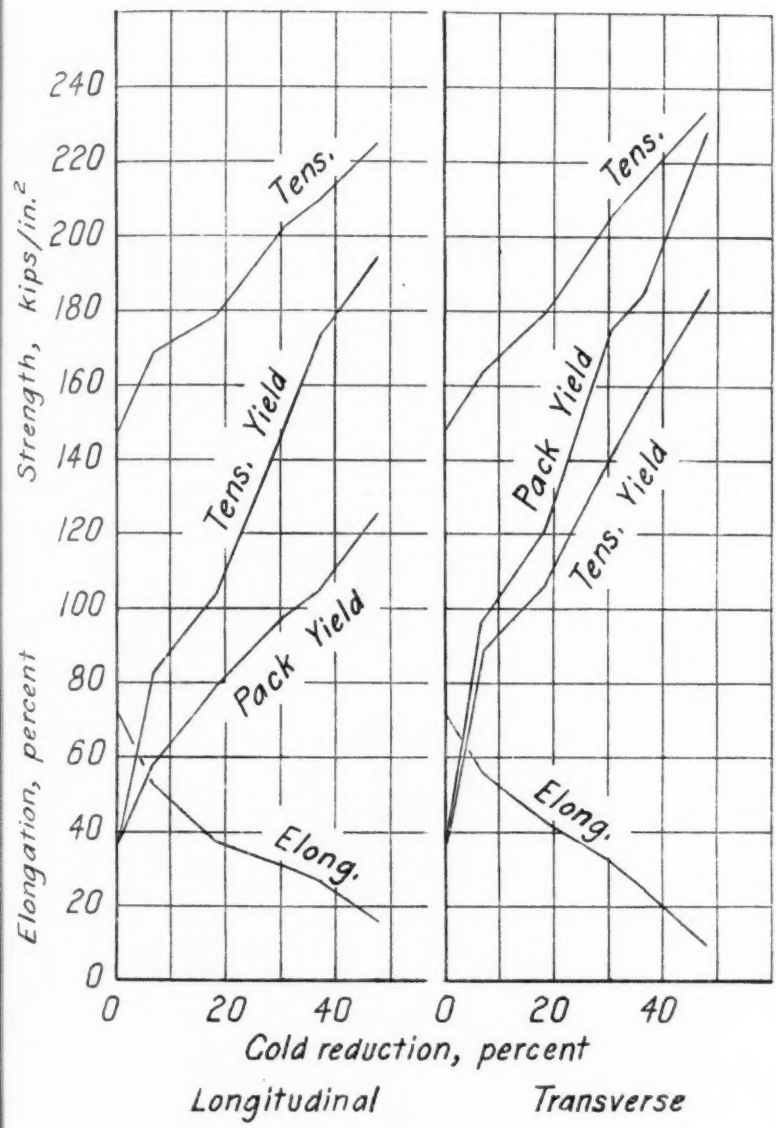

FIGURE 66.—*18–7, 0.06-inch sheet.*

WASHINGTON, March 2, 1942

○